DOCTOR OF SCIENCES

Interactions Between the Outer Membrane and the Peptidoglycan in Brucella abortus

Godessart, Pierre

Award date:
2021

Awarding institution:
University of Namur

Interactions Between the Outer Membrane and the Peptidoglycan in *Brucella abortus*

Pierre Godessart

Unité de Recherche en Biologie des Micro-organismes
Faculty of Sciences

2021

Promoter:

Prof. Xavier De Bolle, Université de Namur, Namur, Belgique

Jury members:

Prof. Waldemar Vollmer, Newcastle University, Newcastle, United Kingdom

Dr. Axel Cloeckaert, INRAE, Nouzilly, France

Prof. Jean-François Collet, Institut de Duve, Université Catholique de Louvain, Bruxelles, Belgique

Dr. Francesco Renzi, Université de Namur, Namur, Belgique

A thesis submitted in fulfilment of the requirements for the degree of

Doctor in Sciences

“I seem to have been only like a boy playing on the seashore, and diverting myself in now and then finding a smoother pebble or a prettier shell than ordinary, whilst the great ocean of truth lay all undiscovered before me”

Isaac Newton

Acknowledgements

First, I would like to thank the members of my jury: **Prof. W. Vollmer**, **Dr. A. Cloeckaert**, **Prof. J.-F. Collet** and **Dr. F. Renzi**. Thank you for the time you have invested in reading the manuscript and improving it and for the critical discussion. A special thanks to **Dr. M. Deghelt** for his involvement in this thesis and the discussion. I also would like to thank my committee that has accompanied me during those four years, **Prof. J.-F. Collet** and **Prof. P. Soumillion**. Thank you for your insights and for participating in taking the right decisions that lead to a successful project.

Un tout grand merci à **Xavier**, je nous revois encore à la foire aux mémoires où je venais me renseigner ! Merci de m'avoir accueilli pour mon mémoire et de m'avoir offert la possibilité de continuer pour une thèse. Merci aussi pour toutes les discussions qui m'auront permis d'y voir plus clair et d'apprendre tant, pour ta disponibilité et pour ta passion contagieuse pour la science. Enfin, merci pour toutes les sorties ainsi que les nombreuses bières partagées (et d'avoir toujours soutenu la Beer Hour quand nous en avions bien besoin) !

Merci aussi à **Jean-Yves, Régis** et **Francesco** (tu ne pourras pas dire que je t'ai oublié, ah ah) pour les discussions constructives et les conseils prodigués lors de ces cinq années en URBM.

Passons ensuite à l'équipe, par ordre chronologique ! Merci à **JF** de m'avoir appris les bases pendant le mémoire qui m'ont permis de bien commencer la thèse. Merci à **Katy** d'avoir répondu à mes nombreuses questions en début de thèse et pour toutes les discussions sur le côté. Thank you **Vicky** for bringing the German spirit to the team and I will never forget how we got Frida back! Merci à **Mathilde** d'avoir été ma

voisine de bureau les premières années et pour toutes tes réflexions qui n'ont jamais manqué de me faire rire.

Aurore, merci d'avoir été là, ça aurait été moins drôle sans toi. Des discussions au BL2 et au BL3, des moments où il fallait que ça sorte (la main !), du partage de cookie (mais du gras en général, ah ah), on pourrait en citer des moments ! Bref, j'espère que tu sais tout le bien que je pense de toi. Je vous souhaite tout le meilleur pour votre nouvelle aventure !

Agnès, du mémoire à la thèse, on en aura vu des choses (surtout en safari !), courage pour la dernière ligne droite ! **Adélie**, je ne te remercierai pas d'avoir fait tomber trois fois ma boite au fond du – 80 °C mais je te remercierai de ta bonne humeur indéfectible, d'avoir constamment voulu t'améliorer. Nous voilà maintenant collègues et je te souhaite de mener cette thèse à bien mais je n'ai aucun doute. Merci à **Eme** d'avoir contribué à la bonne ambiance au bureau. Merci à **Caro** de m'avoir aidé dans les manips (même si ça n'a jamais fonctionné, ah ah) mais aussi pour ton soutien et ta bonne humeur (coucou drunk Caro à Heidelberg). Mais aussi à merci **Angy** et **Elodie** pour l'aide apportée et les discussions. Et bonne chance à **Charline**, la dernière arrivée dans l'équipe. **Kévin**, je pense qu'on forme un bon duo tant pour le BL3 que pour monter des vidéos de thèse hollywoodiennes !

Merci aussi à **Gwen**, n'oublie pas que je compte sur toi pour être la gardienne du temps de la BH ! Et ne baisse pas les bras… je suis sûr qu'un jour, tu arriveras piloter un avion ! Merci à **Pauline** pour l'aide et le soutien apportés. Merci à **Bruce** et ses « Saluuuuut » qui auront rythmé le début de ma thèse et toutes ces bières partagées. Merci à **Jérôme** qui, de par sa bonne humeur, aura représenté l'esprit de l'URBM pendant de nombreuses années et répondu à mes toutes aussi nombreuses

questions. More generally, thanks to all the other URBM members that contributed to the good atmosphere and to successful beer hours, **Aish**, **Elie**, **José**, and sorry to all those that are not mentioned but were part of the adventure! Merci aussi à **Françoise** et **Aurélie** et pour leur travail sans lequel rien de tout cela n'aurait été possible. Les mêmes remerciements vont aussi à **Mathieu** mais avec une mention spéciale pour la touche d'humour ajoutée à l'URBM. Merci à **Patricia** pour ton accueil le matin et ce, malgré mon coin à brols.

Merci à **mes amis** qui se reconnaitront et qui m'auront permis de déconnecter que ce soit autour d'un repas/verre, d'une soirée film/jeux de société, d'une partie de pêche et j'en passe. Si vous lisez ce manuscrit, j'espère que vous comprendrez pourquoi j'ai (parfois) été bougon ces dernières années. Enfin, merci à **mon entourage familial** – et je reprendrai les termes de mon mémoire – de donné la possibilité de devenir ce que j'ai toujours souhaité devenir : un scientifique.

Interactions Between the Outer Membrane and the Peptidoglycan in *Brucella abortus*

The Gram-negative bacteria have an envelope made of three layers. The inner membrane (IM) and the outer membrane (OM) delimit the periplasmic space where the peptidoglycan (PG) is found. *Escherichia coli*, the Gram-negative model bacteria, has an abundant lipoprotein called Lpp, or Braun's lipoprotein, embedded in the inner leaflet of the OM. Lpp is covalently bound to the PG through the amino group of its C-terminal lysine. This linkage is established by enzymes called L,D-transpeptidases (LDts). *Brucella abortus* is a mainly intracellular pathogen and is the etiological agent of bovine brucellosis, a worldwide neglected zoonosis. In *B. abortus*, there is no homolog for Lpp nor any known structure establishing a covalent link between the OM and the PG.

In this thesis, we first aimed to identify OM proteins (OMPs) that would be covalently linked to the PG. Mass spectrometry analysis proved that, in *Brucella*, the PG is anchored via several β-barrel proteins. While these OMPs have no C-terminal lysine, the link occurs between the N-termini of these proteins and the PG. We also showed that the aspartate 2 has a crucial role in the anchoring, as its punctual mutation to alanine completely abolished the linkage of the two major OMPs to PG. Doing so, we showed an OM instability in the mutant, highlighting the physiological relevance of this system. Finally, we have also shown that the β-barrel anchoring system is conserved in *Agrobacterium tumefaciens* and bioinformatic analysis suggests that it could also be broadly found in Rhizobiales.

In a second time, we focused on the eight putative LDts encoded in the *B. abortus* genome to identify those involved in the anchorage of OMPs to the PG. We established a heterologous *E. coli* system where co-expression of one OMP (Omp25) and one LDt of *B. abortus* lead us to identify three LDts able to anchor *B. abortus* OMP to the PG of *E. coli*. The role of one of these LDts (Ldt4) was further confirmed in *Brucella*. We also investigated the remaining LDts and found clues that one of them (Ldt7) is likely to be involved in the PG remodelling.

During this study, we identified an additional putative LDt (BAB1_2034) by homology with *A. tumefaciens*. Surprisingly, BAB1_2034 deletion lead to the opposite expected phenotype as more OMPs were attached to PG. Conversely, over-expression of the protein decreased the amount of OMPs linked to PG. Moreover, infection of murine macrophages with the deletion and the over-expression strains lead to a virulence defect at 24 h post-infection. This suggests that not only the anchorage has a role – direct or not – in the virulence but also that the balance between attached and detached OMPs could be important.

Overall, we characterised a new OM-PG anchorage system and we provided new insights into the mechanisms behind the maintenance of the tethering. These data could be of major significance in the understanding of the envelope structure and resistance towards stress in Rhizobiales.

Table of content

List of abbreviations

- Ab: antibody
- ABC: ATP-binding cassette
- AFM: atomic force microscopy
- BAM: β-barrel assembly machinery
- BCV: *Brucella* containing vacuole
- DDt: D,D-transpeptidase
- DpaA: meso-diaminopimelic acid protein amidase A
- eBCV: endosomal BCV
- EM: electron microscopy
- EP: enolpyruvate
- ER: endoplasmic reticulum
- ERES: ER exit sites
- ERGIC: ER-to-Golgi intermediate compartment
- ES: electron spray
- GlcNAc: N-acetylglucosamine
- GTase: glycosyltransferase
- HMM: heavy molecular mass
- IM: inner membrane
- IMP: inner membrane protein
- LDc: L,D-carboxypeptidase
- LDt: L,D-transpeptidase
- LMM: low molecular mass
- Lol: localisation of lipoproteins
- LPS: lipopolysaccharide
- mAb: monoclonal antibody
- *m*DAP: *meso*-diaminopimelic acid
- MS: mass spectrometry

- MurNAc: N-acetylmuramic acid
- NCDAA: non-canonical D-amino acid
- nPB: non-penicillin-binding
- OM: outer membrane
- OMP: outer membrane protein
- OMV: outer membrane vesicle
- PAMP: pathogen-associated molecular pattern
- PB: penicillin-binding
- PBP: penicillin-binding protein
- PE: phosphatidylethanolamine
- PEP: phosphoenolpyruvate
- PG: peptidoglycan
- PI: post-infection
- PMF: proton motive force
- POTRA: polypeptide transport-associated
- rBCV: replicative BCV
- Sec: secretory
- TAT: twin-arginine translocation
- TM: transmembrane
- TRSE: texas red succinimidyl ester
- WB: western blot
- WT: wild type

INTRODUCTION

1 The bacterial envelope

Bacteria are divided into two main groups, the Gram-negative and the Gram-positive. This nomenclature comes from the crystal violet staining that is not retained by the Gram-negative. Both groups of bacteria have a cytoplasmic membrane (also called inner membrane, IM, in Gram-negative bacteria) that is surrounded by the peptidoglycan (PG) but only the Gram-negative bacteria have an outer membrane (OM). For that reason, they are also termed diderm bacteria as opposed to monoderm. Together, the IM and the OM delimit the periplasm, an aqueous but viscous compartment due to proteins tightly packed. Compared to the cytoplasm, it was estimated that the diffusion coefficient of proteins is about three times lower than in the cytoplasm (Mullineaux *et al.*, 2006).

1.1 The peptidoglycan

The PG, or murein, is a giant, highly dynamic polymer that surrounds the IM of bacteria and therefore, forms a sacculus. Any major defect in its biosynthesis or structure caused either by mutations or by antimicrobials will result in cell lysis, highlighting its importance. It is generally accepted that it withstands the turgor pressure and maintains cell shape as the sacculus retains the initial cell shape, even purified.

A non-mature PG subunit is composed of two hexoses, an N-acetylglucosamine (GlcNAc) and an N-acetylmuramic acid (MurNAc). The latter bears a lactic acid residue on which is grafted a pentapeptide. This manuscript will focus on Gram-negative bacteria and while the peptide stem can be subject to slight variations (Schleifer *et al.*, 1972), the

consensus pentapeptide is L-Ala[1] – D-isoGlu[2*] – *m*DAP[3] – D-Ala[4] – D-Ala[5]. The *m*DAP, *meso*-diaminopimelic acid, is an unconventional amino acid found solely in the PG and resemble a lysine with an additional carboxylic acid residue on the ε carbon of the lateral chain, making it a *meso* compound[†].

It should be noted that bacteria can incorporate non-canonical D-amino acids (NCDAAs) in their PG. For instance, it is known that *Escherichia coli* usually has a small proportion of its peptide stem with a glycine substitution at position four (Glauner *et al.*, 1988a). It was later found that many other bacteria can include NCDAAs in their PG at different positions (Cava *et al.*, 2011). These substitutions can either take place in the periplasm, driven by enzymes – mainly L,D-transpeptidases – that can edit the PG, or during its biosynthesis in the cytoplasm. The nature of the amino acids depends on the species. For example, *Vibrio cholerae* produces D-methionine and D-leucine while *Bacillus subtilis* uses D-tyrosine and D-phenylalanine (Lam *et al.*, 2009). The same study also showed that *V. cholerae* and *B. subtilis* are using these D-forms to down-regulate their growth and coordinate the stationary phase. Interestingly, it has also been shown that *V. cholerae* secretes D-arginine to outcompete other bacteria present in their environment (Alvarez *et al.*, 2018). Hence, the uncontrolled incorporation of NCDAAs can be toxic to bacteria.

The PG subunits are linked on two levels, (i) between the GlcNAc and the MurNAc in a β-1,4 manner and (ii) between the peptide stems. Together,

---

* The iso specifies that the peptide bond is not made with the carboxyl group from the carbon α but with the last carbon of the lateral chain of the glutamate.
† A *meso* molecule is an achiral stereoisomer that has at least two stereogenic centers and a symmetry plan.

these links form a net-like structure that proteins exported to the OM must be able to pass. It is thought that, in its relaxed form, the sacculus has pores that could let diffuse globular proteins up to 24 kDa (Demchick *et al.*, 1996) and the size could even go up to 100 kDa in living conditions where the PG is expanded (Vazquez-Laslop *et al.*, 2001). Despite its repetitive nature, the PG is also a heterogeneous structure. Indeed, when digested with a muramidase (*i.e.* lysozyme), the murein of *E. coli* yields more than fifty different subunits that differ by many factors (*e.g.* the length of the peptide or the peptide crosslink) (Glauner, 1988). It has been estimated that between 40 to 50 % of peptide stems are involved in crosslinking (Glauner *et al.*, 1988a). However, this percentage is subject to variations depending on the strain, the growth condition and also the growth phase.

The thickness of the *E. coli* PG sacculi has been the subject of several studies. The first examination by atomic force microscopy (AFM) found the murein to be 3.0 ± 0.5 nm thick if air-dried and about double when hydrated, 6.0 ± 0.5 nm (Yao *et al.*, 1999). Later, Cryo-EM experiments confirmed these results with a measurement of 6.35 ± 0.53 nm (Matias *et al.*, 2003). This is about the same width as the IM (5.84 ± 0.38 nm) and the OM (6.87 ± 1.01 nm) (Matias *et al.*, 2003). It should be noted that the thickness of the sacculi can vary depending on the species as the same study reported a value of 1.5 ± 0.5 nm for *Pseudomonas aeruginosa*. In addition, the PG of *E. coli* was reported to be single-layered on 75 to 80 % of the sacculi surface and tripled layered on 20 to 25 % (Labischinski *et al.*, 1991) with a thickness of 7 ± 0.5 nm. Remarkably, this study could not demonstrate the existence of a double-layered zone. How these single or triple-layered regions are spread on the surface still has to be determined.

1.1.1 Synthesis

The PG synthesis occurs in three main steps: the synthesis of the precursors that takes place in the cytoplasm, the lipid I and II formation in the IM and, finally, the incorporation of new subunits into the nascent strands of PG in the periplasm (Fig. 1).

The first set of steps consists of the conversion of fructose-6-phosphate to uridine diphosphate, UDP-GlcNAc (Fig. 2). It is achieved in four stages by enzymes of the *glm* (for *glucosamine*) operon: GlmS (Badet *et al.*, 1987), GlmM (Mengin-Lecreulx *et al.*, 1996a) and GlmU (Hove-Jensen, 1992; Mengin-Lecreulx *et al.*, 1993), the latter being a bi-functional enzyme (Mengin-Lecreulx *et al.*, 1994). Once the UDP-GlcNAc is synthesised, the molecule can undergo two modifications to become a UDP-MurNAc. The first consists of the addition of an enolpyruvate (EP) from a phosphoenolpyruvate (PEP) by the transferase MurA (Marquardt *et al.*, 1992), formerly named MurZ. The EP moiety is then further reduced into a lactyl ether by the MurB reductase (Benson *et al.*, 1993) and the consumption of an NADPH molecule. The addition of the peptide stem can then occur through four ligases, MurC (Liger *et al.*, 1995), MurD (Pratviel-Sosa *et al.*, 1991), MurE (Mizuno *et al.*, 1968) and MurF (Duncan *et al.*, 1990), that will subsequently attach the L-Ala, the D-isoGlu, the *m*Dap and the dipeptide D-Ala – D-Ala, respectively. The newly formed intermediate is named UDP-MurNAc-pentapeptide. In most cases, D-amino acids are only found in the PG (Holtje, 1998). Hence, racemases are also required; MurI converts L-Glu into D-Glu (Doublet *et al.*, 1993) and Alr (Wood *et al.*, 1951; Diven *et al.*, 1964) (anabolic) or DadX (Wild *et al.*, 1985) (catabolic) converts the L-Ala into D-Ala. These enzymes are absent from eukaryotic cells hence, designating them as potential targets for antibiotics and will

be briefly discussed below. The D-Ala dipeptide is then formed by the DdlA or DdlB ligases (Zawadzke *et al.*, 1991).

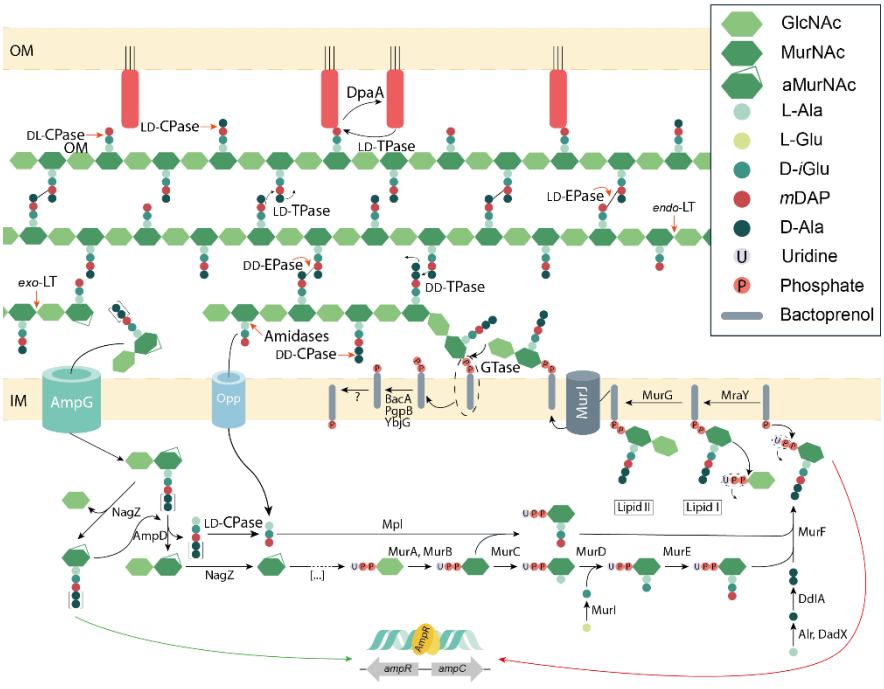

Figure 1 | Peptidoglycan biosynthesis, maturation, editing and recycling. This figure summarises the current knowledge for peptidoglycan synthesis and modification in *E. coli*. The first steps are cytoplasmic and begin with an UDP-GlcNAc to its conversion into UDP-MurNAc pentapeptide by six Mur enzymes. It is then embedded in the inner membrane by linkage to the bactoprenol to form the lipid I. A GlcNAc is transferred from an UDP-GlcNAc to form the lipid II. The latter is then found in the periplasm following flipping by MurJ. There, it can be incorporated into a PG nascent strand by glycosyltransferase (GTase). The nascent strand can then be linked to other strands by 4,3 or 3,3 peptides bridges made by D,D-transpeptidases (DD-TPase) or L,D-transpeptidases (LD-TPase), respectively. These links can be reversed by D,D-endopeptidases (DD-EPase) or L,D-endopeptidases (LD-EPase). Certain LD-TPase can link the peptide stem diaminopimelic acid (*m*DAP) to the C-terminal lysine of Lpp (in red), thus anchoring the OM to the PG. This link can also be reversed by an enzyme named DpaA. The terminal amino acid from the peptide stem can be removed by D,D- L,D- or D,L-carboxypeptidases (DD-, LD- or DL-CPase, respectively). The whole peptide stem can also be removed by amidases. Additionally, sugars bonds can be cleaved either within a strand by endo-lytic transglycosylase (endoLT) or at the end of a strand by exo-lytic transglycosylase (exoLT). The product of the

latter enzyme is the first step of the recycling pathway. Freed anhydro-muropeptides penta-, tetra- or tri-peptides are imported back to the cytoplasm by a transporter named AmpG. The GlcNAc can then be cleaved as well as the peptide chain. Both sub-products can then be processed by different enzymes and reincorporated into the biosynthesis pathway. Upon β-lactam stress, more anhydro-MurNAc-GlcNAc tripeptides are imported and can activate the transcription of *ampC*, a gene coding for a β-lactamase to face the stress through the AmpR transcription regulator. However, this induction does not happen in *E. coli* as *ampR* is not expressed. OM, outer membrane; IM, inner membrane.

The following steps as well as the export to the periplasm take place in the IM and require a carrier called the bactoprenol, or undecaprenyl phosphate (C_{55}-P). The latter is a 55 long carbon lipid that can be found in a functional form when phosphorylated or in an inactive alcohol form (Umbreit *et al.*, 1972). The C_{55}-OH form represents up to 90 % of the molecule pool in several Gram-positive bacteria (Higashi *et al.*, 1970; Umbreit *et al.*, 1972). Given the PG biosynthesis importance but also the involvement of C_{55}-P in the LPS O-chain transport (Whitfield *et al.*, 1993), the alcohol form could represent a reserve pool.

The first step consists of attaching the UDP-MurNAc-pentapeptide to the lipid and is done by the transmembrane translocase, MraY for "murein region a" (Ikeda *et al.*, 1991), thus forming the lipid I. The *mra* region encodes thirteen genes involved in PG biosynthesis and cell division: *pbpB-murE-murF-mraY-murD-ftsW-murG-murC-ddlB-ftsQ-ftsA-ftsZ-envA* (Bouhss *et al.*, 2008). Among them, many were already discussed and others will be further below.

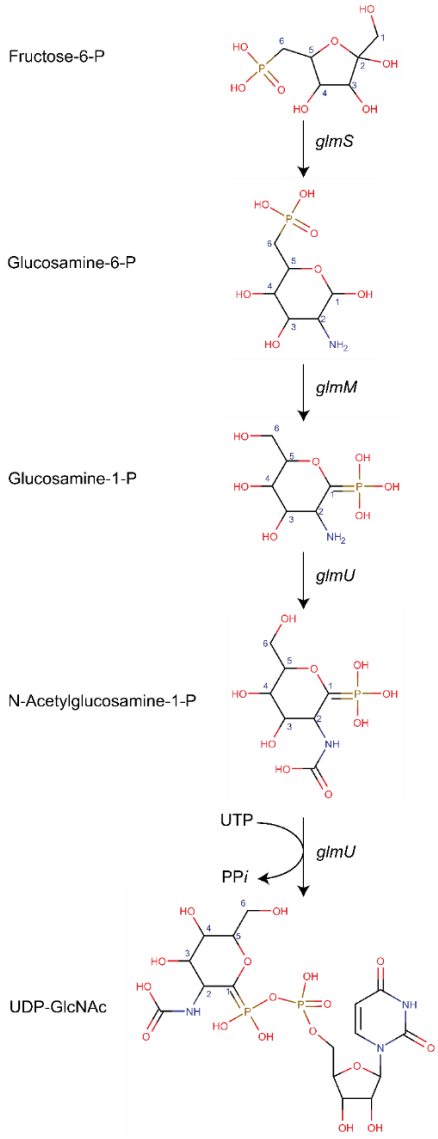

Figure 2 | Conversion of Fructose-6-P to UDP-N-acetylglucosamine The fructose-6-phosphate can be converted into UDP-GlcNAc, the product necessary for *de novo* peptidoglycan synthesis first step, by four enzymes encoded by the *glm* (for glucosamine) operon. The first step is the conversion of fructose-6-P into glucosamine-1-P by GlmS, the D-fructose-6-phosphate amidotransferase. The phosphate is then moved from the 6th to the 1st carbon of the glucosamine by GlmM, a phosphoglucosamine mutase. The two last steps of the process are performed by a bifunctional enzyme, GlmU, the N-acetylglucosamine-1-phosphate uridyltransferase.

The lipid I is further processed and becomes the lipid II by the addition of a UDP-GlcNAc by a second translocase, MurG (Salmond *et al.*, 1980), which forms a β-linked disaccharide. Then, the muropeptide is finally ready to be inserted into a nascent strand of PG. However, one final step must be performed: translocating it to the periplasm, from the inner to the outer leaflet of the IM. Although the majority of the actors of PG synthesis were identified in the second half of the 20th century, the identity of the flippase remained unsure for decades. Based on biochemical evidence, FtsW was first proposed to ensure lipid II transport in a membrane vesicle model (Mohammadi *et al.*, 2011). Opposed to this, a 2014 study proved MurJ to be *E. coli* single flippase and is using the proton motive force (PMF) to drive its conformational changes necessary for molecule transport (Sham *et al.*, 2014) and its structure was later published, suggesting at least two conformational states (Zheng *et al.*, 2018). In addition, the role of MurJ was also confirmed in the Gram-positive *B. subtilis* where an additional flippase, Amj was also identified (Meeske *et al.*, 2015). Reinforcing the connection between the LPS and the PG synthesis, the O-antigen flippase Wzk can sustain the loss of MurJ both in *Helicobacter pylori* and *E. coli* (Elhenawy *et al.*, 2016).

Once the precursor is in the periplasm, it is incorporated into the nascent strand by glycosyltransferases (GTase). These enzymes concomitantly cleave the diphosphate-undecaprenyl from the MurNAc while linking the latter to the C4-OH of the precursor GlcNAc (Sauvage *et al.*, 2008). When polymerised, the strands can then be further linked through their peptide stems by transpeptidase reactions. Since it occurs in the periplasm, no ATP can support the reaction. Hence, a transfer of energy from one peptide bond to another allows the transpeptidation (Cava *et al.*, 2011).

The MurNAc of the chain-ending muropeptide is reduced into an anhydroMurNAc presenting an internal ether bond between carbons 1 and 6 (Holtje *et al.*, 1975). The free undecaprenol pyrophosphate is then dephosphorylated into C55-P by three phosphatases, BacA (El Ghachi *et al.*, 2004), PgpB (El Ghachi *et al.*, 2005) and YbjG (El Ghachi *et al.*, 2005). The actors behind the C55-P transport back to the inner leaflet of the IM are still unknown.

1.1.2 Maturation & editing

Although PG must be sturdy to resist turgor pressure, it also should be plastic enough to accommodate environmental changes but also bacterial growth and division. To this extend, many enzymes are involved in its editing. If classes of enzymes are well conserved across bacteria, the number of enzymes present can greatly vary, underlying the difference of bacterial lifestyle and thus, of needs. In total, no less than 40 enzymes are involved in PG synthesis and degradation in *E. coli* (Typas *et al.*, 2012).

1.1.2.1 Transpeptidases

Two types of links can be found between two peptides as they can be made in D,D or L,D manner by D,D-transpeptidases (DDts) or L,D-transpeptidases (LDts), respectively. D,D links, or 4,3 links, represent most of the links in *E. coli* (Glauner *et al.*, 1988a) which occur between the carboxyl group of the D-Ala^4 and the D-centre of the *m*DAP^3. On the other hand, the 3,3 bond link two *m*DAP^3 from two different peptide stems occurs between their L- and D-centres (Fig. 3).

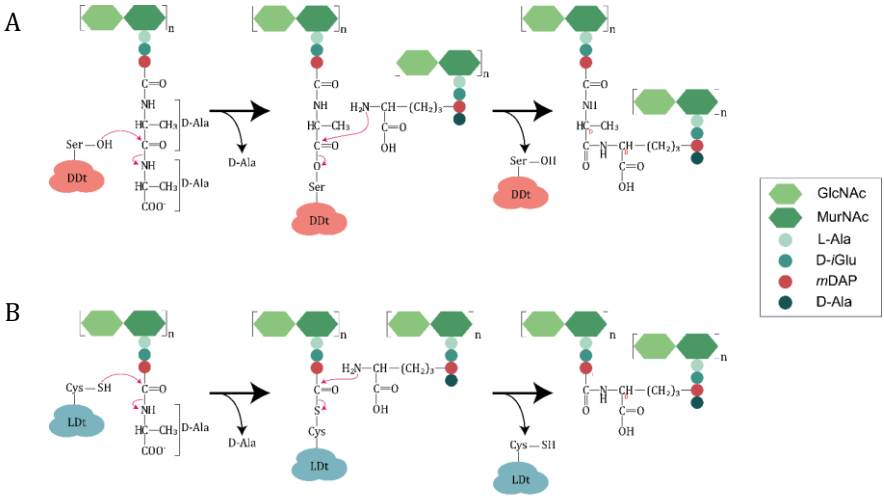

Figure 3 | Mechanism differences between the D,D-transpeptidases and the L,D-transpeptidases. A. In the case of DDts, the first step is the attack of the carbonyl of the D-Ala[4] of the acyl donor by the hydroxyl group of the DDt serine. This leads to the release of the fifth amino acid of the peptide stem and the formation of an enzyme-linked intermediate. Then, the amine group of the lateral chain *m*DAP of the acyl acceptor attack the carbonyl of the enzyme intermediate. This results in the formation of a 4-3 link. **B.** For LDts, the sulfhydryl of the catalytic residue attacks the carbonyl of the *m*DAP[3] of a tetrapeptide stem acyl donor. The intermediate enzyme-linked is then attacked by an acyl acceptor, a tetrapeptide stem and result in the formation of a 3-3 link.

1.1.2.1.1 D,D-transpeptidases

Based on their molecular mass, PBPs have been divided into two groups: high and low molecular mass (HMM and LMM, respectively) (Sauvage *et al.*, 2008). HMM can either be monofunctional transpeptidases or bifunctional with an additional GTase activity. The GTase domain is involved in the glycan strand elongation of PG. Overall, their topology is similar; the N-termini spans into the cytoplasm followed by a transmembrane (TM) domain which precedes two domains separated by a linker. The N-terminal domain is termed “non-penicillin binding” (nPB) and the C-terminal part is a penicillin-binding (PB) module. The former domain is used to divide PBPs into class A or B. Class A PBPs have a GTase

activity (Vollmer *et al.*, 2008a) while the nPB domain of class B does not have a clear enzymatic activity but is rather thought to be involved in the interaction with other proteins (Goffin *et al.*, 1996).

E. coli has three Class A PBPS named PBP1A, PBP1B and PBP1C encoded by *ponA*, *ponB* and *pbpC*, respectively. Class B is composed of the PBP2 and PBP3, encoded by *pbpA* and *ftsI*, respectively. Among them, PBP1a and PBP1b are the most active PBPs and, while not being essential, a double knockout *ponAponB* is lethal due to partially redundant functions (Suzuki *et al.*, 1978a; Denome *et al.*, 1999; Meberg *et al.*, 2001). The role of PBP1c is still unclear; it is seemingly insensitive to most β-lactams and its overexpression does not suppress the lethality induced by the loss of PBP1a and PBP1b (Schiffer *et al.*, 1999). On the contrary, the role of the PBP1a is well understood. It is involved in the elongasome thus, localising at the cell periphery and interacting with PBP2 (Banzhaf *et al.*, 2012). Conversely, PBP1b plays a role in the divisome interacting with PBP3, hence localising at the mid cell (Bertsche *et al.*, 2006). In addition, seven LMM PBPs can be found and are sorted in class C, itself divided into subgroups Type-4, -5, -7 and –AmpH in reference to the eponymous PBPs.

1.1.2.1.2 L,D-transpeptidases

The first L,D-transpeptidase (LDt) was characterised in 2005 by Mainardi and colleagues in a Gram-positive bacterium (Mainardi *et al.*, 2005). They observed that, in an *Enterococcus faecium* ampicillin-resistant strain, the classical D-Ala^{4} – D-isoAsn – L-Lys^{3} crosslink was partially replaced by an undescribed crosslink, L-Lys^{3} – D-isoAsn – L-Lys^{3}. This study also reported the similarity with the PFAM YkuD entry (PF03734). This family (formerly called ErfK/YbiS/YcfS/YnhG domain) was initially described in *Bacillus subtilis* (Bielnicki *et al.*, 2006) where the crystal structure was

solved as a novel tertiary fold made of a β-sandwich. It is composed of a pocket constituted by two leaflets made of five and six β-strands. The two leaflets are topped with an α-helix that figuratively closes the pocket. The active site is well conserved across both Gram-negative and Gram-positive bacteria and, in *B. subtilis*, it encloses four amino acids; His123, Gly124, Cys139 and Arg141 with the cysteine being the catalytic residue. Bielnicki and colleagues also showed *Brucella melitensis* to be no exception to this conservation by *in silico* analysis.

As suggested by their name, *E. faecium* LDts have a substrate specificity towards the L-Lys^{3} – D-Ala^{4} of a tetrapeptide – the acyl donor in the reaction – rather than the D-Ala^{4} – D-Ala^{5} recognised by DDts. In Gram-negative bacteria, LDts specificity is towards *m*DAP^{3} – D-Ala^{4}. Due to the difference of substrates, LDts are naturally β-lactam insensitive as this class of antibiotic mimics the D,D link. Nevertheless, LDts can still be inhibited. Indeed, a study by Mainardi and colleagues reported the *E. faecium* LDt inactivation by imipenem (Mainardi *et al.*, 2007b). Although it is a β-lactam ring–based molecule, it can acylate the catalytic cysteine which inactivates the LDt. In addition, another study from 2018 (Peters *et al.*, 2018) showed that copper, at low concentration, can completely inhibit the formation of 3-3 crosslinks in *E. coli*. The authors suggest a mechanism by which copper ions (Cu^{2+}) would bind the thiol group of the catalytic cysteine, thus preventing the reaction.

If all LDt proteins include a YkuD domain, only some of them also have a LysM motif. The LysM (Lysin Motif, PF01476) domain was discovered in the lysozyme of the *Bacillus* phage Φ29 (Garvey *et al.*, 1986). Then it was reported in bacterial cell wall degrading enzymes in *Enterococcus hirae* and *Enterococcus faecalis* (Joris *et al.*, 1992). It is typically made of 44 to

65 amino acids (Buist *et al.*, 2008) that adopt a βααβ secondary structure (Bateman *et al.*, 2000). The first 16 amino acids are well conserved across species, the rest of the sequence is more variable. Several motifs can be found in one domain and spacer sequences are found in-between. Beginning of 2021, this family (PF01476) had occurrences in over 58,000 proteins from all kingdoms, highlighting its ubiquity. In prokaryotes, LysM allows PG binding and more specifically, recognise the GlcNAc moiety as well as the peptide stem to a lesser extent (Mesnage *et al.*, 2014). In addition, the domain requires a minimal length of four saccharide residues for an efficient binding (Mesnage *et al.*, 2014). LysM domains are present in many proteins with a variety of functions, including hydrolases, lysins, kinases, amidases or virulence factors (Bateman *et al.*, 2000; Mesnage *et al.*, 2014). In eukaryotes, it is suggested that LysM domains presence originates from ancient horizontal gene transfer (Ponting *et al.*, 1999). They are found in animals, insects and plants where they recognise both chitin and PG. The LysM domain is mainly involved in the recognition of pathogens, fungal (Kaku *et al.*, 2006) or bacterial (Willmann *et al.*, 2011), and in the symbiosis for the nodulation factors perception (Broghammer *et al.*, 2012).

In *E. coli*, 6 LDts have been reported up to this day and were originally named ErfK, YbiS, YcfS, YcbB, YnhG and YafK. For the sake of simplicity, a new nomenclature is now used: LdtA (ErfK), LdtB (Ybis), LdtC (YcfS), LdtD (YcbB), LdtE (YnhG) and LdtF (YafK). This family of enzymes was shown to be involved in two different cell wall maintenance aspects. LdtA-C anchors Lpp (Magnet *et al.*, 2007) and LdtB being the major actor as its deletion alone is sufficient to almost completely prevent Lpp anchorage. Lpp is the major OM lipoprotein of *E. coli* and is described in section I.B.1.a.i. of this introduction. LdtD-E are responsible for PG 3-3

crosslinks (Magnet *et al.*, 2008). These enzymes have three catalytic activities, L,D-transpeptidation, L,D-carboxypetidation and substrate exchange. Surprisingly, neither the Lpp anchorage (Hirota *et al.*, 1977) nor the 3-3 transpeptidation (Magnet *et al.*, 2008) activities are essential in *E. coli*. Until recently, the role of LdtF was still elusive and will be treated further below (see section 1.2.1.1.1 of the introduction). Before, ectopic assays could only demonstrate LdtF activity when co-expressed with LdtD or LdtE, suggesting a stimulation role (More *et al.*, 2019). LdtF was already reported to be involved in biofilm formation in the pathogenic enteroaggregative *E. coli* (Sheik *et al.*, 2001). Surprisingly, 3-3 links only represent from 2 to 10 % of all crosslinks in *E. coli* (Pisabarro *et al.*, 1985; Glauner *et al.*, 1988a; Holtje, 1998), the rest being 4-3 crosslinks. This proportion can go up to 16 % during the stationary phase as LdtE and LdtF are under the control of the stationary phase sigma factor RpoS (More *et al.*, 2019). An increase of 3-3 links can also be observed under envelope stress condition responses mediated by Cpx through the activity of LdtD (Bernal-Cabas *et al.*, 2015). Interestingly, in the Rhizobiales *A. tumefaciens* and *Sinorhizobium meliloti*, this crosslink type accounts for about 50 % (Brown *et al.*, 2012). This proportion can even be higher as in *Mycobacterium tuberculosis,* 80 % of the PG crosslinking is due to 3-3 links in stationary phase (Lavollay *et al.*, 2008). The LDt difference of substrate compared to DDts intrinsically provides resistance to β-lactam antibiotics, exception made of carbapenem (Mainardi *et al.*, 2007a).

LDts have also been recently described to have a role in the pathogenicity of *Salmonella enterica* subsp. enterica serovar Typhi (Geiger *et al.*, 2018). This pathogen, closely related to *E. coli* and causing typhoid fever, releases the typhoid toxin, an essential virulence factor. Geiger and

colleagues showed that the export of the typhoid toxin requires the editing of the polar PG by a specific LDt, namely LdtD (or YcbB). Although this is not in line with the low proportion of 3-3 links in *Enterobacteriaceae* PG, it is known that *Salmonella* modulates the proportion of links during the infection of eukaryotic cells (Quintela *et al.*, 1997; Garcia-Del Portillo, 2020). In conclusion, even though the implications of LDts was somewhat neglected, their roles were revealed to be increasingly important and diverse.

1.1.2.2 Carboxypeptidases

The term carboxypeptidase refers to enzymes able to remove a C-terminal amino acid from the peptide stem. Two different types can be found (i) those able to cleave between two D amino acids, consequently named DD-carboxypeptidase (DDc) and (ii) those that can recognise and cleave a bond between an L- and a D- form, termed LD- or DL-carboxypeptidases (Vollmer *et al.*, 2008c). These enzymes can either be found (i) in the periplasm where they participate in the sacculus editing or (ii) in the cytosol where they have a role in the recycling. One example is the cytoplasmic protein LdcA that has for substrate the tetrapeptides, either free or linked to the anhydroMurNAc. LdcA cleaves the link between the *m*DAP^{3} and the D-Ala^{4}, releasing the latter. Additionally, it was shown in *V. cholerae* that LDc have a specificity towards classical peptide stems and their activity on NCDAA is poor (Hernandez *et al.*, 2020).

1.1.3 Recycling and signalling

In *E. coli*, up to 50 % of the murein of the cell can be renewed during a division cycle (Goodell, 1985). Partly because PG represents a pathogen-associated molecular pattern (PAMP) for the innate immune system

(Wolf *et al.*, 2018) and resource optimisation, around 95 % of fragments are recycled (Goodell, 1985). It is also noteworthy that PG fragments can act as signalling molecules for interactions between bacterial species or with the host, they have been reviewed by Irazoki and colleagues (Irazoki *et al.*, 2019). The PG recycling pathway is sharing part of its components with the Amp system, involved in the β-lactam stress signalling and resistance (Fig. 1).

Upon the degradation of the cell wall caused by a β-lactam antibiotic, many Gram-negative bacteria express a β-lactamase named AmpC (Normark *et al.*, 1994). The action of β-lactamase is to hydrolyse the ring, so the reaction with the DDt can no longer take place. The *ampC* gene expression is regulated by a transcriptional factor, AmpR, that also binds its *ampR* gene promoter both in the presence or absence of antibiotics (Lindquist *et al.*, 1989). It should be noted that this regulator is absent from the *E. coli* genome (Honore *et al.*, 1989). Under normal conditions, an intermediate of the PG synthesis pathway, the UDP-MurNAc-pentapeptide bind AmpR and the complex blocks the expression of *ampC* (Jacobs *et al.*, 1997). However, upon β-lactam stress, the cytosolic concentration of 1,6-anhydroMurNAc-peptides imported by the AmpG permease (Jacobs *et al.*, 1994; Cheng *et al.*, 2002) increases due to the catabolism of the PG. This molecule can displace the AmpR repressor and convert it into an activator of the β-lactamase expression (Jacobs *et al.*, 1997).

In the recycling pathway and as above, the result of the catabolism, the GlcNAc-anhMurNAc-peptides, are imported by AmpG back into the cytoplasm (Jacobs *et al.*, 1994; Cheng *et al.*, 2002). There, they first have to be processed by NagZ and AmpD (Fig. 1). NagZ is a β-N-

acetylglucosaminidase that cleaves the bond between the GlcNAc and the anhMurNAc (Cheng *et al.*, 2000). The former can then be reused while the latter needs to be further processed by an anhMurNAc-L-Ala amidase, AmpD, that will release the anhMurNAc on one side and the peptide stem on the other (Jacobs *et al.*, 1995). The sugar can then be modified by a serie of enzymes (not shown) to be converted into GlcNAc-6-P (Park, 2001) that can either be injected back into cell wall synthesis or glycolysis (Park, 2001; Dahl *et al.*, 2004). This allows *E. coli* to be able to grow solely on MurNAc if needed. If the radical is a pentapeptide, then it needs to be shortened to a tripeptide by a L,D-carboxypeptidase, LdcA (Templin *et al.*, 1999). It should be noted that tripeptides can also be generated in the periplasm by the consecutive activities of carboxypeptidases and amidases (Egan *et al.*, 2020). The peptides can then be transported in the cytoplasm by the Opp permease (Park, 1993). The tripeptides can further be grafted onto a UDP-MurNAc by murein peptide ligase, Mpl (Mengin-Lecreulx *et al.*, 1996b). Then, they are directly taken up by MurF for UDP-MurNAc-pentapeptide generation.

It was previously mentioned that NCDAAs can be incorporated in the PG by LDts (see section 1.1 of the introduction) and govern the stationary phase cell wall remodelling (Lam *et al.*, 2009). In addition to this mechanism, a link was made with the recycling pathway in *V. cholerae* (Hernandez *et al.*, 2020). When GlcNAc-anhMurNAc-tetrapeptides modified with NCDAAs at position four are imported, the cytosolic LDc cannot process the fourth amino acid of the stem. Consequently, D-Ala dimer cannot be added and the NCDAAs-containing stem is attached to a sugar backbone and exported to the periplasm. There, these PG subunits can only act as an acceptor for transpeptidation. Thus, the amount of 4,3 crosslinks diminishes proportionally with the increase of NCDAAs-

containing stems. In addition, the pool of canonical precursors is also downregulated by these recycled tetrapeptides. Together, these two phenomena contribute to the control of PG homeostasis.

1.1.4 Peptidoglycan as an antibiotic target

Due to its importance in the bacterial cell, the PG is an obvious antibiotic target. The most famous, Penicillin, was also the first discovered in 1928 by A. Fleming (Fleming, 1929). Penicillin is part of an important family called the β-lactam as they are based on a β-lactam ring. This family contains four subclasses: penicillin, cephalosporins, monobactams and carbapenems (Schneider *et al.*, 2010). Their mode of action is described in the above section *D,D-transpeptidases or Penicillin-binding proteins* and the mechanism of resistance, in the *Recycling and signalling* section.

Since then, other antibiotic families with different modes of action have been reported (Schneider *et al.*, 2010). Another target is the lipid II as it is the most conserved molecule of the synthesis chain and is the most targeted intermediate by several different classes of antibiotics (Breukink *et al.*, 2006). For simplicity, only one example will be mentioned: the glycopeptide antibiotic Vancomycin. It binds to the D-Ala dimer of the immature PG subunit. This prevents crosslink formation and significantly weakens the PG network. However, resistance emerged by modifying the fifth amino acid as in *Staphylococcus aureus*, with a D-lactate that prevents binding of Vancomycin (McGuinness *et al.*, 2017). Additional targets can also be noted in the cytoplasmic steps, for instance, fosfomycin inhibits MurA that converts UDP-GlcNAc into UDP-MurNAc (Kahan *et al.*, 1974). The D-Ala racemase can also be targeted by D-cycloserine, an analogue of D-Ala (Lynch *et al.*, 1966).

1.2 The outer membrane

The OM is an asymmetrical bilayer with an outer leaflet mostly composed of lipopolysaccharides (LPS) and an inner leaflet made of phospholipids. It acts as a permeability barrier to keep harmful components outside of the bacterium and to import nutrients. Two types of OM proteins (OMPs) can be found, integral OMPs that are embedded and face both sides and lipoproteins that are anchored by acyls chains either in the inner or outer leaflet, consequently facing one of the two sides. It should be noted that, albeit it has been long believed that the PG is responsible for the mechanical properties and the stiffness of the envelope (Holtje, 1998), the OM itself has a major stress-bearing capacity (Rojas *et al.*, 2018). Rojas and colleagues showed that the OM resistance is multi-factorial. Its stability and stiffness can be altered by preventing the stabilising ionic interactions between bivalent cations and LPS charges, LPS export, changes in its structure (*i.e.* the O chain) or the presence of OMPs such as OmpA.

1.2.1 Outer membrane proteins

1.2.1.1 Lipoproteins

1.2.1.1.1 Lpp and general structure

In 1969, Braun and Rehn observed a residual lysine on every tenth PG subunit after trypsin digestion (Braun *et al.*, 1969). The authors inferred that this residue was left from a bound protein but also that the latter was probably covalently linked to a complex lipid. In addition, based on ultrathin sections, they already proposed that this protein was playing a major role in the cell wall structure. Due to its dual nature, the authors proposed the name of lipoprotein. Importantly, this lipoprotein was the very first identified of its family and remained to only one reported for at

least ten years (Hayashi *et al.*, 1990). Consequently, Braun's lipoprotein was also known as the lipoprotein or Lpp.

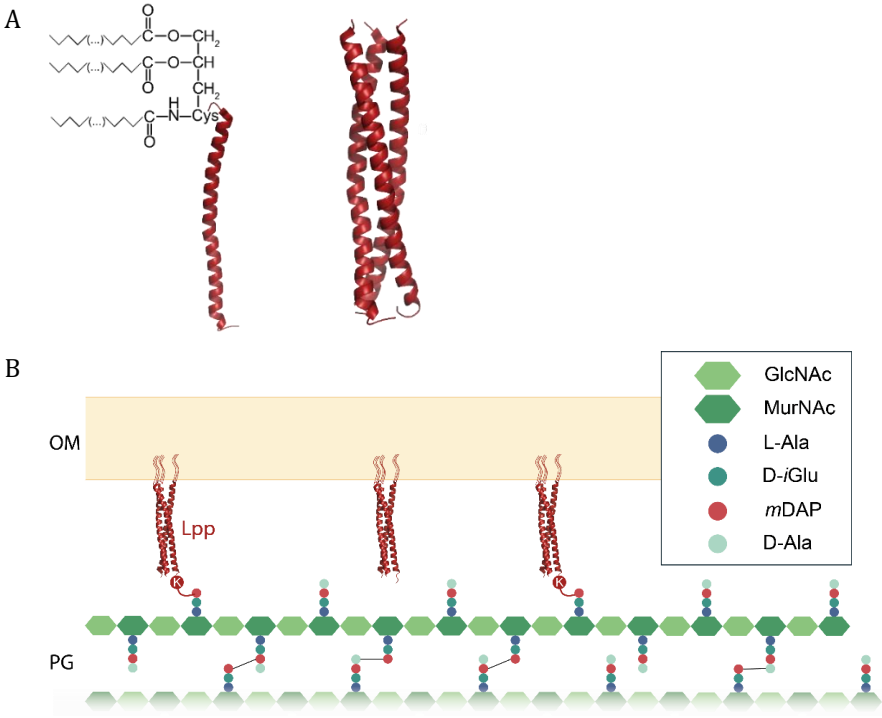

Figure 4 | Structure of Lpp and linkage between the OM and the PG. A. Left, the monomeric structure of mature Lpp (the C1 and K58 are not shown, PDB entry 1EQ7) at 1.9 ångström resolution from X-Ray diffraction. The first cysteine was added as well as the acyl chain and the diacylglyceryl. Right, trimeric Lpp forms an α-helical coiled-coil (PDB entry 1EQ7). **B.** Lpp is embedded in the OM by three acyl chains and can be covalently linked to the *m*DAP of the PG by its C-terminal lysine. Cys, cysteine; OM, outer membrane; PG, peptidoglycan, K, lysine; Ala, alanine; Glu, glutamate; *m*DAP, diaminopimelic acid; GlcNAc, N-acetylglucosamine; MurNAc, N-acetylmuramic acid.

Although the amino acids composition of Lpp was already known, its sequence was published in 1972 (Braun *et al.*, 1972). This study has also shown that the PG subunit was linked through the ε carbon of the C-terminal lysine lateral chain. Regarding the lipid, it was found attached to

the N-terminal end of the lipoprotein. The structure of the lipid was then solved a year later, in 1973 (Hantke *et al.*, 1973). The lipid anchor consists of a diglyceride attached to the cysteine lateral chain by a sulphide bond and an additional fatty acid attached to the N-terminal amino group (Fig. 4A, left). The primary structure of Lpp is an α-helix and has three domains: an N-terminal cap motif (*i.e.* the first amino acid of the helix), a coiled-coil domain and a C-terminal hydrophobic part. The coiled-coil portion is made of three monomers that interact together (Fig. 4A, right).

In *E. coli*, Lpp is the most abundant protein with around one million copies per cell (Braun, 1975; Li *et al.*, 2014). To achieve such a number, Lpp has a highly stable mRNA with a half-life of around 12 minutes (Hirashima *et al.*, 1973) and can represent up to 10 % of all mRNA (Li *et al.*, 2014). Despite the importance of Lpp suggested by its copy number, the coding sequence is not essential. Lpp mutant does not have any survival issues or major defects (Hirota *et al.*, 1977). However, the OM is destabilised and OM vesicles (OMVs or belbs) can be observed at the surface (Suzuki *et al.*, 1978b). These observations were accompanied by the detection of periplasmic proteins in the culture supernatant, suggesting an altered permeability of the OM (Hirota *et al.*, 1977). Nevertheless, mutant cells show higher sensitivity to envelope stresses such as detergents (*i.e.* SDS or sodium deoxycholate) or OM destabilisation with a chelating agent, EDTA (Hirota *et al.*, 1977). Of note, the linkage of Lpp to the PG can be prevented by simply removing the C-terminal lysine (Zhang *et al.*, 1992; Cowles *et al.*, 2011) and such mutation results in the same effects as the deletion of the whole Lpp gene (Asmar *et al.*, 2017).

In the OM, Lpp exists in linked or free states (Fig. 4B) that represent about one-third and two-thirds of the total pool, respectively (Inouye *et al.*, 1972). Of the two, the linked form is the best understood and its involvement in envelope stability has been briefly described above. However, Lpp has an additional, indirect role; it ensures the distance between the OM and the IM (Asmar *et al.*, 2017). Asmar and colleagues could increase the periplasm size by 3 or 4 nm by adding 14 or 21 amino acids to the sequence, respectively. Increasing the distance between the two membranes had direct consequences as it was found that the OM stress sensor, RcsF, was physically unable to interact with its partner in the IM. Accordingly to this observation, Lpp length is well conserved across γ-proteobacteria (Asmar *et al.*, 2018) highlighting its relevance.

On the contrary, the exact role of the free Lpp remains ambiguous. Although one straightforward explanation would be that the free pool can act as a reserve. Indeed, it is known that *E. coli* increases its amount of bound Lpp by 70 % when entering into stationary phase (Glauner *et al.*, 1988b) and having readily available copies could be convenient. Moreover, one could speculate that tighter bonds between the OM and the PG might be needed to face some stresses, although this still needs to be validated. An additional layer of complexity was added when a study (Cowles *et al.*, 2011) showed that the two forms occupy different subcellular compartments. While the N-terminal part of free Lpp is also present in the periplasm, the C-terminal end is surface-exposed. How the free Lpp is transported to the outer environment still requires further investigation.

Until the beginning of 2021, it was still unclear how the covalent bond of Lpp could be reversed. However, two studies (Bahadur *et al.*, 2021;

Winkle *et al.*, 2021a), concomitantly showed that the previously mentioned LdtF was an amidase rather than an LDt. Therefore, LdtF was proposed to be renamed DpaA (for *meso*-diaminopimelic acid protein amidase A) (Winkle *et al.*, 2021b). In addition to DpaA activity on the PG-Lpp link, it was also demonstrated to have an L,D-carboxypeptidase function that allows the enzyme to cleave the *m*DAP^3 and the D-Gly^4 linkages (Bahadur *et al.*, 2021). Interestingly, the DpaA sequence has a YkuD domain (see section 1.1.2.1.1 of the introduction) but it lacks an arginine in position two after the catalytic cysteine (Frirdich *et al.*, 2014; Kim *et al.*, 2015), substituted with alanine or asparagine (Bahadur *et al.*, 2021; Winkle *et al.*, 2021b). This highlights how similar two enzymes sequences can be, yet still have different activities with only a few residues difference. The dynamic and the regulation of Lpp linkage remains to be clarified. Indeed, it is still not known how the number of bound Lpp is determined. It could simply be a passive mechanism where the amount of PG peptide stems available dictates the amount of bound Lpp. Another hypothesis could be that the interplay between the LdtABC and DpaA activities and/or their expression regulates the anchorage. Further study of DpaA will certainly bring further insight into this mechanism.

1.2.1.1.2 The export of lipoproteins

The maturation and the export of lipoproteins to the OM happen in two main stages and are depicted in Fig. 5. Lipoproteins are first produced with an N-terminal signal peptide that ends with a lipobox from the site -3 to +1 relative to the signal peptidase cleavage site. After sequence alignment of several subsequently discovered lipoproteins, the consensus sequence was found to be L-A/S-G/A-C with some variation in the second and third position but with an invariable cysteine across

proteobacteria (Braun *et al.*, 1994; Narita *et al.*, 2007). Lipoproteins are then exported unfolded by the secretory (Sec) system (Crane *et al.*, 2017) although a few of them can be already be folded and thus take the twin-arginine translocation (TAT) system (Palmer *et al.*, 2012). Once in the periplasm, the pro-lipoproteins remain anchored to the IM and will be sequentially processed by three IM proteins (IMPs); Lgt, LspA and Lnt. The first step is to add a diacylglyceryl to the sulfhydryl group of the +1 cysteine and this is achieved by the diacylglyceryl transferase, Lgt (Gan *et al.*, 1993). The diacylated protein is then passed to the signal peptidase II, LspA (Yu *et al.*, 1984), which will remove the peptide anchor. Finally, the last acyl chain is added to the apolipoprotein by Lnt (Rogers *et al.*, 1991; Gupta *et al.*, 1993), an N-acyltransferase, on the N-termini of the +1 cysteine, resulting in a tri-acylated protein. The three enzymes are broadly conserved across Gram-negative bacteria and although all three are essential in *E. coli*, some species, such as *Francisella tularensis* and *Neisseria gonorrhoeae*, can grow without Lnt (LoVullo *et al.*, 2015). In *E. coli*, such a mutant would accumulate Lpp in its IM, wrong PG linking would be made and result in lysis (Robichon *et al.*, 2005). This finding challenges the lipoprotein maturation paradigm and suggests that the final acylation might be dispensable and that the protein export system can still accommodate di-acylated apolipoproteins.

The transport of lipoproteins to the OM is then completed by the localisation of lipoproteins (Lol) pathway. This system is composed of five proteins, LolA-E, with a periplasmic soluble chaperone, LolA (Matsuyama *et al.*, 1995), the OM lipoprotein LolB (Matsuyama *et al.*, 1997) and LolCDE, an ATP-binding cassette (ABC) transporter of the IM composed of two similar proteins, LolC and LolE embedded into the IM and the dimeric ATP-hydrolysing LolD (Yakushi *et al.*, 2000). The first

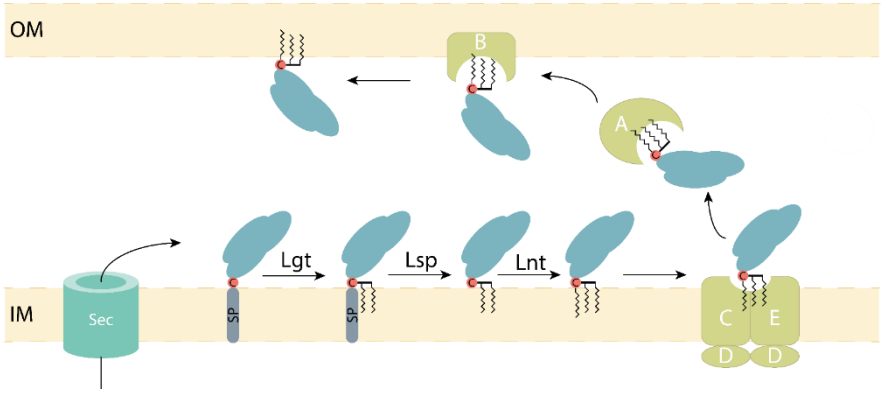

Figure 3 | Export and maturation of lipoproteins. The proteins are synthesised in the cytoplasm before being exported to the periplasm by the Sec or the twin-arginine system (not shown). There, it is embedded in the IM by the signal peptide and the preprolipoprotein can first be processed by Lgt, a dicyglyceryl transferase. The cysteine +1 (in orange) is the protein residue that gets lipidated. The prolipoprotein is then processed by Lsp, the lipoprotein signal peptidase, that cleaves off the signal peptide. Lnt, the lipoprotein acyl transferase, catalyse the addition of the last acyl chain to the amino group of the cysteine. The lipoprotein can be targeted to the IM or be further exported to the OM. In the latter case, this is ensured by the Lol system that is composed of an ABC transporter (LolC, LolD and LolE), a periplasmic carrier (LolA), and an OM receptor protein (LolB). The lipoprotein is first extracted from the IM by LolCDE upon ATP hydrolysis and then transported to the OM by a mouth-to-mouth mechanism. OM, outer membrane; IM, inner membrane; Sec, secretory pathway; SP, signal peptide.

step of the transport is the extraction of the newly acylated protein from the IM. Although LolC and LolE have a similar structure, their roles are distinct; LolE first accommodates the lipoprotein through its hydrophobic cavity then, the lipoprotein is passed on to LolC (Okuda *et al.*, 2009; Kaplan *et al.*, 2018). Despite the structural similarity between LolC and LolE, only the former can interact with LolA (Okuda *et al.*, 2009; Kaplan *et al.*, 2018). It was initially thought that ATP hydrolysis was necessary to transfer the lipoprotein from LolC to LolA (Yakushi *et al.*, 1998) but a more recent study has found that LolA interaction with LolC was independent of ATP (Kaplan *et al.*, 2018). The binding of ATP induces, conformation changes that close the channel and, upon hydrolysis,

further conformational changes allow the transfer of the lipoprotein to LolA (Tang *et al.*, 2021). In *E. coli*, a fully mature lipoprotein (*i.e.* tri-acylated) is required for strong interaction with LolCDE (Gupta *et al.*, 1993; Narita *et al.*, 2007). From LolC, the lipoprotein is then transferred to LolA which forms an incomplete β-barrel thus, creating a hydrophobic pocket to fit the acyl chains (Takeda *et al.*, 2003). However, if this pocket can fit one to three chains is still subject to debate (El Rayes *et al.*, 2021). The protein is then moved by a mouth-to-mouth interaction from the hydrophobic cavity of LolA to the one of LolB (Okuda *et al.*, 2009) by a greater affinity of the latter (Taniguchi *et al.*, 2005). LolB then proceeds to the insertion into the OM (Matsuyama *et al.*, 1997; Tanaka *et al.*, 2001) by a yet unknown mechanism.

As some lipoproteins are meant to stay in the IM, a way to bypass the Lol pathway has emerged in *E. coli*: the Lol avoidance signal. The single substitution of the +2 amino acid, a serine, by an aspartate is sufficient to keep the lipoproteins in the IM (Yamaguchi *et al.*, 1988; Hara *et al.*, 2003). More than the lateral chain, it is the position of the negative charge that is important to avoid the Lol pathway by its interaction with the IM phospholipid, phosphatidylethanolamine (PE) (Hara *et al.*, 2003). In addition, the +3 position could play an additional role; the presence of an aspartate, glutamate or glutamine enhances the retention in the IM (Terada *et al.*, 2001). Although the +2 rule is conserved in several species of the *Enterobacteriaceae*, the avoidance signal could widely vary across bacteria. For instance, *Pseudomonas aeruginosa* rather has a lysine and a serine at positions 3 and 4 respectively that allow avoiding the export in the OM (Narita *et al.*, 2007; Lewenza *et al.*, 2008). *Borrelia burgdorferi* lacks a classical signal and, if no protein-specific retention signal is present, the proteins are exported to the outer leaflet of the OM by default

(Schulze *et al.*, 2006). Similarly, *Yersinia pestis* lipoprotein mutations at sites +2 and +3 do not affect their localisation which is instead dependent on an intact N-terminal region, from residue 1 to 61 (Silva-Herzog *et al.*, 2008). Likewise, the entire Lol system is not conserved across all proteobacteria. While LolA is well conserved, LolB can only be found in β- and γ-proteobacteria (Okuda *et al.*, 2011). This suggests the presence of either a bi-functional LolA or another system for the transfer of lipoprotein to the OM. Furthermore, only a small subset of bacteria, close to *E. coli* (Fig. 6), are encoding LolC and LolE, the others having a hybrid protein called LolF (LoVullo *et al.*, 2015). Because Lnt can be deleted in these bacteria, it was suggested that LolF, in contrast to LolCE of *E. coli*, could recognise both di- and tri-acylated lipoproteins (LoVullo *et al.*, 2015). In line with this, *Wolbachia* has a LolF based pathway and does not encode any Lnt homologue naturally (Turner *et al.*, 2009).

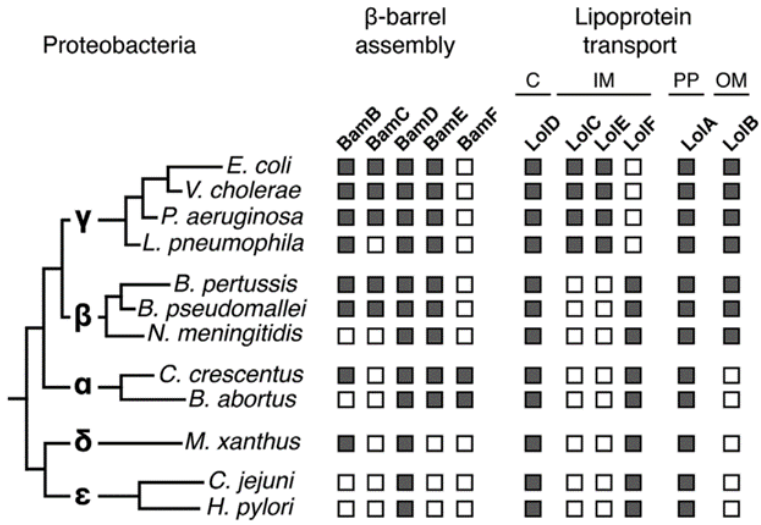

Figure 4 | Conservation of the OMP export system across proteobacteria. BamD, LolA and LolD and LptE are the only proteins conserved across all proteobacteria represented here. Full square means that a homolog protein can be found, and conversely, an empty square indicates an absence. Modified from (Grabowicz, 2018).

1.2.1.2 β-barrel proteins

1.2.1.2.1 General structure

Although OMPs are embedded in the membrane as IM proteins, their topology is completely different. Indeed, while IM proteins are mainly composed of transmembrane α helices, OMPs are composed of an even number of antiparallel β-strands arranged in a single β-sheet. The number of strands can greatly vary from 8 for OmpX (Vogt *et al.*, 1999) to bigger barrels with the type 9 secretion system translocon SprA and its 36 strands (Lauber *et al.*, 2018). The first and last strand of β-barrels can interact together by the mean of hydrogen bonds to form the seam (Konovalova *et al.*, 2017). These interactions close the sheet and form the cylinder or barrel, hence the general name of β-barrels for OMPs. Thus, the top of the barrel is in contact with the environment while the bottom is in contact with the periplasm but both the N- and C-termini are found in the periplasm (Schulz, 2002). The amino acids in between two β-strands form a loop and the ones on the bacterium surface are usually bigger than those spanning in the periplasm (Schulz, 2002). In addition, the variability observed in the loops is much higher than in the sheets (Schulz, 2002). On an amino acid sequence level, the strands are composed of alternating hydrophobic and polar amino acids (Gromiha *et al.*, 1995). In the final three dimensional structure, they are arranged in such a way that polar residues are orientated inwards the barrel while non-polar lateral chains are presented on the exterior. This allows the solutes to pass through the channel if large enough (see next paragraph)

while the barrel can be inserted within the membrane, that has a hydrophilic core. In the OM, the β-barrels can then stay monomeric or associate with others to form di- or trimers. Different families of OMPs were also established based on their function: (i) general porins, (ii) passive transporters, (iii) active transporters, (iv) enzymes, (v) defensive proteins and (vi) structural proteins (Koebnik *et al.*, 2000; Gromiha *et al.*, 2007).

In *E. coli*, several β-barrels have been described. OmpA is the most abundant with 207,000 copies per cell (Li *et al.*, 2014). Some have reported that it forms a 16-stranded β-barrel and would thus have a pore large enough to ensure the transport of polypeptides (Stathopoulos, 1996). Supporting this model, OmpA allows non-specific diffusion of low permeability in proteoliposomes (Sugawara *et al.*, 1992). However, other studies reported a two domains conformation with an N-terminal 8-stranded β-barrel (Pautsch *et al.*, 1998) and a C-terminal globular periplasmic domain (De Mot *et al.*, 1994). In this conformation, the pore is too small for the protein to act as a porin. In addition, the globular domain can bind the PG in a non-covalent manner (Samsudin *et al.*, 2016; Samsudin *et al.*, 2017). Together with Lpp, they could thus help to correctly structure the interactions between the OM and the PG. With the OmpA homolog of *Acinetobacter baumanii*, this interaction was shown to be mediated by a pentapeptide (Park *et al.*, 2012). Moreover, OmpA has been reported to form a homo-dimer in the OM (Stenberg *et al.*, 2005). Despite several decades of studies, the conformation adopted by OmpA is still up to debate and requires further investigation.

Along OmpA, more classical β-barrels can be found, namely OmpC and OmpF. These porins are found with around 163,000 and 89,000 copies

per cell respectively in standard conditions (Li *et al.*, 2014), share 60 % identity and both form trimeric structures (Basle *et al.*, 2006; Yamashita *et al.*, 2008). As porins, they passively let through small solutes with a 600 Da cut-off at a rate that depends on the physicochemical characteristics of both the OMP and the solutes (Nikaido, 1992). The channels have an hourglass shape due to a constriction zone that is made by an extracellular loop (L3) that folds inwards. This allows a stronger selective permeability of the porins (Vergalli *et al.*, 2019).

1.2.1.2.2 The assembly of β-barrels

Even though some aspects remain to be clarified, the assembly of OMPs is now fairly well understood and was recently reviewed (Tomasek *et al.*, 2021). After the synthesis of the protein, the unfolded version is exported to the periplasm through the Sec translocon system (Chaturvedi *et al.*, 2017). There, the protein is maintained unfolded by two chaperones, Skp and SurA, to prevent any misfolding (Chen *et al.*, 1996; Denoncin *et al.*, 2012) and its signal peptide is cleaved. Last but not least, the protein must then be folded and inserted into the membrane and this is performed by the β-barrel assembly machinery (Bam). It is composed of five proteins, BamA, a β-barrel protein and the key component of the system, and four lipoproteins, BamB, BamC, BamD and BamE (Fig. 7A).

In addition to its transmembrane domain, BamA also possesses five N-terminal periplasmic polypeptides transport-associated (POTRA) domains. These soluble domains mediate the interactions with the other Bam proteins. Of the BAM system, only BamA and BamD (Malinverni *et al.*, 2006) are essential and the former was shown to be sufficient for the OMP folding process *in vitro* (Plummer *et al.*, 2015). In addition, it was also reported that a simple substitution in BamA can even bypass the

essentiality of BamD (Hart *et al.*, 2020a; Hart *et al.*, 2020b). This supports the idea that lipoproteins only have a regulatory role and help to optimise the procedure efficiency (Hagan *et al.*, 2010).

Initially, two models were proposed for the folding mechanism: the assisted or the budding model. However, recent studies have brought more evidence in favour of the budding mechanism (see (Tomasek *et al.*, 2021) for more details). In this model (Fig. 7B), BamA exists in two conformational states (Noinaj *et al.*, 2013), open and closed and this could be modulated by BamD (Lee *et al.*, 2018). First, the C-terminus of the OMP is then bound to the BamA N-terminal β-strand by hydrogen bonds (Lee *et al.*, 2019) then, the rest of the protein is assembled inside and stabilised by the interior wall of BamA. Once enough of the OMP β-sheet has been folded, it can bud into the membrane through the seam of BamA as it is in the open conformation. Finally, the initial interactions between the C- and N-termini of the OMP and BamA respectively are exchanged to the profit of the OMP N-terminus that results in the closure of the latter. The OMP is now inserted in the membrane and can, if needed, form oligomers although this mechanism still needs to be deciphered.

A

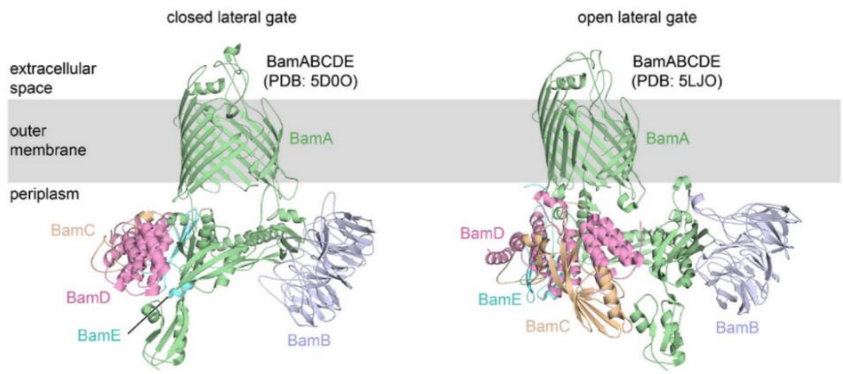

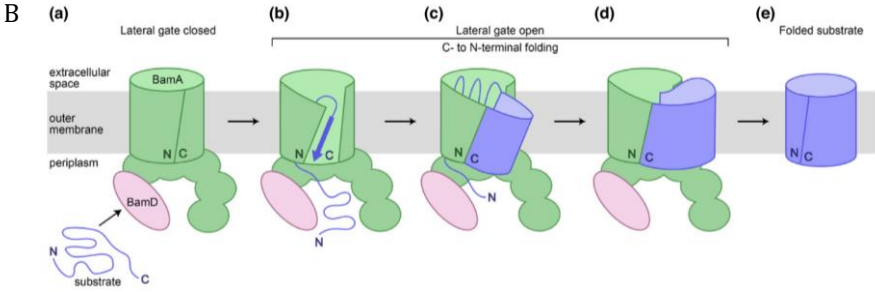

Figure 7 | The BAM assembly system. A. Structure of the BamABCDE complex shown with BamA with lateral gate open (PDB 5D0O) or closed (PDB 5LJO). **B.** The budding model. (a) Following the recruitment of the substrate protein, (b) the seam is opened and the C-terminal end of the unfolded protein can interact with the N-terminal end of BamD. (c) The β-sheet is progressively formed within BamD until (d) completion and insertion into the outer membrane. (e) The final step of the β-barrel formation is the exchange of hydrogen bonds between the BamD and the protein N-terminal end. Only BamA and BamD are shown for simplicity purposes. Adapted from (Tomasek et al., 2021).

2 *Brucella abortus*

2.1 History

In 1886, Malta was under the protectorate of the British Crown and, as such, a garrison is stationed there. Each year, part of the unit is incapacitated by what was called the Malta Fever‡. Consequently, Major-General Sir David Bruce, part of the army medical service, was asked to investigate to undertake this issue. During the *post-mortem* examination, he noticed an enlargement of the spleen and other organs, which – as he highlighted – was similar to other micro-organismal diseases. Proceeding

‡ Depending on the geographical region, the disease took various name. Among them; the rock fever of Gibraltar, the Neapolitan fever of Naples, the country fever of Constantinople, the new fever of Crete, the gastric fever or again the Bang's disease.

to a microscopic examination of the spleen, he identified a Gram-negative micro-coccus. In his notes, he then established its relation to the disease and reported the ability to cultivate the micro-organism *in vitro* (Bruce, 1887). Due to its form and origin, it was first named *Micrococcus melitensis* (*i.e.* the micrococcus of Malta) but then renamed *Brucella melitensis* in Sir Bruce's honour (Meyer *et al.*, 1920). It was later found in 1905, by a Maltese scientist, T. Zammit, that goat milk was the source of disease for human beings (Zammit, 1905).

In 1897 the Danish veterinary Bernhard Bang investigated abortion in cattle and discovered what he named *Bacillus abortus* (Bang, 1897). However, in 1920, a study concluded that both organisms could be discriminated neither morphologically nor biochemically, concluding that both are from the same genus (Evans, 1918; Meyer *et al.*, 1920). Due to the two forms observed (*i.e.* coccoid and rod shapes), it was also proposed to term these bacteria as *coccobacillus*.

Indirect evidence suggests that the relationship between humans and *Brucella* might be as old as 2.5 million years. Paleontological examination of *Australopithecus africanus* partial skeleton revealed that lesions observed on the lumbar vertebrae might be the outcome of brucellosis (D'Anastasio *et al.*, 2009). Hence, linking raw meat consumption to this species of hominid. While Hippocrates describes a disease similar to brucellosis in 400 B.C. already (Cutler *et al.*, 2005; Pappas *et al.*, 2008), the next piece of evidence for *Brucella* presence dates back from 79 of our era. Adult skeletons found buried below volcanic mud – due to Mount Vesuvius eruption that year – showed brucellosis characteristic bones lesions. Furthermore, microscopic analysis of a carbonised cheese piece revealed the presence of bacteria with morphology consistent with

Brucella (Capasso, 2002). However, the oldest case of brucellosis supported by molecular evidence dates back from the middle age, in Albania (Mutolo *et al.*, 2012).

2.2 The *Brucella* genus

Since its first characterisation more than a hundred years ago, the *Brucella* genus has been in continuous expansion with now 21 species (Moreno, 2021). Following the two first species described, other species were discovered and named accordingly to their host. *B. suis* was described in 1914 (Traum, 1914) in pigs, then, *B. ovis* in 1953 in sheep (Buddle *et al.*, 1953), *B. neotomae* in 1957 in the desert woodrat (Stoenner *et al.*, 1957) and *B. canis* in 1968 in dogs (Carmichael *et al.*, 1968). Later, four other main classical species were reported subsequently; *B. pinnipedialis* (Ross *et al.*, 1994), *B. ceti* (Ewalt *et al.*, 1994), *B. microti* (Scholz *et al.*, 2008) and *B. papionis* (Schlabritz-Loutsevitch *et al.*, 2009) infecting respectively seals, cetaceans (including dolphins, porpoises and whales), voles and baboons. The classical category (Fig. 8) was determined based on the close genomic identity compared to *B. melitensis* 16M (>99 %) while non-classical species exhibits a lower identity around 97 % (Guzman-Verri *et al.*, 2019; Suarez-Esquivel *et al.*, 2020). The non-classical species have a broader range of hosts with species isolated from foxes (Hofer *et al.*, 2012), frogs (Eisenberg *et al.*, 2012) or even fish (Eisenberg *et al.*, 2017).

Brucella closest relatives are the members of the *Ochrobactrum* genus that form together the *Brucellacae* family. In 1990, the latter was identified as part of the alphaproteobacteria (Moreno *et al.*, 1990). This class regroups bacteria with diverse lifestyles, from environmental bacteria (*e.g. Caulobacter crescentus*), plant symbionts or pathogens (*e.g.*

Sinorhizobium meliloti and *A. tumefaciens* respectively) to animal pathogens with *Bartonella bacilliformis* and *Brucella*. The latter is a monophylogenetic group. Although all species have their preferential host, a few of them can successfully infect humans, hence causing human brucellosis. Only *B. melitensis*, *B. abortus* and *B. suis* have a high zoonotic potential while the other species only have a low (*e.g. B. ovis*) to null transmission to humans (Table 1).

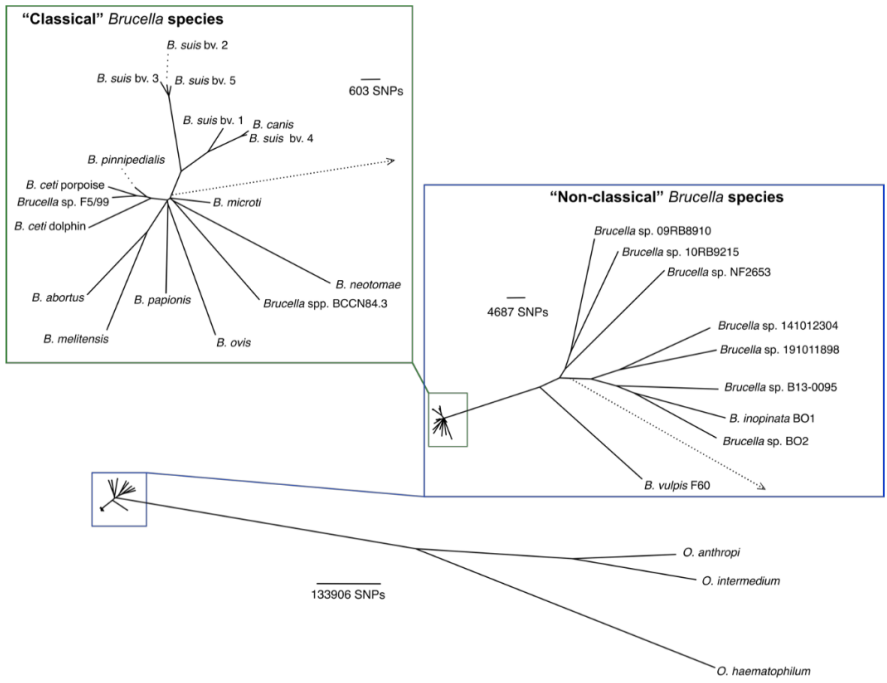

Figur**e 8 | Phylogeny of *Brucella*.** The relationship between *Ochrobactrum* (the closest species to *Brucella*) and the classical (green square) and non-classical (blue square) species of *Brucella*. The dotted arrow lines represent the branch linked to the rest of the tree. From (Suarez-Esquivel et al., 2020).

Species	Host preference	Virulence
Brucella melitensis	Sheep, goat	High
Brucella abortus	Cattle	Moderate
Brucella suis	Pig	Moderate
Brucella canis	Dog	Mild
Brucella ceti	Cetacea	Not reported
Brucella pinnipedialis	Seal	Not reported
Brucella ovis	Sheep	Not reported
Brucella neotomae	Desert woodrat	Not reported
Brucella microti	Common vole	Not reported
Brucella papionis	Baboon	Not reported
Brucella inopinata	Unknown	Not reported

Table 1 | *Brucella* species, host preferences and virulence to humans.

2.3 *Brucella* intracellular cycle

In the course of the natural infection, *Brucella* is mainly found in trophoblastic cells, part of the placental tissue (Anderson *et al.*, 1986). This has been suggested to be the result of a preference for erythritol, a C4 sugar mainly found in the placenta of infected animals (Anderson *et al.*, 1965). Additionally, *Brucella* can also invade professional phagocytes which allow using a variety of cell lines such as HeLa human epithelial cells (Pizarro-Cerda *et al.*, 1998a), JEG-3 human trophoblasts (Salcedo *et al.*, 2013) or RAW264.7 and J774A.1 murine macrophages (Arenas *et al.*, 2000; Starr *et al.*, 2008) to name only a few. These have been useful tools to understand the intracellular trafficking of the bacterium. *Brucella* intracellular cycle will be briefly discussed below and is depicted in Figure 9.

After entry by phagocytosis, *Brucella* is found in a phagosome named *Brucella*-containing vacuole (BCV) that will be subsequently modified. The first interactions will be with the early endosomal pathway that leads

to the acquisition of markers such as EEA-1 (Pizarro-Cerda *et al.*, 1998a; Chaves-Olarte *et al.*, 2002; Celli *et al.*, 2003). Then, consistently with the late endocytic pathway, the eBCV (endosomal BCV) presents markers such as LAMP1 (Pizarro-Cerda *et al.*, 1998a). Although lysosomal markers are present, lysosome fusion with the eBCV was never shown, suggesting that *Brucella* can avoid it and that interactions are only transient (Pizarro-Cerda *et al.*, 1998a; Pizarro-Cerda *et al.*, 1998b; Comerci *et al.*, 2001). Furthermore, these lysosomal interactions were shown to be crucial for the following steps of the intracellular cycle (Starr *et al.*, 2008). The type IV secretion system (T4SS) of *Brucella* was proposed to mediate the transition from eBCV to replicative BCV (rBCV), which harbours markers of the endoplasmic reticulum (Comerci *et al.*, 2001). Expression of *virB*, the operon encoding the T4SS, requires the BCV acidification, which is necessary for normal traffic (Porte *et al.*, 1999; Boschiroli *et al.*, 2002). In HeLa cells, the endosomal stage of the traffic occurs during the first 8 to 12 hours after the entry. During the first hours of this stage of the traffic, bacteria do not grow and do not initiate the replication of their chromosomes (Deghelt *et al.*, 2014). At the end of the eBCV stage, growth and chromosomes replication are resumed and daughter cells are generated once in the rBCV (Deghelt *et al.*, 2014).

During the eBCV to rBCV transition, the T4SS plays its essential role by delivering effectors, outside of the BCV, that will allow the hijacking of vesicles coming from the endoplasmic reticulum (ER)-to-Golgi intermediate compartment (ERGIC). Following interactions with the ER exit sites (ERES), the rBCV is now formed and *Brucella* can begin its replication that occurs between 12 to 24h after phagocytosis (Pizarro-Cerda *et al.*, 1998a; Celli *et al.*, 2003; Celli *et al.*, 2005). The last step is the conversion of the rBCV to an autophagic BCV (aBCV) and it also involves

the T4SS (Smith *et al.*, 2016). However, it is thought that an alternative pathway to classical autophagy is used as only some actors are needed (Starr *et al.*, 2012). Once the aBCV is formed, *Brucella* can then exit the cell and starts the infection cycle again.

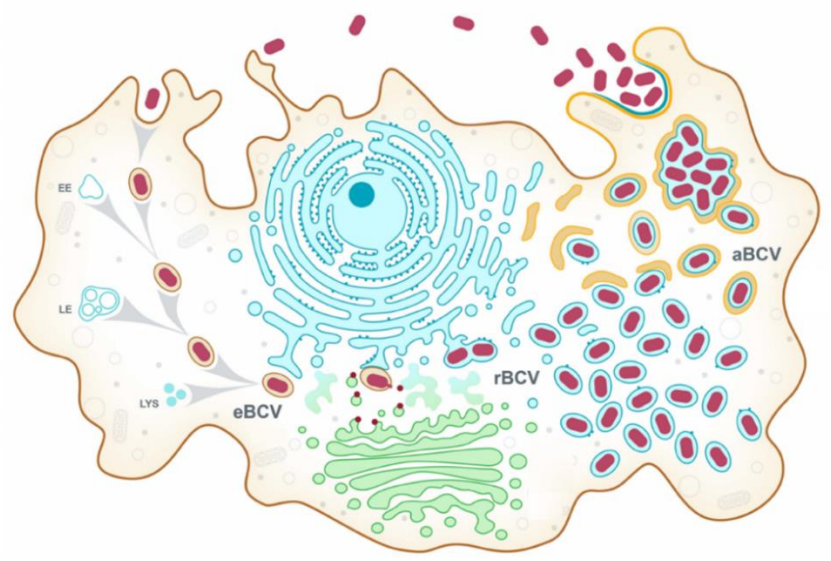

Figure 9 | The intracellular cycle of *Brucella*. Upon the entry by phagocytosis, *Brucella* is found in a BCV that will subsequently interact with early and late endosomes (EE and LE) as well as transiently with lysosomes (LYS) to form the eBCV. Following sustained interaction with the ERGIC, the rBCV is formed and allow *Brucella* replication. Then, spreading outside of the host cell is mediated by subversion of the autophagy pathway and the formation of the aBCV. Modified from (Celli, 2019)

2.4 Peculiarities of *Brucella*

2.4.1 Growth

E. coli, and most rod-shaped bacteria, have a dispersed mode of growth as new envelope material is inserted laterally. Once the bacterium has about doubled in size, the growth is re-localised to the mid-cell and the septation process begins until the cell divides (Typas *et al.*, 2012). This mode of growth principally relies on the MreBCD proteins for the

elongasome and FtsZ for the divisome. Other bacteria have evolved with a different strategy and incorporate new envelope material at the poles, such as *Corynebacterium*, part of the Actinomycetales that elongates from both poles (Daniel *et al.*, 2003).

A common feature of the Rhizobiales is that the growth is zonal and localised at one pole (Brown *et al.*, 2012). This means that upon division, a mother and a daughter cell are generated and each contains a new and an old pole. Consequently, ageing OM material is accumulated in the mother cell. This can be easily visualised by the use of Texas Red-X Succinimidyl Ester (TRSE) that stains surface proteins. In the case of *E. coli*, the signal is gradually dissipated while for *A. tumefaciens* or *B. abortus*, the signal stays on the precursor bacterium while newly generated bacteria are label-free (Fig. 10). This feature could be one advantage of this growth mode as potentially damaged material would stay in the mother cell. Other studies have already shown that division is asymmetrical and underlies a cell ageing that comes with diminished growth, reproduction and an increased death rate (Stewart *et al.*, 2005; Lindner *et al.*, 2008). The polar growth could also help the bacterium to adapt faster to its environment (Kysela *et al.*, 2013). Indeed, in the case of a phase variation event, segregating the older version of the surface exposed molecule could give an advantage to the daughter cell, especially in the case of pathogens.

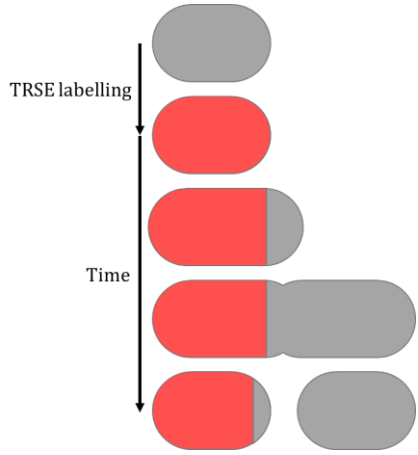

Figure 10 | Polar growth. The schematic represents a polar growing bacterium. Labelling with TRSE allows visualising the pre-existing material as it stays immobile on the outer membrane. Upon growth, new unstained material is added to the new pole (Brown *et al.*, 2012). As new material is also inserted at the constriction site, the mother bacterium has its new pole partially unlabelled.

2.4.2 Peptidoglycan

As for the growth, the most in-depth study of Rhizobiales PG was performed on *A. tumefaciens* (Brown *et al.*, 2012) and this section will thus discuss its features. Expectedly, the composition of the peptide stem is the same as in *E. coli* (see section 1.1 of the introduction). However, *A. tumefaciens* HPLC profile of muramidase-digested PG was found to be more complex than previously reported in other Gram-negative bacteria. Upon the analysis, several differences to *E. coli* were noted. The most interesting in the context of this study is the absence of peptide scar on muropeptides that would suggest a covalently bound lipoprotein, such as Lpp. This could be due to the protease used, a different anchorage system or simply, the absence of attachment. With up to 65 % of all peptide stems engaged into peptide bridge, the crosslinking of the PG is also higher compared to *E. coli*. In addition, around 50 % of these links are between two *m*DAP hence contrasting with the 10 % in *E. coli*. Interestingly, this

higher proportion correlates with a high number of LDts. Fourteen putative LDts were identified in *A. tumefaciens* by *in silico* analysis (Cameron *et al.*, 2014). Comparison with *E. coli* LDts revealed that homology could only be found for LdtB (YbiS) and LdtD (YcbB), with respectively eight and four coding sequences. Because of the higher proportion of 3-3 crosslinks, the high number of LdtD homologs makes sense. However, and quite unexpectedly, the most represented is LdtB, which attaches Lpp C-terminal lysine to the PG. Due to the probable absence of Lpp, this could be due to the similarity between LDts involved in 3-3 crosslink and Lpp anchorage. Of note, two more homologies were found with LdtF that is now described as DpaA and therefore should be considered aside. Efforts were made to localise these LDts in *Agrobacterium* (Cameron *et al.*, 2014). One LDt (Atu0845) exhibited a marked localisation at the growth pole while three others (Atu0669, 2133 and 3332) seemed to localise at the mid-cell during division and one (Atu1164) had a heterogeneous localisation. This, most likely, is the result of distinct spatiotemporal functions.

Another difference was noticed at the end of the sugar strands; they are usually terminated by anhydro-MurNAc (Vollmer *et al.*, 2008b) characterised by an intramolecular ring between the C6 and C1. Consequently, the chains could either be terminated by a different mechanism or could be especially long, with a suggested length of 200 – 250 subunits. For comparison, the average is of 21 subunits for *E. coli* (Harz *et al.*, 1990) and, although it is strongly species-dependent, of about 20 to 40 for Gram-negative bacteria (Vollmer *et al.*, 2008b). The partial amidation (*i.e.* the conversion of a carboxylic acid into a carboxamide) of the glutamate at position two was also reported and has for consequence its conversion into glutamine. Moreover, single glycine bridges between

two *m*DAP were also identified in *A. tumefaciens* (Brown et al., 2012) and while pentaglycine bridge is a long-known feature of *Staphylococcus aureus* PG (Tipper *et al.*, 1969), this was yet unreported for Gram-negative bacteria. Similar observations were made in the same study with *S. meliloti*, allowing a certain degree of confidence to extrapolate these observations to *Brucella*. Regarding the thickness of the PG sacculi in *Brucella*, only information of almost half a century ago can be found and, due to the techniques used, are most likely obsolete.

2.4.3 OMPs

The first study on OMPs was based on the cell wall SDS insoluble fraction of *Brucella*. The SDS-PAGE analysis revealed three major bands at 15, 25 and 37 kDa (Dubray *et al.*, 1980). Then, work on the OM following detergent extraction identified three major clusters at 94, 43 and 30 kDa (Verstreate *et al.*, 1982). For these reasons, OMPs were first classified according to their molecular mass as follows: group 1 (94 kDa), group 2 (36 – 38 kDa) and group 3 (31 – 34 kDa). Group 2 and 3 were shown to be *Brucella* major OMPs (Verstreate *et al.*, 1982) and to be surface exposed due to their recognition by monoclonal antibodies (Cloeckaert *et al.*, 1990). The same study highlighted that OMPs of strains lacking the LPS O-chain (or rough, due to the colony phenotype) were more accessible than smooth strains.

In addition, early studies from the 1980s and 1990s provided evidence that OMPs from groups 2 and 3 are tightly, probably covalently, attached to PG (Dubray *et al.*, 1983; Sowa *et al.*, 1991; Cloeckaert *et al.*, 1992). Indeed, it was shown that Omps remained associated with PG despite harsh detergent treatment (*i.e.* SDS) and the need for lysozyme digestion for release. Although amino acid sequence determination in the search of

possible N- or C-terminal adducts was started already in 1990 (Sowa, 1990), no further molecular characterisation of the nature of the link was later conducted, to the best of our knowledge.

The first group includes the heaviest protein of 94 kDa (sometimes also referred to as Omp85 or 89) that is, by sequence similarity, the BamA homologue (Goolab *et al.*, 2015). All the information on the Bam system and its role in β-barrels incorporation into the OM of *Brucella* was inferred from *in silico* analysis. Hence, the knowledge on β-barrel assembly are still significantly incomplete and requires further investigation.

The group 2 proteins are now named Omp2a and Omp2b and were later shown to be porins (Douglas *et al.*, 1984) similar to OmpC and OmpF of *E. coli* (see section 1.2.1.2.1 of the introduction). Following the identification of the *omp2* locus (Ficht *et al.*, 1988), it was shown to consist of two homologous coding regions, *omp2a* and *omp2b*, that are on the opposite strands but separated by 830 bp (Ficht *et al.*, 1989). Both sequences are very similar with, on average, 85% of identity at the nucleotide level and 96% similarity at the protein level. This difference is mainly due to a 108 nucleotides deletion shortening Omp2a to 33 kDa. Interestingly, Omp2a could not be detected under laboratory conditions although its expression was detected when under the control of an active promoter. To date, the conditions of expression and the role of Omp2a are still unclear. Regarding Omp2b, its role and function are more established. The mature protein is composed of 16 β-strands with large surface loops that assemble to form trimers (Mobasheri *et al.*, 1997) and was found to let sugars in (Douglas *et al.*, 1984). In addition, Omp2b was

shown to be essential in *B. abortus* (Laloux *et al.*, 2010; Sternon *et al.*, 2018).

On a genetic level, the *omp2* locus can be used to differentiate species due to its high variability (Ficht *et al.*, 1990; Cloeckaert *et al.*, 1995; Ficht *et al.*, 1996; Cloeckaert *et al.*, 2001). This diversity is probably caused by several events of recombination, or genetic conversion, between *omp2a* and *omp2b* loci during the course of evolution. In addition, depending on the species, both *omp2a* and *omp2b* genes can be present or only two copies of the same gene are present (Ficht *et al.*, 1990; Ficht *et al.*, 1996; Cloeckaert *et al.*, 2001). Differences are especially found in the surface loops 5 and 8 (respectively L5 and L8). The L5 has been known to be involved in the porin function (Paquet *et al.*, 2001) and its shortening results in an increased sugar permeability (Cloeckaert *et al.*, 2020). The L8 diversity would rather play a role in antigenic variation (Cloeckaert *et al.*, 2020).

Group 3 consist of Omp25 (25 – 27 kDa or formerly Omp3a) and Omp31 (31 – 34 kDa). New members to this group were later added: Omp25b, Omp25c, Omp25d, Omp31b and Omp22 (also previously named Omp3b) (Guzman-Verri *et al.*, 2002; Salhi *et al.*, 2003). However, these OMPs are not present in all *Brucella* species. Omp25b was solely found in *B. suis* (Salhi *et al.*, 2003) and Omp31 is absent for *B. abortus* due to a 10 kb deletion (Vizcaino *et al.*, 1996), for instance. The group 3 OMPs were first proposed to be the *E. coli* OmpA counterpart based on the amino-acid composition (Verstreate *et al.*, 1982), although *omp25* sequencing showed no relevant homologies (de Wergifosse *et al.*, 1995).

Omp25 displays high conservation across *Brucella* species, on the contrary to Omp2b (Cloeckaert *et al.*, 1995) and is also fairly well

conserved in Rhizobiales with homologues in *Mesorhizobium loti*, *Sinorhizobium meliloti* and *A. tumefaciens* (Cloeckaert *et al.*, 2002). The mature protein was predicted to be composed of eight β-strands (Cloeckaert *et al.*, 2002) and to stay monomeric in the OM. Its role has remained ambiguous; it is not a porin but its deletion results in attenuated virulence in animal models (Edmonds *et al.*, 2002). Omp25 of *B. suis* was shown to negatively regulate the production of TNF-α in human macrophages (Jubier-Maurin *et al.*, 2001), but this could be an indirect effect of an alteration of the envelope. In addition, a study showed that *omp25* and *omp22* are under the (direct or indirect) transcriptional control of BvrR/BvrS (Manterola *et al.*, 2007), a regulatory two-component system critical for cell invasion and virulence (Sola-Landa *et al.*, 1998). Omp31, similarly to Omp25 (to which it display 34 % of homologies (Vizcaino *et al.*, 1996)), is an eight β-stranded protein that can form oligomers and it was suggested to be a porin (Cloeckaert *et al.*, 2002).

Lastly, a PhD project studying the OM of *Brucella* was previously conducted in the laboratory. In this study, V. Vassen and colleagues demonstrated that the OM is a heterogeneous structure that presents patches of rough LPS associated with Omp2b and that LPS, Omp2b and Omp25 have limited mobility in the OM (Vassen *et al.*, 2019). In addition, they addressed the question of new material incorporation and showed that newly synthesised PG, LPS and Omp25 are incorporated at the new pole and division site. These results are in line with those already published for the insertion of new PG in *A. tumefaciens* (Kuru *et al.*, 2012).

2.4.4 Lipoproteins

Brucella has an incomplete Lol system since a clear LolB homolog is missing. However, this is a common feature of α-proteobacteria which suggests either a bifunctional LolA or a LolB analogue specific to this bacterial class (Narita, 2011; Sutcliffe *et al.*, 2012).

The *Brucella* genome is predicted to encode forty-eight lipoproteins (see supplementary table 1). However, experimental studies have mainly focused on only three of them, namely Omp10, Omp16 and Omp19. The three of them were proven to be lipoproteins (Tibor *et al.*, 1999), partially surface exposed (Gomez-Miguel *et al.*, 1987; Cloeckaert *et al.*, 1990) and present in all *Brucella* species and their biovar (Tibor *et al.*, 1996; Vizcaíno *et al.*, 2000). The Omp10 was shown to be necessary for full virulence in mice but not in *in vitro* cellular assay and showed a growth defect in minimal medium (Tibor *et al.*, 2002). Omp16 (also named Omp16.5) was reported as the homologue of the PG-associated lipoprotein (Pal) (Tibor *et al.*, 1994). Pal is part of a complex named Tol-Pal and interacts with the PG in a transient and non-covalent manner (Mizuno, 1979; Bouveret *et al.*, 1999). In *C. crescentus,* Pal was found to be essential as in *Brucella* (Sternon *et al.*, 2018) and its depletion leads to OM disruption as well as incomplete cell division (Yeh *et al.*, 2010). Omp19 has sequence homology with a bacterial protease inhibitor and was shown to inhibit gastrointestinal and lysosomal proteases (Coria *et al.*, 2016). Moreover, the importance of Omp19 was shown both for efficient infection by the oral route and for the survival within macrophages (Pasquevich *et al.*, 2019). It could therefore participate in the successful establishment of a chronic infection. Additionally, it was also reported that an Omp19 mutant was more sensitive to OM stress, such as polymyxin B or sodium deoxycholate (Tibor *et al.*, 2002). Because

a double Δ*omp10*Δ*omp19* mutant could not be obtained in *B. ovis*, their roles were proposed to be, at least overlapping and involved in maintaining OM integrity (Sidhu-Munoz *et al.*, 2018). Lastly, a lipoprotein similar to Lpp both in its biochemical properties and its linkage to the peptidoglycan was reported in 1986 (Gomez-Miguel *et al.*, 1986). However, no further publications were made on the subject and the protein was never identified.

3 Objectives

The Gram-negative model bacterium *E. coli* has an abundant lipoprotein, Lpp, covalently attached by its C-terminus to the peptidoglycan. This establishes the basis of the outer membrane anchorage to the peptidoglycan. Three enzymes, called L,D-transpeptidases, are responsible for this binding. Surprisingly, Lpp can only be found conserved in Enterobacteriaceae. In other organisms, no confirmation of Lpp presence or a different mechanism was reported.

Thus, the lack of study in this domain urged us to investigate the case of *B. abortus*, a bacterium phylogenetically distant from *E. coli*. At the start of this work, we realised that the two major OMPs of *B. abortus*, Omp2b and Omp25, although they are phylogenetically distinct, both display an N-terminal extension and the mature protein starts with the same ADAI sequence. We postulated that these two important proteins could be anchored to the PG. In this research, we use a tandem mass spectrometry approach for the unbiased identification of peptidoglycan-linked proteins and the confirmation of the link. We then aim to find the L,D-transpeptidases involved in the protein anchorage mechanism by the use of a bacterial heterologous system, and then by a genetic approach in *B. abortus*. We also use molecular approaches to pinpoint the protein crucial amino acid involved in the reaction and proceed to the effect assessment by western blotting.

Finally, we attempt to characterise a protein initially annotated as a L,D-transpeptidase, but supposed to catalyse the breakage of the links between OMPs and PG.

RESULTS

1 Outer membrane – peptidoglycan interactions

1.1 Publication

1.1.1 Context

The following manuscript is a condensed version of the thesis results about the anchorage of the outer membrane to the peptidoglycan. The manuscript itself is subdivided into three parts, (i) the main manuscript with the key data, (ii) the extended data with information supporting some of the statements made in the manuscript and (iii) the supplementary information composed mainly of the strains, plasmids, primers and antibody tables. Additionally, all raw data can be found on FigShare (https://doi.org/10.6084/m9.figshare.c.5087120.v3). Due to the conciseness imposed by the editorial guidelines of the journal, less relevant or important information were not mentioned. Hence, additional results and interpretation are added after the manuscript section. The mass spectrometry experiments were designed and analysed in collaboration with Marc Dieu and Patsy Renard (MaSUN, UNamur). The *A. tumefaciens* study was conducted by Adélie Lannoy during her master thesis as part of this study. The EM samples preparation and image acquisition were performed by Sander Van Der Verren (Han Remaut team, VUB-VIB).

In this article, we first report the use of mass spectrometry for a without *a priori* identification of proteins possibly bound the PG. Out of the proteins co-purified with PG, seven were predominantly sequenced. Six were predicted – or known - to be β-barrels and one had an unclear predicted localisation. Furthermore, we could confirm the covalent attachment to PG, as previously suggested (Sowa *et al.*, 1991; Cloeckaert

et al., 1992), through a disordered N-terminal extension spanning in the periplasm. In contrast with Lpp, where the side chain amino group of a lysine is bound to the *m*DAP, we showed that the amino group of the N-terminal alanine is linked to *m*DAP.

We then aimed to identify the enzymes involved in the transpeptidation reaction. We show that it is ensured by at least three LDt and identified the main one (Ldt4) while providing evidence for the involvement of the two others (Ldt1 and Ldt2). We also suggest the existence of at least another LDt involved in OMP-PG transpeptidation as we could not completely abolish the OMPs anchorage in a Δ*ldt1,2,4* strain. We provide further insights into the transpeptidation mechanism by abolishing the OMP anchorage by a single amino acid mutation at position two of the major OMPs, an invariant aspartate. Lastly, we could demonstrate the conservation of this anchorage system in another Rhizobiale, *A. tumefaciens.*

Overall, this molecular characterisation – with the companion paper (Sandoz *et al.*, 2021) –of OMP covalently linked to the PG is the first to demonstrate a new mode of covalent anchorage of the OM to the PG, since the Braun's lipoprotein identification. These results suggest that it could exist a broad variety of such links and encourage investigation in other bacteria to unravel its variety.

1.1.2 Article

Nature Microbiology

VOL 6 | January 2021 | 27–33

Letters (DOI: 10.1038/s41564-020-00799-3)

β-Barrels covalently link peptidoglycan and the outer membrane in the α-proteobacterium *Brucella abortus*

Pierre Godessart[1], Adélie Lannoy[1], Marc Dieu[2], Sander E. Van der Verren[3,4], Patrice Soumillion[5], Jean-François Collet[6,7], Han Remaut[3,4], Patricia Renard[2,8] and Xavier De Bolle[1,✉]

[1]Research Unit in Microorganisms Biology (URBM), Department of Biology, Namur Research Institute for Life Sciences (NARILIS), Namur, Belgium.
[2]MaSUN, Mass Spectrometry Facility, University of Namur, Namur, Belgium.
[3]Structural & Molecular Microbiology, VIB-VUB Centre for Structural Biology, Brussels, Belgium.
[4]Structural Biology Brussels, Vrije Universiteit Brussel, Brussels, Belgium.
[5]LIBST, UCLouvain, Louvain-la-Neuve, Belgium.
[6]de Duve Institute, Université Catholique de Louvain, Brussels, Belgium.
[7]WELBIO, Brussels, Belgium.
[8]Laboratory of Biochemistry and Cell Biology (URBC), Department of Biology, Namur Research Institute for Life Sciences (NARILIS), Namur, Belgium.
✉ e-mail: xavier.debolle@unamur.be

1.1.2.1 Abstract

Gram-negative bacteria are surrounded by a cell envelope that comprises an outer membrane (OM) and an inner membrane that, together, delimit the periplasmic space, which contains the peptidoglycan (PG) sacculus. Covalent anchoring of the OM to the PG is crucial for envelope integrity in *Escherichia coli*. When the OM is not attached to the PG, the OM forms blebs and detaches from the cell. The Braun lipoprotein Lpp[1] covalently attaches OM to the PG but is present in only a small number of γ-proteobacteria; the mechanism of OM–PG attachment in other species is unclear. Here, we report that the OM is attached to PG by covalent cross-links between the N-termini of integral OM β-barrel-shaped proteins (OMPs) and the peptide stems of PG in the α-proteobacteria *Brucella abortus* and *Agrobacterium tumefaciens*. Cross-linking is catalysed by L,D-transpeptidases and attached OMPs have a conserved alanyl-aspartyl motif at their N terminus. Mutation of the aspartate in this motif prevents OMP cross-linking and results in OM membrane instability. The alanyl-aspartyl motif is conserved in OMPs from Rhizobiales; it is therefore feasible that OMP–PG cross-links are widespread in α-proteobacteria.

1.1.2.2 Main

The envelope of Gram-negative bacteria is a complex, macromolecular structure that is essential for growth and survival. Since the first observation of its multilayered structure in the 1960s, major efforts have been made to both investigate its unique structural features and unravel the mechanisms that govern its assembly. After decades of intense scrutiny, we now have a reasonably good understanding of the molecular processes that assemble and maintain the envelope of the model organism *E. coli*, although crucial questions remain unresolved. Knowledge gained in *E. coli* can be applied, at least partially, to other less-studied organisms. However, *E. coli* presents some features that are found only in Enterobacteriaceae. For example, the Braun's lipoprotein Lpp is one of the hallmarks of the *E. coli* envelope. With a presence of ~1,000,000 copies per cell, Lpp is numerically the most abundant *E. coli* protein[1]. Lpp has a crucial role in the cell envelope, because it is anchored

to the OM by a lipid moiety at its N terminus and attached to the PG through its C-terminal lysine. Lpp provides the only known covalent connection between the OM and the PG. This anchorage has major implications; when absent, the OM pulls away from the cell and forms blebs[2]. Although other envelope proteins, such as the lipoprotein Pal and the OM protein (OMP) OmpA, bind non-covalently to PG, they cannot fully compensate for the loss of Lpp. Further highlighting its importance in *E. coli*, Lpp has recently been shown to also dictate the size of the periplasm[3,4] the intermembrane distance increases when Lpp becomes longer. Thus, Lpp is a key component of the *E. coli* cell envelope. Given the important function of Lpp in *E. coli*, as well as its role in pathogenesis[5], we were intrigued by the absence of this protein in most Gram-negative bacteria, raising the possibility that other OM–PG covalent tethers remain unidentified. We investigated this prospect using the α-proteobacterium *B. abortus*—which is a Gram-negative intracellular pathogen, and is the aetiological agent of brucellosis, a zoonosis that causes major social and economic impacts worldwide[6].

To investigate whether OM proteins are covalently attached to PG in *B. abortus*, PG sacculi were purified and digested with either lysozyme (cleaving the β-1-4 bond between the *N*-acetylglucosamine (NAG) and *N*-acetylmuramic acid (NAM) residues) or an amidase (cleaving the amide bond between NAM and the l-alanine residue of the peptide stem), while the potentially linked proteins were digested with trypsin either alone or in combination with chymotrypsin. The resulting fragments were then analysed using liquid chromatography coupled with tandem mass spectrometry (LC–MS/MS). Out of 66 proteins identified, the most predominant proteins (in terms of spectra per protein) were predicted to be located in the OM (Fig. 1a). We found hybrid peptides between the *meso*-diaminopimelic acid (*m*DAP) residue from the peptide stems and the N termini of seven different proteins (Fig. 1b). All of the proteins are predicted to have a β-barrel-like structure and all except for one are OMPs. In the lysozyme-digested condition, we found that the oxonium ions corresponded to the NAG fragmentation (Extended Data Fig. 1a), therefore confirming the glycosylated nature of the hybrid fragments[7]. Supporting these data, when lysozyme-digested PG fragments were analysed using sodium dodecyl sulphate–polyacrylamide gel

electrophoresis (SDS–PAGE), released Omp2b and Omp25 could be detected using immunoblotting (Extended Data Fig. 2).

Our data above indicate that OMPs are covalently attached to the PG in *B. abortus* (Fig. 1b). In *E. coli*, three l,d-transpeptidases (Ldts) catalyse the attachment of Lpp to the PG[8]. These enzymes use a cysteine-based enzymatic mechanism[9] to covalently link the C-terminal lysine residue of Lpp to the *m*DAP[10]. This prompted us to search for *B. abortus* Ldts. Analysis of the *B. abortus* genome revealed that it encodes eight proteins with sequence homology to *E. coli* Ldts. These putative Ldt genes were named *ldt1* to *ldt8* (Supplementary Table 3). To test whether these Ldts were able to covalently link OMPs to the PG, the coding sequences of these enzymes were expressed separately in *E. coli* cells also producing *B. abortus* Omp25. We then purified the PG of these *E. coli* strains and digested it with lysozyme. Omp25 was found attached to the PG only in cells expressing Ldt1, Ldt2 and Ldt4 (Fig. 2a). These three Ldts have a lipobox, being the only putative lipoproteins among the eight Ldts, and also form a monophyletic group (Extended Data Fig. 3).

Next, we deleted the eight identified Ldts either separately or in combination to assess their roles in OMP–PG attachment in *B. abortus*. We used the attachment of Omp2b and Omp25 to PG in *B. abortus* as a readout (Extended Data Fig. 4). Increased proportions of free OMPs were observed in the lysozyme-treated samples generated from cells lacking Ldt4, either alone or in combination with Ldt1 or Ldt2 (Fig. 2b and Extended Data Fig. 4). Complementation of both Δ*ldt4* and Δ*ldt1*,*2*,*4* strains with the *ldt4* gene increased the PG-bound protein forms and led to decreased pools of free Omp25 and Omp2b (Fig. 2b). By contrast, deletion of *ldt1* and *ldt2* had no impact. These results led us to conclude that Ldt4 is the main Ldt involved in OMP tethering to the PG in *B. abortus*. A fraction of OMPs remained linked in all of the mutants, indicating that at least one other unidentified enzyme might anchor OMPs to PG.

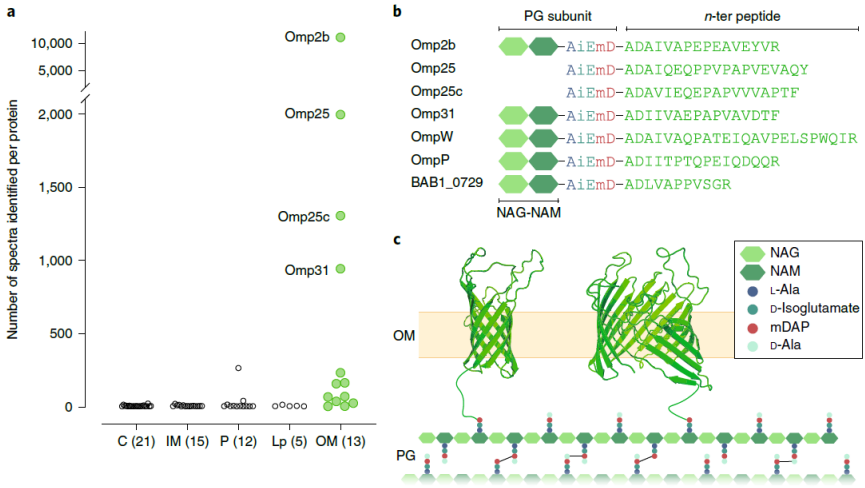

Fig. 1 | Multiple OM proteins are bound to PG. **a**, Classification of the 66 proteins purified with PG and identified in MS according to the number of spectra per protein and their predicted subcellular localization. Four proteins, which are all predicted to be β-barrels, were prevalent. The numbers in brackets correspond to the number of proteins predicted per subcellular localization. C, cytoplasmic; IM, inner membrane; Lp, lipoprotein; P, periplasmic. **b**, PG-linked identified proteins and their corresponding sequenced fragments at the N terminus of mature forms (*n*-ter). Proteins identified in lysozyme-treated samples were linked to the disaccharide NAG-NAM (Supplementary Fig. 1a). iE, isoglutamate; mD, *m*DAP. **c**, Model of OMPs linked through their N-terminal amino group to the *m*DAP of the PG. The 3D structures of the proteins were predicted using I-Tasser[45–47] and displayed with PyMol v.2.0, and represent Omp25 (left) and Omp2b (right).

Brucella spp. release OM vesicles containing OM material[11]. We therefore hypothesized that altered OM–PG interactions might increase the production of OM vesicles under stress conditions. We exposed the wild-type (WT), Δ*ldt4* and Δ*ldt1,2,4* strains to heat stress. Whereas the WT strain released only small amounts of Omp25 at 60 °C, the deletion strains released detectable levels of Omp25 at 50 °C (Fig. 2c). We observed that Ldt1 and Ldt2 had a bigger impact on the envelope integrity when deleted in combination with the Ldt4 (Extended Data Fig. 5c). After heat stress, large OM blebs were observed for the Δ*ldt1,2,4* strain in cryo-electron microscopy (cryo-EM; Fig. 2d), consistent with the release of Omp25 in the culture supernatant. No change in periplasm size was observed between the WT and Δ*ldt1,2,4* strains (Extended Data Fig. 5a,b) in these conditions, suggesting that the remaining links between OM and PG

preserve the global envelope structure. In agreement with this hypothesis, the Δ*ldt1*,*2*,*4* strain remained as infectious as the WT in murine macrophage infection assays (Extended Data Fig. 6). Together, these data indicate that, although the OM structure is not visibly affected under normal growth conditions, it is more sensitive to heat stress.

In *B. abortus*, all mature PG-bound OMPs begin with an alanyl-aspartyl motif that is conserved in other Rhizobiales (Fig. 3a). We next investigated the role of the aspartate residue in anchoring Omp25 and Omp2b to the PG. We replaced the *omp25* or *omp2b* genes with an allele in which the conserved aspartate 2 was substituted with an alanine residue, therefore generating two single mutants encoding Omp25^{D2A} or Omp2b^{D2A}. Although both proteins were still exported to the OM (Extended Data Fig. 7), they were no longer attached to the PG (Fig. 3b). The aspartate residue is therefore crucial for anchoring these OMPs to the PG. In the absence of the Omp25 linkage, a higher proportion of Omp2b was linked to the PG and conversely. On the basis of phase-contrast microscopy, the mutation of Omp25 or Omp2b alone had no phenotypical effect. However, the combination of both mutations led to a higher proportion of rounder cells compared with the WT (Extended Data Fig. 8a). The double mutant carrying Omp25^{D2A} and Omp2b^{D2A} (Omp25-2b^{D2A}) also showed the release of small blebs under normal growth conditions in EM (Fig. 3c,d). Furthermore, Omp25 could be detected in the supernatant of an Omp25-2b^{D2A} mutant suspension (Extended Data Fig. 8b), suggesting that there is increased blebbing in this strain. Similar to the Δ*ldt1*,*2*,*4* mutant, the Omp25^{D2A} strain also released OM material at a lower temperature compared with the WT. In line with the results above, the Omp25-2b^{D2A} mutant showed no reduced infectivity in macrophage infection assays, despite the altered structure of its envelope (Extended Data Fig. 6). The alanyl-aspartyl motif is conserved in many mature OMPs homologues in several Rhizobiales, raising the interesting possibility that the anchorage described above is conserved in this bacterial clade. To assess this hypothesis, the PG from the plant pathogen *A. tumefaciens* was isolated to identify PG-bound OMPs. We found two

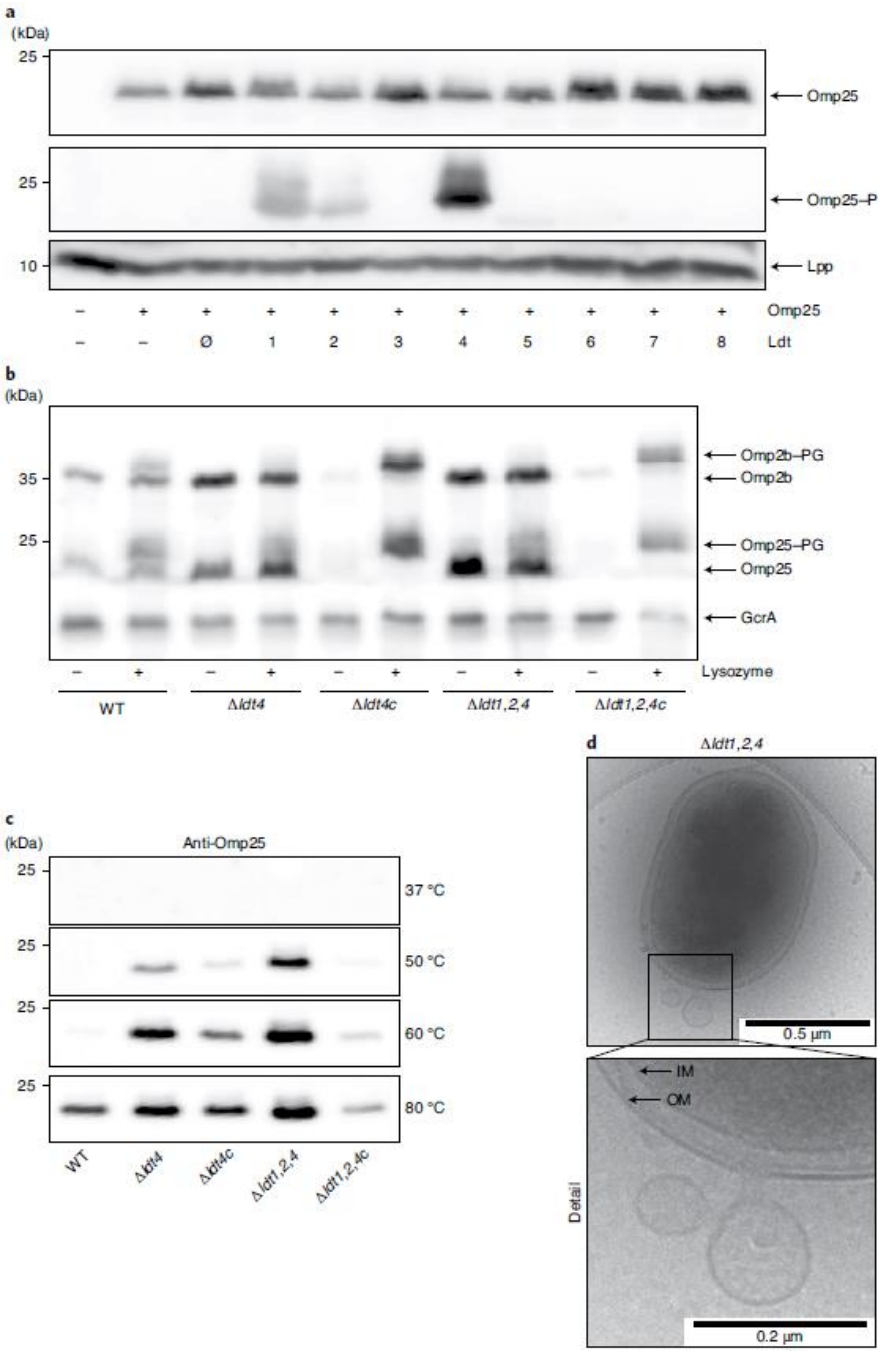
a
(kDa)
25
Omp25
25
Omp25–P
10
Lpp
– + + + + + + + + + + Omp25
– – Ø 1 2 3 4 5 6 7 8 Ldt
b
(kDa)
35
25
Omp2b–PG
Omp2b
Omp25–PG
Omp25
GcrA
– + – + – + – + – + Lysozyme
WT
Δldt4
Δldt4c
Δldt1,2,4
Δldt1,2,4c
c
(kDa)
Anti-Omp25
25
37 °C
50 °C
60 °C
80 °C
WT
Δldt4
Δldt4c
Δldt1,2,4
Δldt1,2,4c
d
Δldt1,2,4
0.5 µm
IM
OM
Detail
0.2 µm

Fig. 2 | Ldts are involved in OMP-PG linkage and envelope stability. a, Coexpression of Omp25 and Ldts from *B. abortus* in *E. coli*. Omp25 was detected using western blot analysis of the cell lysates (top). When PG was isolated, Omp25 was detected only when coexpressed with *ldt1*, *ldt2* and *ldt4*, suggesting an anchorage of Omp25 to the *E. coli* PG (middle). Lpp was used as a loading control for PG (bottom). 'Ø' refers to the empty vector (without the *omp25* gene). **b**, The effect of deleting and complementing *ldt4* alone or in combination with *ldt1* and *ldt2* in *B. abortus*. A decrease in the bound forms of Omp25 and Omp2b and an increase in the free forms were observed in the deletion strains. Complementation with *ldt4* (Δ*ldt4c* and Δ*ldt1*,*2*,*4c*) led, in both cases, to a strong increase in the bound form with a depletion of the free form. GcrA was used as the loading control. **c**, Heat-stressed Δ*ldt4* and Δ*ldt1*,*2*,*4* strains release Omp25 at a lower temperature compared with the WT. Omp25 was detected using western blot analysis of the culture supernatants. Complementation strains have a partially restored phenotype. **d**, Cryo-EM observations of the Δ*ldt1*,*2*,*4* strain heat-stressed at 60 °C. The strain exhibits formation of blebs along the OM, supporting the release of Omp25. Scale bars, 0.5 μm (top) and 0.2 μm (bottom). For **a**–**d**, data are representative of experiments from three biologically independent replicates.

proteins that are homologous to Omp2b and Omp25, named RopA1/A2 and RopB, respectively, that bind covalently to the *m*DAP of the PG through their N terminus (Extended Data Fig. 9). This suggests that a similar organization of OM–PG interactions is shared by the Rhizobiales, enabling the prediction of covalent anchorage of OMPs with an alanyl-aspartyl N terminus to the *m*DAP of the PG.

Our results address a long-standing question concerning the covalent attachment of the OM to the PG in bacteria that do not produce a Lpp homologue. Notably, we found that the identified linkage involves the N-terminal part of multiple integral OMPs. Depending on the OMP, this linker has a variable length and is thought to be flexible due to the absence of secondary structure. We also found that the formation of the covalent link is catalysed by L,D-transpeptidases, therefore revealing a new function for this large class of enzymes that is widely conserved in bacteria. In addition to being conserved in Rhizobiales, this mechanism is also found in other proteobacteria[12]. In the future, it will be important to characterize the envelope structure of other Gram-negative bacteria, as OM–PG tethering could be different in other clades. These investigations might result in leads for therapeutics to treat bacterial infections.

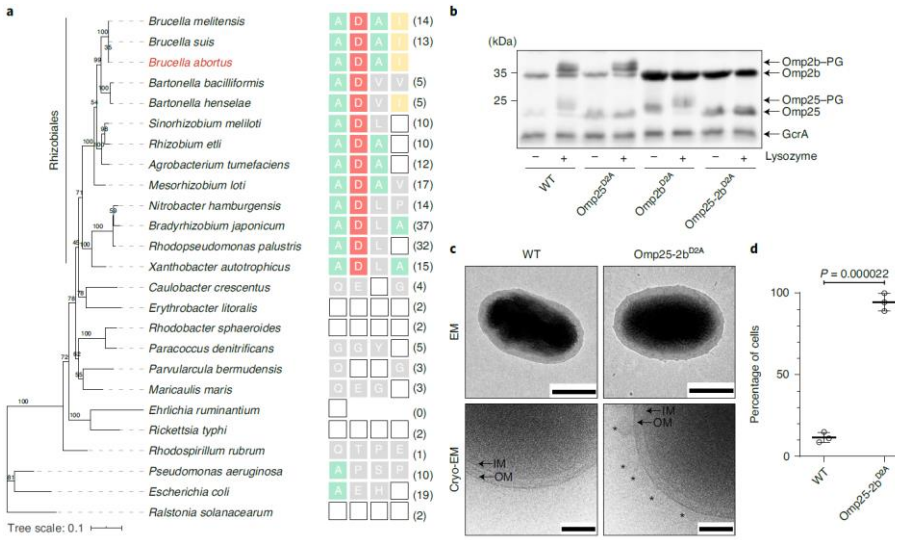

Fig. 3 | Aspartate 2 is crucial for the OMP anchorage to PG. a, Comparison between the first four amino acid consensus of *B. abortus* OMPs and their homologues found in α-proteobacteria. The phylogeny was inferred from the 16S and 23S RNA and bootstrap values are represented. The two first residues are conserved across Rhizobiales. The numbers in brackets represent the total number of homologues found in the listed organisms. An empty square indicates that there is no consensus sequence. **b**, Mutation of the Omp25 or Omp2b aspartate 2 into an alanine (D2A) abolished their linkage to PG, whereas an increased free form of Omp2b or Omp25, respectively, was concomitantly observed. GcrA was used as the loading control. The representative western blot was consistently observed over three biologically independent replicates. **c**, Electron microscopy (top) and cryo-EM (bottom) analysis of the WT and the Omp25-2b^{D2A} strains. The mutant strain shows an envelope instability with small blebs originating from the OM. The asterisks indicate blebs, which were consistently observed over three biologically independent replicates. Scale bars, 0.5 µm (top) and 0.1 µm (bottom). **d**, The Omp25-2b^{D2A} strain has a significantly higher proportion of bacterial cells that have at least one bleb detected on its envelope in EM. $n = 101$ for WT and $n = 111$ for Omp25-2b^{D2A} strains over three biologically independent experiments. Statistical significance was determined using unpaired two-tailed *t*-tests with the Holm–Sidak method. Data are mean ± s.d.

1.1.2.3 Methods

Plasmids and strains

E. coli DH10B, S17-1 and derivative strains were grown in Luria–Bertani (LB) medium at 37 °C under constant agitation. *B. abortus* 544 and derivative strains were grown in TSB-rich medium (3% Bacto Tryptic Soy Broth) at 37 °C under constant agitation. *A. tumefaciens* C58 was grown in 2YT-rich medium (1% yeast extract, 1.6% peptone, 0.5% NaCl) at 30 °C. When necessary, culture medium was supplemented with the appropriate antibiotics at the following concentrations: kanamycin, 10 μg ml^{-1} or 50 μg ml^{-1} for genomic or plasmidic resistance, respectively; chloramphenicol, 20 μg ml^{-1}; and nalidixic acid, 25 μg ml^{-1}.

Strain construction

A list of the strains, plasmids, open reading frames and primers used in this study is provided in Supplementary Tables 1–4, respectively. Deletion strains were constructed by allelic exchange with a pNPTS138 carrying a kanamycin resistance cassette and a sucrose sensitivity cassette as previously described[13]. For the expression of Ldts in *E. coli*, the Ldt sequences were amplified with 500 bp upstream and 100 bp downstream of the coding sequence and the amplicon was then inserted into a pNPTS138 restricted at the EcoRV site.

PG purification for MS

PG purification was performed using a modified version of a previously published method[14]. Bacteria were collected from exponential-phase culture by centrifugation (7,000*g* for 5 min at 4 °C), and then resuspended in lysis buffer (Tris-HCl 10 mM pH 7.5, NaCl 100 mM, DNase 100 μg ml^{-1} (Roche, 10104159001) and protease inhibitor cocktail EDTA-free (Roche, 11873580001)). Cells were then disrupted with 0.1 mm zirconia/silica beads (Biospec Products, 11079101z) in a Cell Disruptor Genie (Scientific Industries) at maximal amplitude (2,800 rotations per minute) for 60 min at 4 °C. Samples were then inactivated at 80 °C for 1 h. Envelopes were collected by centrifugation at 10,000*g* for 10 min at room temperature and resuspended in 5% SDS. The samples were boiled until the solution become translucent at 95 °C, 500 r.p.m. (Thermomixer, Eppendorf) and were then centrifuged (16,200*g* for 30 min at 14 °C). The samples were then resuspended in 5% SDS and boiled again for 30 min at 95 °C. This step was repeated five times to ensure that most of contaminant proteins were removed. The samples

were then washed repeatedly with distilled water until SDS-free. PG pellets were resuspended in PBS and stored at −20 °C.

Proteomic analysis

PG was digested overnight with either lysozyme (Roche, 10006829, 10 µg for 45 µl of PG at ~1 mg ml^{-1}) or with the recombinant amidase Atl from *Staphylococcus aureus* (60 µg for 100 µl of a PG sample ±50 mg ml^{-1}), purified and used as described previously[15]. The samples were then reduced with dithiothreitol (10 mM at 37 °C for 45 min) and then alkylated with iodoacetamide (40 mM at 37 °C for 45 min) before protein digestion with trypsin (0.5 µg, Promega) overnight or trypsin overnight followed by treatment with chymotrypsin (0.25 µg, Promega) for 2 h for the amidase-treated samples. The digested samples were then analysed using nanoLC (UltiMate 3000, Thermo Fisher Scientific) coupled to electrospray MS/MS (maXis Impact UHR-TOF, Bruker). Peptides were separated by reverse-phase LC using a 75 µm × 250 mm column (Acclaim PepMap 100 C18). Mobile phase A was composed of 95% H_2O, 5% acetonitrile and 0.1% formic acid. Mobile phase B was composed of 80% acetonitrile, 20% H_2O and 0.1% formic acid. After injection of the peptides, the gradient started linearly from 5% B to 40% B in 220 min and from 40% B to 90% B in 10 min. The column was directly connected to a CaptiveSpray source (Bruker). In survey scans, MS spectra were acquired for 0.5 s in the m/z range of 400–2,200. The most intense peptides (2^+, 3^+ or 4^+ ions) were sequenced during a cycle time of 3 s. The collision-induced dissociation energy was automatically set according to the m/z ratio and the charge state of the precursor ion. To improve oxonium ion detection and glycopeptide sequencing, a second nanoLC–MS/MS analysis was performed using a basic stepping mode in MS/MS for which the collision energy was increased by 30% (ref. 7) to half the sequencing time. The MaXis and Ultimate systems were controlled by Compass HyStar 3.2 (Bruker). Peak lists for all of the samples were created using DataAnalysis v.4.0 (Bruker) and saved as MGF files. Mascot v.2.4 (Matrix Science) and X! Tandem (The GPM; https://thegpm.org; version, CYCLONE 2010.12.01.1) were used as the search engine for protein identification. Enzyme specificity was set to trypsin or trypsin and chymotrypsin, and the maximum number of missed cleavages per peptide was set to one for trypsin alone or two when trypsin was used in combination with chymotrypsin. Carbamidomethyl (Cys), oxidation (Met), deamidation (Asn, Gln) for the amidase-treated samples and NAG(1)NAM(1) (478.179 Da) modification were variably enabled on alanines. The non-conventional amino acid *m*DAP (172.085 Da) was

added to the amino acid configuration file from Mascot (Matrix Science). Mass tolerance for the monoisotopic peptide was 10 ppm and the MS/MS tolerance window was set to 0.05 Da.

For protein identification, we used a custom-made database comprising the *B. melitensis* biovar *abortus* 2308 or *A. tumefaciens* C58 proteome downloaded from UniProt (July 2018 or June 2019, respectively) with the candidate protein modified sequences. The modified sequences consisted of a duplication of the sequence, a removal of the signal peptide to correspond to the mature proteins and the addition of the PG amino acids AEJ (where J is *m*DAP). The list of proteins with modified sequences is provided in Source Data Fig. 1 and Source Data Extended Data Fig. 9.

Scaffold v.4.8 (Proteome Software) was used to validate MS/MS-based peptide and protein identifications. Peptide identifications were accepted if they could be established at a probability of greater than 95% using the PeptideProphet algorithm[16] with Scaffold delta-mass correction. Protein identifications were accepted if they could be established at greater than 5.0% probability to achieve a false-detection rate of less than 1.0% and contained at least two identified peptides. Protein probabilities were assigned by the ProteinProphet algorithm[17]. Subcellular localization determination for the identified proteins was performed according to a decisional tree (Supplementary Fig. 1).

PG isolation for validation in *E. coli*

PG for western blot analysis was prepared according to a previously published method[18]. *E. coli* overnight cultures of 50 ml were normalized between them and centrifuged to recover bacteria (7,000*g* for 5 min at room temperature). The pellets were resuspended in 5% SDS and incubated at 95 °C, 500 r.p.m. (Thermomixer, Eppendorf) until the solution became translucent. PG was pelleted by centrifuging the samples at 16,200*g* for 30 min at 14 °C. The pellets were then washed by resuspension in distilled water, and the centrifugation steps described above were repeated until the sample was SDS-free. The pellets were resuspended in PBS and digested overnight with 2.5 U of mutanolysin (Sigma-Aldrich, M9901) per 50 µl of PG suspension.

PG isolation for validation in *B. abortus*

Exponential-phase cultures (optical density at 600 nm (OD_{600}) of 0.3–0.6) of *B. abortus* were normalized to an OD_{600} of 2 in 50 µl and inactivated for

1 h at 80 °C. Half of the sample was then digested overnight at 37 °C with lysozyme (8 µg). The digested and undigested samples were then treated with DNase I (10 µg, Roche) for 30 min at 37 °C. The sample volumes were then adjusted to 30 µl.

Western blot analysis

SDS-β-mercaptoethanol loading buffer, at final concentrations of 2% and 5%, was added (1:4 of final volume) before heating the samples at 95 °C for 10 min. Samples were loaded on 12% acrylamide gels. After migration, proteins were transferred in a semi-dry manner onto a nitrocellulose membrane (GE Healthcare Amersham Protran 0.45 NC) and then blocked in PBS supplemented with 0.05% Tween-20 (VWR) and 5% (w/v) milk (Nestlé, Foam topping) overnight at 4 °C on rollers. Before antibody incubation, the membranes were washed three times with PBS with 0.05% Tween-20. Membranes were incubated with primary antibodies (anti-Omp25 and anti-Omp2b, 1:200; anti-PG, 1:100; and anti-GcrA, 1:1,000; Supplementary Table 5) for 1 h followed by the corresponding secondary horseradish-peroxidase-coupled antibody (1:5,000, Supplementary Table 6). Both antibodies were diluted in PBS supplemented with 0.05% Tween-20 and 0.5% milk, and the membranes were washed as described after both incubations. The membranes were revealed using Clarity ECL Substrate (Bio-Rad) solutions and images were acquired using a GE Healthcare Amersham Imager 600. The specificity of anti-Omp25 and anti-Omp2b monoclonal antibodies was checked (Supplementary Fig. 2). Lpp was detected by immunoblot analysis using anti-Lpp antibodies (dilution, 1:10,000) produced from a rabbit (Eurogentec) immunized with the purified synthetized peptide KVDQLSNDVNAMRSDVQAAK from the middle part of the Lpp protein.

OM vesicle analysis

Exponential-phase bacteria were concentrated at an OD_{600} of 5 in 1 ml and washed twice in PBS, and then 200 µl of the sample was used for incubation at the different temperatures for 1 h. After incubation, bacteria were pelleted at 8,000*g* for 150 s and 100 µl of the supernatants were recovered and inactivated at 80 °C for 1 h. Then, 30 µl of the sample was added to 10 µl of 4× SDS-β-mercaptoethanol loading buffer and processed as described above for western blotting.

RAW 264.7 macrophage culture and infection

RAW 264.7 murine macrophages (ATCC) were cultured at 37 °C under 5% CO_2 in DMEM (GIBCO) supplemented with 10% decomplemented fetal bovine serum (GIBCO). For infections, RAW 264.7 macrophages were seeded in 24-well plates at a density of 10^5 cells per well and left overnight for growth and adhesion. The next day, *B. abortus* infectious doses were prepared in DMEM from exponential cultures (OD_{600} of 0.3–0.6) washed twice at a multiplicity of infection of 50. Bacteria and cells were centrifuged at 169*g* at 4 °C for 10 min and incubated until the appropriate time point at 37 °C, 5% CO_2. One hour after the beginning of infection, the culture medium was replaced with DMEM supplemented with 50 μg ml^{-1} of gentamycin to kill the remaining extracellular bacteria. One hour later, culture medium was changed again with fresh DMEM supplemented with 10 μg ml^{-1} of gentamycin. At the different time points (that is, 2 h, 5 h, 24 h and 48 h after infection), the cells were washed twice in PBS, and then lysed with PBS with 0.1% Triton X-100 for 10 min at 37 °C. Dilutions were then spotted (20 μl) onto TSB agar, incubated at 37 °C and colony-forming units were counted.

OMP labelling

Exponential-phase bacteria (OD_{600} of 0.3–0.6) were collected by centrifugation (8,000*g* for 150 s), washed twice in PBS then resuspended in undiluted hybridoma culture supernatant (Supplementary Table 5) and incubated at room temperature for 40 min on a wheel. Cells were then washed twice as described above and resuspended in the corresponding secondary antibody (Supplementary Table 6) diluted 500-fold in PBS and incubated at room temperature for 40 min on a wheel, protected from light. Cells were then washed as described above and resuspended in PBS for imaging.

Microscopy and analysis

Bacterial suspensions (2 μl) were spotted onto 1% agarose PBS pads for imaging. Images were acquired using a Nikon Eclipse Ti2 equipped with a phase-contrast objective Plan Apo λ DM100XK 1.45/0.13 PH3 and a Hamamatsu C13440-20CU ORCA-FLASH 4.0. Images were processed using FIJI v.2.0.0 (ref. [19]), a distribution of ImageJ. Look-up tables were adjusted to the best signal–noise ratio. Bacteria were detected and analysed using the ImageJ plugin MicrobeJ[20]. The parameters and pictures used for bacterial detection and measurements can be found at https://doi.org/10.6084/m9.figshare.12800795. Only bacteria with a maximal length of 1.4 μm were taken into account.

EM and cryo-EM analyses

Sample preparation was performed on the basis of a previously published protocol[21]. In brief, bacteria were collected in exponential phase by centrifugation (2 min at 8,000*g*), washed once with PBS and resuspended in paraformaldehyde (Merck) 4%. Fixation was performed at room temperature for 1 h. Cells were then washed once in EM buffer (20 mM Tris-HCl pH 7.6, 50 mM glucose, 10 mM EDTA) before resuspension in EM buffer. Cell killing was confirmed before imaging. To assess the OM integrity of the Omp25-2b^{D2A} strain, biological triplicates of WT and mutant fixed bacteria were imaged using transmission EM, in the absence of negative staining reagents. All of the samples were prepared for EM by applying 5 µl sample to a non-glow discharged formvar copper 400 mesh grid (EMS) and washing once with 10 µl double-distilled H_2O. The prepared samples were imaged at ×15,000 nominal magnification (pixel size, 7.64 Å) using an in-house 120 kV JEM 1400+ (JEOL) microscope equipped with a LaB_6 filament and CMOS camera (TVIPS TemCam F-416). To assess periplasm size in the Δ*ldt1*,*2*,*4* strain and OM defects in the Omp25^{D2A} mutant, samples were additionally prepared for cryo-EM. Fixed bacteria were vitrified on glow-discharged Lacey carbon films on 300 mesh copper EM-grids (Agar-scientific). For each grid, 3 µl of sample was manually back-blotted and plunged into liquid ethane using a CP3 Cryoplunge (Gatan). For the Δ*ldt1*,*2*,*4* strain, images were acquired using a JEM-1400+ (JEOL) microscope. Images were obtained with a defocus of between −7 µm and −10 µm at ×25,000 nominal magnification, corresponding to a pixel size of 4.584 Å. For the Omp25^{D2A} mutant, images were acquired using a 300 kV JEOL CryoARM300 system (BECM, Brussels) equipped with an omega energy filter and a K3 detector (Gatan). Images were collected with a defocus range of −3 µm to −4 µm at a nominal magnification of ×25,000, corresponding to a pixel size of 2.01 Å. The detector was used in counting mode with a cumulative dose of 63.8 electrons per Å^2 spread over 60 frames. The images were motion-corrected and dose-weighted using MotionCor2.1 (ref. [22]) and defocus values were determined using ctffind4.1 (ref. [23]). Periplasmic space was measured using FIJI v.2.0.0 (ref. [19]), a distribution of ImageJ. In brief, membranes were manually delimited and distances between both membranes were computed at a 1 nm interval using a custom script (PeriSizer; https://doi.org/10.6084/m9.figshare.12806876) to produce the histogram. The pictures used for periplasm measurements are provided at https://doi.org/10.6084/m9.figshare.12806876.

Phylogeny analysis

For *ldt* phylogeny, *ldt* sequences from *B. abortus* were aligned with Clustal Omega v.1.2.4 (refs. [24,25,26]) without signal peptides (SignalP 4.1 Server[27]) and trimmed using TrimAI v.1.3 (ref. [28]). The best model was then determined using SMS[29], the phylogenetic analysis was performed using PhyML v.3.0 (refs. [30,31]) primed with BIONJ[32], and 100 bootstraps were performed. Visualization and tree annotation were performed using iTOL[33].

The tree of the alanyl-aspartyl motif conservation was constructed on the basis of the 16S and 23S RNA. Sequences were recovered for each organism listed from KEGG[34,35,36] and aligned separately using Clustal Omega v.1.2.4 (refs. [24,25,26]). The aligned sequences were then curated with Gblocks v.0.91b[37,38] and concatenated. The best model was then determined using jModeltest v.2.1 (ref. [39]). The phylogeny analysis was performed using PhyML v.3.0 (refs. [30,31]) primed with BIONJ[32], and 100 bootstraps were performed. Visualization and tree annotation were performed using iTOL[33].

Homology search and alignment

B. abortus OMPs homologues were searched using BLAST with the DELTA-BLAST[40,41,42] algorithm and an expected threshold of 10^{-5}. Signal peptides were then predicted using the SignalP 4.1 Server[27] and removed. Mature sequences were aligned using Clustal Omega[25] and viewed using Jalview v.2.10.5 (ref. [43]) to determine the consensus sequence. Protein sequences annotated as auto-transporter were manually removed.

Reporting Summary

Further information on research design is available in the Nature Research Reporting Summary linked to this article.

Data availability

All data are available at Figshare (https://doi.org/10.6084/m9.figshare.c.5087120) and raw MS data were deposited at the ProteomeXchange Consortium through the PRIDE[44] partner repository with the dataset identifier PXD019023. Source data are provided with this paper.

Code availability

The ImageJ script written for periplasm measurement is available on GitHub (https://github.com/pgodessa/PeriSizer).

1.1.2.4 References

1. Asmar, A. T. & Collet, J. F. Lpp, the Braun lipoprotein, turns 50—major achievements and remaining issues. *FEMS Microbiol. Lett.* **365**, fny199 (2018).
2. Suzuki, H. et al. Murein-lipoprotein of *Escherichia coli*: a protein involved in the stabilization of bacterial cell envelope. *Mol. Gen. Genet.* **167**, 1–9 (1978).
3. Asmar, A. T. et al. Communication across the bacterial cell envelope depends on the size of the periplasm. *PLoS Biol.* **15**, e2004303 (2017).
4. Cohen, E. J., Ferreira, J. L., Ladinsky, M. S., Beeby, M. & Hughes, K. T. Nanoscale-length control of the flagellar driveshaft requires hitting the tethered outer membrane. *Science* **356**, 197–200 (2017).
5. Diao, J. et al. Peptidoglycan association of murein lipoprotein is required for KpsD-dependent group 2 capsular polysaccharide expression and serum resistance in a uropathogenic *Escherichia coli* Isolate. *mBio* **8**, e00603-17 (2017).
6. Moreno, E. & Moriyon, I. in *The Prokaryotes* Vol. 5 (Dworkin, M. et al.) Ch. 3.1.16, 315–456 (Springer, 2006).
7. Halim, A. et al. Assignment of saccharide identities through analysis of oxoniumion fragmentation profiles in LC–MS/MS of glycopeptides. *J. Proteome Res.* **13**, 6024–6032 (2014).
8. Magnet, S. et al. Identification of the l,d-transpeptidases responsible for attachment of the Braun lipoprotein to *Escherichia coli* peptidoglycan. *J. Bacteriol.* **189**, 3927–3931 (2007).
9. Mainardi, J. L. et al. A novel peptidoglycan cross-linking enzyme for a β-lactam-resistant transpeptidation pathway. *J. Biol. Chem.* **280**, 38146–38152 (2005).
10. Braun, V. & Bosch, V. Sequence of the murein-lipoprotein and the attachment site of the lipid. *Eur. J. Biochem.* **28**, 51–69 (1972).
11. Gamazo, C. & Moriyon, I. Release of outer membrane fragments by exponentially growing *Brucella melitensis* cells. *Infect. Immun.* **55**, 609–615 (1987).
12. Sandoz, K. M. et al. *Nat. Microbiol.* https://doi.org/10.1038/s41564-020-00798-4 (2020).
13. Deghelt, M. et al. G1-arrested newborn cells are the predominant infectious form of the pathogen *Brucella abortus*. *Nat. Commun.* **5**, 4366 (2014).
14. Moriyon, I. & Berman, D. T. Isolation, purification, and partial characterization of *Brucella abortus* matrix protein. *Infect. Immun.* **39**, 394–402 (1983).
15. Wheeler, R., Mesnage, S., Boneca, I. G., Hobbs, J. K. & Foster, S. J. Super-resolution microscopy reveals cell wall dynamics and peptidoglycan architecture in ovococcal bacteria. *Mol. Microbiol.* **82**, 1096–1109 (2011).

16. Keller, A., Nesvizhskii, A. I., Kolker, E. & Aebersold, R. Empirical statistical model to estimate the accuracy of peptide identifications made by MS/MS and database search. *Anal. Chem.* **74**, 5383–5392 (2012).
17. Nesvizhskii, A. I., Keller, A., Kolker, E. & Aebersold, R. A statistical model for identifying proteins by tandem mass spectrometry. *Anal. Chem.* **75**, 4646–4658 (2003).
18. Peters, K. et al. Copper inhibits peptidoglycan LD-transpeptidases suppressing β-lactam resistance due to bypass of penicillin-binding proteins. *Proc. Natl Acad. Sci. USA* **115**, 10786–10791 (2018).
19. Schindelin, J. et al. Fiji: an open-source platform for biological-image analysis. *Nat. Methods* **9**, 676–682 (2012).
20. Ducret, A., Quardokus, E. M. & Brun, Y. V. MicrobeJ, a tool for high throughput bacterial cell detection and quantitative analysis. *Nat. Microbiol.* **1**, 16077 (2016).
21. Herrou, J. et al. Periplasmic protein EipA determines envelope stress resistance and virulence in *Brucella abortus*. *Mol. Microbiol.* **111**, 637–661 (2019).
22. Zheng, S. Q. et al. MotionCor2: anisotropic correction of beam-induced motion for improved cryo-electron microscopy. *Nat. Methods* **14**, 331–332 (2017).
23. Rohou, A. & Grigorieff, N. CTFFIND4: fast and accurate defocus estimation from electron micrographs. *J. Struct. Biol.* **192**, 216–221 (2015).
24. Goujon, M. et al. A new bioinformatics analysis tools framework at EMBL-EBI. *Nucleic Acids Res.* **38**, W695–W699 (2010).
25. Li, W. et al. The EMBL-EBI bioinformatics web and programmatic tools framework. *Nucleic Acids Res.* **43**, W580–W584 (2015).
26. McWilliam, H. et al. Analysis tool web services from the EMBL-EBI. *Nucleic Acids Res.* **41**, W597–W600 (2013).
27. Petersen, T. N., Brunak, S., von Heijne, G. & Nielsen, H. SignalP 4.0: discriminating signal peptides from transmembrane regions. *Nat. Methods* **8**, 785–786 (2011).
28. Capella-Gutierrez, S., Silla-Martinez, J. M. & Gabaldon, T. trimAl: a tool for automated alignment trimming in large-scale phylogenetic analyses. *Bioinformatics* **25**, 1972–1973 (2009).
29. Lefort, V., Longueville, J. E. & Gascuel, O. SMS: smart model selection in PhyML. *Mol. Biol. Evol.* **34**, 2422–2424 (2017).
30. Guindon, S. et al. New algorithms and methods to estimate maximum-likelihood phylogenies: assessing the performance of PhyML 3.0. *Syst. Biol.* **59**, 307–321 (2010).
31. Guindon, S. & Gascuel, O. A simple, fast, and accurate algorithm to estimate large phylogenies by maximum likelihood. *Syst. Biol.* **52**, 696–704 (2003).
32. Gascuel, O. BIONJ: an improved version of the NJ algorithm based on a simple model of sequence data. *Mol. Biol. Evol.* **14**, 685–695 (1997).
33. Letunic, I. & Bork, P. Interactive Tree Of Life (iTOL) v4: recent updates and new developments. *Nucleic Acids Res.* **47**, W256–W259 (2019).
34. Kanehisa, M. Toward understanding the origin and evolution of cellular organisms. *Protein Sci.* **28**, 1947–1951 (2019).

35. Kanehisa, M. & Goto, S. KEGG: Kyoto Encyclopedia of Genes and Genomes.*Nucleic Acids Res.* **28**, 27–30 (2000).
36. Kanehisa, M., Sato, Y., Furumichi, M., Morishima, K. & Tanabe, M. New approach for understanding genome variations in KEGG. *Nucleic Acids Res.* **47**, D590–D595 (2019).
37. Dereeper, A. et al. Phylogeny.fr: robust phylogenetic analysis for the non-specialist. *Nucleic Acids Res.* **36**, W465–W469 (2008).
38. Castresana, J. Selection of conserved blocks from multiple alignments for their use in phylogenetic analysis. *Mol. Biol. Evol.* **17**, 540–552 (2000).
39. Darriba, D., Taboada, G. L., Doallo, R. & Posada, D. jModelTest 2: more models, new heuristics and parallel computing. *Nat. Methods* **9**, 772 (2012).
40. Altschul, S. F. et al. Gapped BLAST and PSI-BLAST: a new generation of protein database search programs. *Nucleic Acids Res.* **25**, 3389–3402 (1997).
41. Boratyn, G. M. et al. Domain enhanced lookup time accelerated BLAST. *Biol. Direct* **7**, 12 (2012).
42. Schaffer, A. A. et al. Improving the accuracy of PSI-BLAST protein database searches with composition-based statistics and other refinements. *Nucleic Acids Res.* **29**, 2994–3005 (2001).
43. Waterhouse, A. M., Procter, J. B., Martin, D. M., Clamp, M. & Barton, G. J. Jalview version 2—a multiple sequence alignment editor and analysis workbench. *Bioinformatics* **25**, 1189–1191 (2009).
44. Perez-Riverol, Y. et al. The PRIDE database and related tools and resources in 2019: improving support for quantification data. *Nucleic Acids Res.* **47**, D442–D450 (2019).
45. Roy, A., Kucukural, A. & Zhang, Y. I-TASSER: a unified platform for automated protein structure and function prediction. *Nat. Protoc.* **5**, 725–738 (2010).
46. Yang, J. et al. The I-TASSER Suite: protein structure and function prediction. *Nat. Methods* **12**, 7–8 (2015).
47. Zhang, Y. I-TASSER server for protein 3D structure prediction. *BMC Bioinform.* **9**, 40 (2008).

Acknowledgements

We thank the members of the URBM for their discussions of the data; F. Tilquin and M. Waroquier for their logistic support; P. Cherry and C. Servais for their help with this project; V. Vassen for the *B. abortus* strains; C. Demazy for the MS sample preparation; I. Moriyon for his insights and ideas; S. Gillet for his help and knowledge regarding the script; S. Mesnage for sharing the amidase expression vector, M. Boutry for the *A. tumefaciens* strain and A. Asmar for the Lpp antibody; A. Cehovin and E. Lawarée for their reading of the manuscript; and staff at UNamur (https://www.unamur.be/) for financial and logistical support. P.G. was supported by a FRIA PhD fellowship. S.E.V.d.V. is supported by a FWO PhD fellowship. This work was funded by the Fédération Wallonie-

Bruxelles (no. ARC 17/22-087), and by the FRS-FNRS (nos. PDR T.0060.15 and T.0058.20).

Author information

Contributions

A.L. conducted PG extraction of *A. tumefaciens*. M.D. and P.R. performed the MS analysis. S.E.V.d.V. and H.R. performed the EM sample preparation and image acquisition. P.G. performed all of the other experiments. P.S. contributed to the initial conception of the work. P.G. and X.D.B. designed the experiments. P.G., X.D.B. and J.-F.C. wrote the manuscript.

1.1.2.5 Extended data

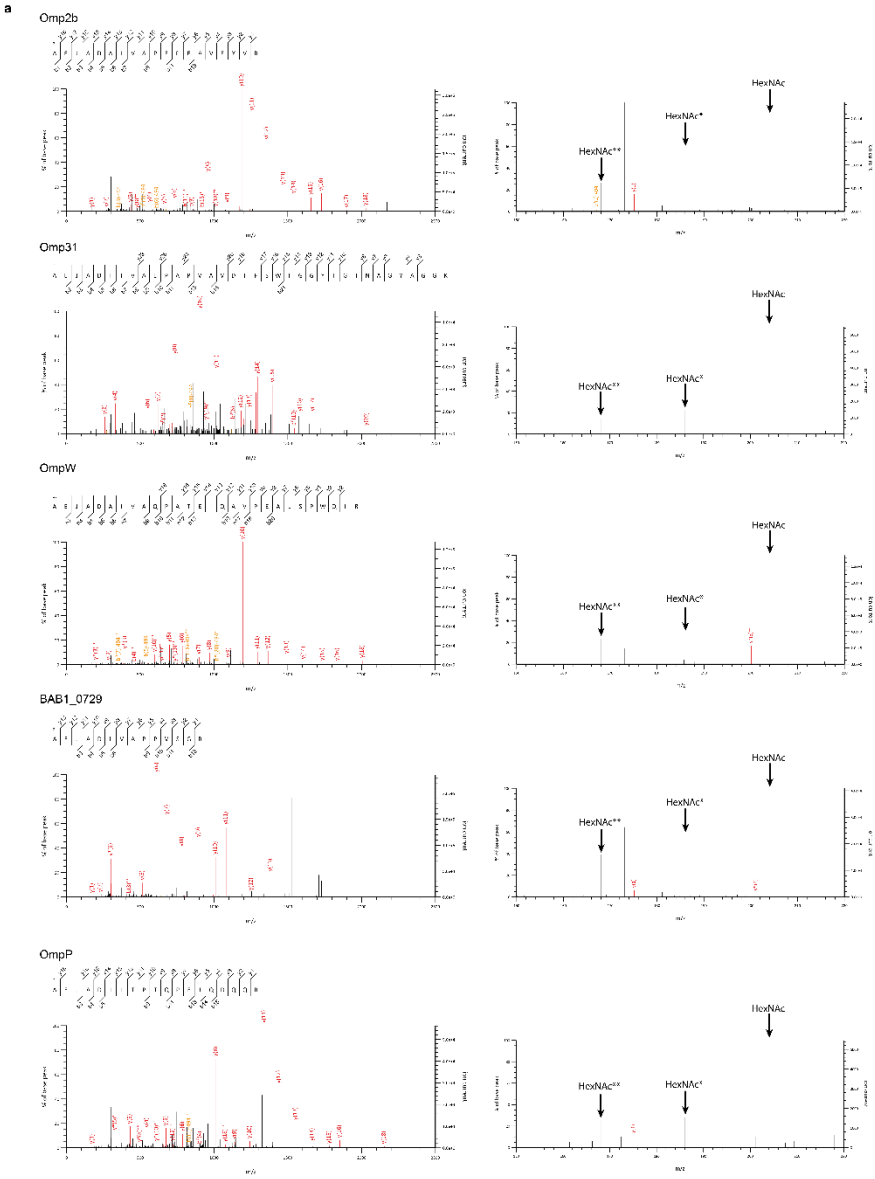

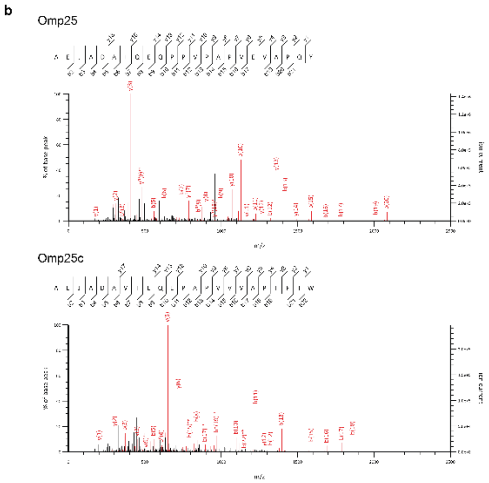

Extended Data Fig. 1 | MS-MS fragmentation spectra of OMPs N-terminal peptides. a, Left panel, spectra obtained for Omp2b/31/W/P and BAB1_0729 from the analysis of lysozyme treated samples. PG disaccharide (NAG-NAM) modifications are indicated by « GL » on the sequence. Right panel, enlargement of the left spectra from 150 to 220 M/Z ratio. Glycosylation of peptides is confirmed by the presence of saccharide oxonium ions: HexNAc, $[C_8H_{14}NO_5]^+$ with a mass of 204.087; HexNAc*, HexNAc – H_2O, $[C_8H_{12}NO_4]^+$ with a mass of 186.076 and HexNAc**, HexNAc – 2 H_2O, $[C_8H_{10}NO_3]^+$ with a mass of 168.066. J corresponds to *m*DAP. **b**, Fragmentation spectra of the N-terminal peptides of Omp25 and 25c were obtained upon treatment with the amidase. The absence of glycosylation is due to the amidase activity.

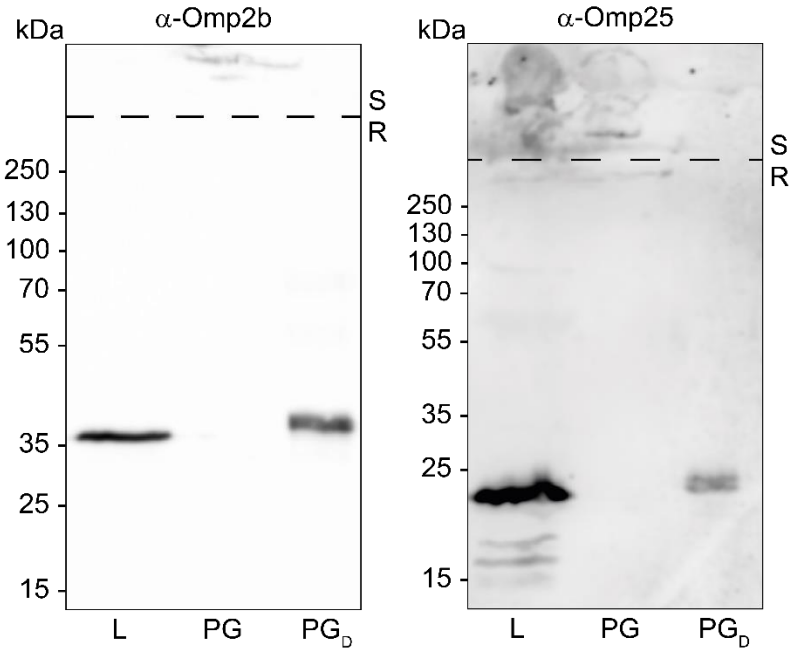

Extended Data Fig. 2 | Peptidoglycan binding induces a shift in the migration of Omp2b and Omp25 in Western blot. Upon digestion of purified *B. abortus* peptidoglycan with lysozyme, an apparent heavier weight is observed for Omp2b (left) and Omp25 (right) compared to the signal obtained with a lysate. A signal is observed in the stacking gel when the purified peptidoglycan is undigested. S, stacking gel; R, running gel; L, lysate; PG, peptidoglycan; PG$_D$, lysozyme-digested peptidoglycan. This experiment was not repeated. The shift induced by the PG binding is consistently observed in Fig. 3b.

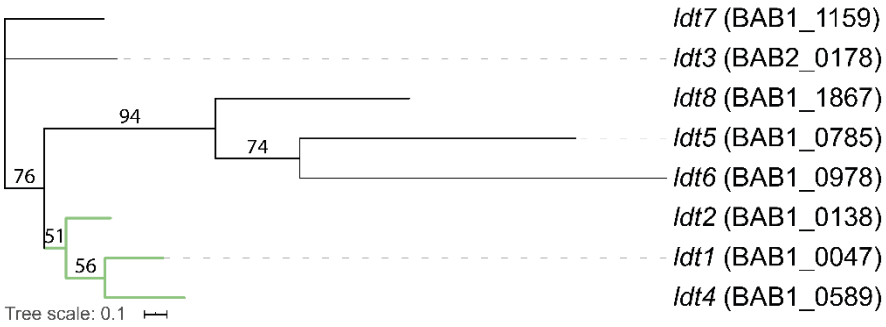

Extended Data Fig. 3 | Ldt1, Ldt2 and Ldt4 form a monophyletic cluster. Bootstrap values are represented above branches.

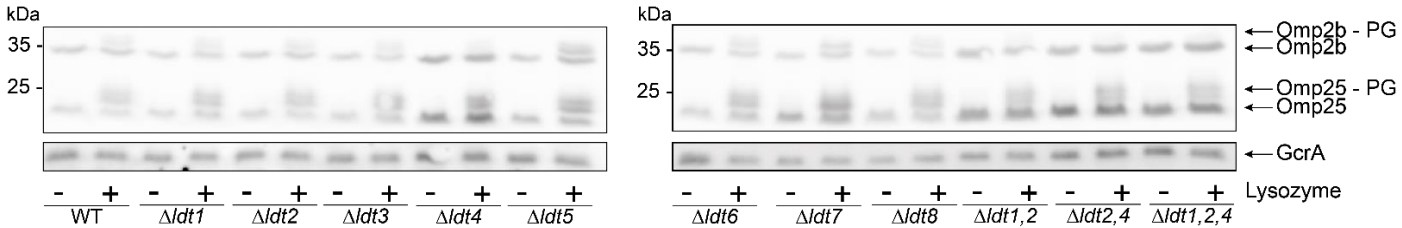

Extended Data Fig. 4 Ldt4 has an impact on the linkage of Omp25 and Omp2b. Effect of the deletion of the eight *ldt* genes in *B. abortus*. The *ldt4* strain and derivatives (Δ*ldt1,4*, Δ*ldt2,4* and Δ*ldt1,2,4*) have a noticeable effect on the linkage of Omp25 and Omp2b. An increased signal corresponding to the free form of both OMPs is observed in these strains. GcrA was used as loading control.

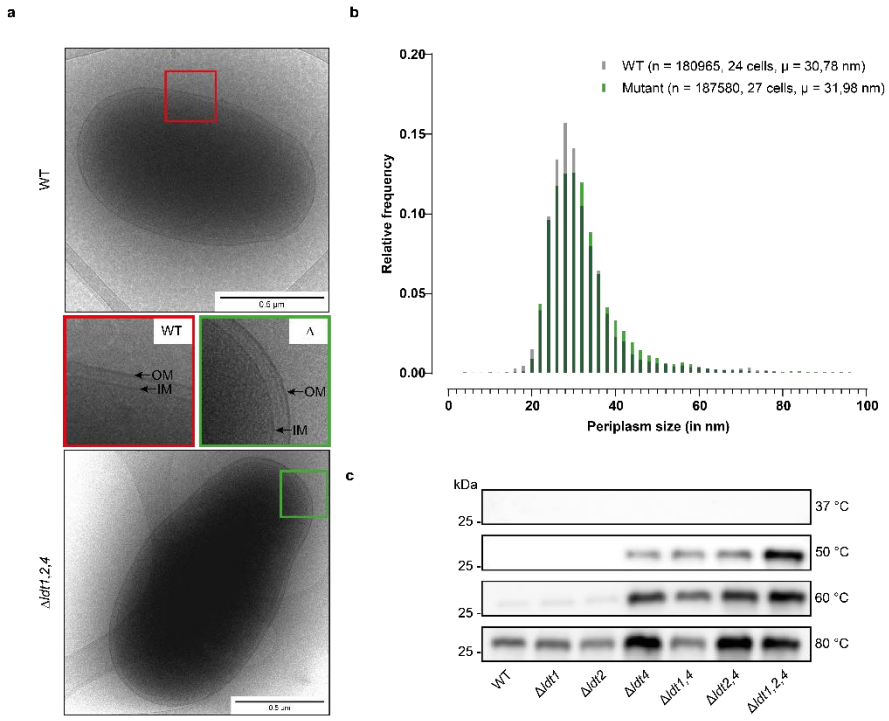

Extended Data Fig. 5 | Δ*ldt1,2,4* has no phenotype defect under normal growth conditions but is more sensitive to heat. a, Cryo-EM imaging of WT and Δ*ldt1,2,4* strains (« Δ »). No obvious defect can be seen between both strains. Enlarged portion delimited with coloured squares is shown in detail with the same colour code. Images were acquired with a defocus in the range of −7 to −10 µm. IM, inner membrane; OM, outer membrane. **b**, Comparison of the periplasm size distribution between the WT and the Δ*ldt1,2,4* strains. From 3 biological replicates, 24 cells were used and 180,965 measures were taken for the WT strain and 187,580 measures were obtained from 27 cells for the mutant. No significant difference was observed in the periplasm size between both strains. **c** Heat-stressed *ldt1* and *ldt2* strains have a WT-like phenotype for the release of Omp25 in culture supernatant. These results support the previous observations that Ldt1 and Ldt2 do not seem to have a major role in the OMP anchorage under normal growth conditions. This experiment is representative of 2 biologically independent replicates.

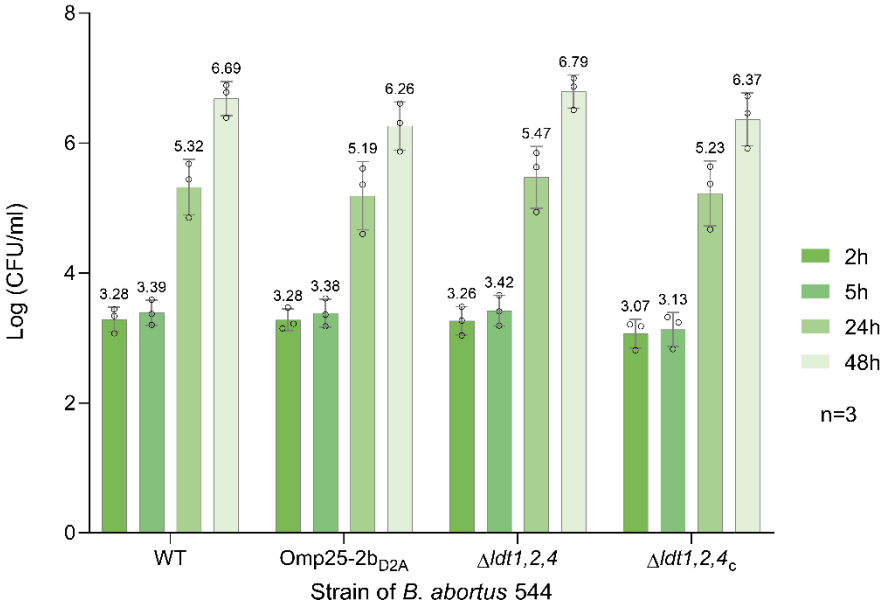

Extended Data Fig. 6 | Infectivity is not impacted in the Omp25-2b$_{D2A}$ or Δ*ldt1,2,4* strains. Murine RAW 264.7 macrophages were infected with *Brucella abortus* 544 WT, Omp25-2b$_{D2A}$, Δ*ldt1,2,4* or Δ*ldt1,2,4*c strains. Entry was assessed at 2 h post-infection (PI), survival at 5 h PI and replication at 24 h and 48 h PI. No difference was observed between the WT and the mutants. n = 3 biologically independent experiments, error bars, mean ± s.d.

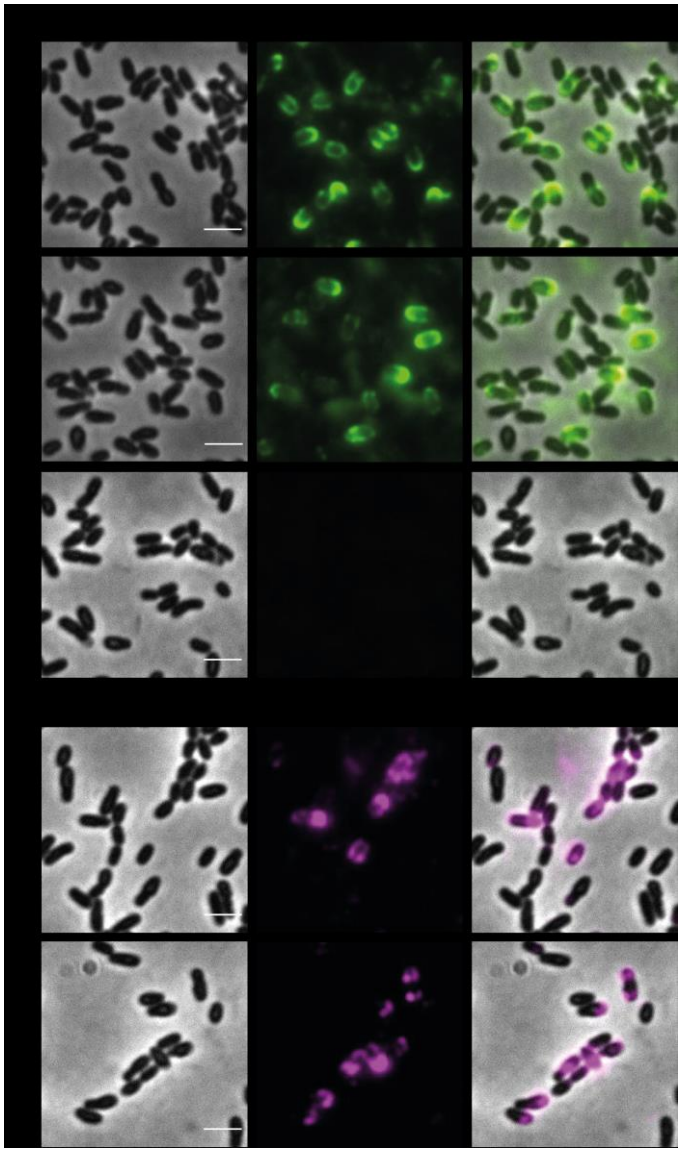

Extended Data Fig. 7 | Omp25$_{D2A}$ and Omp2b$_{D2A}$ are exported in the OM and detectable on the surface. a, Immunolabelling of Omp25 on the WT, *omp25*$_{D2A}$ and Δ*omp25* strains. A signal similar to the WT is observed in the *omp25*$_{D2A}$, suggesting a normal export of Omp25 and insertion at the OM. **b**, Immunolabelling of Omp2b on the WT and *omp2b*$_{D2A}$ strains. As for Omp25$_{D2A}$, Omp2b$_{D2A}$ is detectable on the bacterial surface. Scale bar is 2 μm.

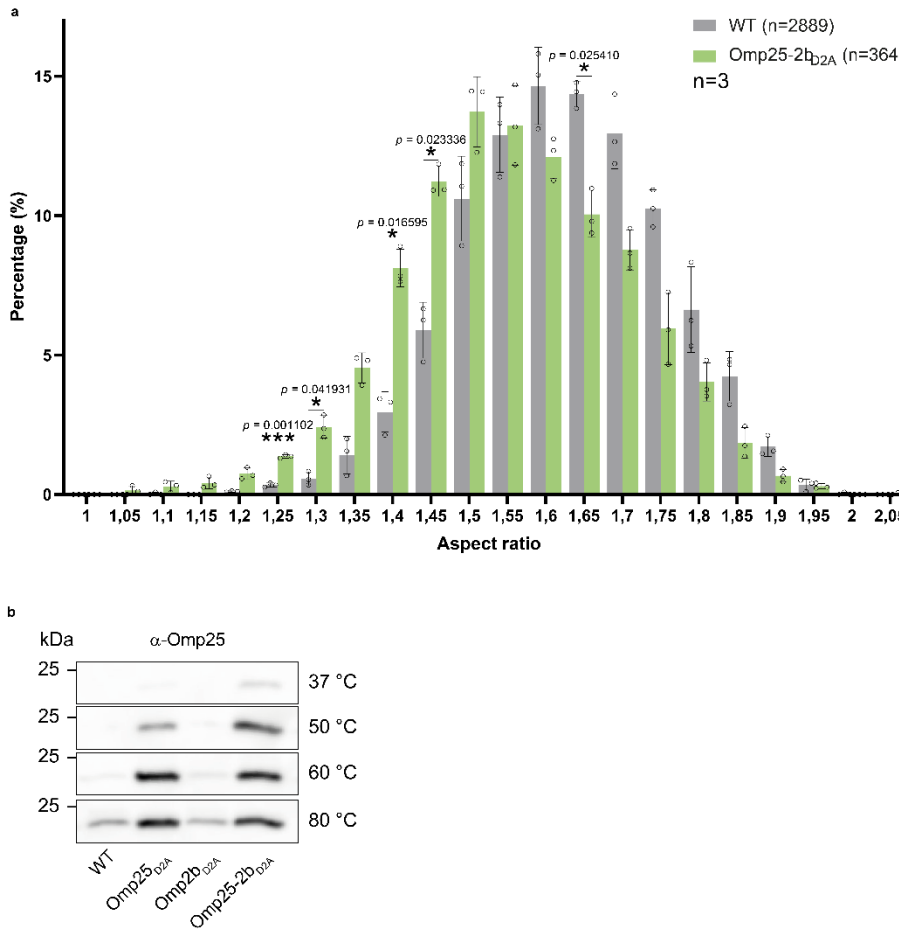

Extended Data Fig. 8 | Omp25-2b$_{D2A}$ strain has an envelope defect. a, The aspect ratio (major axis/minor axis) of both the WT and the Omp25-2b$_{D2A}$ strains was calculated and sorted according to their frequency. A shift of the distribution towards lower aspect ratios is observed for the mutant strains reflecting rounder cell shape. Statistical significance was determined using two-tailed unpaired *t*-tests with the Holm-Sidak method (with P<0.05), n = 2889 for WT and 3644 for Omp25-2b$_{D2A}$ strains cells examined over 3 independent experiments, error bars, mean ± s.d. **b**, Western blot analysis of the WT and D2A OMPs strains supernatants after incubation at different temperatures. The Omp25-2b$_{D2A}$ already release Omp25 at growth temperature indicating an outer-membrane instability.

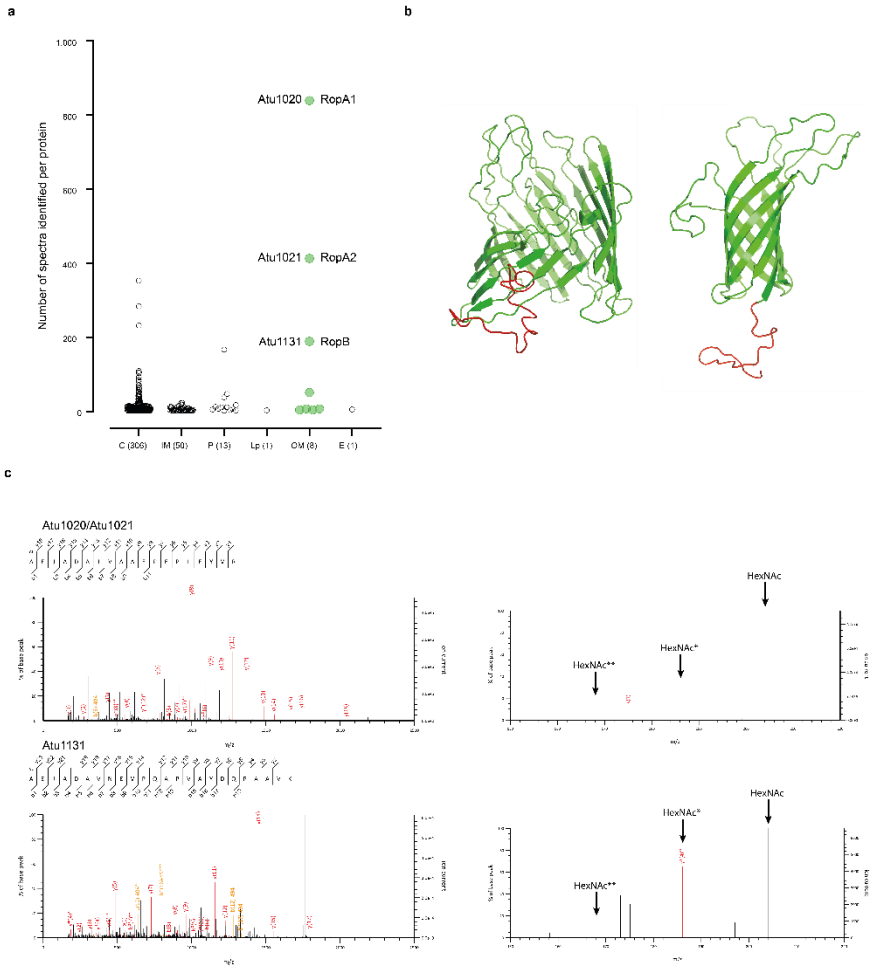

Extended Data Fig. 9 | *Agrobacterium tumefaciens* has a similar structure for the OMP-PG link to that of *B. abortus*. **a**, Classification of the 379 proteins isolated with PG and identified in mass spectrometry according to the number of spectra per protein and their subcellular localisation. Numbers in brackets correspond to the number of proteins predicted per subcellular localisation. C, Cytoplasmic; IM, Inner Membrane; P, Periplasmic; OM, Outer Membrane; E, extracellular. **b**, Three-dimensional predicted structure of the two predominant protein (Atu1020/1021, left; Atu1131, right) identified by mass spectrometry. Prediction were made using protein sequences without signal peptides and the I-TASSER server[44,45,46], and displayed with PyMol v.2.0. **c**, Spectra obtained for Atu1020/1021 and Atu1131 upon analysis of lysozyme treated samples. PG disaccharide (NAG-NAM) modifications are indicated by « GL » on the sequence. Glycosylation of peptides is confirmed by the presence of saccharide oxonium ions on the enlargement of the left spectra from 150 to 220 M/Z ratio. Glycosylation of peptides is confirmed by the

presence of saccharide oxonium ions: HexNAc, $[C_8H_{14}NO_5]^+$ with a mass of 204.087; HexNAc*, HexNAc – H_2O, $[C_8H_{12}NO_4]^+$ with a mass of 186.076 and HexNAc**, HexNAc – 2 H_2O, $[C_8H_{10}NO_3]^+$ with a mass of 168.066. J corresponds to *m*DAP.

1.1.2.6 Supplementary information

Supplementary Information for

β-barrels covalently link the peptidoglycan in the α-proteobacterium *Brucella abortus*

Pierre GODESSART[1], Adélie LANNOY[1], Marc DIEU[2], Sander E. VAN DER VERREN[3,4], Patrice SOUMILLION[5], Jean-François COLLET[6,7], Han REMAUT[3,4], Patricia RENARD[2,8] and Xavier DE BOLLE[1,*]

[1]Research Unit in Microorganisms Biology (URBM), Namur Research Institute for Life Sciences (NARILIS), UNamur, rue de Bruxelles 61, 5000 Namur, Belgium.

[2]MaSUN, Mass Spectrometry Facility, UNamur, rue de Bruxelles 61, 5000 Namur, Belgium.

[3]Structural & Molecular Microbiology, VIB-VUB Centre for Structural Biology, VIB, Pleinlaan 2, 1050 Brussels, Belgium.

[4]Structural Biology Brussels, Vrije Universiteit Brussel, Pleinlaan 2, 1050 Brussels, Belgium.

[5]LIBST, UCLouvain, Croix du Sud, Bte L7.07.06, 1348 Louvain-la-Neuve, Belgium.

[6]de Duve Institute, Université catholique de Louvain, Avenue Hippocrate 75 – B1.75.08, 1200 Brussels, Belgium.

[7]WELBIO, Avenue Hippocrate 75 – B1.75.08, 1200 Brussels, Belgium.

[8]Laboratory of Biochemistry and Cell Biology (URBC), Namur Research Institute for Life Sciences (NARILIS), UNamur, rue de Bruxelles 61, 5000 Namur, Belgium.

In this file:

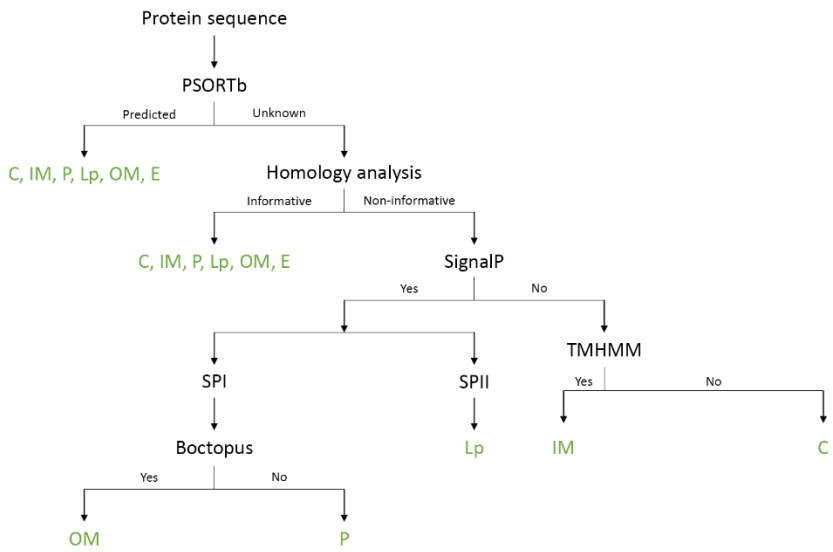

Supplementary Figure S1 | Decisional tree for protein subcellular localisation. The subcellular localisations of proteins identified in mass were determined following this decisional tree. Prediction from sequence, PSORTb v3.0.2[1]; Signal peptide prediction, SignalP-5.0 server[2]; Trans-membrane helix prediction, TMHMM v.2.0[3] and β-barrel prediction, Boctopus 2[4] were used. C, cytoplasmic; IM, inner membrane; P, periplasmic; Lp, lipoprotein; OM, outer membrane; E, extracellular.

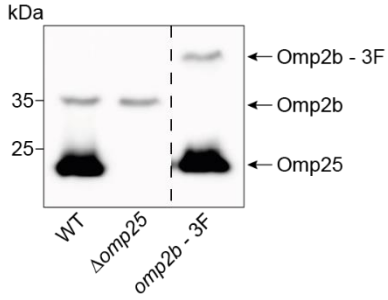

Supplementary Figure S2 | Omp25 and Omp2b monoclonal antibodies specificity. The specificity of the antibodies recognizing the Omp25 and Omp2b in western blotting was shown by using two *B. abortus* mutants: a strain deleted for the Omp25 gene (Δ*omp25*) and, being an essential gene, Omp2b was added a 3Flag (*omp2b* – 3F). No signal can be observed in the absence of the Omp25 (lane 2) and a higher molecular weight is observed for when a 3Flag is added to the Omp2b (lane 3). This experiment was done once.

Supplementary information Table 1 | List of strains used in this study

Name	Description and relevant genotype	Reference
	Brucella abortus	
Wild type (WT)	*B. abortus* 544, Nal^R	J.-M. Verger, INRA, Tours, FR
Δomp25	*B. abortus* 544 Δ*omp25*	Vassen *et al.,* 2019[5]
Δ*ldt1*	*B. abortus* 544 Δ*BAB1_0047*	This study
Δ*ldt2*	*B. abortus* 544 Δ*BAB1_0138*	This study
Δ*ldt3*	*B. abortus* 544 Δ*BAB2_0178*	This study
Δ*ldt4*	*B. abortus* 544 Δ*BAB1_0589*	This study
Δ*ldt5*	*B. abortus* 544 Δ*BAB1_0785*	This study
Δ*ldt6*	*B. abortus* 544 Δ*BAB1_0978*	This study
Δ*ldt7*	*B. abortus* 544 Δ*BAB1_1159*	This study
Δ*ldt8*	*B. abortus* 544 Δ*BAB1_1837*	This study
Δ*ldt1,4*	*B. abortus* 544 Δ*BAB1_0047* Δ*BAB1_0589*	This study
Δ*ldt2,4*	*B. abortus* 544 Δ*BAB1_0138* Δ*BAB1_0589*	This study
Δ*ldt1,2,4*	*B. abortus* 544 Δ*BAB1_0047* Δ*BAB1_0138* Δ*BAB1_0589*	This study
Δ*BAB1_2034*	*B. abortus* 544 Δ*BAB1_2034*	This study
$\Delta ldt4_c$	*B. abortus* 544 Δ*BAB1_0589, BAB1_0589::pBBR1*	This study
$\Delta ldt1,2,4_c$	*B. abortus* 544 Δ*BAB1_0047* Δ*BAB1_0138* Δ*BAB1_0589, BAB1_0589::pBBR1*	This study
$omp25_{D2A}$	*B. abortus* 544 *Omp25D2A*	This study
$omp2b_{D2A}$	*B. abortus* 544 *Omp2bD2A*	This study
$omp25\text{-}2b_{D2A}$	*B. abortus* 544 *Omp25-2bD2A*	This study
Omp2b-3F	*B. abortus* 544 *Omp2b*-3F	V. Vassen PhD thesis, UNamur, BE

	Escherichia coli	
DH10B	F- endA1 recA1 galE15 galK16 nupG rpsL ΔlacX74 Φ80lacZΔM15 araD139 Δ(ara,leu)7697 mcrA Δ(mrr-hsdRMS- mcrBC) λ	Invitrogen
S17-1	M294::RP4-2 (Tc::Mu)(Km::Tn7)	Simon *et al*., 1983[6]
omp25, ldt1	*E. coli* DH10B *Omp25*::pBBR MCS1, *ldt1*::pNPTS138	This study
omp25, ldt2	*E. coli* DH10B *Omp25*::pBBR MCS1, *ldt2*::pNPTS138	This study
omp25, ldt3	*E. coli* DH10B *Omp25*::pBBR MCS1, *ldt3*::pNPTS138	This study
omp25, ldt4	*E. coli* DH10B *Omp25*::pBBR MCS1, *ldt4*::pNPTS138	This study
omp25, ldt5	*E. coli* DH10B *Omp25*::pBBR MCS1, *ldt5*::pNPTS138	This study
omp25, ldt6	*E. coli* DH10B *Omp25*::pBBR MCS1, *ldt6*::pNPTS138	This study
omp25, ldt7	*E. coli* DH10B *Omp25*::pBBR MCS1, *ldt7*::pNPTS138	This study
omp25, ldt8	*E. coli* DH10B *Omp25*::pBBR MCS1, *ldt8*::pNPTS138	This study

Supplementary information Table 2 | List pf plasmids used in this study

Description	Reference
pNPTS138	M. R. K. Alley, Imperial College of Science, UK
pNPTS138_ΔLdt1	This study
pNPTS138_ΔLdt2	This study
pNPTS138_ΔLdt3	This study
pNPTS138_ΔLdt4	This study
pNPTS138_ΔLdt5	This study
pNPTS138_ΔLdt6	This study
pNPTS138_ΔLdt7	This study
pNPTS138_ΔLdt8	This study
pBBR1_Ldt4	This study
pBBR1_Omp25	V. Vassen, PhD thesis, UNamur, BE
pNPTS138_Ldt1	This study
pNPTS138_Ldt2	This study
pNPTS138_Ldt3	This study
pNPTS138_Ldt4	This study
pNPTS138_Ldt5	This study
pNPTS138_Ldt6	This study
pNPTS138_Ldt7	This study
pNPTS138_Ldt8	This study
pNPTS_Omp25$_{D2A}$	This study
pNPTS_Omp2b$_{D2A}$	This study
pBBR MCS1	Elzer *et al.*, 1995[7]

Supplementary information Table 3 | List of ORFs used in this study.

Gene	ORF #	Accession number*
omp25	BAB1_0722	Q2YN33
omp2b	BAB1_0660	Q2YMY7
ldt1	BAB1_0047	Q2YPP6
ldt2	BAB1_0138	Q2YNZ6
ldt3	BAB2_0178	KFJ50266.1
ldt4	BAB1_0589	Q2YMR8
ldt5	BAB1_0785	Q2YN97
ldt6	BAB1_0978	AIN90423.1
ldt7	BAB1_1159	KFJ54317.1
ldt8	BAB1_1867	KFJ51593.1

* Uniprot acession number available, NCBI otherwise.

Supplementary information Table 4 | List of primers used in this study.
Bold characters represents bases that do not hybridize on DNA template.

Primer	Sequence
Ldt47_UP_F	agtgctggcgcaattgatcttca
Ldt47_UP_R	**ggctccacat**ataaatctcctaagaaattgctgtcaaa
Ldt47_DW_F	**ggagatttat**atgtggagcctcaaccgagaa
Ldt47_DW_R	tctcaggcatgcagaatcaggat
Ldt138_UP_F	aggatttgatttccacgatccagat
Ldt138_UP_R	**attccgtcga**gtatccccccaatcaagtggattc
Ldt138_DW_F	**ggggggatac**tcgacggaatgaaaaaggccg
Ldt138_DW_R	ttcggctatgatttcatcaccgtca
Ldt589_UP_F	atatggtgaagaaatacaagacctcgct
Ldt589_UP_R	**tgccctaaac**atgaaaaccagattgatgatgggagag
Ldt589_DW_F	**tggttttcat**gtttagggcagtagggctgta
Ldt589_DW_R	tctggaccgtgattctgcttttg
Ldt785_UP_F	agggcaatgaaatcgccaatca
Ldt785_UP_R	**tttgacgcaa**ttgattaacgtcccaaaaggctaa
Ldt785_DW_F	**cgttaatcaa**ttgcgtcaaaaaccacctgttgc
Ldt785_DW_R	aagcttcttggcgcgttcga
Ldt978_UP_F	aagctggagcttcaaggcatattc
Ldt978_UP_R	**gcactccagt**cgtcacgcgctgctgaac
Ldt978_DW_F	**gcgcgtgacg**actggagtgcggttgcaac
Ldt978_DW_R	aagccaatctcatcgccctgt
Ldt1159_UP_F	acatcgctgctgcttggcataa
Ldt1159_UP_R	**attcccggtg**cacgagcggaaaatacctgc
Ldt1159_DW_F	**cgctcgtgca**ccgggaattcctgtatgggatc
Ldt1159_DW_R	tcgtaatggcccagatcgaggt
Ldt1867_UP_F	taggctgtagtggcgaattaacttgt
Ldt1867_UP_R	**gccccggaaa**cgtgacccggcgtccatatg
Ldt1867_DW_F	**ccgggtcacg**tttccggggctttatcccgaa
Ldt1867_DW_R	tgggctatacccggatgcatac
Ldt178_UP_F	gtcataggtggcaatgcgatgaaa
Ldt178_UP_R	**taaaggtcgg**ggttttgatccgtctatctttgcgc
Ldt178_DW_F	**gatcaaaacc**ccgacctttacgaacgcacac
Ldt178_DW_R	aaccgttgatcgccttgcc
Ldt_47_Out_F	cacggtggacgatctcaacatc
Ldt_47_Out_R	tgcgcgcctttcctttcg
Ldt_138_Out_F	acaggatgaagccgcattcct

Ldt_138_Out_R	aagtttctccccggcaaggt
Ldt_178_Out_F	accagaaataggcggcaagc
Ldt_178_Out_R	tcagatagagatccacatagtcggtg
Ldt_589_Out_F	aaggccctgaaggatcgtg
Ldt_589_Out_R	ggtgtaccatccatggtgcag
Ldt_785_Out_F	catccaccatcagcgttccc
Ldt_785_Out_R	gattcatctggctgccggaat
Ldt_978_Out_F	cttcgccaagagggaaaagatcg
Ldt_978_Out_R	agctcgaagggcgcgtag
Ldt_1159_Out_F	atcgtgctggcgcttgtc
Ldt_1159_Out_R	atgaggaatgacctgaaccgtcg
Ldt_1867_Out_F	acaaacctgcccggcttc
Ldt_1867_Out_R	cgccaagcagttcctgctg
0047_F	acggtggacgatctcaacatc
0047_R	tggcgtatgaagaacagattcaactg
0138_F	attccggccatttgtggtcc
0138_R	tgcagcaggtcgaacagatct
0178_F	tccacatcgctttcgtcataggt
0178_R	tctttccttgcaggaaattcggat
0589_F	agacctcgcttgcggtctat
0589_R	tctagagcgcatcccgaaaagt
0785_F	atgaaatcgccaatcaggtcgc
0785_R	tatcacacttgagtaggcaaggc
0978_F	aacccggaagctggagct
0978_R	tgcgcattcgggaagagaatc
1159_F	atcggtttctttgccacatcgc
1159_R	attccaacctcttaatacccgcg
1876_F	atcgcaagatcaccttgcagc
1876_R	tcaacagcgacgaaaacggt
25_D2A_UP_F	ttgcaaccatgcgggcttc
25_D2A_UP_R	**cggaggctgt**tcctggatggca**gc**ggca
25_D2A_DW_F	**ccatccagga**acagcctccggttccggc
25_D2A_DW_R	caaaggatttcaggcatccggta
Omp2b_D2A_UP_F	cgaacacataaagatttgctgggatatt
Omp2b_D2A_UP_R	**gggctctggc**gcgacgattgcggcggca
Omp2b_D2A_DW_F	**caatcgtcgc**gccagagcccgaagccgt
Omp2b_D2A_DW_R	cgtagttctgatccggcgtag

Supplementary information Table 5 | List of primary antibodies used in this study

Reference	Target	Type	Species	Application	Reference
A59/5F1/C5	Omp25	Monoclonal	Mouse	WB	Cloeckaert *et al*., 1992[8,9]
A68/4B10/F5	Omp25	Monoclonal	Mouse (IgG2a)	IF	Cloeckaert *et al*., 1992[8,9]
A63/3H2/B1	Omp2b	Monoclonal	Mouse (IgG1)	WB	Letesson *et al*., 1997[10]
A68/25G5/A5	Omp2b	Monoclonal	Mouse (IgG2a)	IF	Cloeckaert *et al*., 1990[11]
290.S3	GcrA	Polyclonal	Rabbit	WB	Poncin *et al.*, 2019[12]
N/A	Lpp	Polyclonal	Lapin	WB	This study

Supplementary information Table 6 | List of secondary antibodies used in this study

Target	Conjugate	Application	Reference (#)
Rabbit Ig	HRP	WB	Dako (P0217)
Mouse Ig	HRP	WB	Dako (P0260)
Mouse IgG (H+L)	Alexa Fluor 488	IF	Life technologies (A11001)
Mouse IgG2a	Alexa Fluor 647	IF	Life technologies (A21241)

Supplementary references

1 Yu, N. Y. *et al.* PSORTb 3.0: improved protein subcellular localization prediction with refined localization subcategories and predictive capabilities for all prokaryotes. *Bioinformatics* **26**, 1608-1615, doi:10.1093/bioinformatics/btq249 (2010).

2 Almagro Armenteros, J. J. *et al.* SignalP 5.0 improves signal peptide predictions using deep neural networks. *Nature Biotechnology* **37**, 420-423 (2019).

3 Sonnhammer, E. L., von Heijne, G. & Krogh, A. A hidden Markov model for predicting transmembrane helices in protein sequences. *Proc Int Conf Intell Syst Mol Biol* **6**, 175-182 (1998).

4 Hayat, S., Peters, C., Shu, N., Tsirigos, K. D. & Elofsson, A. Inclusion of dyad-repeat pattern improves topology prediction of transmembrane beta-barrel proteins. *Bioinformatics* **32**, 1571-1573, doi:10.1093/bioinformatics/btw025 (2016).

5 Vassen, V. *et al.* Localized incorporation of outer membrane components in the pathogen *Brucella* abortus. *EMBO J* **38**, doi:10.15252/embj.2018100323 (2019).

6 Simon, R., Priefer, U. & Pühler, A. A Broad Host Range Mobilization System for In Vivo Genetic Engineering: Transposon Mutagenesis in

Gram Negative Bacteria. *Nature Biotechnology* **1**, 784-791, doi:10.1038/nbt1183-784 (1983).
7 Elzer, P. H. *et al.* In vivo and in vitro stability of the broad-host-range cloning vector pBBR1MCS in six *Brucella* species. *Plasmid* **33**, 51-57, doi:10.1006/plas.1995.1006 (1995).
8 Cloeckaert, A., Zygmunt, M. S., De Wergifosse, P., Dubray, G. & Limet, J. N. Demonstration of peptidoglycan-associated *Brucella* outer-membrane proteins by use of monoclonal antibodies. *Journal of General Microbiology* **138**, 1543-1550 (1992).
9 Alena, A. *et al.* A D-amino acid produced by plant-bacteria metabolic crosstalk empowers interspecies competition. *bioRxiv* (2020).
10 Letesson, J. J. *et al.* Humoral immune responses of *Brucella*-infected cattle, sheep, and goats to eight purified recombinant *Brucella* proteins in an indirect enzyme-linked immunosorbent assay. *Clin Diagn Lab Immunol* **4**, 556-564 (1997).
11 Cloeckaert, A., De Wergifosse, P., Dubray, G. & Limet, J. N. Identification of Seven Surface-Exposed *Brucella* Outer Membrane Proteins by Use of Monoclonal Antibodies: Immunogold Labeling for Electron Microscopy and Enzyme-Linked Immunosorbent Assay. *Infection and Immunity* **58**, 3980-3987 (1990).
12 Poncin, K. *et al.* Occurrence and repair of alkylating stress in the intracellular pathogen *Brucella abortus*. *Nat Commun* **10**, 4847, doi:10.1038/s41467-019-12516-8 (2019).

1.2 Additional results

1.2.1 LDts

As stated in the article (see section 1.1.2.2 of the results), eight putative LDts were initially found in *B. abortus* genome and more information about them can be found the supplementary figures 1 and 2. The growth of the eight Δ*ldt* strains was assessed and the profiles are shown in Fig. 11. No growth defect could be observed for any of the mutants. To further characterise the effects of the LDts removal, the strains were observed in microscopy using phase-contrast (Fig. 12). Of the eight mutants, only the Δ*ldt7* showed a clear effect with rounder swollen cells. Because LDts can either be involved in the PG remodelling or the anchorage of OMPs, we then aimed to discriminate between these two categories. With the LDts being able to bypass β-lactam resistance (see section 1.1.2.1.2 of the introduction), we hypothesised that exposing the Δ*ldt* strains to such stress could highlight a growth defect. For this, we chose carbenicillin as an antibiotic and then determined a sub-lethal concentration for *B. abortus* WT strain. Based on the growth curves in TSB (Tryptic Soy Broth) rich medium (Fig. 13A), 16 µg/ml was chosen as the strain can still grow but reaches the stationary phase earlier. Exposing the Δ*ldt* strains revealed that only the Δ*ldt7* was affected during its growth (Fig. 13B). Further experiments with this mutant are described below (see section 1.2.1.1 of the results).

The investigation of LDts described in the manuscript led us to the conclusion that the Ldt1, Ldt2 and Ldt4 are involved in the covalent OMP anchorage to the PG, with Ldt4 being the most important. Nevertheless, the WB performed on the Δ*ldt1,2,4* strain lysate clearly showed that a small amount of OMPs remained anchored to the PG. Hence, we

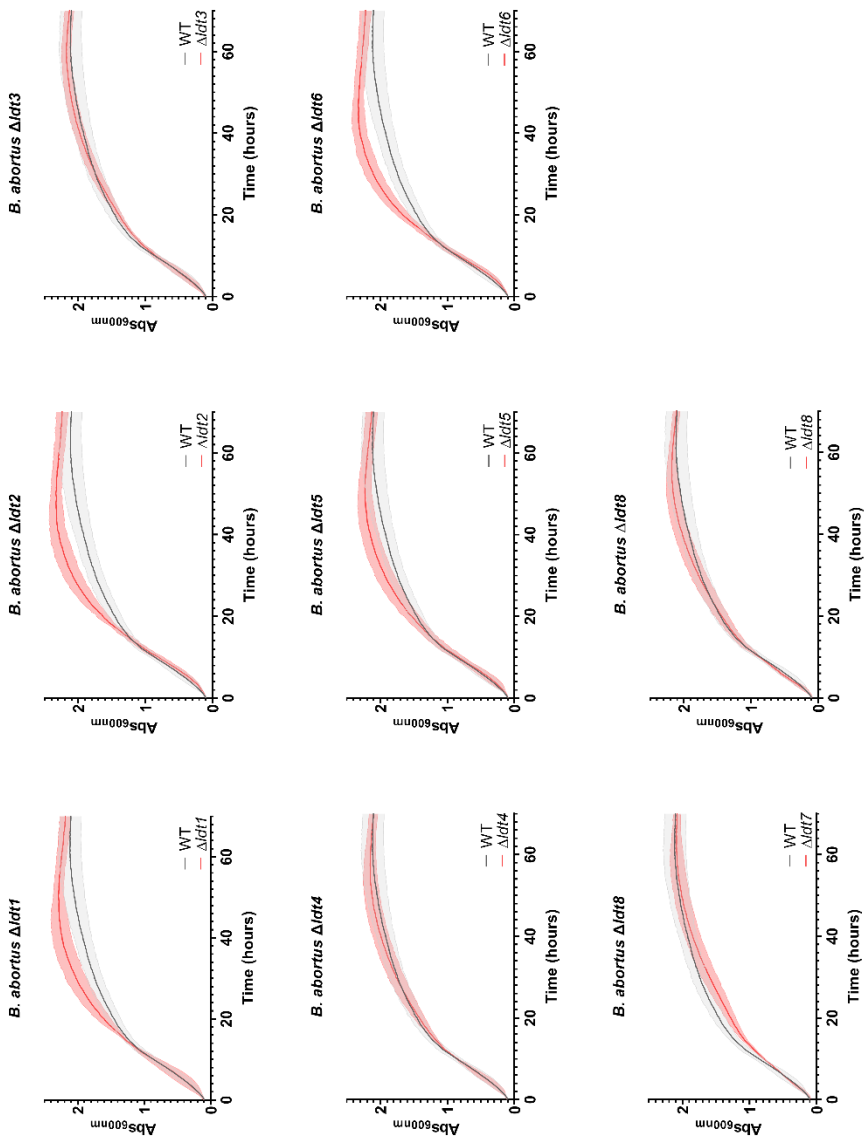

Figure 11 | Growth of the LDt deletion strains. None of the eight single deletion strains (in red) showed a significantly different growth profile compared to *B. abortus* WT (in black).

attempted to identify the other LDts involved. In a Δ*ldt1,2,4* background, we could also remove the *ldt3*, *ldt6*, *ldt7* and *ldt8* gene and the strains generated were all viable with no obvious growth defect on plates. By western blotting, it was observed that some Omp2b and Omp25 remained attached no matter the combination (Fig. 14). However, our attempt at gene deletion remained unsuccessful regarding *ldt5*. Because completely abolishing the anchorage between the OM and the PG might be toxic, we decided to use a CRSIPRi approach (see section 2.1 of the results).

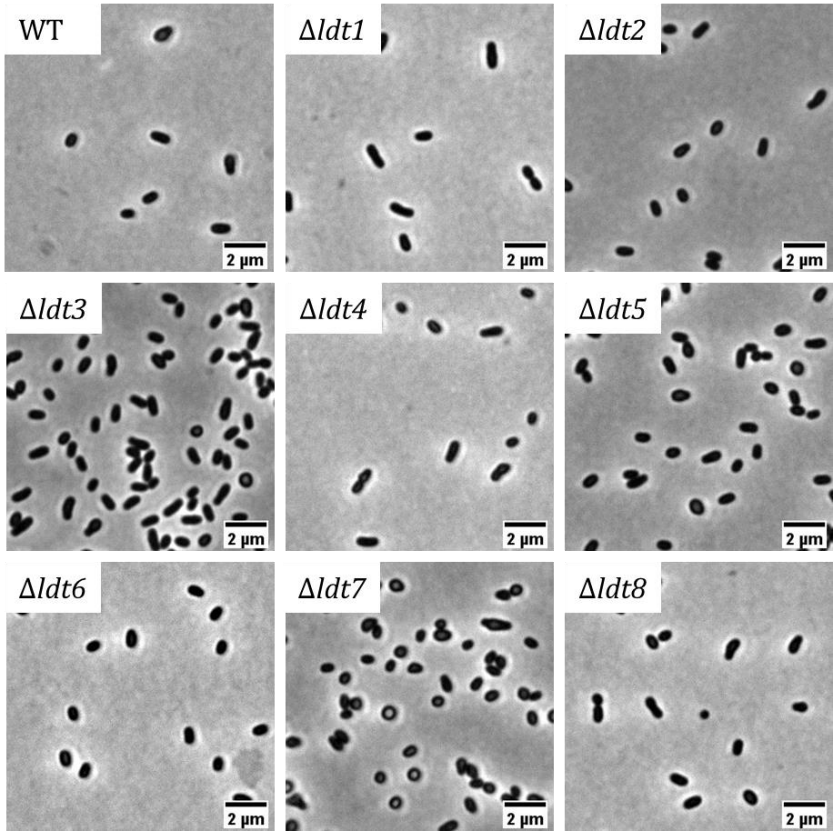

Figure 12 | Phenotype of the LDt deletion strains. Phase microscopy of *B. abortus* WT and the Δ*ldt* strains. Only the Δ*ldt7* mutant shows a morphological difference with smaller and rounder cells. Scale bars are 5 µm.

A

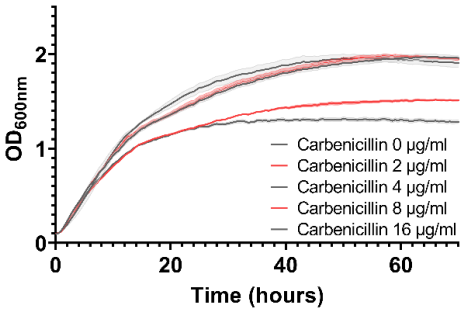
OD600nm
Time (hours)
Carbenicillin 0 µg/ml
Carbenicillin 2 µg/ml
Carbenicillin 4 µg/ml
Carbenicillin 8 µg/ml
Carbenicillin 16 µg/ml

B

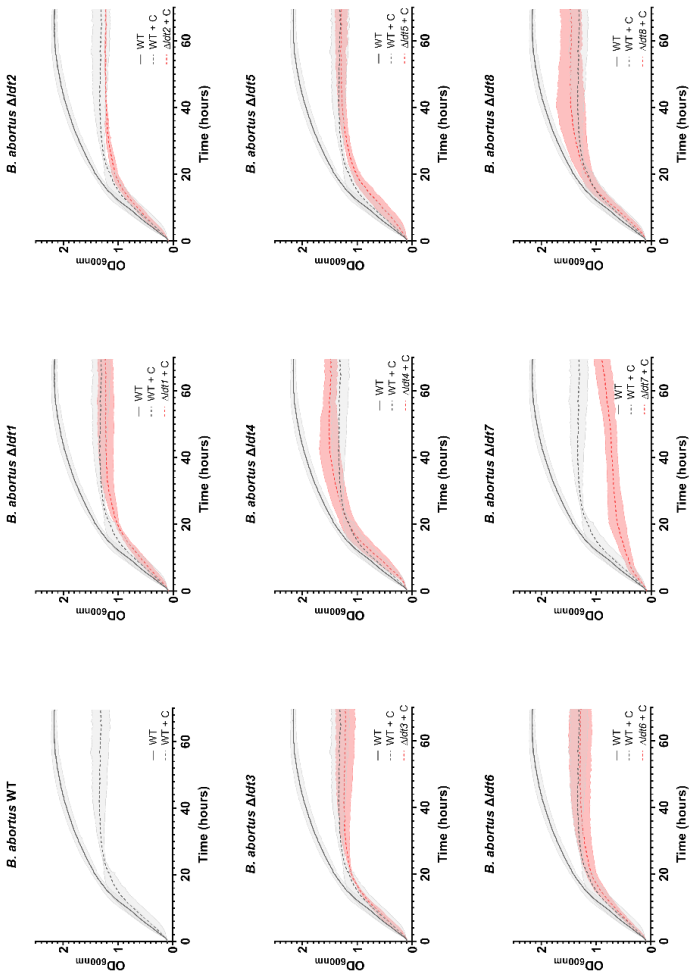
B. abortus WT
B. abortus Δldt1
B. abortus Δldt2
B. abortus Δldt3
B. abortus Δldt4
B. abortus Δldt5
B. abortus Δldt6
B. abortus Δldt7
B. abortus Δldt8
WT
WT + C
Δldt1 + C
Δldt2 + C
Δldt3 + C
Δldt4 + C
Δldt5 + C
Δldt6 + C
Δldt7 + C
Δldt8 + C
OD600nm
Time (hours)

Figure 13 | Effects of carbenicillin on the growth of *Brucella*. A. Determination of a sub-lethal concentration of carbenicillin on *B. abortus* WT. Because *Brucella* could still grow in presence of carbenicillin 16 µg / ml (dark red) but reaches its plateau earlier, this concentration was chosen for further tests. **B.** The growth of the *B. abortus* LDt single mutants (solid red lines) was compared to the WT (solid grey lines) strain in presence of carbenicillin (dashed lines). Of the eight strains, only the Δ*ldt7* mutant showed an impacted growth in this condition. Other strains profiles were similar to the WT.

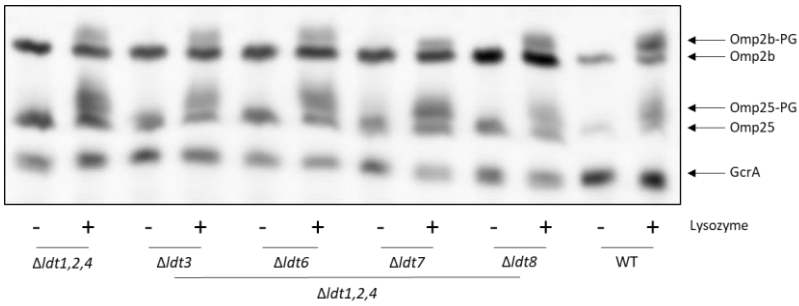

Figure 14 | Quadruple LDts mutants. As for the Δ*ldt1,2,4* strain, a fraction of the Omp25 remains linked to the PG in the combination of Δ*ldt1,2,4* strain with Δ*ldt3*, Δ*ldt6*, Δ*ldt7* or Δ*ldt8*. This suggests that a least one other enzyme is involved in the PG anchorage. The *ldt5* is an interesting candidate as attempts at deleting it in a Δ*ldt1,2,4* background remained unsuccessful.

1.2.1.1 Ldt5

To this extent, a single guide RNA hybridising on the +1 site of *ldt5* was designed and the CRISPRi elements were inserted in a Δ*ldt1,2,4* background. It should be noted that the mRNA quantification before and after induction could not be done in the time constraints of this study. Although bacteria still had a normal morphology after a short time post-induction (*e.g.* 8 h, data not shown), structures consistent with blebs were observed after 24 h of AHTC treatment (Fig. 15A). Additionally, the formation of blebs-like structures could be observed in time-lapse microscopy (Fig. 15B). Growth monitoring of the induced strain showed defect only after 16 h compared to the non-induced strain (Fig. 15C). Consequently, cultures induced for 24 h were used to detect bound or

free OMPs by western blotting. The results show that no bound Omp2b can be observed, already in the non-induced condition. For Omp25, a fraction of the pool remained bound to the PG (Fig. 15D).

A

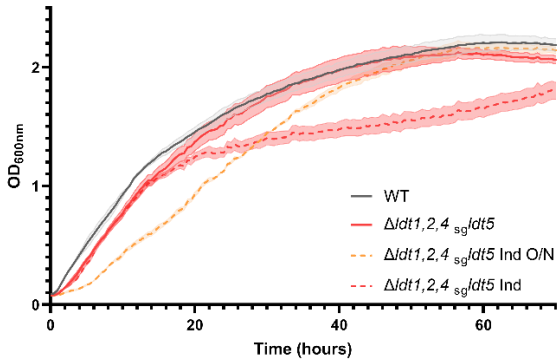

B

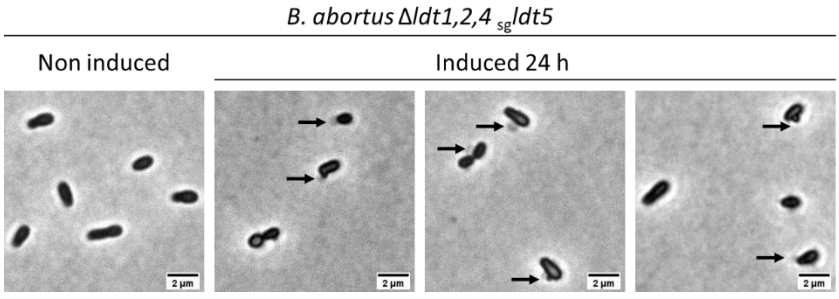

C

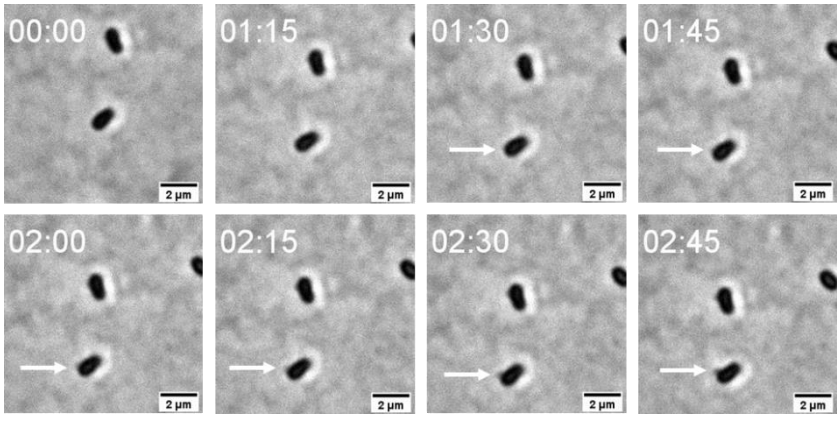

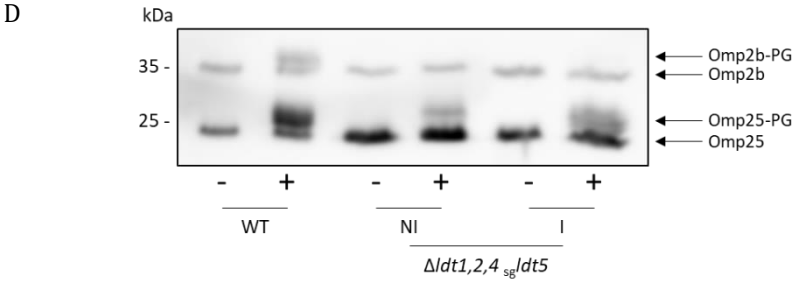

Fig. 15 | Depletion of Ldt5 in a *B. abortus* Δ*ldt1,2,4* background leads to defects. A Growth monitoring shows no major difference between the WT (black line) and the non-induced CRISPRi strain (solid red line). When the inducer is added (red dashed line), an effect can be observed after 14h. The orange dashed line depicts the removal of the inducer after O/N induction and suggests a rapid recovery. **B** Observation of the strain induced for 24 h shows abnormal structures compared to the non-induced condition that suggests the presence of blebs (black arrows). **C** Time-lapse microscopy allowed to visualise the formation of blebs-like structures after 21 h hours of induction. **D** Western blot against Omp25 and Omp2b in the WT, the NI or I Δ*ldt1,2,4* $_{sg}$*ldt5* strains. Compared to the WT, the NI condition already shows no detectable Omp2b-PG and less Omp25-PG. No difference is observed after induction. For all microscopy images, scale bars are 2 µm.

1.2.1.2 Ldt7

Microscopy on *ldt* mutant strains revealed that the *Δldt7* has a morphological defect. Furthermore, it was also the only *ldt* mutant to have an aggravated growth defect under β-lactam stress. We first aimed to characterise its morphology by measuring the average width and length of the cells with MicrobeJ. This was done with the deletion and complementation strains in exponential as well as in stationary phase. The results are shown in Fig. 16 and highlight that the deletion of the *ldt7* leads to smaller, rounder bacteria and this is reinforced when the bacteria are in stationary phase. However, the complementation induces the opposite phenotype with cells longer and narrower than the WT. Because the Δ*ldt7* cells are rounder we wondered if the growth was still polar. To this end, we used HADA, a fluorescent D-alanine that can be incorporated at the sites of new PG insertion, as well as sites of PG remodelling

(Williams *et al.*, 2021). As shown with the WT (Fig. 17, upper panel), the fluorescence is mainly localised at a pole or the constriction site of the bacterium. In the mutant (Fig. 17, middle panel), although there is no visible pole, the insertion of HADA still takes place at discrete sites on the cell periphery. This is in sharp contrast with the pattern of HADA insertion in a *B. abortus* Δ*pdeA* mutant (Reboul *et al.*, 2021), in which HADA insertion occurs on a wide polar surface, even though both mutants (Δ*ldt7* and Δ*pdeA*) have a similar coccoid morphology. The HADA staining is also shown for the complementation strain (Fig. 17, lower panel). Because shape determination strongly depends on PG in many bacteria, these results lead us to think that this LDt was rather involved in the creation of 3-3 links within the PG sacculi. However, to validate this role, MS analysis was necessary. At the time of this manuscript, it was not yet possible.

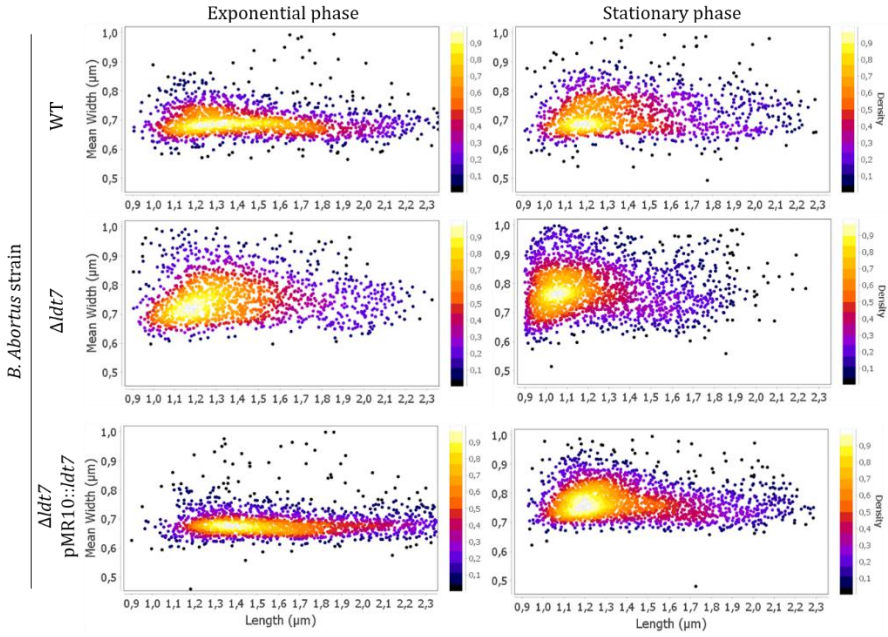

Figure 16 | Morphology of the *B. abortus* Δ*ldt7* mutant. Width and length were measured for bacteria of the three strains in exponential (WT, 1562; Δ*ldt7*, 1385 and Δ*ldt7* pMR10::*ldt7*, 1725) and in stationary phase (WT, 1331; Δ*ldt7*, 2050 and Δ*ldt7* pMR10::*ldt7*, 2102) with MicrobeJ. Each point represents a bacterium. The length (x-axis) was then graphed over the width (y-axis) for each condition. In both culture phases, the Δ*ldt7* strain shows a shift towards smaller and wider cells. This is in agreement with the phase microscopy images (Fig. 12) that shows rounder bacteria. On the contrary, the complementation strain has a shift towards the right side of the graph, which suggests longer cells and thus efficient complementation.

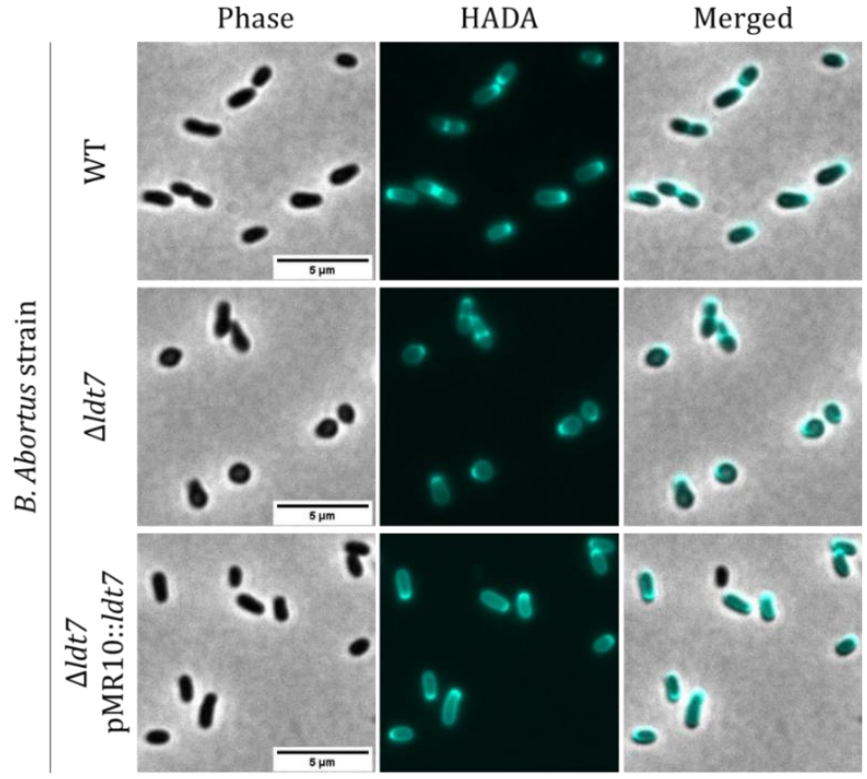

Figure 17 | HADA staining in the *B. abortus* Δ*ldt7* strain. The staining was performed with the fluorescent D-amino acid, HADA, over five minutes. This compound labels the active sites of PG incorporation/remodelling in a bacterium. In the WT strain, the polar growth, as well as the constriction site, can be seen. Even though the Δ*ldt7* strain has a rounder shape, the growth is still polar as shown by localised HADA incorporation. In the complementation strain, the morphology is restored and the HADA incorporation profile is similar to the WT. Scale bars are 5 µm.

If the hypothesis that the Ldt7 is involved in the PG crosslink was correct, we thought that this localisation might be predominantly at the growing part of the cell, hence at the pole and the constriction site (see section 2.3.1 of the introduction). To this end, we translationally fused the mNG CDS to the 3' end of the *ldt7* gene with a tetra glycine linker in between. The chromosomal copy was then replaced with the fusion construction. Even though we were able to observe fluorescence in the strain, no specific localisation was found (Fig. 18).

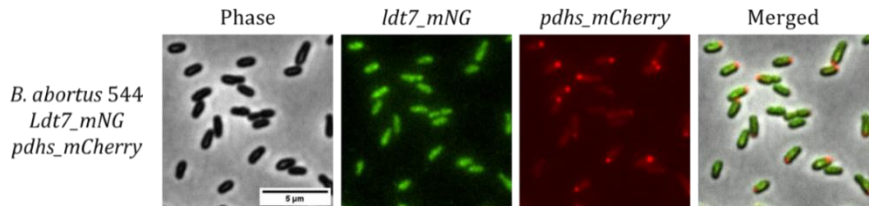

Figure 18 | Localisation of the Ldt7 in *B. abortus*. The CDS of the mNeonGreen (*mNG*) was fused to the 3' end of *ldt7* with a four glycine linker in between. The *pdhS_mCherry* allows spotting the old pole of the bacterium. As shown on the green channel image, no particular localisation could be observed for the Ldt7. Scale bars are 5 µm.

Finally, we tested the effect of the *ldt7* deletion in the context of eukaryotic cells infections. Indeed, we hypothesised that a defect in the PG crosslinking might lead to a virulence defect due to vulnerability to the cell defences. For this, we used RAW 264.7 murine macrophages, infected them either with the WT or the deletion strain and recovered bacteria after 2, 5, 24 and 48 h post-infection for CFUs counting. The results (Fig. 19) showed no difference compared to the WT and this was not further investigated.

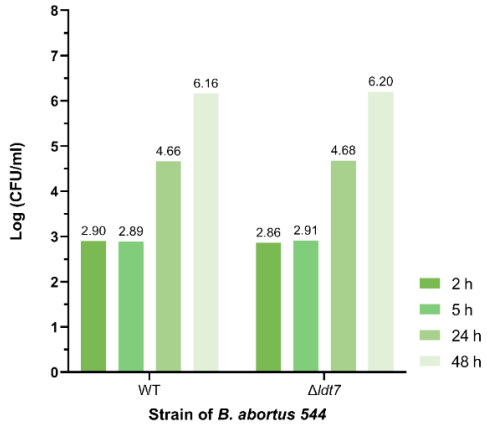

Figure 19 | Infection of RAW macrophages with the Δ*ldt7* strain. RAW 264.7 murine macrophages were infected with the Δ*ldt7* strain. Bacteria were recovered at 2, 5, 24 and 48 h post-infection and CFUs counted. As shown with *B. abortus* WT, the CFU count is stable at 2 and 5h PI and increases once *Brucella* has reached its replication niche at 24 and 48 h PI. In comparison, the deletion strain shows similar CFU counts across all time points. CFU, colony-forming unit; PI, post-infection; n=1.

1.2.2 The anchorage signal

As described in further details in the manuscript, we found the +2 aspartate to be essential for the OMP linkage to the PG (see section 1.1.2.1 of the results). Omp2b is known to be an essential porin (Sternon *et al.*, 2018), and because the function as an OM anchor is not essential, it is likely that to be the function as a nutrients importer that is crucial. Despite Omp2b and Omp25 being the most prevalent OMPs linked to the PG, we managed to obtain a double point mutant (Omp25-2b$_{D2A}$). Unexpectedly, this only resulted in a mild phenotype where small OMVs were present at the surface of the mutant (Fig. 3c and 3d of the published article). Thus, we aimed to further destabilise the OM by removing additional contacts between OMPs and PG. The next logical step was thus to mutate the aspartate of the next most prevalent OMP, *i.e.* Omp25c (BAB1_0116), in the Omp25-2b^{D2A} strain. While the Omp25c$_{D2A}$ mutant

alone could easily be obtained in about a 1:1 WT/mutant ratio at the last screening stage of the allelic replacement[§], no screened cloned were mutant in an Omp2b-25$_{D2A}$ background. This lead us to think that the combination of these mutations was lethal. To overcome this issue, we used to CRISPRi technique as explained above. However, this approach is less elegant as, under induction, no Omp25c should be present in the OM and this could have unintended effects. Nevertheless, this was the only option to evaluate the OM stability in this context.

A single guide RNA (sgRNA) was thus designed to hybridise on the *omp25c* +1 site. Unfortunately, the addition of AHTC did not show any reduction of the mRNA level (data not shown). Consequently, a second sgRNA was designed further on the coding sequence (starting at position 34 after the ATG). Although it was not possible to quantify the mRNA before the end of this project the following results are in accordance with a depletion of Omp25c. The growth monitoring showed a strong defect of the *B. abortus* Omp25-2b$_{D2A\ sg}$*omp25c* two hours after the induction of CRISPRi (Fig. 20A, dashed red line). Conversely, when the inducer is removed, the strain can grow back to the non-induced condition level, which could be due to a bacteriostatic effect or a surviving part of the population (orange dashed line). In agreement with the growth defects, phase microscopy showed abnormal morphologies after overnight induction, further supporting the Omp25c depletion. The cells showed a

[§] In *Brucella* the generation of mutants, either of deletion or point mutation, is done by double homologous recombination. For this, we used a plasmid that contains both a kanamycin resistance cassette and a sucrose sensitivity gene. The last step of clone selection requires parallel streaks on kanamycin and sucrose. Clones resistant to sucrose but sensitive to kanamycin have correctly undergone the second homologous recombination. Candidates can either be back to WT or be mutant in a theoretical ratio of 1 to 1.

rounder morphology with structures that could suggest the formation of blebs (Fig. 20B). To ascertain the rounder morphology, the mean width of the cells was measured and plotted (Fig. 20C). The induced mutant indeed showed a shifted distribution of the width suggesting wider cells. The growth curves suggest that the effects of the Omp25c depletion in the Omp25-2b$_{D2A}$ background could already be observed at shorter timing. Thus, to observe the formation of blebs, time-lapse microscopy was performed (Fig. 20D). In addition to blebs, some bacteria seemed to discharge part of their content. As shown in Fig. 20E, the swollen cell appears to undergo a contraction (represented by the change of phase-contrast at 06:15) that is accompanied by the presence of a darker structure on its left (white arrow), suggesting material discharge. Together, these results, although preliminary, highlight the importance of the covalent anchorage in *Brucella* and pinpoint the β-barrels needed for normal growth.

A

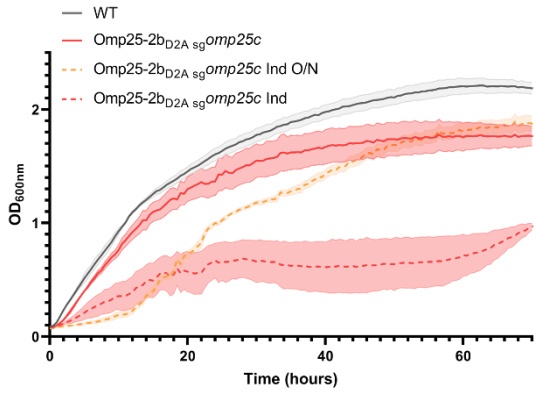

B

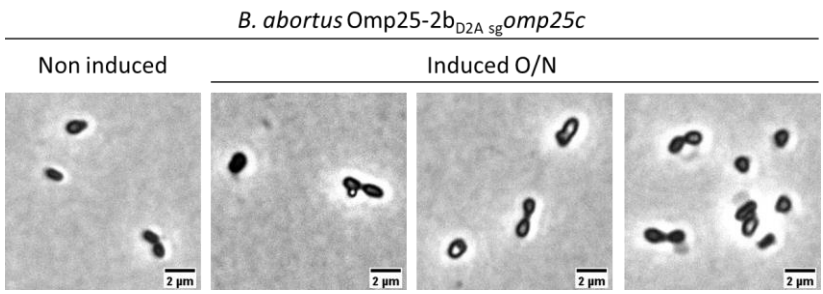
B. abortus Omp25-2b$_{D2A\ sg}$*omp25c*
Non induced
Induced O/N
2 µm
2 µm
2 µm
2 µm

C

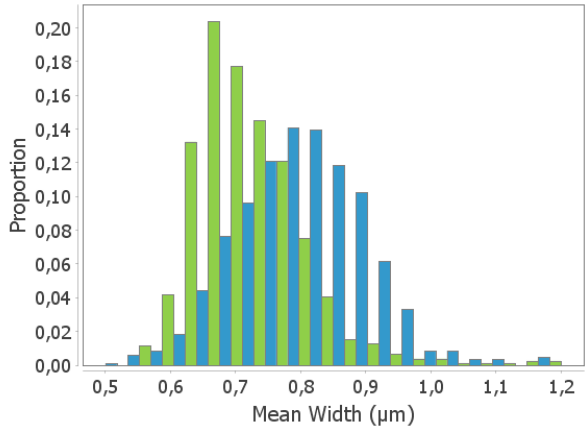
Proportion
0,20
0,18
0,16
0,14
0,12
0,10
0,08
0,06
0,04
0,02
0,00
0,5
0,6
0,7
0,8
0,9
1,0
1,1
1,2
Mean Width (µm)

D

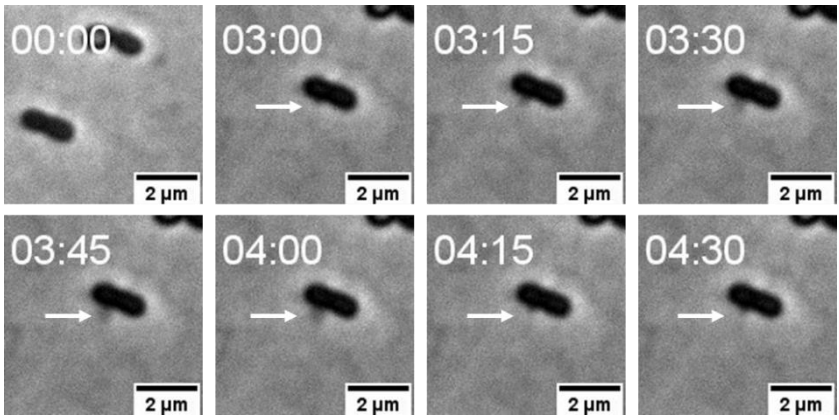
00:00
03:00
03:15
03:30
03:45
04:00
04:15
04:30
2 µm

E

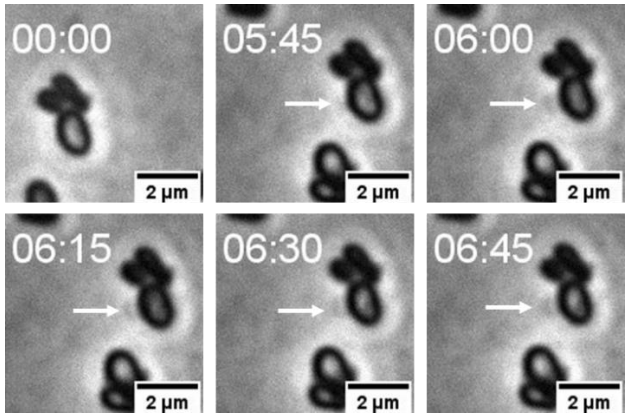

Fig. 20 | Depletion of Omp25c in a *B. abortus* Omp25-2b$_{D2A}$ background leads to defects. A Without the inducer (solid lines), the CRISPRi strain (red lines) shows only a slight difference of growth compared to the WT (black line). Upon induction (dashed red line) an important growth defect is observed already in the first hours of monitoring. However, when the inducer is removed from an overnight induced CRISPRi strain culture, the strain can grow back to the non-induced CRIPSRi strain level. This would be consistent with a bacteriostatic effect. **B** The *B. abortus* Omp25-2b$_{D2A\ sg}$*omp25c* strain was imaged after overnight growth without or with the inducer. As shown by the images on the right, morphological defects consistent with blebbing can be observed. **C** The induced *B. abortus* Omp25-2b$_{D2A\ sg}$*omp25c* is wider after an overnight induction (in blue, n = 809) compared to the non-induced condition (in green, n = 785), suggesting a rounder morphology. **D** The formation of blebs (white arrow) could be observed in time-lapse microscopy. **E** Depletion of Omp25c in a *B. abortus* Omp25-2b$_{D2A}$ background might lead to bursting as shown by the grey structure appearing (white arrow). For microscopy data, scale bars are 2 µm. For time-lapse microscopy, the time (hh:mm) is shown in the upper left corner and imaging was started 7 hours after induction.

In parallel, we assessed the role of the charge by replacing the aspartate with glutamate for the Omp25 (Omp25^{D2E}). Both residues are negatively charged at physiological pH. As shown in Fig. 21, the amount of free Omp25^{D2E} is similar to the one of Omp25^{D2A}. However, a small portion of the Omp25^{D2E} pool shows a slower migration in the form of a smear. This suggests that a small proportion of the Omp25^{D2E} is still able to bind PG. Thus, the charge by itself is not sufficient to allow a strong recognition of the OMPs in the anchorage mechanism. The failure to restore a WT level

of binding might be due to the additional carbon on the lateral chain that would somehow perturb the recognition. This shows that the anchoring mechanism is very precise at the atomic level, and is consistent with the perfect conservation of D2, which was never replaced with E2 in the homologs that we analysed so far.

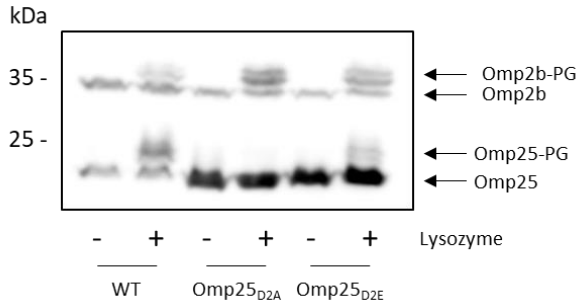

Figure 21 | Mutation of the aspartate into glutamate partially allows the anchorage. Treatment of bacterial lysate with lysozyme allows to visualise the PG-bound form of the OMPs (here, Omp25 on the bottom and Omp2b and the upper part of the image). As previously shown in the manuscript, the mutation of the second aspartate of Omp25 into an alanine effectively prevent the anchorage to the PG. However, changing the aspartate into glutamate leads to the anchorage of only a small amount of Omp25 to the PG, as shown by the light bands above the free Omp25 on the last lane. No loading control was used here, n=3.

1.2.3 Reversing the anchorage of OMPs

As a side project, the conservation of the anchorage was studied in *A. tumefaciens* (A. Lannoy, master thesis). In this organism, no less than fourteen LDts were reported (Cameron *et al.*, 2014) and thus were blasted against *Brucella* genome. Interestingly, this allowed the identification of three new putative LDts compared to the first screening with *E. coli* LDts as reference sequences. These three CDS are BAB1_0979 (also called Ldt9), BAB1_2007 (Ldt10) and BAB1_2034 (Ldt11) and more information can be found in supplementary figures 1 and 2. The *ldt6* and

ldt9 genes seem to form a pseudogene interrupted by a frameshift, and the lipoprotein signal sequence of Ldt10 (VLEC) is poorly consistent with the consensus sequences. The deletion mutants were generated and, when the amount of PG-bound and unbound protein were compared, only the Δ*BAB1_2034* strain showed a clear phenotype. However, it was the exact opposite of what is expected for an LDt. Indeed, when deleted, the amount of PG-bound proteins increased and conversely when over-expressed (Fig. 22).

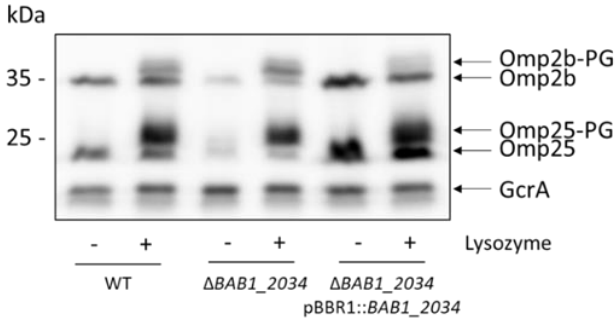

Figure 22 | BAB1_2034 is not a L,D-transpeptidase. The Δ*BAB1_2034* strain shows a smaller pool of free OMPs and a higher proportion of PG-bound OMPs. This strain was complemented with the *BAB1_2034* gene expressed on a medium copy plasmid, the pBBR1, under the control of the *E. coli* lac promoter. In this strain, the opposite phenotype is observed with a stronger signal for the free OMPs. Taken together, these results contradict the prediction of *BAB1_2034* as encoding an L,D-transpeptidase. GcrA was used as a loading control, n=3.

The most straightforward explanation was that this protein can reverse the covalent anchorage of OMPs to PG (*i.e.* an amidase). However, the deletion of an L,D-carboxypeptidase could also induce this phenotype. Indeed, this enzyme has the tetrapeptide stems for substrate and it removes the last D-alanine, turning it into a tripeptide. As in *E. coli* (Magnet *et al.*, 2007), our data (see section 1.1.2.1 of the results) show that the β-barrels are linked to tripeptides. This suggests that the initial

substrate for the transpeptidation reaction is most likely a tetrapeptide. Consequently, diminishing the pool of free tetrapeptide could, in turn, reduce the amount of linked OMPs

To ascertain the role of this protein, we then proceeded to a MS analysis of the Δ*BAB1_2034* strain muropeptides. In the case of an LDc, the amount of tripeptide would be increased. On the contrary, deleting an OMP-PG amidase would rather leave more free tetrapeptide. One major obstacle in this part of the study was that the muropeptide composition of the *Brucella* PG has never been studied. The characterisation of *B. abortus* PG needs to be addressed in future work.

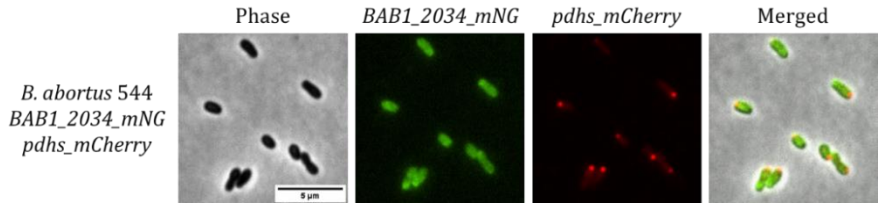

Figure 23 | Localisation of BAB1_2034 in *B. abortus*. The CDS of the mNeonGreen (*mNG*) was fused to the 3' end of *BAB1_2034* with a four glycine linker in between. The *pdhS_mCherry* allows spotting the old pole of the bacterium. As shown on the green channel image, no particular localisation could be observed for BAB1_2034. Scale bars are 5 µm.

In parallel, we tried to localise BAB1_2034 by fusing it translationally to the mNeonGreen fluorochrome to the C-terminal, because the N-terminal is occupied with the signal peptide. As for the Ldt7, a tetra glycine linker was inserted in between the two coding sequences and the genomic copy was replaced by the fluorescent fusion. Although we were able to visualise fluorescence in the engineered strain, no particular localisation could be observed (Fig. 23). The signal can be patchy but varies from one cell to the other.

We then hypothesised that, due to the increased anchorage of the OM to the PG, the Δ*BAB1_2034* strain could be impacted during the course of the infection. We first tested the virulence of this strain *in vitro* with the RAW 264.7 murine macrophages. As shown in Fig. 24A, the mutant strain has no difference in the CFU count at the early post-infection (PI) time points compared to the WT. However, it seems that around ten times fewer Δ*BAB1_2034* bacteria (*i.e.* around one log) can reach the replication niche as fewer CFU are observed at 24 PI. The increase observed at 48 h PI suggest that the mutant strain is still able to proliferate. However, the phenotype is not complemented when a copy of the gene is introduced on a pBBR1. To further investigate this decreased virulence, we used a different cell type for *Brucella*, the J774A.1. These are murine macrophages that are more challenging for the bacteria in terms of stress endured and more specifically, oxidative stress. In J774.A1 (Fig. 24B), the decrease of CFUs is similar to the RAW 264.7 macrophages, confirming the observed diminished virulence.

A

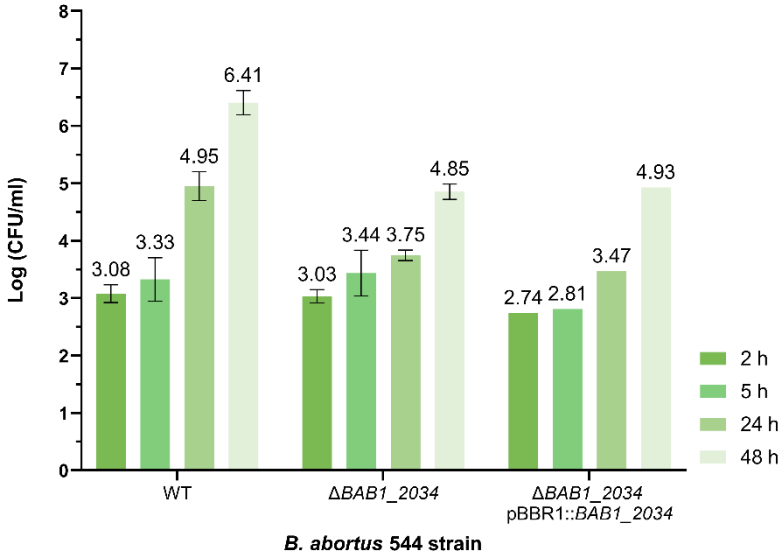
Log (CFU/ml)
8
7
6
5
4
3
2
1
0
3.08
3.33
4.95
6.41
3.03
3.44
3.75
4.85
2.74
2.81
3.47
4.93
2 h
5 h
24 h
48 h
WT
ΔBAB1_2034
ΔBAB1_2034
pBBR1::BAB1_2034
B. abortus 544 strain

B

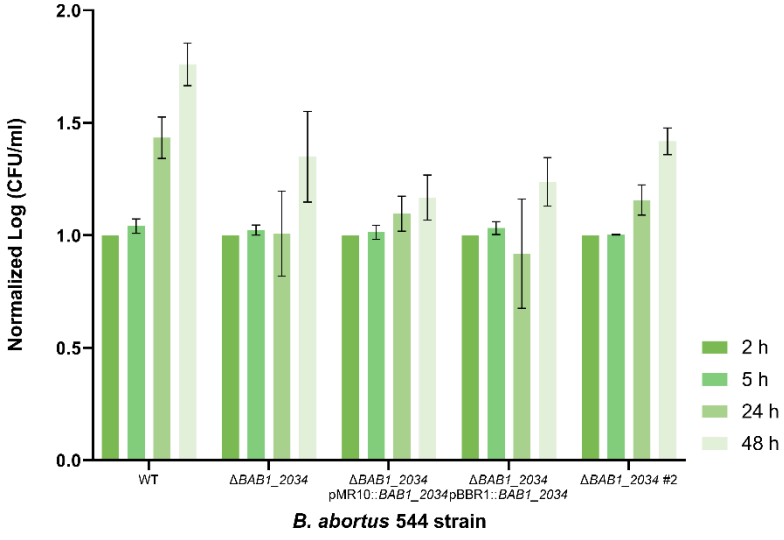
Normalized Log (CFU/ml)
2.0
1.5
1.0
0.5
0.0
2 h
5 h
24 h
48 h
WT
ΔBAB1_2034
ΔBAB1_2034
pMR10::BAB1_2034
ΔBAB1_2034
pBBR1::BAB1_2034
ΔBAB1_2034 #2
B. abortus 544 strain

Figure 24 | Infection of murine macrophages with the Δ*BAB1_2034*. A. RAW 264.7 or **B.** J774A.1 murine macrophages were infected with the *ΔBAB1_2034* or complementation strains (pMR10::*BAB1_2034* and pBBR1::*BAB1_2034*). Bacteria were recovered at 2, 5, 24 and 48 h post-infection and CFUs counted. As shown with *Brucella* WT, the CFU count is stable at 2 and 5h PI and increases once *Brucella* has reached its replication niche at 24 and 48 h PI. In comparison, the deletion strain shows similar CFU counts at 2 and 5 h PI but lower at 24 and 48 h PI in both cell types. However, the WT virulence is not restored with any of the complementation strains. CFU, colony-forming unit; PI, post-infection. n=3 when error bars are shown, n=2 for Δ*BAB1_2034* #2 and, n=1 otherwise.

Because pBBR1 is a medium copy number plasmid, we hypothesised that it could be the right balance of links between the OM and the PG that is needed to restore the virulence. Indeed, we previously showed in Fig. 22 that in the pBBR1::*BAB1_2034* complemented strain, the amount of bound OMPs was higher than the WT. This argues for complementation accompanied by overexpression of *BAB1_2034*. This was is further supported by the growth curve shown in Fig. 25 where the pBBR1::*BAB1_2034* complementation strain shows a slower growth and a lower plateau compared to the WT or the Δ*BAB1_2034* strains. The level of Omp25 linked was also assessed in the pMR10::*BAB1_2034* strain and is shown in Fig. 26. Although the amount of linked Omp25 is still lower, the free pool seems to be closer to the one of the WT strain.

To get as close as possible to the endogenous level of *BAB1_2034* expression, we used a pMR10 construction as it is a low copy plasmid. Unlike the pBBR1-derived strains, the pMR10::*BAB1_2034* only shows a slight growth difference at the end of the growth curve. In infection of J774A.1 macrophages, the WT virulence level was not restored by the presence of pMR10::*BAB1_2034* in the Δ*BAB1_2034* strain (Fig. 24B). Due to the lack of complementation, the hypothesis arose that the phenotype could not be due to the deletion itself but rather to a side mutation that

could have occurred in the strain. Since it is unlikely that such a mutation occurs a second time, a second independent clone was tested and showed the same phenotype as the first clone (Fig. 24B, Δ*BAB1_2034* #2). Although a knock-in approach was also started, the strain was not obtained before the end of the thesis.

Hence, we decided to go for a CRISPRi approach that would allow better control. Rather than the mRNA level, the effect on the free or bound Omp25 was evaluated by western blotting. As shown in Fig. 27, upon induction with AHTC, the level of free Omp25 decreased to the profit of the linked form. These effects are in line with the previous data obtained for the *BAB1_2034* deletion mutant. Additionally, it is known that AHTC is used for induction during cellular infection with *Brucella* (Smith *et al.*, 2016). Figure 28 shows that no strong difference is observed between the non-induced and the induced condition, half a CFU log is lost at 24 and 48 h PI in induced conditions, *i.e.* conditions in which the *BAB1_2034* mRNA level is expected to decrease.

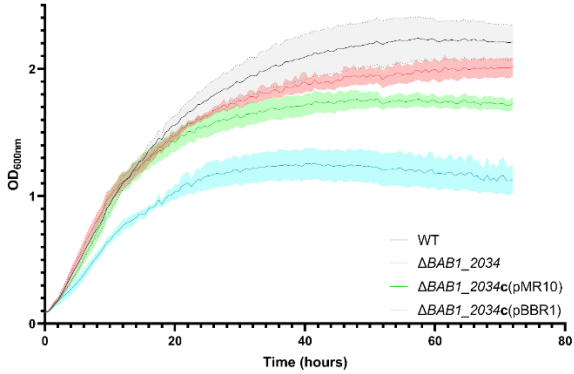

Figure 25 | Growth of the Δ*BAB1_2034* and complementation strains. Growth was performed at 37 °C and the OD was measured every 30 minutes for 72 hours. While the deletion and pMR10::*BAB1_2034* complementation show no difference compared to the WT during the exponential phase, they do show a plateau sooner. The pBBR1::*BAB1_2034* complemented strain

however shows a slower growth from the beginning and a plateau at lower OD. OD, optical density; n=2 for the pMR10::*BAB1_2034* strain and n=3 for the other strains.

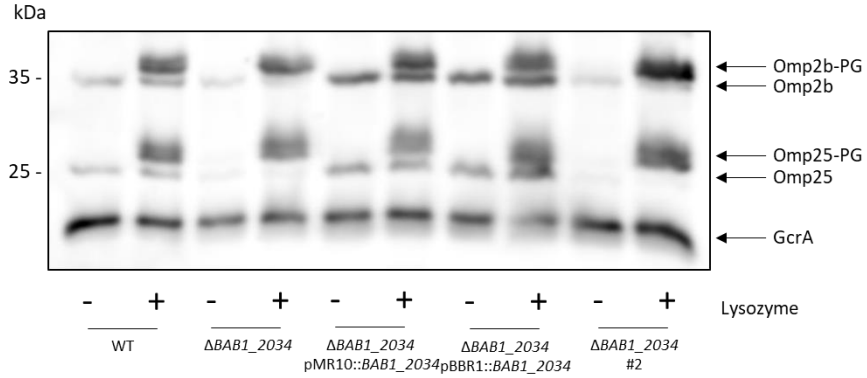

Figure 26 | BAB1_2034 expression on a pMR10 does not fully restore the WT condition. The WT, Δ*BAB1_2034* and pBBR1::*BAB1_2034* and their effect were introduced and are the same as in Fig. 22. Here, the complementation of BAB1_2034 was tried on a pMR10, a low copy plasmid. Although the normal situation is not restored, the balance between free and linked Omp25 is closer to the WT.

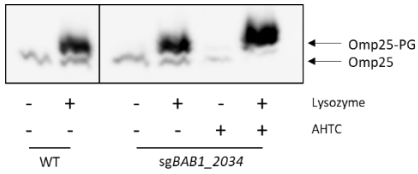

Figure 27 | Control of the *BAB1_2034* expression by CRISPRi. The pJMP1339t2 construction was used with a sgRNA targeting *BAB1_2034* (sg*BAB1_2034*). To maximise protein depletion, the lysates were made after an O/N AHTC induction. In the AHTC condition, the ratio of free and linked Omp25 is close to the Δ*BAB1_2034* strain (see Fig. 22 or 26), suggesting that the inhibition is effective. The second and third lanes were not adjacent on the gel as depicted by the black line.

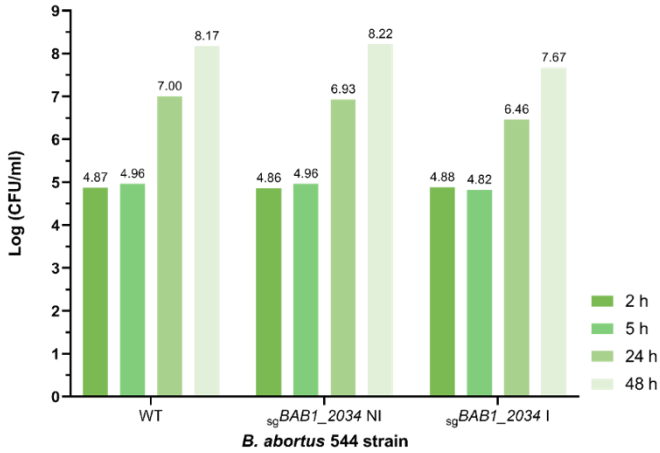

Figure 28 | Infection of J774 macrophages with the BAB1_2034 CRISPRi strain. J774 A.1 murine macrophages were infected with the BAB1_2034 CRISPRi strain-induced or not. Bacteria were recovered at 2, 5, 24 and 48 h post-infection and CFUs counted. No CFU count difference can be observed when not induced, compared to the WT. The induction of the CRISPRi does not lead to a strong defect as the deletion mutant. n = 1; NI, non-induced; I, induced.

1.2.4 Protein purification

The activity of some *E. coli* LDts can be assessed *in vitro* by incubation of the purified enzyme with different PG substrates (More *et al.*, 2019; Winkle *et al.*, 2021a). Therefore, we intended to produce, purify and, if possible, test the *in vitro* activity of three of our proteins: Ldt4, Ldt7 and BAB1_2034. The aim was different depending on the protein. For Ldt4, it was to compute structural data by crystallography in collaboration with J. Hermoso (CISC, Spain). For Ldt7 and BAB1_2034, it was to incubate these purified proteins with different substrates to test their proposed functions, hence Ldt7 establishing 3-3 crosslinks and BAB1_2034 detaching OMPs from PG.

For this, the coding sequence of these proteins, without the lipoprotein export signal and cysteine, was inserted in an expression vector

(pET28a). This plasmid, when cut with the restriction enzyme *Nde*I, allows the direct in-frame fusion of the protein N-termini to a His-Tag with a thrombin cleavage site in between. This way, the protein can be purified on a Ni-NTA column and the His-tag could be cleaved by thrombin after purification. As shown on the left panel of Fig. 29A, the Ldt4 (expected size, 25 kDa) was detected and soluble in Coomassie blue staining after 3 h of induction at 37 °C. It could also be detected by western blotting with an antibody against the His-tag as shown on the left panel. The construct was sent to the Hermoso lab to try to get protein crystals from the purified Ldt4, which could hopefully diffract and allow structural determination. For Ldt7 and BAB1_2034 (Fig. 29B and 29C, 28 and 45 kDa expected, respectively), although they could be observed by Coomassie blue staining upon induction, they were in the insoluble fraction. Induction at a lower temperature (20 °C) was tested to lower the production rate and thus increase the soluble fraction, but it gave no different results (data not shown). Consequently, this part was not further investigated.

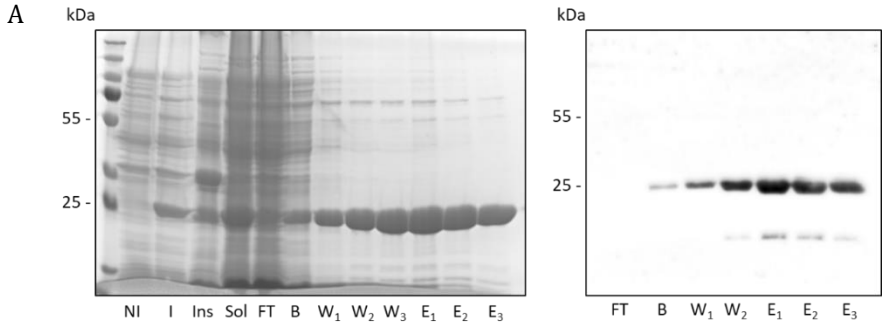

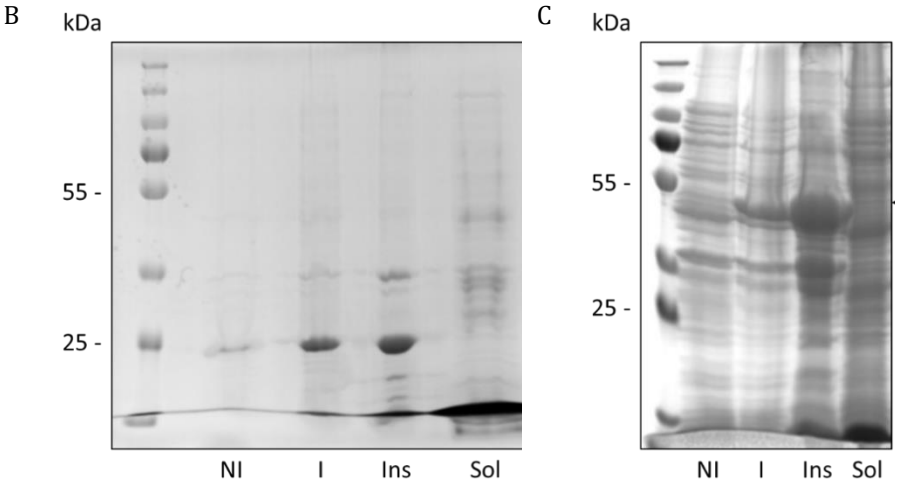

Figure 29 | Production of the Ldt4, Ldt7 and BAB1_2034. A. Production and purification of the Ldt4. The left panel shows that the protein is indeed produced (expected size, 25 kDa) when induced and is soluble. On the right panel is shown the detection of the His-tag fused protein by western blotting with anti-His antibody. **B.** Although the Ldt7 (left panel, expected size, 25 kDa shown by the arrow) and the BAB1_2034 (right panel, expected size, 45 kDa) were produced, they were insoluble. Ni, non-induced; I, induced; Ins, insoluble; Sol, soluble; FT, flow-through; B, buffer; W, wash; E, elution with 100 mM imidazole.

2 Tools development

2.1 CRISPRi

To study essential genes in *Brucella*, a depletion strain is usually used in our laboratory. The principle is to first introduce a second copy of the studied gene on a plasmid that is expressed upon the addition of IPTG in the medium, via the p_{lac}. Then, the genomic copy is deleted by classical pop-in – pop-out and the effect of the depletion of the protein can be studied when IPTG is removed. For example, this was done with the essential response regulator CtrA in *Brucella* (Francis *et al.*, 2017). Nevertheless, this technique is time consuming due to the plasmid construction and subsequent deletion. We thus aimed to have a more

time-efficient technique with an expression level that would also be more physiologically relevant. To this end, we chose the CRISPRi (see Box 1) technique, in a mobile version recently published (Peters *et al.*, 2019).

Before using the CRISPRi system in this project, it was necessary to first validate it in *B. abortus*. Indeed, this mobile version had not been assessed in this bacterium. In the publication, Peters and colleagues report the construction and validation of an IPTG or anhydrotetracycline (AHTC) inducible system for the Gram-negative or Firmicutes, respectively. However, our first attempts revealed the *E. coli lac* system was too leaky to be used with *Brucella* essential genes as no clones could be observed after a triple mating with a CRISPRi system targeting CtrA. We thus proceeded to the construction of an AHTC inducible system that would work in Gram-negative bacteria, hence with the dCas9 and guide sequences adapted to Gram-negative bacteria. To this extend, we based our construction on the two plasmids from the study of Peters and colleagues: the pJMP1339 and pJMP1337 (Supplementary Fig. 3 for their maps). Briefly, the pJMP1339 was used for Gram-negative bacteria and it contains a CRISPRi IPTG-inducible system as well as the sequences (Tn7L and Tn7R) allowing insertion downstream of the *glmS* gene (BAB2_0658) using the Tn*7* system. The pJMP1337 was used for Firmicutes and the transfer of the system is based on integrative and conjugative elements (ICE). On the pJMP1337, the expression of the dCas9 is under the control of the tetracycline-responsive promoter but the $_{sg}$RNA is constitutively expressed by p_{Veg} from the P43 protein of *Bacillus subtilis*. Moreover, the scaffold RNA are also different between the two plasmids, although the

two dCas9 genes encode proteins with the same amino acid sequence, the GC content is higher for Gram-negative bacteria (55.6 % vs. 35.2 %).

Based on this, we used the pJMP1339 as the backbone and kept everything but the part in between the $_{sg}$RNA and the Cas9. This was replaced by Gibson assembly with the p_{veg} for the $_{sg}$RNA, the *tetR* gene and a p_{tetA} for the dCas9 as shown in Fig. 30. The newly created plasmid was named pJMP1339t, in reference to its backbone (pJMP1339) and the tetracycline (t). Although we have no data on the efficiency of the pVeg in *B. abortus*, we were concerned about a constitutive expression of the

BOX 1 | CRISPRi stands for Clustered Regularly Interspaced Short Palindromic Repeats interference. It is a derivate from the classical CRISPR. This system relies on an endonuclease (called Cas9 for CRISPR associated protein 9) and on a single guide RNA (sgRNA) that targets a specific sequence and that is accompanied by a scaffolding RNA for Cas9 recognition. As indicated by its name, the CRISPRi prevents the expression of a gene rather than cleaving the DNA. The Cas9 used is catalytically inactive due to two point mutations (RuvC-like and HNH nuclease domains] and is thus referred to as dead Cas9 (dCas9). The sgRNA-dCas9 complex is targeted to the promoter or the beginning of the gene to be silenced; the binding of this complex in the promoter blocks the RNA polymerase, hence blocking the transcription initiation. The system used here is based on a recent publication of a mobile CRISPRi (Peters *et al.*, 2019). It is said mobile as it can be mobilised in a bacterium by the means of a Tn*7* system. It is based on two plasmids, one carries the transposase gene and the other the sgRNA and the dCas9 genes from *Streptococcus pyogenes,* flanked by the Tn*7* sequences involved in DNA integration by the transposase. Following a tri-parental mating, the system is introduced in *Brucella*, the dCas9 and sgRNA genes are integrated downstream the *glmS* gene by the Tn*7* transposase, where the transcription of the dCas9 and $_{sg}$RNA gene is then transcriptionally controlled through an inducer, IPTG or anhydrotetracycline.

$_{sg}$RNA. To prevent any undesirable effects due to this uncontrolled expression, we designed an AHTC-inducible promoter based on the one controlling the dCas9 expression in the pJMP1337. In this promoter, upstream of the $_{sg}$RNA, one Tet operator was removed to shorten the distance between the -10 box and the $_{sg}$RNA. Its sequence is shown in the box of Fig. 30. This new plasmid was consequently named pJMP1339t2.

The functionality of the AHTC system was first assessed with *omp25* (BAB1_0722), which was a challenge since this gene is probably highly expressed and thus difficult to silence. The mRNA relative expression of *omp25* was determined by RT-qPCR on the WT strain with and without AHTC after 2 hours of growth in TSB medium. As shown in Fig. 31A, the strain with the CRISPRi system in the induced condition shows a significant drop in the mRNA level. However, the non-induced strain does show a small decrease in the mRNA level, suggesting a small leak of the system. Because CRISPRi is here used to impact the level of proteins, we then proceeded to a western blot. Fig. 31B shows no visible difference of Omp25 amount between the WT with or without AHTC. Expectedly, the non-induced strain with the sgOmp25 showed a decrease of the Omp25 amount and no signal was observed in presence of AHTC. Although partial inhibition has to be taken into account, these results demonstrate that this CRISPRi setup is efficient in *B. abortus*.

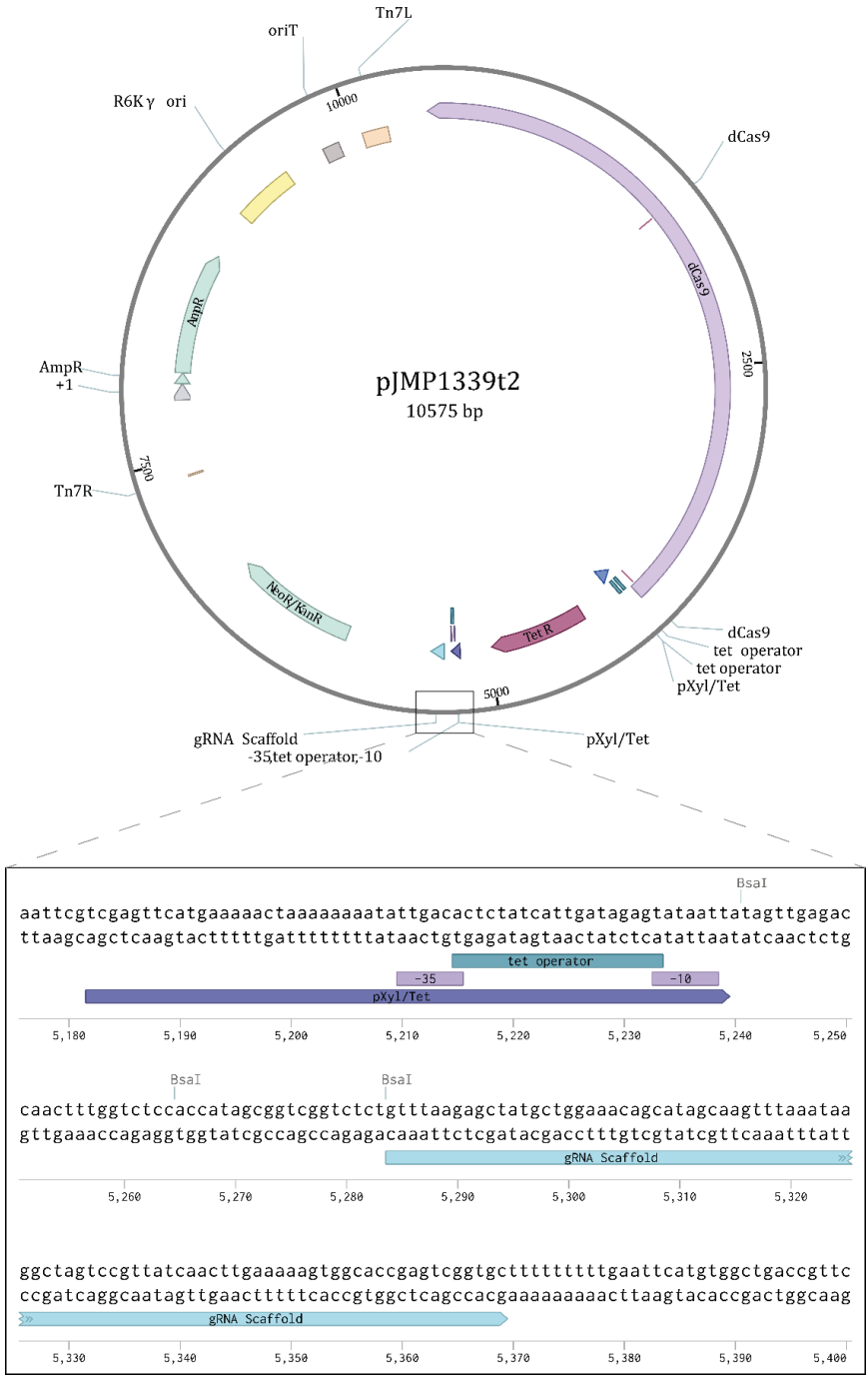

Figure 30 | Map of the custom pJMP1339t2 plasmid. The backbone of the plasmid is the pJMP1339, from right after the gRNA scaffold termination

system (position 5380) to the beginning of the dCas9 sequence (position 4010). The tet system (from bases 4011 to 5175) comes from the pJMP1337 and the $_{sg}$RNA/gRNA scaffold (bases 5176 to 5379) is a custom gene fragment ordered to have a single tet operator regulating its expression. The latter is shown in greater detail in the box and was based on the original p_{TetA} found in the pJMP1337. The restriction sites BsaI for the $_{sg}$RNA insertion are also shown.

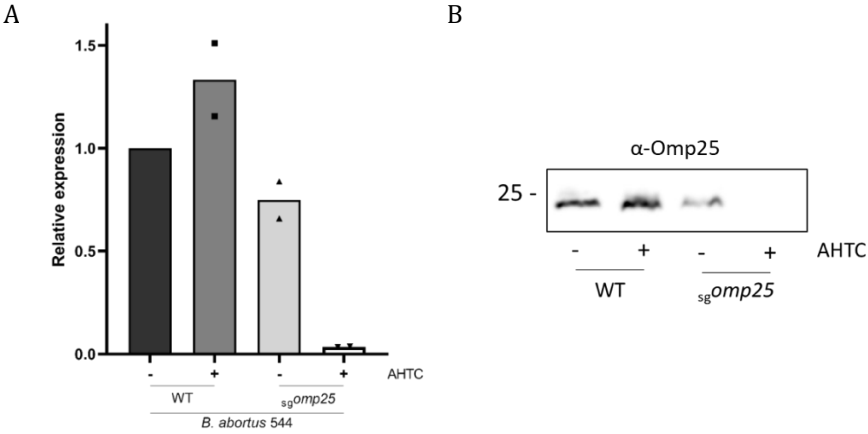

Figure 31 | AHTC-inducible CRISPRi system validation in *Brucella abortus*. A. The level of omp25 mRNA of the WT and the $_{sg}$*omp25* was evaluated after a two hours AHTC induction by RT-qPCR. Whilst this could be due to some variation, the NI $_{sg}$*omp25* strain has a lower level of mRNA. When induced, the transcription of the omp25 gene was almost completely repressed. This graph is the result of two technical replicates. **B.** The amount of Omp25 was evaluated by western blotting after two hours of induction. Consistently with the RT-qPCR data, the level of proteins in the NI $_{sg}$*omp25* strain appears to be lower than in the WT. When the CRISPRi system was induced, no signal for Omp25 could be observed. AHTC, anhydrotetracycline.

DISCUSSION & PERSPECTIVES

1 Discussion related to the manuscript

1.1 OMPs are covalently linked to the PG

In the course of our study, we collected mass spectrometry data highlighting the link between seven proteins and the PG (*i.e.* Omp2b, Omp25, Omp25c, Omp31, OmpW, OmpP and BAB1_0729). Six of them are known or predicted to be found in the OM based on their topology as they are eight- or sixteen-stranded β-barrel. While some are well known (*e.g.* Omp2b and Omp25), the role of the others is not well defined yet. Omp25c, and possibly Omp31 too, could have a redundant function with Omp25, since they are paralogs. It would also be interesting to have more insight into the role of OmpW and OmpP as they are unlikely to only be structural OMPs, and nothing is known about their function.

It is interesting to note that the Rhizobiales have evolved a way to combine two functions in one protein. For example, Omp2b imports peptides while anchoring the OM to the PG. This duality of function is less straightforward with Lpp in *E. coli* although it was reported to be indirectly involved in virulence to some extent. In addition, while all covalent linkages rely solely on Lpp in *E. coli*, along with evolution *Brucella* selected six β-barrel proteins with an N-terminal sequence allowing covalent linkage to PG. One reason might be to ensure sufficient anchorage even if one protein is less produced or damaged. This hypothesis is consistent with our results as preventing the anchorage of both Omp2b and Omp25 only lead to a small phenotypic defect.

Lpp has also been shown to dictate the size of the periplasm as increasing Lpp length resulted in a larger periplasmic space (Asmar *et al.*, 2017). However, in *Brucella*, the predicted length of the N-terminal part

spanning in the periplasm varies between the OMPs. For example, Omp2b has a thirty-two amino acids long extension while Omp25 has twenty-three and OmpW only has seventeen amino acids. It is thus hard to extrapolate the model existing in *E. coli*. If this was true in *Brucella*, one might assume that the major linked proteins would have the smallest extension as they would be more efficient to regulate the PG-OM distance due to their number. Here, however, the most abundant, *i.e.* Omp2b, has the longest extension. Interestingly, a short segment of sequence, located just before the β-barrel, is probably folded because it contains a conserved pair of cysteine residues. This sequence, about 30 residues in length, is very well conserved among homologs in Rhizobiales. However, if Omp2b is the distance determinant, less abundant OMPs with a shorter extension might not be attached to the PG due to physical distance. Due to the number of OMPs involved and extension length heterogeneity, trying to change periplasm size by elongating every extension would be quite fastidious and unlikely to succeed. Although we can only speculate, one might suppose that other proteins, hence interacting non covalently with the PG, could then play a role in the regulation of the periplasm size. The abundant and essential Pal lipoprotein could be an interesting candidate for this role.

The last PG-linked identified protein, BAB1_0729, remains puzzling as it was initially predicted to be periplasmic. Indeed, its sequence includes a signal peptide and its topology does not resemble a β-barrel. However, further modelling using AlphaFold2 (Mirdita *et al.*, 2017; Mirdita *et al.*, 2019; Mitchell *et al.*, 2020; Jumper *et al.*, 2021; Mirdita *et al.*, 2021) and Robetta (Raman *et al.*, 2009; Song *et al.*, 2013; Yang *et al.*, 2020; Baek *et al.*, 2021; Hiranuma *et al.*, 2021) revealed a possible β-barrel structure (supplementary figure 4). By sequence homology, it has a domain of

unknown function (DUF992) that is found in 277 species, mostly Rhizobiales, according to PFAM (PF06186). Thus, further investigation on this protein is needed to assess its localisation.

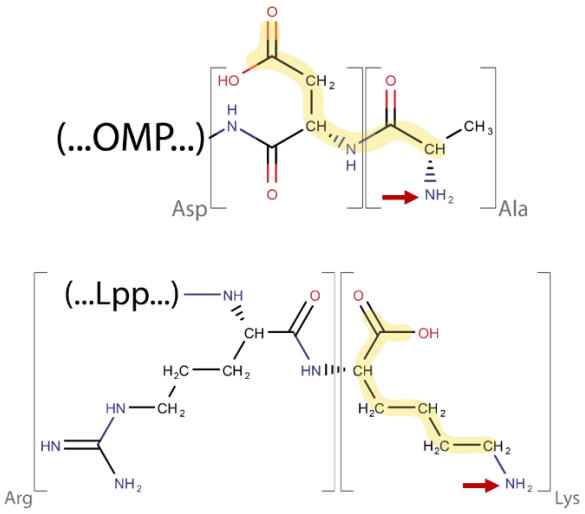

Figure 32 | Molecular similarities between *Brucella* OMPs and *E. coli* Lpp. The N-terminal alanyl-aspartyl moiety of the OMPs is represented above and the two last amino acids of Lpp, below. The yellow highlighting shows the similarity between the two structures. Six atoms are present in between the reactive amine and the carboxyl group. Thus the substrate of the LDt attaching Lpp to PG in *E. coli* (YbiS/LdtB) could be similar to the substrate attached by Ldt4 to the PG in *B. abortus*. The PG attachment site is shown by the red arrow.

Although Lpp and the OMPs are fundamentally different, it is interesting to note that they have a molecular similarity. Indeed, the number of atoms between the reactive amine and the carboxyl group is the same for both (Fig. 32). This could be an important feature when it comes to the attack of the enzyme-linked complex. This is supported by our data as when we added only one carbon in between the two groups (the D2E substitution), the anchorage of the Omp25 to PG was greatly reduced although still possible (see section 1.2.3 of the results). Nevertheless, we also showed that the Lpp- or OMP-based system are incompatible since the expression

of Omp25 in *E. coli* does not lead to attachment to PG, unless Ldt4, Ldt2 or Ldt1 of *Brucella* is also expressed (see section 1.1.2.2 of the results, Fig. 2a). Whereas the number of atoms between the two groups is a genuine mechanism or a coincidence thus remains to be determined, but this is consistent with the fact that LDts anchor both types of proteins to PG.

1.2 LDts are linking OMPs to the PG

In the published research, we showed that three LDt (Ldt1, Ldt2 and Ldt4) from *Brucella* can link Omp25 to the PG of *E. coli* see section 1.1.2.2 of the results, Fig. 2a). Intriguingly, only the Ldt4 had a visible effect on the amount of linked OMPs when deleted in *Brucella*. In that, *Brucella* situation is similar to *E. coli* where LdtB (or YbiS) is the main LDt and the role of the two other remains elusive.

It would therefore be interesting to gain more insight into the role of Ldt1 and Ldt2. According to RNA-Seq data (M. Roop, unpublished data), the Ldt1 appears to be transcribed under standard laboratory conditions while the Ldt2 does not seem to be expressed. Consequently, the approaches for their study would be radically different. For Ldt1, the first step would be to know if its deletion has any form of impact on the PG structure. Such information could be obtained by MS/MS analysis of the mutant muropeptides. It is also possible that this LDt only acts at discrete sites of the cell or specific timings of the cell cycle. Therefore, fusing Ldt1 to a fluorescent protein, such as the mNG, could give some clues about its function. Regarding Ldt2, the first step of its study would be to know when it is expressed. To answer, the *ldt2* gene could be replaced by the CDS of a fluorescent protein that would be produced instead of the Ldt2. It is possible that *ldt2* has a low level of expression, hence placing its promoter fused to the fluorophore on a medium copy plasmid might also

be a solution. Thus, several conditions could be tested and fluorescence rapidly visualised. Among the conditions that could be tested, the classical stress against bacteria (*i.e.* temperature, pH, salts, β-lactam antibiotics, SDS or Polymyxin B) could be relevant as well the infection of eukaryotic cells such as HeLa cells that are easier for micrographs due to their flatness.

However, one should not rule out the possibility we concluded that the Ldt1 had no effect simply because we did not look at the right OMP(s). We chose to evaluate the effect of Ldt(s) deletion by detecting the amount of bound and unbound Omp25 and Omp2b because the antibodies were available. Thus, we introduced a bias in our assessment as we only evaluated the effects on two out of six OMPs. Additionally, the heat stress data showed previously (see section 1.1.2.2 of the results, Fig. 2c) suggest that the combined deletion of the Ldt4 with the Ldt1 and 2 further destabilise the envelope as more Omp25 is detected in the suspension supernatant. WB may not be sensitive enough to detect the additional effect of the combined deletion of the Ldt1 and 4 (see section 1.1.2.5 of the results, Extended Data Fig. 4). To have a definitive answer, a semi-quantitative MS analysis should be performed on a *Δldt1* strain and compared to the WT.

1.3 Conservation of the system

We showed that the OMPs anchorage is conserved in their homologues across all the Rhizobiales. However, outside this order, the system does not appear to be conserved and naturally give rise to the question of how other bacteria tether the OM to the PG. The companion paper to our publication (Sandoz *et al.*, 2021) partially answered by showing OMP anchorage is also conserved in the γ-proteobacteria *Coxiella burnetii* and

Legionella pneumophila. Additionally, they showed that both systems can co-exist as *C. burnetii* has a PG-linked lipoprotein although the link happens with an internal lysine. One can thus assume bacteria have evolved systems either based on β-barrels or lipoproteins and possibly anchorage signals that are restricted to a small part of their phylogeny.

2 Discussion related to the additional results

2.1 CRISPRi

During this project, CRISPRi was used as a tool to study presumably essential genes or to stay in a physiologically relevant level of expression. To this end, we used a mobile system recently published (Peters *et al.*, 2019). However, the initial p_{lac} IPTG-inducible promoter was too leaky to be used in our model bacterium. We thus replaced the *lac* with a *tet* system, as it was shown to be not leaky for *virB11* at the Tn7 locus in *B. abortus* (Smith *et al.*, 2016). Although the control by AHTC was more effective, partial repression was still observed in the absence of AHTC by RT-qPCR in our validation assays suggesting a leak of the promoters. Unfortunately, no other inducible promoter than the IPTG and the Tet have been reported to work in *Brucella*. Still, as long as the mutant is viable even with the partial repression, this system can be used. It should also be mentioned that the first $_{sg}$RNA targeting the Omp25c showed no inhibition of the mRNA in RT-qPCR. Because the design method did not change compared to the others, it is complicated to answer why it did not work as sgRNAs were targeted to the ATG sites or in the close vicinity. In some cases, it might be better to design it more upstream or downstream, Therefore, a new $_{sg}$RNA was designed downstream the *omp25c* ATG to evaluate its potency. Although no mRNA level quantification was made,

the effects observed suggest it was efficient. Consequently, it is very likely that the $_{sg}$RNA efficiency greatly varies depending on the gene.

As a future direction, it would be very useful to be able to fuse several $_{sg}$RNA in a row. Indeed, this could help to understand the interplay between several essential genes at the same time. To this end, as many IIs type restriction enzymes as $_{sg}$RNA should be planned and cloning should be done sequentially. The main challenge here will be to find a way to put $_{sg}$RNA systems one after the other and then cleaved them afterwards. One option could be to use a mini-III RNase, an enzyme first characterised in *Bacillus subtilis* (BsMiniIII) and absent from proteobacteria. It is originally involved in the 23S rRNA (ribosomal RNA) maturation where it cleaves its 5' and 3' ends (Redko *et al.*, 2008). The BsMiniIII was shown to cleave specifically double-stranded RNA through the recognition of a sequence with the following consensus: GACC^UCG, with the scissile phosphodiester shown by the ^ mark (Glow *et al.*, 2015). Thus, it could be possible to add this sequence after the $_{g}$RNA scaffold termination signal and before repeating the $_{sg}$RNA construct. However, it should be first verified that introducing the BsMiniIII CDS in *Brucella* is not harmful for its physiology. Indeed, as this type of enzyme was never shown to be present in proteobacteria so far, it is possible that some of the *Brucella* dsRNA present the BsMiniIII cleavage site. If no effects are seen on the *Brucella* growth, then the BsMiniIII CDS could be added on the pJMP1339$_{t2}$ either with a p_{lac} for constitutive expression or under the same p_{tetA} as the dCas9 for an inducible control. Because RT-qPCR is rather a delicate method, a test strain could be set up where several fluorescent proteins could be expressed to rapidly and efficiently assess the system functionality.

2.2 The LDts

This work has partially focused on the identification and characterisation of the LDts of *B. abortus*. Upon single deletion of the eight putative LDts, only the Ldt7 mutant showed a morphology defect. Further data lead to the hypothesis that this enzyme could be involved in the PG remodelling. Although the absence of fluorescence localisation might be due to a problem with the fusion, it is also possible that it is localised all across the periplasm at all times of the cell cycle. The fact that the mutant has a rounder morphology, and that the Ldt7-mNG strain does not, supports the idea that the Ldt7-mNG fusion is at least partially functional. In addition, it has been reported in *C. crescentus* that even if LdtD is the major LDt involved in stalk synthesis, it is homogeneously distributed across the cell body and stalk (Stankeviciute *et al.*, 2019). This exemplifies that the function ensured by an enzyme does not always require its presence only at the site of reaction, or the enzyme may have several functions at different locations, and only one is discovered so far. Another option is that it could be involved in the general PG maturation and editing. In *A. tumefaciens*, it was shown that the unipolar growth involved an increase of the length of the cell but also the width (Cameron *et al.*, 2014). Consequently, if the mutant is unable to perform the PG editing necessary for diameter enlargement, it could lead to a swollen phenotype.

To have more insights into this LDt role, it is crucial to be able to determine the muropeptide composition of the mutant and compare it to the WT strain. It is a common practice to evaluate the muropeptide variation of a given mutant by comparing its purified and digested PG HPLC profile to the WT. However, as the PG composition can be quite different from a strain to another, it is first necessary to identify the muropeptides that correspond to the HPLC peaks. As this has never been

done for *Brucella* before, we aimed to establish its profile by a collaboration. As explained before, this was initiated but will have to be further pursued. Once the WT profile is determined, all the other mutants could be investigated by starting to check if there are any differences in the muropeptide content.

In our published data, we failed to completely prevent the anchorage of OMPs through LDts deletions. Hence, at least one more LDt has this function. Based on LDt sequences, no obvious candidate arose as the Ldt1, 2 and 4 were forming a monophyletic group in our analysis due to similar amino acid sequence (see section 1.1.2.5 of the results, Extended Data Fig. 3). In addition, these three LDts were the only lipoproteins, exception made of BAB1_2034. As explained in the results, based on the quadruple mutants, Ldt5 is our most potent candidate. While it was simple to obtain in the WT background, we could not get its deletion in the Δ*ldt1,2,4* background. Thus it is most likely essential in the absence of Ldt1, 2 and 4, presumably because the OM-PG attachment is essential for growth or survival.

To further characterise OMP-PG attachment, a CRISPRi system with a $_{sg}$RNA targeting the *ldt5* was inserted in the Δ*ldt1,2,4* background and phenotypes consistent with OM-PG anchorage defect were observed. Although these data are very preliminary, it is tempting to consider future directions.

Now that another key LDt has been identified, new mutant combinations should be tested. For instance, a Δ*ldt4,5* could answer whether the Ldt1 and Ldt2 are accessories and only the Ldt4 and Ldt5 play a major role. It is noteworthy that, according to the growth curves (Fig. 15), the effects are only visible after at least five replication times. This could be due to a

limit dilution; although no new Ldt5 are produced, some are still present in the periplasm that can be partly transmitted to the daughter(s) and can ensure their role. However, with dilution by divisions and proteolysis, the pool gradually diminishes until the breaking point and growth is no longer possible. Nevertheless, this is not lethal as removing the inducer results in restored growth.

As structures consistent with blebs were observed in phase contrast microscopy, the next step would be to validate the blebbing in cryo-EM and the homogeneity of the periplasm size could also be verified as it was shown to be constant in the Δ*ldt1,2,4* mutant (see section 1.1.2.5 of the results, extended data fig. 5). Surprisingly, the WB (Fig. 15) showed no obvious OMP-PG difference between the non- or induced mutant. Because we know the AHTC-induced CRISPRi system to be leaky, it is possible that, in the non-induced condition, the Ldt5 production is already largely reduced to a level that is still sufficient for growth without defect. While, when induced, a threshold is passed and, although not much difference is seen by western blotting, it could be sufficient to lead to blebbing. The remaining pool of bound Omp25 in the induced condition could also be an artefact. As the effect is not immediately following the induction, the WB sample still contains a substantial part of mother cells with, presumably, enough Omp25 bound to the PG. It is also striking that no more bound Omp2b can be detected in the non-induced condition and raise the question of enzyme specificity. Although we have no data supporting such a mechanism, it could be relevant to perform quantitative MS on the Δ*ldt1,2,4* and the Δ*ldt5* as we could only monitor the anchorage of two OMPs out of the seven.

2.3 Anchorage essentiality

As the cumulative D2A point mutation was not possible for the Omp2b, Omp25 and Omp25c, the simplest explanation was the toxicity of these multiple mutations, for growth or survival. This hypothesis was supported by the use of a $_{sg}$RNA silencing *omp25c*. However, due to the preliminary nature of these data, speculation should be done with caution. While Omp25c is not predicted as essential (Sternon *et al.*, 2018), the CRISPRi system should also be inserted in the Omp2b$_{D2A}$ or Omp25$_{D2A}$ mutant alone to validate the absence of phenotype. It is, however, interesting to note that *Brucella* covalent OM-PG linkage would not be dispensable, contrary to *E. coli*. One major difference between both bacteria is that, while both possess Pal, *E. coli* still has OM-PG non-covalent interactions mediated through the abundant OmpA. Supporting this, it was shown that a Δ*lpp*Δ*ompA* mutant exhibits extensive blebbing, has a spherical morphology and needs increased concentration of Mg^{++} or Ca^{++} for optimal growth (Sonntag *et al.*, 1978). In addition, some induced Omp25-2b$_{D2A}$ $_{sg}$*omp25c* bacteria undergo a discharge as suggested by time-lapse microscopy data (Fig. 20). Therefore, the nature of the released material should be assessed. This could be achieved by western blotting with antibodies against proteins from the OM, the periplasm and most importantly, from the cytoplasm on an induced culture supernatant. Finally, because growth in liquid culture and on a pad is very different, microfluidic could be used to finely determine the time necessary for the apparition of the first morphological defects. This technique could also be used to evaluate if all bacteria can recover after the induction or if some, such as those that seem to experience a discharge, are dead.

2.4 Reversing the anchorage

While Lpp was characterised fifty years ago, the mechanism by which the link between Lpp and the PG was cleaved was still unknown. Beginning of 2021, two teams simultaneously reported that LdtF is an amidase (Bahadur *et al.*, 2021; Winkle *et al.*, 2021a). The fact that it was thought to be an LDt for years shows that two genes can encode highly similar proteins with two opposite activities. In our study, we showed that an ORF, first identified as an LDt *in silico* had the opposite expected effect on the OMPs anchorage when deleted (see results, Fig. 22). However, this phenotype could be due to two distinct enzymatic activities: carboxypeptidase or amidase.

In the first case, an L,D-carboxypeptidase would specifically chop off the fourth D-alanine from a tetrapeptide stem, the substrate for OMP transpeptidation. In a deletion strain, more substrate would be available for the LDts such as the Ldt4 and consequently, more OMPs could be linked. This could be detected in a MS analysis, using the *ΔBAB1_2034* and the pBBR1 over-expression strain. Indeed, when comparing the muropeptide profiles, a decrease of tripeptide stems should be observed in the deletion strain and conversely in the over-expression mutant. In the case of an amidase, the amount of tripeptide should remain unchanged either in a deletion or an over-expression strain while the variation of the tetrapeptide could be observed. However, this first requires the characterisation of the HPLC muropeptide profile of *Brucella* peptidoglycan as it has never been done so far. It could also be of interest to look at the variations in the number of linked-OMPs although this would imply heavier semi- or quantitative mass spectrometry.

Although the amidase of *E. coli* is already published, it is still relevant to continue the investigation of BAB1_2034 as the virulence of *Brucella* is impacted. Indeed, we have shown that the deletion strain has a lower CFUs count at the late time point of infection. As a reminder (see section 2.3 of the introduction for more information), the 2 h PI reflects the bacterium ability to enter the cell and form the eBCV. The 5 h PI reflects its potential to survive the stress of the late endosomal pathway and to evade it. The 24 h PI shows the capacity to interact with the ERGIC to form the rBCV and to proliferate. Finally, the 48 h PI time point, the ability to further proliferate. Considering this, the data obtained lead to questions in many aspects.

First, because the deletion of BAB1_2034 modifies the anchorage level of the envelope layers, one might expect to see defects under stressful conditions, hence at 5 h PI. Still, the decrease of CFUs happens at 24 h. Two explanations can be proposed; (i) the bacteria are somehow killed in the process of reaching their niche. Although it is known that a bottleneck happens during the first hours of the infection, no stress sufficient to induce killing has been reported after the transition of the eBCV to the rBCV, to our knowledge. Or, (ii) once in the rBCV, a replication issue occurs. This could be either a greater doubling time, an accident during cell division as well as a delay to start growth and division. We know from the growth data in rich medium that the deletion strain has no defect compared to the WT in rich medium. The conditions of the infection might affect growth while it is unlikely as the CFUs increase between the 24 h and the 48 h PI are consistent with the WT. Hence, a delay between the rBCV establishment and the beginning of replication might be the best hypothesis. To discriminate the two hypotheses, (i) or (ii), the sensitivity to relevant stresses such as pH or lysozyme could be assessed to help

decide if killing could occur later than usually thought. The intracellular trafficking, as well as the replication, could be monitored by creating a Δ*BAB1_2034* strain expressing constitutively the mCherry and by immunofluorescence, to detect typical markers of the rBCV (*e.g.* calreticulin). Imaging cells at intermediate time points between 5 and 24 h PI could help to detect a problem to reach the niche, a delay to start replication or a growth issue.

Another interesting observation is that it seems that the equilibrium of bound and unbound OMPs is decisive for the bacterium. While an excess of bound proteins induces a decreased virulence, less tethering between the two layers leads to a similar phenotype. Although one could argue that the pBBR1::*BAB1_2034* strain has a growth defect in rich medium, the recovery of CFUs number between 24 and 48 h PI excludes the simple defect and suggests that there is something more to it. This is further supported by the results of the pMR10 complementation as the CFU counts at 24 h PI gets higher than the 5 h PI. This suggests that although the virulence is not restored at the WT level, the pMR10::*BAB1_2034* allows an expression closer to the endogenous level, hence partially restoring the balance. Yet the CFUs count at 48 h does not increase compared at 24 h as it would be expected, based on the WT or the Δ*BAB1_2034* derivative strains. It could also be interesting to introduce either the pMR10 or the pBBR1 expressing the *BAB1_2034* in the WT to produce a mild or strong over-expression respectively and verify if we can modulate the virulence defect.

Although an increased anchorage of OMPs to the PG was observed by western blotting for the $_{sg}$*BAB1_2034* strain upon induction, the CFU counts were the same as the WT in an infection context. This could be the

result of poor inducer availability once in the cell and thus, less efficient repression of *BAB1_2034*. While AHTC use has already been reported during *Brucella* infection (Smith *et al.*, 2016), a major difference is that the authors used it to induce the production of their protein while here the aim was to silence it. Hence, AHTC usability may be different depending on the application. Because it would be difficult to verify its level of expression during the infection, a possibility could be to use an existing *Brucella* mCherry strain and to assess the repression of the fluorescence in the course of the infection, using the CRISPRi system.

However, the infection results are hard to conceal with those of both the Omp2b/25$_{D2A}$ and *Δldt1,2,4*(**c**) mutants, even if these data were generated in RAW 264.7 macrophages instead of J774A.1. In the Omp2b/25$_{D2A}$ and *Δldt1,2,4*, the amount of free-OMPs is significantly increased while in the *Δldt1,2,4*c, it is decreased to the profit of bound OMPs (see section 1.1.2.1 of the results, Fig. 2b). Still, none of the three strains has a virulence defect (see section 1.1.2.2 of the results, Extended Data Fig. 6). For the Omp2b/25$_{D2A}$ strain, it might be because only these two OMPs are affected and the rest can stand up for their anchorage loss. However, in the *Δldt1,2,4* and complemented strain, all OMPs should be affected the same way and thus, the absence of virulence defect suggests that the effects seen with the Δ*BAB1_2034* might be indirect.

Ultimately, insights about the virulence defect might be obtained by going back to forward genetic approaches. A classical approach would be to look after suppressors that regain a WT virulence after systematic passage in macrophages. However, this experiment is quite heavy due to the number of bacteria necessary for the emergence of suppressing mutations. Another – but heavy – approach could be to perform a Tn-seq;

by using a mini-Tn*5* that randomly inserts in the genome, the fitness of the disruption mutants could be assessed during a cellular challenge. This could unveil a combination that could have either a virulence worse than the deletion strain alone or better.

Finally, we have seen consistently – although we could not quantify it – that when mutating the Omp25 aspartate D2, the amount of linked Omp2b would increase and conversely (see Results, Fig. 22). This also leads us to think that the anchorage dynamics might be a passive mechanism in the sense that as long as there are substrates, OMPs linkage will take place disregarding the OMP type. The regulation might rather take place through the position of the involved enzymes. Indeed, it is possible that the amidase would preferentially be located at the sites where detachment and plasticity of the envelope are needed, *e.g.* the constriction site. We have tried to localise the BAB1_2034 by fusing its C-terminal end to a mNG fluorescent protein. Unfortunately, no specific localisation could be shown although the signal sometimes appeared patchy at the growing poles. Because no antibodies against the mNG are available, degradation or subcellular mislocalisation could occur. To circumvent this issue, a tag (*e.g.* FLAG-tag) could be inserted in the construction, either between the two CDS or at the end, to check the degradation. Checking the protein localisation would be trickier but could possibly be achieved by fractionation, although if it is not degraded, it is likely to be correctly exported. Fusion with a different fluorophore, the mTurquoise2Ox, was also tried as antibodies are available but no fluorescence was observed (data not shown). It should be noted that its use has never been reported in *Brucella*.

GENERAL CONCLUSION

Over this study, we have investigated the interactions between the OM and the PG in *Brucella abortus*. We showed that, contrary to *E. coli*, which relies on a single lipoprotein to tether these two envelope layers, *Brucella* has developed a multiple β-barrels based anchorage system. However, the advantage of β-barrels over a lipoprotein remains unclear. Although it seems reasonable that grouping two functions in one protein would be an energy-saving process. With these findings, we showed that, despite being useful tools, model bacteria show their limitations and that bacterial variability should be readily explored.

In line with *E. coli*, we brought evidence that the attachment of *Brucella* OMPs is dependent on LDts. Even if we identified three LDts able to attach Omp25 to *E. coli* PG, we could only demonstrate the activity of Ldt4 in *Brucella*. Even by creating a triple deletion strain, the anchorage of OMPs to the PG was never fully abolished. Identifying the remaining LDt involved would be of interest as a quadruple mutant – if there is only one more – could have a further destabilised membrane that could lead to virulence defects in an infection model. In addition, we showed that the +2 aspartate of the OMPs is crucial for anchorage. While the charge is probably important, it also seems that the length of the amino acid lateral chain is also a determinant of enzyme recognition.

Out of the eight putative LDts, the role for four of them still requires investigation but would require glycan proteomic analysis. Furthermore, we provided insight for two other proteins with an LDt domain: Ldt7 and BAB1_2034. The clues obtained for Ldt7 suggest a role in the PG remodelling and establishment of 3-3 links. On the other hand, data collected on BAB1_2034 indicate an amidase rather than an LDt activity as originally predicted. In addition, we showed that the equilibrium of

linked OMPs is likely to have a role – direct or not – in the cellular infection models used. However, MS data are needed to determine their activity with confidence.

In conclusion, while we provided some new insights into *Brucella* envelope, many aspects are still largely unknown. Intense investigation to better understand the structure, biogenesis, repair and adaptation of the bacterial envelope of this pathogen is essential in the prospect of targeting the envelope as a part of the crucial targets for a potential therapeutic approach.

SUPPLEMENTARY

1 Supplementary methods

Plasmids and strains

E. coli DH5α, BL21(DE3), BW25141, MFD pir and derivatives strains were grown in Luria-Bertani (LB) medium at 37 °C under constant agitation. When necessary, culture media were supplemented with the appropriate antibiotic at the following concentrations: ampicillin, 100 µg/ml; carbenicillin, 50 µg/ml; *meso*-DAP (Sigma), 300 µM; AHTC, 0.2 µg/ml.

Strains construction

The additional list of *E. coli and B. abortus* strains and primers used in this study can be found in Supplementary Table 2, 3, and 4 respectively.

J774.A1 macrophages culture and infection

RAW J774A.1 murine macrophages (ATCC) were cultured at 37°C, 5 % CO_2 in DMEM (GIBCO) supplemented with 10 % heat-inactivated foetal bovine serum (GIBCO). For infections, J774A.1 macrophages were seeded in 24-well plates at a density of 10^5 cells per well and let O/N for growth and adhesion. The day after, *Brucella abortus* infections doses were prepared in DMEM from exponential cultures (OD_{600nm} 0.3-0.6) washed twice at a multiplicity of infection of 50. Bacteria and cells were centrifuged at 169 × *g*, 4 °C, 10 minutes and incubated until the time point at 37 °C, 5 % CO_2. One hour after the beginning of infection, the culture medium was replaced with DMEM supplemented with 50 µg/ml of gentamycin to kill any remaining extracellular bacteria. One hour later, culture media was changed again with fresh DMEM supplemented with 10 µg/ml of gentamycin. At the different time points (i.e. 2, 5, 24 and 48 h post-infection), cells were washed twice in PBS, then lysed with PBS - 0.1 % Triton X-100 for 10 min at 37 °C. Dilutions were then spotted (20 µl) on TSB agar, incubated at 37 °C and colony-forming units were counted.

Microscopy and analysis

Two µl of bacterial suspension were spotted on 1 % agarose PBS pads for imaging. Images were acquired with a Nikon Eclipse Ti2 equipped with a phase-contrast objective Plan Apo λ DM100XK 1.45/0.13 PH3 and a Hamamatsu C13440-20CU ORCA-FLASH 4.0. Images were processed with FIJI 2.0.0 (Schindelin *et al.*, 2012), a distribution of ImageJ. LUTs were adjusted to the best signal-noise ratio. Bacteria were detected, analysed and plotted by the ImageJ plugin MicrobeJ (Ducret *et al.*, 2016).

HADA labelling

Cells from exponential phase culture (50 µl) were incubated for 5 min at 37 °C with HADA at a final concentration of 500 µM. Cells were then washed twice with

PBS by centrifugation at 7000 RPM, 2:30 min, RT. Cells were then observed by fluorescence microscopy.

Growth curve

Growth was assessed by using an Epoch2 Microplate Reader from BioTek. O/N cultures were diluted to OD_{600nm} 0.1 and supplemented with the appropriate complement. OD was then measured every 30 min over 72 h at 37 °C. GraphPad Prism was then used to visualise results.

Gibson Assembly

The Gibson assembly was performed as follows: to 10 µl of 2x mix were added the vector and the insert(s) in a 1:1 ratio with 100 ng of vector as the basis. The reaction was assembled on ice, incubated at RT for 30 seconds and then incubated O/N at 50°C. Primers used for the inserts amplification were designed with Benchling and had 40 overlapping bases. The 2x Gibson Mix was made *in house* and for 800 µl, made of 0.6 µl T5 exonuclease (10 U/µl, NEB), 20 µl Phusion DNA polymerase (2 U/µl, NEB), 160 µl *Taq* DNA ligase (40 U/µl, NEB), 320 µl 5x reaction buffer (see below) and 300 µl of water. The 5x reaction buffer consisted of Tris-HCl 0.5 M, $MgCl_2$ 50 mM, 1mM of each dNTPs, DTT 50 mM, ¼ W/V PEG 8000, NAD 5mM and water.

CRISPRi

The CRISPRi plasmids (pJMP1039, pJMP1339, pJMP1356 and pJMP1339) were bought from Addgene (see supplementary table 2) and were a gift from Carol Gross & Jason Peters & Oren Rosenberg. The pJMP1339t2 was constructed by Gibson Assembly (see section 7). Single guides were designed with Benchling and chosen on the minus strand, then assembled on the *Bsa*I sites of the $pJMP1339t_2$ as detailed by the authors in a later and more detailed publication (Banta *et al.*, 2020). The dimerisation of the sgRNAs and subsequent steps until conjugation with *Brucella* were made as described by Banta and colleagues (Banta *et al.*, 2020). Dimerisation was made by adding 1 µL of each primer (100 µM) to 5 µl of CutSmart 10X buffer (NEB) and scaled up to 50 µL with $_{dd}H_2O$. The mix was then heated at 95 °C for 5 min and let cool down at RT for 15 min. Annealed oligos were diluted 40X and 2 µl were used for ligation with the BsaI restricted plasmid.

Preparation of electro-competent cells

500 mL of pre-warmed LB were inoculated with 5 mL of O/N culture and incubated at 37 °C until OD_{600nm} 0.5 – 0.6 was reached. Cells were collected by centrifugation at 4 °C, 4000 RPM for 10 min and resuspended in 50 ml of sterile ice-cold $_{dd}H_2O$. This process was repeated 4 times to eliminate residual salts. The

final pellet was resuspended in a small volume of $_{dd}H_2O$ – 15 % glycerol (typically 2 mL) and aliquoted in tubes of 50 µL.

Transformation by electroporation

DNA was first dialysed on 0.025 µm membranes (Merck) and 10 µl were added to thawed *E. coli* BW25141 or MFD pir electro-competent cells and transferred to 2 mm electroporation cuvettes (Eurogentec). Cells were then shocked with a pulser (BioRad, Gene Pulser Xcell Electroporation system) with the following parameters: 25 µF, 200 Ohms, 2500 V for a shock duration between 4.7 and 5.3 ms. Cells were then resuspended in 1 ml of RT LB medium and incubated at 37 °C, shaking for 45 min. Bacteria were recovered by centrifugation (3 min, 2350 × *g*), resuspended in 100 µl of LB and the transformants were then selected on LB agar supplemented with the appropriate antibiotic.

RNA extraction and reverse transcription

Cells were recovered from exponential phase culture or after 2 h AHTC induction by centrifugation at 7000 RPM, 5 min, 4 °C and washed twice with PBS. Pellets were resuspended with 100 µl SDS 10 % (Sigma), 10 µl of proteinase K (20 mg/ml, VWR) and were incubated at 37 °C for 1 hour under agitation to lyse the cells. Then, 1 ml of TriPure (Roche) was added, the suspension was homogenised by pipetting and incubated for 10 min at 65 °C. To this, 200 µl of chloroform were added, homogenised by inversion for 30 sec and let to rest for 10 min at RT. Tubes were then centrifuged at 13.500 RPM, 15 min, 4 °C and 400 µl were recovered from the aqueous phase. Then, 400 µl of isopropanol were added (with or without Glycoblue co-precipitant[5] (Invitrogen)) and were centrifuged at 14.000 RPM, 30 min, 4 °C. Supernatants were eliminated and 1 ml of 75 % RNase-free ethanol was added. Upon centrifugation at 8000 RPM, 5 min, 4 °C, supernatants were removed and tubes were centrifuged at 10.000 RPM, 1 min to ensure complete removal of alcohol. Pellets were then resuspended in 50 µl of DEPC (Sigma) $_{dd}H_2O$ and incubated at 55 °C, 10 min for optimal solubilisation.

Samples were further treated with DNase I (1 U/µl, ThermoFisher). In a volume of 9 µl were added, 1 µl of 10X buffer, 1 µl of DNase I, 1 µg of RNA and filled up with DEPC $_{dd}H_2O$. Samples were incubated at 37 °C, 30 min and then, 1 µl of EDTA 50 mM was added to stop the reaction and incubated at 65°C for 10 min. The reverse transcriptase was performed with the High Capacity cDNA Reverse Transcriptase kit (Applied Biosystems). To the 10 µl of DNase I-treated RNA were added, 2 µl of 10X random hexamer and 4.2 µl of DEPC $_{dd}H_2O$ and

[5] If available, Glycoblue can be used to easily visualise the RNA pellets.

hybridisation was made at 65 °C for 10 min followed by a 1 min incubation at 4 °C. To this, 2 µl of RT buffer 10X, 0.8 µl of dNTPs 100 mM and 1 µl of reverse transcriptase were added. It should be noted that every step since the DNaseI treatment was made in double for each condition to have an RT- control where reverse transcriptase was replaced by water. The mix was then incubated at 25 °C for 10 min, 37 °C for 120 min and 85 °C for 5 min. The $_{c}$DNA was then diluted 10 fold with DEPC $_{dd}H_2O$.

qPCR

Plates were designed by using the manufacturer software (LightCycler 96, v 1.1, Roche). The master mix included, per reaction, 1 µl of each primer at a final concentration of 300 nM, 5 µl of Takyon SYBR MasterMix blue dTTP (Eurogentec) and 3 µl of $_{c}$DNA was added to each well. The amplification program was the following: a pre-incubation at 95 °C for 10 min, 45 cycles of 3 step amplification (95°c, 10 sec; 60 °C, 10 sec; 72 °C, 10 sec) and melting step (95 °C, 10 sec; 65 °C, 60 sec and 97 °C, 1 sec). GAPDH was used as reference, with the following primers at a final concentration of 200 nM: forward, 5'- GAT ACG ATC GAT GTT GGC TAC G -3'; reverse, 3'- CAA GAT GAA GTG CTG CCT TGT C -3'. Data were subsequently analysed with LightCycler 96 and Excel (Microsoft). The fold change was calculated as $2^{-\Delta\Delta Ct}$.

Protein overexpression and purification

Over-expression plasmids were made by using the pET20a. A flask with 1 l LB supplemented with the appropriate antibiotic was inoculated with 1 ml of O/N culture of the over-expression strain and let grown until OD_{600nm} reached 0.3 – 0.6. At this point, 1 ml was withdrawn for the non-induced control and the culture was induced with IPTG at a final concentration of 1 mM for 3 to 4 h. As previously, 1 ml was taken for the induced control. The rest of the culture was centrifuged at 5000 RPM, 15 min, 4 °C and cells were resuspended in 20 ml of PBS-PI buffer (one pill of protease inhibitor (Roche) for 50 ml of PBS) to which was added 400 mg of lysosyme (Sigma) and 10 mg of DNaseI (Roche) and let at RT for 30 min. Cells were further lysed by sonication for 6 cycles of 30 sec (power 6, Sonifier, Branson Ultrasonic Corporation) followed by 30 sec on ice. Samples were centrifuged at 12.000 RPM for 30 min at 4 °C and the supernatants were recovered.

The purification was made by using a column loaded with 1.2 ml of Ni-NTA HisBind Superflow (Millipore) diluted in 5 ml of $_{dd}H_2O$. Water was let through and the sample was loaded for an incubation of 1 h at 4 °C. Then, 1 ml of flowthrough was recovered for control and 5 ml of binding buffer was loaded and let through. Subsequently, 3 ml of the wash buffer 1, 2 and 3 and of the elution buffer (see below) were loaded. The elution product was divided into

fractions of about 300 µl and kept on ice. All samples from the NI induced control to the elution fractions were loaded on a gel for verification.

	Binding Buffer*	Wash Buffer 1	Wash Buffer 2	Wash Buffer 3	Elution Buffer
5 M NaCl	5 ml	5 ml	5 ml	5 ml	5 ml
1 M Imidazole	0,625 ml	1,25 ml	2,5 ml	3,75 ml	5 ml
Glycerol	5 ml	5 ml	5ml	5 ml	5 ml
1 M Tris-HCl pH 8.0	1ml	1 ml	1 ml	1 ml	1 ml
H_2O	38,375 ml	37,25 ml	36,25 ml	35,25 ml	34 ml

2 Supplementary figures

Supplementary Figure 1 | Additional informations on *B. abortus* putative LDts. In dark and light blue are shown the YkuD or YcbB domains, respectively. The catalytic cysteine are shown in red and the polypeptide binding sites in yellow. The domains were predicted with a Conserved Domains search (Marchler-Bauer *et al.*, 2017), the 3D structure was computed by alphaFold (Mirdita *et al.*, 2017; Mirdita *et al.*, 2019; Mitchell *et al.*, 2020; Jumper *et al.*, 2021; Mirdita *et al.*, 2021) and visualised with PyMOL.

Ldt1	BAB1_0047	
Export signal	TAT/SPI (1-36)	
Length	241 AA	
Domains	**Position**	**E-value**
YkuD-like	107-240	$2.38e^{-29}$
ErfK	104-240	$1.71e^{-60}$
Comment		

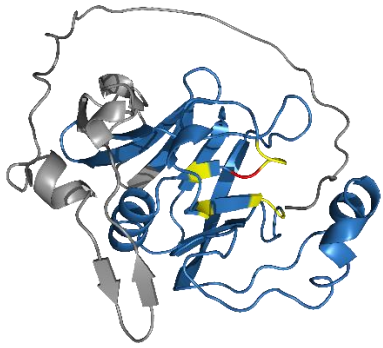

Ldt2	BAB1_0138	
Export signal	SPII (1-20)	
Length	206 AA	
Domains	**Position**	**E-value**
YkuD-like	71-204	$6.76e^{-30}$
ErfK	30-206	$1.85e^{-60}$
Comment		

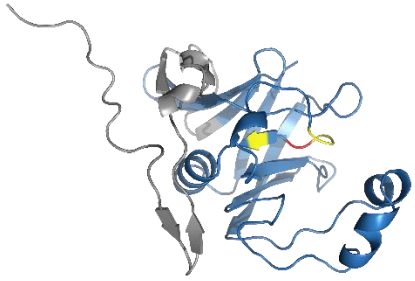

Ldt3	BAB2_0178	
Export signal	Sec/SPI (1-27)	
Length	227 AA	
Domains	**Position**	**E-value**
YkuD-like	113-215	$8.69e^{-17}$
ErfK	1-218	$5.68e^{-44}$
Comment	No catalytic moiety	

Ldt4	BAB1_0589	
Export signal	SPII (1-24)	
Length	238 AA	
Domains	**Position**	**E-value**
YkuD-like	101-237	$1.40e^{-25}$
ErfK	22-237	$3.49e^{-61}$
Comment		

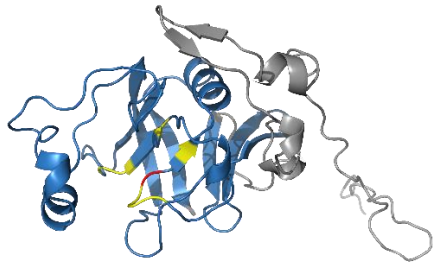

Ldt5	BAB1_0785	
Export signal	TAT/SPI (1-40)	
Length	433 AA	
Domains	**Position**	**e-value**
YkuD-like	204-369	$1.46e^{-12}$
YcbB	15-433	0^{e00}
PG-binding	115-173	2.49^{e-9}
Comment		

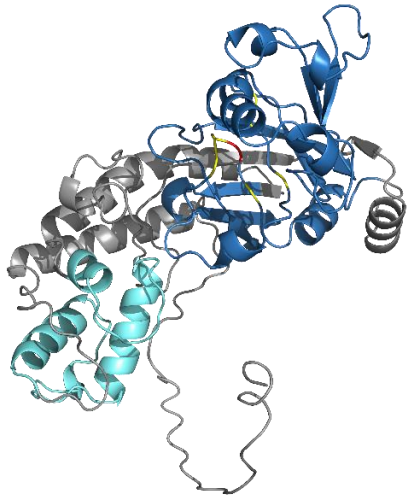

Ldt6	BAB1_0978	
Export signal	TAT/SPI (0-42)	
Length	523 AA	
Domains	**Position**	**e-value**
YcbB	133-466	$2{,}88e^{-108}$
PG-binding	372-404	$4{,}25e^{-4}$
Comment	Possible pseudo-gene with BAB1_0979	

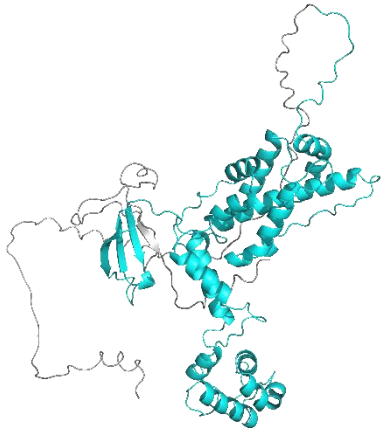

Ldt7	BAB1_1159	
Export signal	TAT/SPI (1-31)	
Length	237 AA	
Domains	**Position**	**e-value**
YkuD-like	102-236	$5.12e^{-28}$
ErfK	7-236	$1.94e^{-54}$
Comment		

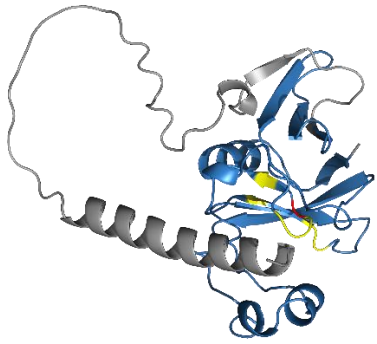

Ldt8	BAB1_1836	
Export signal	None	
Length	408 AA	
Domains	**Position**	**e-value**
YkuD-like	275-405	$3.77e^{-27}$
ErfK	196-408	$8.23e^{-43}$
Comment		

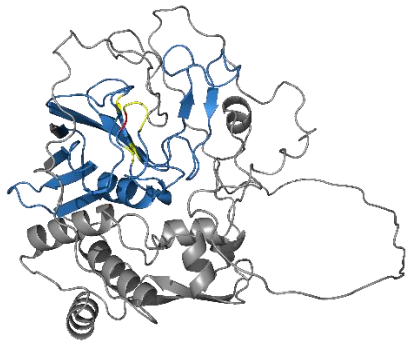

Ldt9	BAB1_0979	
Export signal	None	
Length	173 AA	
Domains	**Position**	**e-value**
YkuD-like	275-405	$3.66e^{-7}$
YcbB	1-173	$1.14e^{-90}$
Comment	Possible pseudo-gene with BAB1_0978	

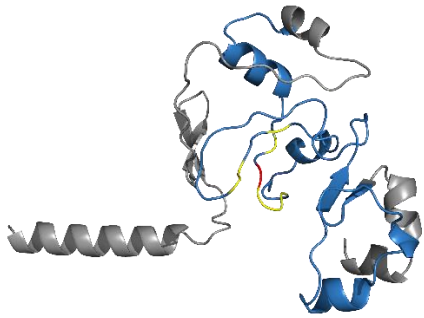

Ldt10	BAB1_2007		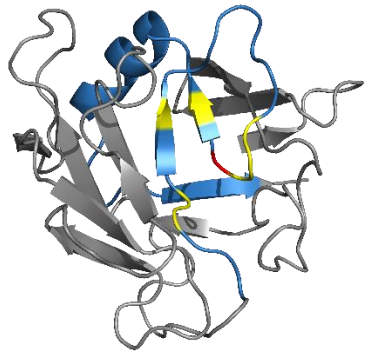
Export signal	None		
Length	167 AA		
Domain	**Position**	**e-value**	
YkuD-like	122-165	$9.51e^{-4}$	
Comment	Could be an hydrolase		
Ldt11	BAB1_2034		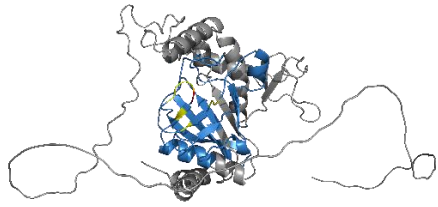
Export signal	SPII (1-19)		
Length	403 AA		
Domains	**Position**	**e-value**	
YkuD-like	56-169	$3.33e^{-4}$	
YafK	2-299	4.13^{-136}	
Comment	Possible amidase		

Supplementary Figure 2 | Putative *Brucella* LDts active sites. A. Alignment of putative LDts exception made of those without any predicted catalytic sites and BAB1_2034, the catalytic cysteine is shown in red and the surrounding binding sites in yellow. **B.** Catalytic site of BAB1_2034, the color code is the same as above. Numbers on the right correspond to the amino acid position.

```
A  BAB1_0047   QSMSSGCIRLMNQDIID-LYNRVQGKA 236
   BAB1_0138   KAMSSGCIRLMNQDIID-LYNRVEQGA 200
   BAB1_0589   KAVSSGCVRFLNQDIID-LYDRVPAKT 233
   BAB1_0785   RFDSSGCVRVQNVRDLDVWLLKNTLGW 372
   BAB1_1159   SSASNGCFRMINEDVMD-LYDRVTLGT 232
   BAB1_1867   KISSHGCVRLTNWDAEE-LAKLVKPGV 402
   BAB1_0979   RALSHGCIRLERPRDMAAAVLGTSV-- 108
   BAB1_2007   YTPTEGCIALKRADMARLLPHLTDRTV 162

B  BAB1_2034   ANGRTGQHLMVHGACSSSGCYSMTDEQ 143
```

Supplementary Figure 3 | Plasmid maps of the pJMP1337 and pJMP1339.

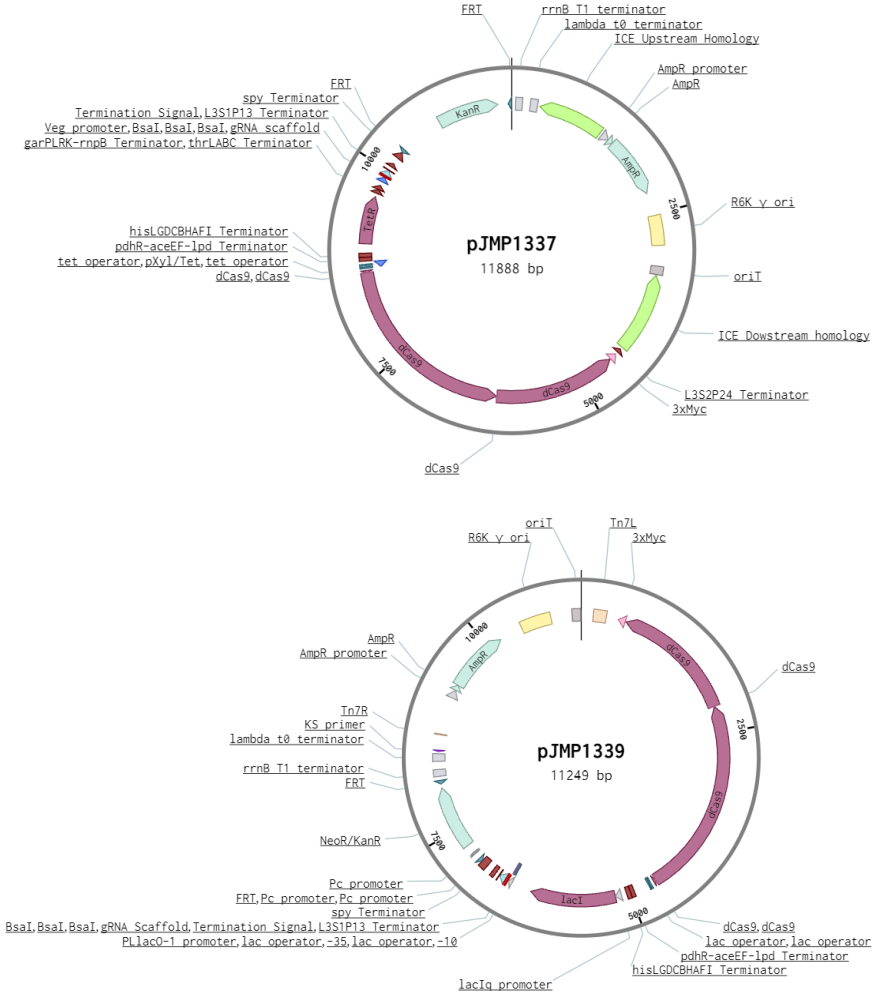

Supplementary figure 4 | BAB1_0729 predicted structure. These predictions were made by using **A** I-TASSER, **B** Robetta and **C** AlphaFold2. The models of Robetta (grey) and AlphaFold2 (blue) are superimposed in **D**.

A

B

C

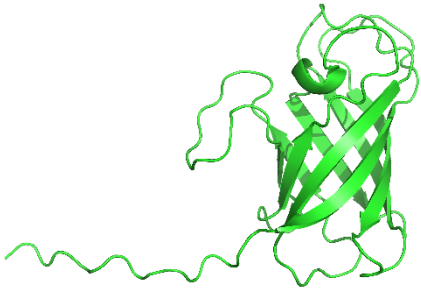

D

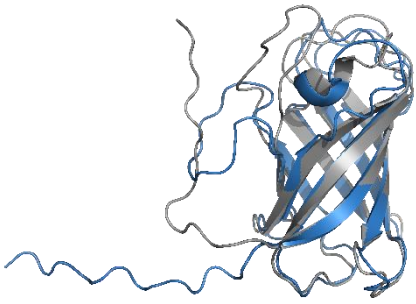

3 Supplementary tables

Supplementary table 1 | Predicted lipoproteins in the *Brucella* abortus genome. Lipoproteins were predicted on the whole proteome by using LipoP. NE, not essential; E, essential; NIV, not involved in virulence; IV, involved in virulence; DP, defect on plate

ORF	Tn-Seq Data	Predicted function
BAB1_0038	NE, NIV	*bamD*
BAB1_0047	NE, NIV	*lptE*
BAB1_0064	NE, NIV	*pal*
BAB1_0138	NE, NIV	*cdlP*, Zn-dept peptidase
BAB1_0358	NE, NIV	*bamE*
BAB1_0511	NE, NIV	*exoR*
BAB1_0589	NE, NIV	*mlaA*
BAB1_0630	DF	*omp19*
BAB1_0663	NE, NIV	*omp10*
BAB1_0758	NE, NIV	*virB7*
BAB1_0794	E	Possible polysaccharide export protein
BAB1_0804	NE, slightly IV	Conserved hypothetical
BAB1_0819	NE, NIV	Hypothetical
BAB1_0858	NE, NIV	L,D-transpeptidase
BAB1_0891	E	Hypothetical
BAB1_1009	NE, NIV	Hypothetical
BAB1_1035	NE, NIV	Hypothetical
BAB1_1041	NE, DF	Hypothetical
BAB1_1208	NE, NIV	PG-binding domain in C-term
BAB1_1226	NE, NIV	Lytic transglycosylase lysozyme-like
BAB1_1227	NE, NIV	Hypothetical
BAB1_1295	NE, NIV	Hypothetical (extensin-like)
BAB1_1296	NE, NIV	Hypothetical
BAB1_1308	Slight DF, NIV	Hypothetical (*lemA*)
BAB1_1336	NE, NIV	Hypothetical
BAB1_1441	E	Hypothetical
BAB1_1464	NE, NIV	L,D-transpeptidase
BAB1_1527	NE, NIV	lytic transglycosylase lysozyme-like
BAB1_1548	NE, NIV	L,D-transpeptidase
BAB1_1640	NE, NIV	*mopB*
BAB1_1707	E	*dppB* (ABC transporter)

BAB1_1773	E	Hypothetical (*hlyD*-like)
BAB1_1814	E	*nosL*
BAB1_1830	NE, NIV	*oprF*
BAB1_1930	NE, DP	Hypothetical (molydopterin-binding domain)
BAB1_1983	NE, NIV	*flgH*
BAB1_2034	NE, NIV	Hypothetical
BAB1_2148	NE, NIV	Hypothetical
BAB2_0017	NE, NIV	patatin-like on a small portion
BAB2_0057	NE, NIV	rare lipoprotein A
BAB2_0062	NE, IV	Hypothetical
BAB2_0076	NE, DP	Hypothetical
BAB2_0156	NE, NIV	Hypothetical
BAB2_0195	NE, NIV	*cyoA*
BAB2_0316	NE, NIV	*yifL*
BAB2_0319	NE, NIV	Hypothetical peptidase
BAB2_0452	NE, NIV	Hypothetical
BAB2_0773	NE, NIV	Hypothetical
BAB2_0924	NE, NIV	Hypothetical (*lipA*)

Supplementary table 2 | Additional list of *E. coli* strain and plasmids used in this study. The dark gray strain correspond to the WT and the light grey to strain containing empty plasmids. The numbers correspond to the position in the bank.

#	Strain	Description and relevant genotype	Plasmid	Resistance	Other marker	Comments
1	S17		pNPTs *omp25* $_{D2A}$	Kan	SacB	Replacement of *omp25* by *omp25* $_{D2A}$ in *Brucella*
3	K12 MG 1655	F-, λ-, ilvG-, rfb-50, rph-1	/	/	/	From F. Renzi (Milano Lab)
7	S17		pNPTS138 *ΔBAB1_0047*	Kan	SacB	Deletion of *B. abortus* 544 Ldts
8	S17		pNPTS138 *ΔBAB1_0138*	Kan	SacB	Deletion of *B. abortus* 544 Ldts
9	S17		pNPTS138 *ΔBAB1_0178*	Kan	SacB	Deletion of *B. abortus* 544 Ldts
10	S17		pNPTS138 *ΔBAB1_0589*	Kan	SacB	Deletion of *B. abortus* 544 Ldts
11	S17		pNPTS138 *ΔBAB1_0785*	Kan	SacB	Deletion of *B. abortus* 544 Ldts
12	S17		pNPTS138 *ΔBAB1_0978*	Kan	SacB	Deletion of *B. abortus* 544 Ldts
13	S17		pNPTS138 *ΔBAB1_1159*	Kan	SacB	Deletion of *B. abortus* 544 Ldts
14	S17		pNPTS138 *ΔBAB1_1867*	Kan	SacB	Deletion of *B. abortus* 544 Ldts
16	DH10B		pBBR1 *omp25*	Cm	/	From V.Vassen, URBM
21	DH10B		pNPTS138 *BAB1_0047*	Kan	SacB	Expression Ldt in *E. coli*
22	DH10B		pNPTS138 *BAB1_0138*	Kan	SacB	Expression Ldt in *E. coli*
23	DH10B		pNPTS138 *BAB1_0178*	Kan	SacB	Expression Ldt in *E. coli*
24	DH10B		pNPTS138 *BAB1_0589*	Kan	SacB	Expression Ldt in *E. coli*
25	DH10B		pNPTS138 *BAB1_0785*	Kan	SacB	Expression Ldt in *E. coli*
26	DH10B		pNPTS138 *BAB1_0978*	Kan	SacB	Expression Ldt in *E. coli*
27	DH10B		pNPTS138 *BAB1_1159*	Kan	SacB	Expression Ldt in *E. coli*
28	DH10B		pNPTS138 *BAB1_1867*	Kan	SacB	Expression Ldt in *E. coli*
33	DH10B		pBBR1 *omp25*, pNPTS138 Ø	Cm/Kan	SacB	Control expression OMP
74	DH10B		pBBR1 Ø	Cm	/	From "Banque de Monique", URBM
75	DH10B		pBBRi Ø	Cm	/	From V. Vassen, URBM
76	BL21 (DE3)		pET21a Atl	Amp	/	From S. Mesnage, Sheffield, UK
77	BL21 (DE3)	F- ompT gal dcm lon hsdSB (r-m-) λ (DE3 [lacI lacUV5-T7 gene 1 ind1 sam7 nin5])	/	/	/	From R. Hallez (RH603), URBM
78	S17		pBBR1 *BAB1_2034*	Cm	/	For BAB1_2034 (Ldt11) over-expression
85	S17		pBBR1 *BAB1_0047*	Cm	/	For BAB1_0047 (Ldt1) over-expression
86	S17		pBBR1 *BAB1_0138*	Cm	/	For BAB1_0138 (Ldt2) over-expression
87	S17		pBBR1 *BAB1_0589*	Cm	/	For BAB1_0589 (Ldt4) over-expression
88	S17		pMR10 *BAB1_0047*	Kan	/	For BAB1_0047 (Ldt1) complementation
89	S17		pMR10 *BAB1_0138*	Kan	/	For BAB1_0138 (Ldt2) complementation
90	S17		pMR10 *BAB1_0589*	Kan	/	For BAB1_0589 (Ldt4) complementation
91	DH10B		pNTPS138 Ø	Kan	SacB	From M. Deghelt (10D7)
92	BL21 (DE3)		pET28a	Kan	/	From R. Hallez (RH1471), URBM
93	DH5α		pET21b-yebA-His	Amp	/	From W. Vollmer Lab
94	BW25113	Δ6Ldts	/	/	/	From W. Vollmer Lab
95	S17		pNPTS138 *omp2b* $_{D2A}$	Kan	SacB	Replacement of *omp2b* by *omp2b* $_{D2A}$ in *Brucella*
96	S17		pNPTS138 *omp25* $_{D2E}$	Kan	SacB	Replacement of *omp25* by *omp25* $_{D2E}$ in *Brucella*
98	BL21 (DE3)		pET28a Ldt4r	Kan	/	For Ldt4 (BAB1_0589) purification

99	BL21 (DE3)		pET28a Ldt11r	Kan	/	For Ldt11 (BAB1_2034) purification
102	BL21 (DE3)		pET21b-yebA-His	Amp	/	For YebA purification
105	BL21 (DE3)		pET28a Ldt7r	Kan	/	For Ldt7 (BAB1_1159) purification
109	S17		pBBR1 *BAB1_1159*	Cm	/	For Ldt7 (BAB1_1159) over-expression
110	S17		pMR10 *BAB1_1159*	Kan	/	For Ldt7 (BAB1_1159) complementation
111	S17		pMR10 *BAB1_2034*	Kan	/	For Ldt11 (*BAB1_2034*) complementation
112	DH10B		pMR10 Ø	Kan	/	From M. Deghelt (10D9)
113	DH10B		pRET3a-TEV	Amp	/	From J. A. Hermoso Lab,
114	DH10B		pETEV-15b	Amp	/	From J. A. Hermoso Lab
115	S17		pNTPS138 *BAB1_2034-mNG*	Kan	Suc	For Ldt11 (BAB1_2034) localisation
116	S17		pNPTS138 *omp25c*$_{D2A}$	Kan	Suc	Replacement of *omp25c* by *omp25c*$_{D2E}$ in *Brucella*
117	S17		pNPTS138 *omp31* $_{D2A}$	Kan	Suc	Replacement of *omp31* by *omp31* $_{D2E}$ in *Brucella*
119	S17		pNTPS138 *BAB1_1159-mNG*	Kan	Suc	For Ldt7 (BAB1_1159) localisation
120	BW25141		pJMP1039	Amp	/	Initial CRISPRi plasmid (Addgene Plasmid #119239)
121	BW25141		pJMP1356	Amp	Cm	Initial CRISPRi plasmid (Addgene Plasmid #119276)
122	BW25141		pJMP1339	Amp	Kan	Initial CRISPRi plasmid (Addgene Plasmid #119271)
123	MFD pir		pJMP1039	Amp	DAP	For conjugation with *Brucella*
128	MFD pir	F- λ- ilvG- rfb-50 rph-1 RP4-2-Tc::[ΔMu1::aac(3)IV-ΔaphA-Δnic35-ΔMu2::zeo] ΔdapA::(erm-pir) ΔrecA			DAP	From R. Hallez (RH2845), see Ferrières et al., 2017
134	DH5α	F-, endA1, glnV44, thi-1, recA1, relA1, gyrA96, deoR, nupG, purB20, φ80dlacZΔM15, Δ(lacZYA-argF)U169, hsdR17(rK-mK+), λ-				
135	MFD pir		pJPMP1339 Ø	Amp	Kan, DAP	For conjugation with *Brucella*
136	MFD pir		pJPMP1356 Ø	Amp	Cm, DAP	For conjugation with *Brucella*
142	BW25141		pJMP1337	Amp	Kan	Initial CRISPRi plasmid (Addgene Plasmid #119270)
143	BW 25141	F-, Δ(araD-araB)567, ΔlacZ4787(::rrnB-3), Δ(phoB-phoR)580, λ-, galU95, ΔuidA3::pir+, recA1, endA9(del-ins)::FRT, rph-1, Δ(rhaD-rhaB)568, hsdR514				From L. Van Melderen Lab
144	S17		pNTPS *BAB1_0589-mNG*	Kan	SacB	For Ldt4 (BAB1_05689) localisation
146	Bl21 (DE3)		pET28a ldt11r	Kan	/	For Ldt11 (BAB1_2034) purification
147	DH5α		pJMP1339t	Amp	/	Construction intermediate for pJMP1339$_{t2}$
148	BW25141		pJMP1339t	Amp	/	Construction intermediate for pJMP1339t2
149	DH5α		pJMP1339 EcoRI Ø	Amp	/	Construction intermediate for pJMP1339t2
150	DH10B		pBBRi Ø	Cm	/	From 12H4 (V. Vassen)
151	S17		pNPTS138 *Omp25c*$_{D2A}$ PstI	Kan	SacB	Construction with PstI site for PCR check

152	S17		pNPTS138 *BAB1_2034 C155A*	Kan	SacB	For catalytically dead mutant
153	DH5α		pJMP1339$_{t2}$ Ø	Amp	Kan	CRISPRi plasmid with AHTC control
155	MFD pir		pJMP1339$_{t2}$ 290/291	Amp	Kan	sgRNA for Omp25 (primers 290/291)
158	MFD pir		pJMP1339$_{t2}$ Ø	Amp	Kan	For conjugation with *Brucella*
164	S17		pNTPS138 *BAB1_2034-Linker-mTQ*	Kan	SacB	For BAB1_2034 localisation
173	MFD pir		CRISPRi 39$_{t2}$ 369/370	Amp	Kan	sgRNA for *ldt5* (*BAB1_0785*,primers 369/370)
174	MFD pir		CRISPRi 39$_{t2}$ 357/358	Amp	Kan	sgRNA for *BAB1_2034* (primers 357/358)

Supplementary table 3 | Additional list of *B. abortus* strains used in this study. The numbers correspond to the position in the bank.

#	Strain	Plasmid	Resistance	Comment
28	*B. abortus* 544 ΔLdt4,2,1,3	None	None	Quadruple Ldt deletion
30	*B. abortus* 544 ΔLdt4,2,1,6	None	None	Quadruple Ldt deletion
32	*B. abortus* 544 ΔLdt4,2,1,8	None	None	Quadruple Ldt deletion
35	*B. abortus* 544 ΔLdt4,2,1,7	None	None	Quadruple Ldt deletion
38	*B. abortus* 544 Δ*BAB1_2034* #2	None	None	BAB1_2034 deletion
38	*B. abortus* 544 Δ*BAB1_2034* #1	None	None	BAB1_2034 deletion
41	*B. abortus* 544 Δ*BAB1_2034*	pBBR1 *BAB1_2034*	Cm	BAB1_2034 over-expression
67	*B. abortus* 544 Omp25/2b D2A	None	None	Double D2A punctual mutation
69	*B. abortus* 544 Omp25 D2E	None	None	D2E punctual mutation
74	*B. abortus* 544 Δ*ldt7*	pMR10::*ldt7*	Kan	Ldt7 (BAB1_1159) complementation strain
76	*B. abortus* 544 *BAB1_2034-mNG*	None	None	BAB1_2034 localisation
78	*B. abortus* 544 *BAB1_2034-mNG* pSK *pdhS-mcherry*	pSK	None	BAB1_2034 localisation
80	*B. abortus* 544 $Omp25c_{D2A}$	None	None	D2A punctual mutation
81	*B. abortus* 544 $Omp31_{D2A}$	None	None	D2A punctual mutation
82	*B. abortus* 544 *ldt7-mNG*	None	None	Ldt7 (BAB1_1159) localisation
86	*B. abortus* 544 *ldt7-mNG* pSK *pdhS-mCherry*	pSK	Kan	Ldt7 (BAB1_1159) localisation
88	*B. abortus* 544 Δ*BAB1_2034*	pMR10 *BAB1_2034*	Kan	BAB1_2034 complementation
99	*B. abortus* 544 CRISPRi 39t2 290/291	None	Kan	sgRNA for *omp25*
106	*B. abortus* 544 CRISPRi 39t2 Ø	None	Kan	Empty CRISPRi system
119	*B. abortus* 544 $Omp25/2b_{D2A}$ CRISPRi 39t2 251/252	None	Kan	sgRNA for *omp25c*
127	*B. abortus* 544 CRISPRi 39t2::sg2034	None	Kan	Used for BAB1_2034 depletion
128	*B. abortus* 544 Δ*ldt1,2,4* CRISPRi 39t2::sg*ldt5*	None	Kan	Used for Ldt5 depletion
130	*B. abortus* 544 Omp25/2b D2A CRISPRi 39t2::sg*omp25c* # /		Kan	Used for Omp25c depletion

Supplementary table 4 | Additional list of primers used in this study. Bold characters show bases that do not hybridise on DNA template. The numbers correspond to the position in the bank.

#	Primer name	Sequence
166	Omp2b_D2A_UP_F	cgaacacataaagatttgctgggatatt
167	Omp2b_D2A_UP_R	**gggctctggc**gcgacgattgcggcggca
168	Omp2b_D2A_DW_F	**caatcgtcgc**gccagagcccgaagccgt
174	Omp2b_D2A_DW_R	cgtagttctgatccggcgtag
175	Omp25_D2E_AM_R	**cggaggctgt**tcctggatggcttcggca
176	Ldt4_REC_F	aacatatggctcagttggggcagacc
177	Ldt4_REC_R	aagaattctcacatgacgaggataggcgtc
178	Ldt7_REC_F	aacatatggcttcgccggtcaatgct
179	Ldt7_REC_R	aagaattcttacagaacaaccacttccgtacca
180	2034_REC_F	aacatatgcagggatcgtcggtgtcc
181	2034_REC_R	aagaattctcagttgccgatgattttccacc
184	Omp2b_D2A_C_F	tcgtgtcatttctgcaacaactgc
185	Omp2b_D2A_C_R	cattaccatatttaccatctacgcccgaat
188	Ldtt11_mNG-1_F	ggttgctattcgatgacggacg
193	Ldtt11_mNG-3_R	tgcggtcacgaccatcatc
194	Ldtt11_mNG_S-2_R	**gtctgttaga**ctacttatacagttcatccatgccca
195	Ldtt11_mNG_S-3_F	**gtataagtag**tctaacagacttgatgcgacatgaatattgaacagccgggacca
196	Ldtt11_mNG_X_1-R	**ccactcgagc**ctccgttgccgatgattttccaccac
197	Ldtt11_mNG_X_2-F	**catcggcaac**ggaggctcgagtggcggtgtctcgaagg
198	Omp25c_D2A_AM_F	gccgaagtgctgtcccag
199	Omp25c_D2A_AM_R	**caggttcctg**ttcaatgacggcagcagca
200	Omp25c_D2A_AV_F	**cgtcattgaa**caggaacctgcaccggttg
201	Omp25c_D2A_AV_R	gcgtcgtcgaagccgtaat
202	Ldt11-mNG-C_F	tatgtcttccgcaagaccgaac
203	Ldt11-mNG-C_R	gattgtgaaggacttgccgga
204	15b_ldt4r_F	catatggctcagttggggcagacc
205	15b_ldt4r_R	ggatcctcacatgacgaggataggcgt
206	1639_D2A-AM_F	cttgattatggtgcgatgcggat
207	1639_D2A-AM_R	**ggtgccggtt**cagcaacgatgatagcggca
208	1639_D2A-AV_F	**atcgttgctg**aaccggcacccgttgcag
209	1639_D2A-AV_R	gtattccgacttcagggtccaat
216	ldt7-mNG_1F	caacaatacggccaaggcca
217	ldt7-mNG_1R	**cgccacctcc**cagaacaaccacttccgtaccaa
218	ldt7-mNG_2F	**ggttgttctg**ggaggtggcggtgtctcga
219	ldt7-mNG_2R	**aattcccggt**ctacttatacagttcatccatgccca
220	ldt7-mNG_3F	**gtataagtag**accgggaattcctgtatgggat
221	ldt7-mNG_3R	gaccggtaaaccgctcgtaatg
238	Omp25c_D2A_C_F	ggcgcaaacgctgctgct
239	Omp25c_WT_C_F	ggcgcaaacgctgctgac
240	Omp31_D2A_C_F	tcggctatggctgccgct
241	Omp31_WT_C_F	tcggctatggctgccgac
280	pTEV_Ldt4rNdeI_F	catatgggctgggtgcaaatgtatgc

281	pTEV_Ldt4rXhoI_R	ctcgagtcacatgacgaggataggcgtc
290	sgRNA_omp25_D-F	tagtgagagacttaagagtgcgca
291	sgRNA_omp25_D-R	aaactgcgcactcttaagtctctc
296	glmS_check_F	ccgcgcaatctcaacaaggt
297	pJMP1337_Check_R	ttctcgtctggtcagttt
298	pJMP1337_Check_F	agcactgacttttgttatcaat
313	1339_TetR_C-F	gtatgccgccattattacgacaag
320	RTqPCR_Omp25-1F	accttggctatggctggaac
321	RTqPCR_Omp25-1R	ggcccaggaataacctgcat
326	1339ori_F	gagttctgaggtcattactggatctatc
327	1339ori_R	tacgagacacggatcgacctgtct
328	1339ori_check_R	taccgctgttgagatccagttcgatg
329	1356ori2-F	agctagcttatcgataccgacgacctcg
334	116D2A_PstI_AM_R	caggttcctgttcaatgacggctgcagca
349	1339t2_Ampli_R	actaatagtacataaggaggaactagctagtatggacaagaagtac
350	1339t2_Ampli_F	gagtcggtgctttttttttgaattcatgtggctgaccgtt
351	sgOmp25c_1	tagtgagcttcatgataaacctct
352	sgOmp25c_2	aaacagaggtttatcatgaagctc
353	39t3_CtrA-2 FWD	tagtgagccgaccagatgtccctca
354	39t3_CtrA-2 REV	aaactgagggacatctggtcggctc
355	2034_C1554A_AM-R	gtcgggtgttcgtccgtcatcgaataggcacc
356	2034_C1554A_AV-F	atgacggacgaacacccgacgacgaacatgc
357	39t2_sg2034_F	tagtgcagaatggagcctagaagtg
358	39t2_sg2034_R	aaaccacttctaggctccattctgc
363	omp25c_RT_1_F	tcggcgatataaagccggac
364	omp25c_RT_1_R	actgttgccgaggtcgaaat
365	omp25c_RT_2_F	accggcttctctcaaagcaa
366	omp25c_RT_2_R	cgatattcgaggcgcaggat
367	sgOmp25c_2_FWD	tagtggtcgcggcaacgagaacga
368	sgOmp25c_2_REV	aaactcgttctcgttgccgcgacc
369	39t2_sgLDt5_F	tagtgcatttgattaacgtcccaaa
370	39t2_sgLDt5_R	aaactttgggacgttaatcaaatgc
AL29	2034_AM_F	cggtggcaaaccgcgtctatat
AL30	2034_AM_R	**cctgatcgga**gtcgcatcaagtctgttagagcca
AL31	2034_AV_F	**ttgatgcgac**ccgatcaggaaaacacacctgtttac
AL33	2034_AV_R	tcccggtttcgaccttcgagat
CN25	pJMP1337 FWD	**gtacttcttgtccatactag**ctagttcctccttatgtactattagt
CN26	pJMP1337 REV	**aacggtcagccacatgaatt**cctagtaaaaaaagcaccga

REFERENCES

Alvarez, L., Aliashkevich, A., de Pedro, M. A., & Cava, F. (2018). Bacterial secretion of D-arginine controls environmental microbial biodiversity. *ISME J, 12*(2), 438-450. doi:10.1038/ismej.2017.176

Anderson, J. D., & Smith, H. (1965). The Metabolism of Erythritol by *Brucella Abortus*. *J Gen Microbiol, 38*, 109-124. doi:10.1099/00221287-38-1-109

Anderson, T. D., Cheville, N. F., & Meador, V. P. (1986). Pathogenesis of placentitis in the goat inoculated with *Brucella abortus*. II. Ultrastructural studies. *Vet Pathol, 23*(3), 227-239. doi:10.1177/030098588602300302

Arenas, G. N., Staskevich, A. S., Aballay, A., & Mayorga, L. S. (2000). Intracellular trafficking of *Brucella abortus* in J774 macrophages. *Infect Immun, 68*(7), 4255-4263. doi:10.1128/IAI.68.7.4255-4263.2000

Asmar, A. T., & Collet, J. F. (2018). Lpp, the Braun lipoprotein, turns 50-major achievements and remaining issues. *FEMS Microbiol Lett, 365*(18). doi:10.1093/femsle/fny199

Asmar, A. T., Ferreira, J. L., Cohen, E. J., Cho, S. H., Beeby, M., Hughes, K. T., & Collet, J. F. (2017). Communication across the bacterial cell envelope depends on the size of the periplasm. *PLoS Biol, 15*(12), e2004303. doi:10.1371/journal.pbio.2004303

Badet, B., Vermoote, P., Haumont, P. Y., Lederer, F., & LeGoffic, F. (1987). Glucosamine synthetase from *Escherichia coli*: purification, properties, and glutamine-utilizing site location. *Biochemistry, 26*(7), 1940-1948. doi:10.1021/bi00381a023

Baek, M., DiMaio, F., Anishchenko, I., Dauparas, J., Ovchinnikov, S., Lee, G. R., Wang, J., Cong, Q., Kinch, L. N., Schaeffer, R. D., Millan, C., Park, H., Adams, C., Glassman, C. R., DeGiovanni, A., Pereira, J. H., Rodrigues, A. V., van Dijk, A. A., Ebrecht, A. C., Opperman, D. J., Sagmeister, T., Buhlheller, C., Pavkov-Keller, T., Rathinaswamy, M. K., Dalwadi, U., Yip, C. K., Burke, J. E., Garcia, K. C., Grishin, N. V., Adams, P. D., Read, R. J., & Baker, D. (2021). Accurate prediction of protein structures and interactions using a three-track neural network. *Science, 373*(6557), 871-876. doi:10.1126/science.abj8754

Bahadur, R., Chodisetti, P. K., & Reddy, M. (2021). Cleavage of Braun's lipoprotein Lpp from the bacterial peptidoglycan by a paralog of L,D-

transpeptidases, LdtF. *Proc Natl Acad Sci U S A, 118*(19). doi:10.1073/pnas.2101989118

Bang, B. (1897). The Etiology of Epizootic Abortion. *Journal of Comparative Pathology and Therapeutics, 10*, 125-IN122. doi:10.1016/s0368-1742(97)80014-8

Banta, A. B., Ward, R. D., Tran, J. S., Bacon, E. E., & Peters, J. M. (2020). Programmable Gene Knockdown in Diverse Bacteria Using Mobile-CRISPRi. *Curr Protoc Microbiol, 59*(1), e130. doi:10.1002/cpmc.130

Banzhaf, M., van den Berg van Saparoea, B., Terrak, M., Fraipont, C., Egan, A., Philippe, J., Zapun, A., Breukink, E., Nguyen-Disteche, M., den Blaauwen, T., & Vollmer, W. (2012). Cooperativity of peptidoglycan synthases active in bacterial cell elongation. *Mol Microbiol, 85*(1), 179-194. doi:10.1111/j.1365-2958.2012.08103.x

Basle, A., Rummel, G., Storici, P., Rosenbusch, J. P., & Schirmer, T. (2006). Crystal structure of osmoporin OmpC from *E. coli* at 2.0 A. *J Mol Biol, 362*(5), 933-942. doi:10.1016/j.jmb.2006.08.002

Bateman, A., & Bycroft, M. (2000). The structure of a LysM domain from *E. coli* membrane-bound lytic murein transglycosylase D (MltD). *J Mol Biol, 299*(4), 1113-1119. doi:10.1006/jmbi.2000.3778

Benson, T. E., Marquardt, J. L., Marquardt, A. C., Etzkorn, F. A., & Walsh, C. T. (1993). Overexpression, purification, and mechanistic study of UDP-N-acetylenolpyruvylglucosamine reductase. *Biochemistry, 32*(8), 2024-2030. doi:10.1021/bi00059a019

Bernal-Cabas, M., Ayala, J. A., & Raivio, T. L. (2015). The Cpx envelope stress response modifies peptidoglycan cross-linking via the L,D-transpeptidase LdtD and the novel protein YgaU. *J Bacteriol, 197*(3), 603-614. doi:10.1128/JB.02449-14

Bertsche, U., Kast, T., Wolf, B., Fraipont, C., Aarsman, M. E., Kannenberg, K., von Rechenberg, M., Nguyen-Disteche, M., den Blaauwen, T., Holtje, J. V., & Vollmer, W. (2006). Interaction between two murein (peptidoglycan) synthases, PBP3 and PBP1B, in *Escherichia coli*. *Mol Microbiol, 61*(3), 675-690. doi:10.1111/j.1365-2958.2006.05280.x

Bielnicki, J., Devedjiev, Y., Derewenda, U., Dauter, Z., Joachimiak, A., & Derewenda, Z. S. (2006). *B. subtilis* ykuD protein at 2.0 A resolution: insights into the structure and function of a novel, ubiquitous family of bacterial enzymes. *Proteins, 62*(1), 144-151. doi:10.1002/prot.20702

Boschiroli, M. L., Ouahrani-Bettache, S., Foulongne, V., Michaux-Charachon, S., Bourg, G., Allardet-Servent, A., Cazevieille, C., Liautard, J. P., Ramuz, M., & O'Callaghan, D. (2002). The *Brucella suis* virB operon is

induced intracellularly in macrophages. *Proc Natl Acad Sci U S A, 99*(3), 1544-1549. doi:10.1073/pnas.032514299

Bouhss, A., Trunkfield, A. E., Bugg, T. D., & Mengin-Lecreulx, D. (2008). The biosynthesis of peptidoglycan lipid-linked intermediates. *FEMS Microbiol Rev, 32*(2), 208-233. doi:10.1111/j.1574-6976.2007.00089.x

Bouveret, E., Benedetti, H., Rigal, A., Loret, E., & Lazdunski, C. (1999). *In vitro* characterization of peptidoglycan-associated lipoprotein (PAL)-peptidoglycan and PAL-TolB interactions. *J Bacteriol, 181*(20), 6306-6311. doi:10.1128/JB.181.20.6306-6311.1999

Braun, V. (1975). Covalent lipoprotein from the outer membrane of *Escherichia coli*. *Biochimica et Biophysica Acta (BBA) - Reviews on Biomembranes, 415*(3), 335-377. doi:10.1016/0304-4157(75)90013-1

Braun, V., & Bosch, V. (1972). Sequence of the murein-lipoprotein and the attachment site of the lipid. *Eur J Biochem, 28*(1), 51-69. doi:10.1111/j.1432-1033.1972.tb01883.x

Braun, V., & Rehn, K. (1969). Chemical characterization, spatial distribution and function of a lipoprotein (murein-lipoprotein) of the *E. coli* cell wall. The specific effect of trypsin on the membrane structure. *Eur J Biochem, 10*(3), 426-438. doi:10.1111/j.1432-1033.1969.tb00707.x

Braun, V., & Wu, H. C. (1994). Lipoproteins, structure, function, biosynthesis and model for protein export. In *Bacterial Cell Wall* (pp. 319-341).

Breukink, E., & de Kruijff, B. (2006). Lipid II as a target for antibiotics. *Nat Rev Drug Discov, 5*(4), 321-332. doi:10.1038/nrd2004

Broghammer, A., Krusell, L., Blaise, M., Sauer, J., Sullivan, J. T., Maolanon, N., Vinther, M., Lorentzen, A., Madsen, E. B., Jensen, K. J., Roepstorff, P., Thirup, S., Ronson, C. W., Thygesen, M. B., & Stougaard, J. (2012). Legume receptors perceive the rhizobial lipochitin oligosaccharide signal molecules by direct binding. *Proc Natl Acad Sci U S A, 109*(34), 13859-13864. doi:10.1073/pnas.1205171109

Brown, P. J., de Pedro, M. A., Kysela, D. T., Van der Henst, C., Kim, J., De Bolle, X., Fuqua, C., & Brun, Y. V. (2012). Polar growth in the Alphaproteobacterial order Rhizobiales. *Proc Natl Acad Sci U S A, 109*(5), 1697-1701. doi:10.1073/pnas.1114476109

Bruce, D. (1887). Note on the discovery of a microorganism in Malta fever. *The Practitioner, 39*, 161-170.

Buddle, M. B., & Boyes, B. W. (1953). A *Brucella* Mutant Causing Genital Disease of Sheep in New Zealand. *Australian Veterinary Journal, 29*(6), 145-153. doi:10.1111/j.1751-0813.1953.tb05257.x

Buist, G., Steen, A., Kok, J., & Kuipers, O. P. (2008). LysM, a widely distributed protein motif for binding to (peptido)glycans. *Mol Microbiol, 68*(4), 838-847. doi:10.1111/j.1365-2958.2008.06211.x

Cameron, T. A., Anderson-Furgeson, J., Zupan, J. R., Zik, J. J., & Zambryski, P. C. (2014). Peptidoglycan synthesis machinery in *Agrobacterium tumefaciens* during unipolar growth and cell division. *MBio, 5*(3), e01219-01214. doi:10.1128/mBio.01219-14

Capasso, L. (2002). Bacteria in two-millennia-old cheese, and related epizoonoses in Roman populations. *J Infect, 45*(2), 122-127. doi:10.1053/jinf.2002.0996

Carmichael, L. E., & Bruner, D. W. (1968). Characteristics of a newly-recognized species of *Brucella* responsible for infectious canine abortions. *Cornell Vet, 48*(4), 579-592.

Cava, F., de Pedro, M. A., Lam, H., Davis, B. M., & Waldor, M. K. (2011). Distinct pathways for modification of the bacterial cell wall by non-canonical D-amino acids. *EMBO J, 30*(16), 3442-3453. doi:10.1038/emboj.2011.246

Celli, J. (2019). The Intracellular Life Cycle of *Brucella* spp. *Microbiol Spectr, 7*(2). doi:10.1128/microbiolspec.BAI-0006-2019

Celli, J., de Chastellier, C., Franchini, D. M., Pizarro-Cerda, J., Moreno, E., & Gorvel, J. P. (2003). *Brucella* evades macrophage killing via VirB-dependent sustained interactions with the endoplasmic reticulum. *J Exp Med, 198*(4), 545-556. doi:10.1084/jem.20030088

Celli, J., Salcedo, S. P., & Gorvel, J. P. (2005). *Brucella* coopts the small GTPase Sar1 for intracellular replication. *Proc Natl Acad Sci U S A, 102*(5), 1673-1678. doi:10.1073/pnas.0406873102

Chaturvedi, D., & Mahalakshmi, R. (2017). Transmembrane beta-barrels: Evolution, folding and energetics. *Biochim Biophys Acta Biomembr, 1859*(12), 2467-2482. doi:10.1016/j.bbamem.2017.09.020

Chaves-Olarte, E., Guzman-Verri, C., Meresse, S., Desjardins, M., Pizarro-Cerda, J., Badilla, J., Gorvel, J. P., & Moreno, E. (2002). Activation of Rho and Rab GTPases dissociates *Brucella abortus* internalization from intracellular trafficking. *Cell Microbiol, 4*(10), 663-676. doi:10.1046/j.1462-5822.2002.00221.x

Chen, R., & Henning, U. (1996). A periplasmic protein (Skp) of *Escherichia coli* selectively binds a class of outer membrane proteins. *Mol Microbiol, 19*(6), 1287-1294. doi:10.1111/j.1365-2958.1996.tb02473.x

Cheng, Q., Li, H., Merdek, K., & Park, J. T. (2000). Molecular characterization of the beta-N-acetylglucosaminidase of *Escherichia coli* and its role

in cell wall recycling. *J Bacteriol, 182*(17), 4836-4840. doi:10.1128/JB.182.17.4836-4840.2000

Cheng, Q., & Park, J. T. (2002). Substrate specificity of the AmpG permease required for recycling of cell wall anhydro-muropeptides. *J Bacteriol, 184*(23), 6434-6436. doi:10.1128/JB.184.23.6434-6436.2002

Cloeckaert, A., De Wergifosse, P., Dubray, G., & Limet, J. N. (1990). Identification of Seven Surface-Exposed *Brucella* Outer Membrane Proteins by Use of Monoclonal Antibodies: Immunogold Labeling for Electron Microscopy and Enzyme-Linked Immunosorbent Assay. *Infection and Immunity, 58*(12), 3980-3987.

Cloeckaert, A., Verger, J.-M., Grayon, M., Paquet, J.-Y., Garin-Bastuji, B., Foster, G., & Godfroid, J. (2001). Classification of Brucella spp. isolated from marine mammals by DNA polymorphism at the omp2 locus. *Microbes and Infection, 3*(9), 729-738. doi:10.1016/s1286-4579(01)01427-7

Cloeckaert, A., Verger, J. M., Grayon, M., & Grepinet, O. (1995). Restriction site polymorphism of the genes encoding the major 25 kDa and 36 kDa outer-membrane proteins of *Brucella*. *Microbiology (Reading), 141 (Pt 9)*, 2111-2121. doi:10.1099/13500872-141-9-2111

Cloeckaert, A., Vergnaud, G., & Zygmunt, M. S. (2020). Omp2b Porin Alteration in the Course of Evolution of *Brucella* spp. *Frontiers in Microbiology, 11*.

Cloeckaert, A., Vizcaíno, N., Paquet, J.-Y., Bowden, R. A., & Elzer, P. H. (2002). Major outer membrane proteins of *Brucella* spp.: past, present and future. *Veterinary Microbiology, 90*(1-4), 229-247. doi:10.1016/s0378-1135(02)00211-0

Cloeckaert, A., Zygmunt, M. S., De Wergifosse, P., Dubray, G., & Limet, J. N. (1992). Demonstration of peptidoglycan-associated *Brucella* outer-membrane proteins by use of monoclonal antibodies. *Journal of General Microbiology, 138*, 1543-1550.

Comerci, D. J., Martinez-Lorenzo, M. J., Sieira, R., Gorvel, J. P., & Ugalde, R. A. (2001). Essential role of the VirB machinery in the maturation of the Brucella abortus-containing vacuole. *Cell Microbiol, 3*(3), 159-168. doi:10.1046/j.1462-5822.2001.00102.x

Coria, L. M., Ibanez, A. E., Tkach, M., Sabbione, F., Bruno, L., Carabajal, M. V., Berguer, P. M., Barrionuevo, P., Schillaci, R., Trevani, A. S., Giambartolomei, G. H., Pasquevich, K. A., & Cassataro, J. (2016). A *Brucella* spp. Protease Inhibitor Limits Antigen Lysosomal Proteolysis, Increases Cross-Presentation, and Enhances CD8+ T Cell

Responses. *J Immunol, 196*(10), 4014-4029. doi:10.4049/jimmunol.1501188

Cowles, C. E., Li, Y., Semmelhack, M. F., Cristea, I. M., & Silhavy, T. J. (2011). The free and bound forms of Lpp occupy distinct subcellular locations in *Escherichia coli*. *Mol Microbiol, 79*(5), 1168-1181. doi:10.1111/j.1365-2958.2011.07539.x

Crane, J. M., & Randall, L. L. (2017). The Sec System: Protein Export in *Escherichia coli*. *EcoSal Plus, 7*(2). doi:10.1128/ecosalplus.ESP-0002-2017

Cutler, S. J., Whatmore, A. M., & Commander, N. J. (2005). Brucellosis - new aspects of an old disease. *J Appl Microbiol, 98*(6), 1270-1281. doi:10.1111/j.1365-2672.2005.02622.x

D'Anastasio, R., Zipfel, B., Moggi-Cecchi, J., Stanyon, R., & Capasso, L. (2009). Possible brucellosis in an early hominin skeleton from Sterkfontein, South Africa. *PLOs one, 4*(7), e6439. doi:10.1371/journal.pone.0006439

Dahl, U., Jaeger, T., Nguyen, B. T., Sattler, J. M., & Mayer, C. (2004). Identification of a phosphotransferase system of *Escherichia coli* required for growth on N-acetylmuramic acid. *J Bacteriol, 186*(8), 2385-2392. doi:10.1128/JB.186.8.2385-2392.2004

Daniel, R. A., & Errington, J. (2003). Control of Cell Morphogenesis in Bacteria. *Cell, 113*(6), 767-776. doi:10.1016/s0092-8674(03)00421-5

De Mot, R., & Vanderleyden, J. (1994). The C-terminal sequence conservation between OmpA-related outer membrane proteins and MotB suggests a common function in both Gram-positive and gram-negative bacteria, possibly in the interaction of these domains with peptidoglycan. *Mol Microbiol, 12*(2), 333-334. doi:10.1111/j.1365-2958.1994.tb01021.x

de Wergifosse, P., Lintermans, P., Limet, J. N., & Cloeckaert, A. (1995). Cloning and nucleotide sequence of the gene coding for the major 25-kilodalton outer membrane protein of *Brucella abortus*. *J Bacteriol, 177*(7), 1911-1914. doi:10.1128/jb.177.7.1911-1914.1995

Deghelt, M., Mullier, C., Sternon, J. F., Francis, N., Laloux, G., Dotreppe, D., Van der Henst, C., Jacobs-Wagner, C., Letesson, J. J., & De Bolle, X. (2014). G1-arrested newborn cells are the predominant infectious form of the pathogen *Brucella abortus*. *Nat Commun, 5*, 4366. doi:10.1038/ncomms5366

Demchick, P., & Koch, A. L. (1996). The permeability of the wall fabric of *Escherichia coli* and *Bacillus subtilis*. *J Bacteriol, 178*(3), 768-773. doi:10.1128/jb.178.3.768-773.1996

Denome, S. A., Elf, P. K., Henderson, T. A., Nelson, D. E., & Young, K. D. (1999). *Escherichia coli* mutants lacking all possible combinations of eight penicillin binding proteins: viability, characteristics, and implications for peptidoglycan synthesis. *J Bacteriol, 181*(13), 3981-3993. doi:10.1128/JB.181.13.3981-3993.1999

Denoncin, K., Schwalm, J., Vertommen, D., Silhavy, T. J., & Collet, J. F. (2012). Dissecting the *Escherichia coli* periplasmic chaperone network using differential proteomics. *Proteomics, 12*(9), 1391-1401. doi:10.1002/pmic.201100633

Diven, W. F., Scholz, J. J., & Johnston, R. B. (1964). Purification and properties of the alanine racemase from *Bacillus subtilis*. *Biochimica et Biophysica Acta (BBA) - Specialized Section on Enzymological Subjects, 85*(2), 322-332. doi:10.1016/0926-6569(64)90253-6

Doublet, P., van Heijenoort, J., Bohin, J. P., & Mengin-Lecreulx, D. (1993). The *murI* gene of *Escherichia coli* is an essential gene that encodes a glutamate racemase activity. *J Bacteriol, 175*(10), 2970-2979. doi:10.1128/jb.175.10.2970-2979.1993

Douglas, J. T., Rosenberg, E. Y., Nikaido, H., Verstreate, D. R., & Winter, A. J. (1984). Porins of *Brucella* species. *Infect Immun, 44*(1), 16-21. doi:10.1128/iai.44.1.16-21.1984

Dubray, G., & Bezard, G. (1980). Isolation of three *Brucella abortus* cell-wall antigens protective in murine experimental brucellosis. *Ann Rech Vet, 11*(4), 367-373.

Dubray, G., & Charriaut, C. (1983). Evidence of three major polypeptide species and two major polysaccharide species in the *Brucella* outer membrane. *Ann Rech Vet, 14*(3), 311-318.

Ducret, A., Quardokus, E. M., & Brun, Y. V. (2016). MicrobeJ, a tool for high throughput bacterial cell detection and quantitative analysis. *Nat Microbiol, 1*(7), 16077. doi:10.1038/nmicrobiol.2016.77

Duncan, K., van Heijenoort, J., & Walsh, C. T. (1990). Purification and characterization of the D-alanyl-D-alanine-adding enzyme from *Escherichia coli*. *Biochemistry, 29*(9), 2379-2386. doi:10.1021/bi00461a023

Edmonds, M. D., Cloeckaert, A., & Elzer, P. H. (2002). *Brucella* species lacking the major outer membrane protein Omp25 are attenuated in mice and protect against *Brucella melitensis* and *Brucella ovis*. *Veterinary Microbiology, 88*(3), 205-221. doi:10.1016/s0378-1135(02)00110-4

Egan, A. J. F., Errington, J., & Vollmer, W. (2020). Regulation of peptidoglycan synthesis and remodelling. *Nat Rev Microbiol*. doi:10.1038/s41579-020-0366-3

Eisenberg, T., Hamann, H. P., Kaim, U., Schlez, K., Seeger, H., Schauerte, N., Melzer, F., Tomaso, H., Scholz, H. C., Koylass, M. S., Whatmore, A. M., & Zschock, M. (2012). Isolation of potentially novel *Brucella* spp. from frogs. *Appl Environ Microbiol, 78*(10), 3753-3755. doi:10.1128/AEM.07509-11

Eisenberg, T., Risse, K., Schauerte, N., Geiger, C., Blom, J., & Scholz, H. C. (2017). Isolation of a novel 'atypical' Brucella strain from a bluespotted ribbontail ray (*Taeniura lymma*). *Antonie Van Leeuwenhoek, 110*(2), 221-234. doi:10.1007/s10482-016-0792-4

El Ghachi, M., Bouhss, A., Blanot, D., & Mengin-Lecreulx, D. (2004). The *bacA* gene of *Escherichia coli* encodes an undecaprenyl pyrophosphate phosphatase activity. *J Biol Chem, 279*(29), 30106-30113. doi:10.1074/jbc.M401701200

El Ghachi, M., Derbise, A., Bouhss, A., & Mengin-Lecreulx, D. (2005). Identification of multiple genes encoding membrane proteins with undecaprenyl pyrophosphate phosphatase (UppP) activity in *Escherichia coli*. *J Biol Chem, 280*(19), 18689-18695. doi:10.1074/jbc.M412277200

El Rayes, J., Rodriguez-Alonso, R., & Collet, J. F. (2021). Lipoproteins in Gram-negative bacteria: new insights into their biogenesis, subcellular targeting and functional roles. *Curr Opin Microbiol, 61*, 25-34. doi:10.1016/j.mib.2021.02.003

Elhenawy, W., Davis, R. M., Fero, J., Salama, N. R., Felman, M. F., & Ruiz, N. (2016). The O-Antigen Flippase Wzk Can Substitute for MurJ in Peptidoglycan Synthesis in *Helicobacter pylori* and *Escherichia coli*. *PLOs one, 11*(8), e0161587. doi:10.1371/journal.pone.0161587

Evans, A. C. (1918). Further Studies on *Bacterium Abortus* and Related Bacteria: II. A Comparison of *Bacterium Abortus* with *Bacterium Bronchisepticus* and with the Organism which Causes Malta Fever. *Journal of Infectious Diseases, 22*(6), 580-593. doi:10.1093/infdis/22.6.580

Ewalt, D. R., Payeur, J. B., Martin, B. M., Cummins, D. R., & Miller, W. G. (1994). Characteristics of a *Brucella* species from a bottlenose dolphin (*Tursiops truncatus*). *J Vet Diagn Invest, 6*(4), 448-452. doi:10.1177/104063879400600408

Ficht, T. A., Bearden, S. W., Sowa, B. A., & Adams, L. G. (1988). A 36-kilodalton *Brucella abortus* cell envelope protein is encoded by repeated sequences closely linked in the genomic DNA. *Infect Immun, 56*(8), 2036-2046. doi:10.1128/iai.56.8.2036-2046.1988

Ficht, T. A., Bearden, S. W., Sowa, B. A., & Adams, L. G. (1989). DNA sequence and expression of the 36-kilodalton outer membrane protein gene of *Brucella abortus*. *Infect Immun, 57*(11), 3281-3291. doi:10.1128/iai.57.11.3281-3291.1989

Ficht, T. A., Bearden, S. W., Sowa, B. A., & Marquis, H. (1990). Genetic variation at the *omp2* porin locus of the brucellae: species-specific markers. *Mol Microbiol, 4*(7), 1135-1142. doi:10.1111/j.1365-2958.1990.tb00688.x

Ficht, T. A., Husseinen, H. S., Derr, J., & Bearden, S. W. (1996). Species-specific sequences at the *omp2* locus of *Brucella* type strains. *Int J Syst Bacteriol, 46*(1), 329-331. doi:10.1099/00207713-46-1-329

Fleming, A. (1929). On the Antibacterial Action of Cultures of a Penicillium, with Special Reference to Their Use in the Isolation of *B. influenzae*. *Br J Exp Pathol.* (10), 226-236.

Francis, N., Poncin, K., Fioravanti, A., Vassen, V., Willemart, K., Ong, T. A., Rappez, L., Letesson, J. J., Biondi, E. G., & De Bolle, X. (2017). CtrA controls cell division and outer membrane composition of the pathogen *Brucella abortus*. *Mol Microbiol, 103*(5), 780-797. doi:10.1111/mmi.13589

Frirdich, E., Vermeulen, J., Biboy, J., Soares, F., Taveirne, M. E., Johnson, J. G., DiRita, V. J., Girardin, S. E., Vollmer, W., & Gaynor, E. C. (2014). Peptidoglycan LD-carboxypeptidase Pgp2 influences *Campylobacter jejuni* helical cell shape and pathogenic properties and provides the substrate for the DL-carboxypeptidase Pgp1. *J Biol Chem, 289*(12), 8007-8018. doi:10.1074/jbc.M113.491829

Gan, K., Gupta, S. D., Sankaran, K., Schmid, M. B., & Wu, H. C. (1993). Isolation and characterization of a temperature-sensitive mutant of Salmonella typhimurium defective in prolipoprotein modification. *Journal of Biological Chemistry, 268*(22), 16544-16550. doi:10.1016/s0021-9258(19)85453-4

Garcia-Del Portillo, F. (2020). Building peptidoglycan inside eukaryotic cells: A view from symbiotic and pathogenic bacteria. *Mol Microbiol, 113*(3), 613-626. doi:10.1111/mmi.14452

Garvey, K. J., Saedi, M. S., & Ito, J. (1986). Nucleotide sequence of *Bacillus* phage phi 29 genes 14 and 15: homology of gene 15 with other phage lysozymes. *Nucleic Acids Res, 14*(24), 10001-10008. doi:10.1093/nar/14.24.10001

Geiger, T., Pazos, M., Lara-Tejero, M., Vollmer, W., & Galan, J. E. (2018). Peptidoglycan editing by a specific LD-transpeptidase controls the

muramidase-dependent secretion of typhoid toxin. *Nat Microbiol, 3*(11), 1243-1254. doi:10.1038/s41564-018-0248-x

Glauner, B. (1988). Separation and quantification of muropeptides with high-performance liquid chromatography. *Anal Biochem, 172*(2), 451-464. doi:10.1016/0003-2697(88)90468-x

Glauner, B., Holtje, J. V., & Schwarz, U. (1988a). The composition of the murein of *Escherichia coli*. *J Biol Chem, 263*(21), 10088-10095.

Glauner, B., Höltje, J. V., & Schwarz, U. (1988b). The composition of the murein of Escherichia coli. *Journal of Biological Chemistry, 263*(21), 10088-10095. doi:10.1016/s0021-9258(19)81481-3

Glow, D., Pianka, D., Sulej, A. A., Kozlowski, L. P., Czarnecka, J., Chojnowski, G., Skowronek, K. J., & Bujnicki, J. M. (2015). Sequence-specific cleavage of dsRNA by Mini-III RNase. *Nucleic Acids Res, 43*(5), 2864-2873. doi:10.1093/nar/gkv009

Goffin, C., Fraipont, C., Ayala, J., Terrak, M., Nguyen-Disteche, M., & Ghuysen, J. M. (1996). The non-penicillin-binding module of the tripartite penicillin-binding protein 3 of *Escherichia coli* is required for folding and/or stability of the penicillin-binding module and the membrane-anchoring module confers cell septation activity on the folded structure. *J Bacteriol, 178*(18), 5402-5409. doi:10.1128/jb.178.18.5402-5409.1996

Gomez-Miguel, M. J., & Moriyon, I. (1986). Demonstration of a peptidoglycan-linked lipoprotein and characterization of its trypsin fragment in the outer membrane of *Brucella* spp. *Infect Immun, 53*(3), 678-684. doi:10.1128/iai.53.3.678-684.1986

Gomez-Miguel, M. J., Moriyon, I., & Lopez, J. (1987). *Brucella* outer membrane lipoprotein shares antigenic determinants with *Escherichia coli* Braun lipoprotein and is exposed on the cell surface. *Infect Immun, 55*(1), 258-262. doi:10.1128/iai.55.1.258-262.1987

Goodell, E. W. (1985). Recycling of murein by *Escherichia coli*. *J Bacteriol, 163*(1), 305-310. doi:10.1128/JB.163.1.305-310.1985

Goolab, S., Roth, R. L., van Heerden, H., & Crampton, M. C. (2015). Analyzing the molecular mechanism of lipoprotein localization in *Brucella*. *Front Microbiol, 6*, 1189. doi:10.3389/fmicb.2015.01189

Grabowicz, M. (2018). Lipoprotein Transport: Greasing the Machines of Outer Membrane Biogenesis: Re-Examining Lipoprotein Transport Mechanisms Among Diverse Gram-Negative Bacteria While Exploring New Discoveries and Questions. *Bioessays, 40*(4), e1700187. doi:10.1002/bies.201700187

Gromiha, M. M., & Ponnuswamy, P. K. (1995). Prediction of protein secondary structures from their hydrophobic characteristics. *Int J Pept Protein Res, 45*(3), 225-240. doi:10.1111/j.1399-3011.1995.tb01484.x

Gromiha, M. M., & Suwa, M. (2007). Current developments on beta-barrel membrane proteins: sequence and structure analysis, discrimination and prediction. *Curr Protein Pept Sci, 8*(6), 580-599. doi:10.2174/138920307783018712

Gupta, S. D., Gan, K., Schmid, M. B., & Wu, H. C. (1993). Characterization of a temperature-sensitive mutant of *Salmonella typhimurium* defective in apolipoprotein N-acyltransferase. *Journal of Biological Chemistry, 268*(22), 16551-16556. doi:10.1016/s0021-9258(19)85454-6

Guzman-Verri, C., Manterola, L., Sola-Landa, A., Parra, A., Cloeckaert, A., Garin, J., Gorvel, J. P., Moriyon, I., Moreno, E., & Lopez-Goni, I. (2002). The two-component system BvrR/BvrS essential for *Brucella abortus* virulence regulates the expression of outer membrane proteins with counterparts in members of the Rhizobiaceae. *Proc Natl Acad Sci U S A, 99*(19), 12375-12380. doi:10.1073/pnas.192439399

Guzman-Verri, C., Suarez-Esquivel, M., Ruiz-Villalobos, N., Zygmunt, M. S., Gonnet, M., Campos, E., Viquez-Ruiz, E., Chacon-Diaz, C., Aragon-Aranda, B., Conde-Alvarez, R., Moriyon, I., Blasco, J. M., Munoz, P. M., Baker, K. S., Thomson, N. R., Cloeckaert, A., & Moreno, E. (2019). Genetic and Phenotypic Characterization of the Etiological Agent of Canine Orchiepididymitis Smooth *Brucella* sp. BCCN84.3. *Front Vet Sci, 6*, 175. doi:10.3389/fvets.2019.00175

Hagan, C. L., Kim, S., & Kahne, D. (2010). Reconstitution of outer membrane protein assembly from purified components. *Science, 328*(5980), 890-892. doi:10.1126/science.1188919

Hantke, K., & Braun, V. (1973). Covalent binding of lipid to protein. Diglyceride and amide-linked fatty acid at the N-terminal end of the murein-lipoprotein of the *Escherichia coli* outer membrane. *Eur J Biochem, 34*(2), 284-296. doi:10.1111/j.1432-1033.1973.tb02757.x

Hara, T., Matsuyama, S., & Tokuda, H. (2003). Mechanism underlying the inner membrane retention of *Escherichia coli* lipoproteins caused by Lol avoidance signals. *J Biol Chem, 278*(41), 40408-40414. doi:10.1074/jbc.M307836200

Hart, E. M., Gupta, M., Wuhr, M., & Silhavy, T. J. (2020a). The gain-of-function allele *bamA* E470K bypasses the essential requirement for BamD in

beta-barrel outer membrane protein assembly. *Proc Natl Acad Sci U S A, 117*(31), 18737-18743. doi:10.1073/pnas.2007696117

Hart, E. M., & Silhavy, T. J. (2020b). Functions of the BamBCDE Lipoproteins Revealed by Bypass Mutations in BamA. *J Bacteriol, 202*(21). doi:10.1128/JB.00401-20

Harz, H., Burgdorf, K., & Höltje, J.-V. (1990). Isolation and separation of the glycan strands from murein of *Escherichia coli* by reversed-phase high-performance liquid chromatography. *Analytical Biochemistry, 190*(1), 120-128. doi:10.1016/0003-2697(90)90144-x

Hayashi, S., & Wu, H. C. (1990). Lipoproteins in bacteria. *J Bioenerg Biomembr, 22*(3), 451-471. doi:10.1007/BF00763177

Hernandez, S. B., Dörr, T., Waldor, M. K., & Cava, F. (2020). Modulation of Peptidoglycan Synthesis by Recycled Cell Wall Tetrapeptides. *Cell Reports*(31).

Higashi, Y., Strominger, J. L., & Sweeley, C. C. (1970). Biosynthesis of the Peptidoglycan of Bacterial Cell Walls. *Journal of Biological Chemistry, 245*(14), 3697-3702. doi:10.1016/s0021-9258(18)62982-5

Hiranuma, N., Park, H., Baek, M., Anishchenko, I., Dauparas, J., & Baker, D. (2021). Improved protein structure refinement guided by deep learning based accuracy estimation. *Nat Commun, 12*(1), 1340. doi:10.1038/s41467-021-21511-x

Hirashima, A., Childs, G., & Inouye, M. (1973). Differential inhibitory effects of antibiotics on the biosynthesis of envelope proteins of *Escherichia coli*. *Journal of Molecular Biology, 79*(2), 373-389. doi:10.1016/0022-2836(73)90012-0

Hirota, Y., Suzuki, H., Nishimura, Y., & Yasuda, S. (1977). On the process of cellular division in Escherichia coli: a mutant of E. coli lacking a murein-lipoprotein. *Proc Natl Acad Sci U S A, 74*(4), 1417-1420. doi:10.1073/pnas.74.4.1417

Hofer, E., Revilla-Fernandez, S., Al Dahouk, S., Riehm, J. M., Nockler, K., Zygmunt, M. S., Cloeckaert, A., Tomaso, H., & Scholz, H. C. (2012). A potential novel *Brucella* species isolated from mandibular lymph nodes of red foxes in Austria. *Vet Microbiol, 155*(1), 93-99. doi:10.1016/j.vetmic.2011.08.009

Holtje, J. V. (1998). Growth of the stress-bearing and shape-maintaining murein sacculus of *Escherichia coli*. *Microbiol Mol Biol Rev, 62*(1), 181-203. doi:10.1128/MMBR.62.1.181-203.1998

Holtje, J. V., Mirelman, D., Sharon, N., & Schwarz, U. (1975). Novel type of murein transglycosylase in *Escherichia coli*. *J Bacteriol, 124*(3), 1067-1076. doi:10.1128/JB.124.3.1067-1076.1975

Honore, N., Nicolas, M. H., & Cole, S. T. (1989). Regulation of enterobacterial cephalosporinase production: the role of a membrane-bound sensory transducer. *Mol Microbiol, 3*(8), 1121-1130. doi:10.1111/j.1365-2958.1989.tb00262.x

Hove-Jensen, B. (1992). Identification of *tms-26* as an allele of the *gcaD* gene, which encodes N-acetylglucosamine 1-phosphate uridyltransferase in *Bacillus subtilis*. *J Bacteriol, 174*(21), 6852-6856. doi:10.1128/jb.174.21.6852-6856.1992

Ikeda, M., Wachi, M., Jung, H. K., Ishino, F., & Matsuhashi, M. (1991). The Escherichia coli mraY gene encoding UDP-N-acetylmuramoyl-pentapeptide: undecaprenyl-phosphate phospho-N-acetylmuramoyl-pentapeptide transferase. *J Bacteriol, 173*(3), 1021-1026. doi:10.1128/jb.173.3.1021-1026.1991

Inouye, M., Shaw, J., & Shen, C. (1972). The Assembly of a Structural Lipoprotein in the Envelope of *Escherichia coli*. *Journal of Biological Chemistry, 247*(24), 8154-8159. doi:10.1016/s0021-9258(20)81822-5

Irazoki, O., Hernandez, S. B., & Cava, F. (2019). Peptidoglycan Muropeptides: Release, Perception, and Functions as Signaling Molecules. *Front Microbiol, 10*, 500. doi:10.3389/fmicb.2019.00500

Jacobs, C., Frère, J.-M., & Normark, S. (1997). Cytosolic Intermediates for Cell Wall Biosynthesis and Degradation Control Inducible β-Lactam Resistance in Gram-Negative Bacteria. *Cell, 88*(6), 823-832. doi:10.1016/s0092-8674(00)81928-5

Jacobs, C., Huang, L. J., Bartowsky, E., Normark, S., & Park, J. T. (1994). Bacterial cell wall recycling provides cytosolic muropeptides as effectors for beta-lactamase induction. *The EMBO Journal, 13*(19), 4684-4694. doi:10.1002/j.1460-2075.1994.tb06792.x

Jacobs, C., Joris, B., Jamin, M., Klarsov, K., Van Beeumen, J., Mengin-Lecreulx, D., van Heijenoort, J., Park, J. T., Normark, S., & Frere, J. M. (1995). AmpD, essential for both beta-lactamase regulation and cell wall recycling, is a novel cytosolic N-acetylmuramyl-L-alanine amidase. *Mol Microbiol, 15*(3), 553-559. doi:10.1111/j.1365-2958.1995.tb02268.x

Joris, B., Englebert, S., Chu, C. P., Kariyama, R., Daneo-Moore, L., Shockman, G. D., & Ghuysen, J. M. (1992). Modular design of the *Enterococcus hirae* muramidase-2 and *Streptococcus faecalis* autolysin. *FEMS Microbiol Lett, 70*(3), 257-264. doi:10.1016/0378-1097(92)90707-u

Jubier-Maurin, V., Boigegrain, R. A., Cloeckaert, A., Gross, A., Alvarez-Martinez, M. T., Terraza, A., Liautard, J., Kohler, S., Rouot, B.,

Dornand, J., & Liautard, J. P. (2001). Major outer membrane protein Omp25 of *Brucella suis* is involved in inhibition of tumor necrosis factor alpha production during infection of human macrophages. *Infect Immun, 69*(8), 4823-4830. doi:10.1128/IAI.69.8.4823-4830.2001

Jumper, J., Evans, R., Pritzel, A., Green, T., Figurnov, M., Ronneberger, O., Tunyasuvunakool, K., Bates, R., Zidek, A., Potapenko, A., Bridgland, A., Meyer, C., Kohl, S. A. A., Ballard, A. J., Cowie, A., Romera-Paredes, B., Nikolov, S., Jain, R., Adler, J., Back, T., Petersen, S., Reiman, D., Clancy, E., Zielinski, M., Steinegger, M., Pacholska, M., Berghammer, T., Bodenstein, S., Silver, D., Vinyals, O., Senior, A. W., Kavukcuoglu, K., Kohli, P., & Hassabis, D. (2021). Highly accurate protein structure prediction with AlphaFold. *Nature, 596*(7873), 583-589. doi:10.1038/s41586-021-03819-2

Kahan, F. M., Kahan, J. S., Cassidy, P. J., & Kropp, H. (1974). The mechanism of action of fosfomycin (phosphonomycin). *Ann N Y Acad Sci, 235*(0), 364-386. doi:10.1111/j.1749-6632.1974.tb43277.x

Kaku, H., Nishizawa, Y., Ishii-Minami, N., Akimoto-Tomiyama, C., Dohmae, N., Takio, K., Minami, E., & Shibuya, N. (2006). Plant cells recognize chitin fragments for defense signaling through a plasma membrane receptor. *Proc Natl Acad Sci U S A, 103*(29), 11086-11091. doi:10.1073/pnas.0508882103

Kaplan, E., Greene, N. P., Crow, A., & Koronakis, V. (2018). Insights into bacterial lipoprotein trafficking from a structure of LolA bound to the LolC periplasmic domain. *Proc Natl Acad Sci U S A, 115*(31), E7389-E7397. doi:10.1073/pnas.1806822115

Kim, H. S., Im, H. N., An, D. R., Yoon, J. Y., Jang, J. Y., Mobashery, S., Hesek, D., Lee, M., Yoo, J., Cui, M., Choi, S., Kim, C., Lee, N. K., Kim, S. J., Kim, J. Y., Bang, G., Han, B. W., Lee, B. I., Yoon, H. J., & Suh, S. W. (2015). The Cell Shape-determining Csd6 Protein from *Helicobacter pylori* Constitutes a New Family of L,D-Carboxypeptidase. *J Biol Chem, 290*(41), 25103-25117. doi:10.1074/jbc.M115.658781

Koebnik, R., Locher, K. P., & Van Gelder, P. (2000). Structure and function of bacterial outer membrane proteins: barrels in a nutshell. *Mol Microbiol, 37*(2), 239-253. doi:10.1046/j.1365-2958.2000.01983.x

Konovalova, A., Kahne, D. E., & Silhavy, T. J. (2017). Outer Membrane Biogenesis. *Annu Rev Microbiol, 71*, 539-556. doi:10.1146/annurev-micro-090816-093754

Kuru, E., Hughes, H. V., Brown, P. J., Hall, E., Tekkam, S., Cava, F., de Pedro, M. A., Brun, Y. V., & VanNieuwenhze, M. S. (2012). *In Situ* probing of

newly synthesized peptidoglycan in live bacteria with fluorescent D-amino acids. *Angew Chem Int Ed Engl, 51*(50), 12519-12523. doi:10.1002/anie.201206749

Kysela, D. T., Brown, P. J., Huang, K. C., & Brun, Y. V. (2013). Biological consequences and advantages of asymmetric bacterial growth. *Annu Rev Microbiol, 67*, 417-435. doi:10.1146/annurev-micro-092412-155622

Labischinski, H., Goodell, E. W., Goodell, A., & Hochberg, M. L. (1991). Direct proof of a "more-than-single-layered" peptidoglycan architecture of *Escherichia coli* W7: a neutron small-angle scattering study. *J Bacteriol, 173*(2), 751-756. doi:10.1128/jb.173.2.751-756.1991

Laloux, G., Deghelt, M., de Barsy, M., Letesson, J.-J., & De Bolle, X. (2010). Identification of the Essential *Brucella melitensis* Porin Omp2b as a Suppressor of Bax-Induced Cell Death in Yeast in a Genome-Wide Screening. *PLOs one, 5*(10).

Lam, H., Oh, D. C., Cava, F., Takacs, C. N., Clardy, J., de Pedro, M. A., & Waldor, M. K. (2009). D-amino acids govern stationary phase cell wall remodeling in bacteria. *Science, 325*(5947), 1552-1555. doi:10.1126/science.1178123

Lauber, F., Deme, J. C., Lea, S. M., & Berks, B. C. (2018). Type 9 secretion system structures reveal a new protein transport mechanism. *Nature, 564*(7734), 77-82. doi:10.1038/s41586-018-0693-y

Lavollay, M., Arthur, M., Fourgeaud, M., Dubost, L., Marie, A., Veziris, N., Blanot, D., Gutmann, L., & Mainardi, J. L. (2008). The peptidoglycan of stationary-phase *Mycobacterium tuberculosis* predominantly contains cross-links generated by L,D-transpeptidation. *J Bacteriol, 190*(12), 4360-4366. doi:10.1128/JB.00239-08

Lee, J., Sutterlin, H. A., Wzorek, J. S., Mandler, M. D., Hagan, C. L., Grabowicz, M., Tomasek, D., May, M. D., Hart, E. M., Silhavy, T. J., & Kahne, D. (2018). Substrate binding to BamD triggers a conformational change in BamA to control membrane insertion. *Proc Natl Acad Sci U S A, 115*(10), 2359-2364. doi:10.1073/pnas.1711727115

Lee, J., Tomasek, D., Santos, T. M., May, M. D., Meuskens, I., & Kahne, D. (2019). Formation of a beta-barrel membrane protein is catalyzed by the interior surface of the assembly machine protein BamA. *Elife, 8*. doi:10.7554/eLife.49787

Lewenza, S., Mhlanga, M. M., & Pugsley, A. P. (2008). Novel inner membrane retention signals in *Pseudomonas aeruginosa* lipoproteins. *J Bacteriol, 190*(18), 6119-6125. doi:10.1128/JB.00603-08

Li, G. W., Burkhardt, D., Gross, C., & Weissman, J. S. (2014). Quantifying absolute protein synthesis rates reveals principles underlying allocation of cellular resources. *Cell, 157*(3), 624-635. doi:10.1016/j.cell.2014.02.033

Liger, D., Masson, A., Blanot, D., van Heijenoort, J., & Parquet, C. (1995). Over-production, purification and properties of the uridine-diphosphate-N-acetylmuramate: L-alanine ligase from *Escherichia coli*. *Eur J Biochem, 230*(1), 80-87. doi:10.1111/j.1432-1033.1995.0080i.x

Lindner, A. B., Madden, R., Demarez, A., Stewart, E. J., & Taddei, F. (2008). Asymmetric segregation of protein aggregates is associated with cellular aging and rejuvenation. *Proc Natl Acad Sci U S A, 105*(8), 3076-3081. doi:10.1073/pnas.0708931105

Lindquist, S., Lindberg, F., & Normark, S. (1989). Binding of the *Citrobacter freundii* AmpR regulator to a single DNA site provides both autoregulation and activation of the inducible ampC beta-lactamase gene. *J Bacteriol, 171*(7), 3746-3753. doi:10.1128/jb.171.7.3746-3753.1989

LoVullo, E. D., Wright, L. F., Isabella, V., Huntley, J. F., & Pavelka, M. S., Jr. (2015). Revisiting the Gram-negative lipoprotein paradigm. *J Bacteriol, 197*(10), 1705-1715. doi:10.1128/JB.02414-14

Lynch, J. L., & Neuhaus, F. C. (1966). On the mechanism of action of the antibiotic O-carbamyld-serine in *Streptococcus faecalis*. *J Bacteriol, 91*(1), 449-460. doi:10.1128/jb.91.1.449-460.1966

Magnet, S., Bellais, S., Dubost, L., Fourgeaud, M., Mainardi, J. L., Petit-Frere, S., Marie, A., Mengin-Lecreulx, D., Arthur, M., & Gutmann, L. (2007). Identification of the L,D-transpeptidases responsible for attachment of the Braun lipoprotein to *Escherichia coli* peptidoglycan. *J Bacteriol, 189*(10), 3927-3931. doi:10.1128/JB.00084-07

Magnet, S., Dubost, L., Marie, A., Arthur, M., & Gutmann, L. (2008). Identification of the L,D-transpeptidases for peptidoglycan cross-linking in *Escherichia coli*. *J Bacteriol, 190*(13), 4782-4785. doi:10.1128/JB.00025-08

Mainardi, J. L., Fourgeaud, M., Hugonnet, J. E., Dubost, L., Brouard, J. P., Ouazzani, J., Rice, L. B., Gutmann, L., & Arthur, M. (2005). A novel peptidoglycan cross-linking enzyme for a beta-lactam-resistant transpeptidation pathway. *J Biol Chem, 280*(46), 38146-38152. doi:10.1074/jbc.M507384200

Mainardi, J. L., Hugonnet, J. E., Rusconi, F., Fourgeaud, M., Dubost, L., Moumi, A. N., Delfosse, V., Mayer, C., Gutmann, L., Rice, L. B., & Arthur, M.

(2007a). Unexpected Inhibition of Peptidoglycan LD-Transpeptidase from Enterococcus faecium by the β-Lactam Imipenem. *J Biol Chem, 282*(42), 30414-30422.

Mainardi, J. L., Hugonnet, J. E., Rusconi, F., Fourgeaud, M., Dubost, L., Moumi, A. N., Delfosse, V., Mayer, C., Gutmann, L., Rice, L. B., & Arthur, M. (2007b). Unexpected inhibition of peptidoglycan LD-transpeptidase from *Enterococcus faecium* by the beta-lactam imipenem. *J Biol Chem, 282*(42), 30414-30422. doi:10.1074/jbc.M704286200

Malinverni, J. C., Werner, J., Kim, S., Sklar, J. G., Kahne, D., Misra, R., & Silhavy, T. J. (2006). YfiO stabilizes the YaeT complex and is essential for outer membrane protein assembly in *Escherichia coli*. *Mol Microbiol, 61*(1), 151-164. doi:10.1111/j.1365-2958.2006.05211.x

Manterola, L., Guzman-Verri, C., Chaves-Olarte, E., Barquero-Calvo, E., de Miguel, M. J., Moriyon, I., Grillo, M. J., Lopez-Goni, I., & Moreno, E. (2007). BvrR/BvrS-controlled outer membrane proteins Omp3a and Omp3b are not essential for *Brucella abortus* virulence. *Infect Immun, 75*(10), 4867-4874. doi:10.1128/IAI.00439-07

Marchler-Bauer, A., Bo, Y., Han, L., He, J., Lanczycki, C. J., Lu, S., Chitsaz, F., Derbyshire, M. K., Geer, R. C., Gonzales, N. R., Gwadz, M., Hurwitz, D. I., Lu, F., Marchler, G. H., Song, J. S., Thanki, N., Wang, Z., Yamashita, R. A., Zhang, D., Zheng, C., Geer, L. Y., & Bryant, S. H. (2017). CDD/SPARCLE: functional classification of proteins via subfamily domain architectures. *Nucleic Acids Res, 45*(D1), D200-D203. doi:10.1093/nar/gkw1129

Marquardt, J. L., Siegele, D. A., Kolter, R., & Walsh, C. T. (1992). Cloning and sequencing of *Escherichia coli murZ* and purification of its product, a UDP-N-acetylglucosamine enolpyruvyl transferase. *J Bacteriol, 174*(17), 5748-5752. doi:10.1128/jb.174.17.5748-5752.1992

Matias, V. R., Al-Amoudi, A., Dubochet, J., & Beveridge, T. J. (2003). Cryo-transmission electron microscopy of frozen-hydrated sections of *Escherichia coli* and *Pseudomonas aeruginosa*. *J Bacteriol, 185*(20), 6112-6118. doi:10.1128/JB.185.20.6112-6118.2003

Matsuyama, S., Tajima, T., & Tokuda, H. (1995). A novel periplasmic carrier protein involved in the sorting and transport of *Escherichia coli* lipoproteins destined for the outer membrane. *The EMBO Journal, 14*(14), 3365-3372. doi:10.1002/j.1460-2075.1995.tb07342.x

Matsuyama, S., Yokota, N., & Tokuda, H. (1997). A novel outer membrane lipoprotein, LolB (HemM), involved in the LolA (p20)-dependent localization of lipoproteins to the outer membrane of *Escherichia coli*. *EMBO J, 16*(23), 6947-6955. doi:10.1093/emboj/16.23.6947

McGuinness, W. A., Malachowa, N., & DeLeo, F. R. (2017). Vancomycin Resistance in *Staphylococcus aureus*. *Yale J Biol Med, 90*(2), 269-281.

Meberg, B. M., Sailer, F. C., Nelson, D. E., & Young, K. D. (2001). Reconstruction of *Escherichia coli mrcA* (PBP1a) mutants lacking multiple combinations of penicillin binding proteins. *J Bacteriol, 183*(20), 6148-6149. doi:10.1128/JB.183.20.6148-6149.2001

Meeske, A. J., Sham, L. T., Kimsey, H., Koo, B. M., Gross, C. A., Bernhardt, T. G., & Rudner, D. Z. (2015). MurJ and a novel lipid II flippase are required for cell wall biogenesis in Bacillus subtilis. *Proc Natl Acad Sci U S A, 112*(20), 6437-6442. doi:10.1073/pnas.1504967112

Mengin-Lecreulx, D., & van Heijenoort, J. (1993). Identification of the *glmU* gene encoding N-acetylglucosamine-1-phosphate uridyltransferase in *Escherichia coli*. *J Bacteriol, 175*(19), 6150-6157. doi:10.1128/jb.175.19.6150-6157.1993

Mengin-Lecreulx, D., & van Heijenoort, J. (1994). Copurification of glucosamine-1-phosphate acetyltransferase and N-acetylglucosamine-1-phosphate uridyltransferase activities of *Escherichia coli*: characterization of the *glmU* gene product as a bifunctional enzyme catalyzing two subsequent steps in the pathway for UDP-N-acetylglucosamine synthesis. *J Bacteriol, 176*(18), 5788-5795. doi:10.1128/jb.176.18.5788-5795.1994

Mengin-Lecreulx, D., & van Heijenoort, J. (1996a). Characterization of the essential gene *glmM* encoding phosphoglucosamine mutase in *Escherichia coli*. *J Biol Chem, 271*(1), 32-39. doi:10.1074/jbc.271.1.32

Mengin-Lecreulx, D., van Heijenoort, J., & Park, J. T. (1996b). Identification of the *mpl* gene encoding UDP-N-acetylmuramate: L-alanyl-gamma-D-glutamyl-*meso*-diaminopimelate ligase in *Escherichia coli* and its role in recycling of cell wall peptidoglycan. *J Bacteriol, 178*(18), 5347-5352. doi:10.1128/jb.178.18.5347-5352.1996

Mesnage, S., Dellarole, M., Baxter, N. J., Rouget, J. B., Dimitrov, J. D., Wang, N., Fujimoto, Y., Hounslow, A. M., Lacroix-Desmazes, S., Fukase, K., Foster, S. J., & Williamson, M. P. (2014). Molecular basis for bacterial peptidoglycan recognition by LysM domains. *Nat Commun, 5*, 4269. doi:10.1038/ncomms5269

Meyer, K. F., & Shaw, E. B. (1920). A Comparison of the Morphologic, Cultural and Biochemical Characteristics of *B. Abortus* and *B. Melitensis*: Studies on the Genus *Brucella* Nov. Gen. I. *The Journal of Infectious Diseases, 27*(3), 173-184.

Mirdita, M., Schütze, K., Moriwaki, Y., Heo, L., Ovchinnikov, S., & Steinegger, M. (2021). ColabFold - Making protein folding accessible to all. *bioRxiv*. doi:10.1101/2021.08.15.456425

Mirdita, M., Steinegger, M., & Soding, J. (2019). MMseqs2 desktop and local web server app for fast, interactive sequence searches. *Bioinformatics, 35*(16), 2856-2858. doi:10.1093/bioinformatics/bty1057

Mirdita, M., von den Driesch, L., Galiez, C., Martin, M. J., Soding, J., & Steinegger, M. (2017). Uniclust databases of clustered and deeply annotated protein sequences and alignments. *Nucleic Acids Res, 45*(D1), D170-D176. doi:10.1093/nar/gkw1081

Mitchell, A. L., Almeida, A., Beracochea, M., Boland, M., Burgin, J., Cochrane, G., Crusoe, M. R., Kale, V., Potter, S. C., Richardson, L. J., Sakharova, E., Scheremetjew, M., Korobeynikov, A., Shlemov, A., Kunyavskaya, O., Lapidus, A., & Finn, R. D. (2020). MGnify: the microbiome analysis resource in 2020. *Nucleic Acids Res, 48*(D1), D570-D578. doi:10.1093/nar/gkz1035

Mizuno, T. (1979). A novel peptidoglycan-associated lipoprotein found in the cell envelope of *Pseudomonas aeruginosa* and *Escherichia coli*. *J Biochem, 86*(4), 991-1000. doi:10.1093/oxfordjournals.jbchem.a132631

Mizuno, Y., & Ito, E. (1968). Purification and Properties of Uridine Diphosphate N-Acetylmuramyl-L-alanyl-D-glutamate:*meso*-2,6-diaminopimelate Ligase. *Journal of Biological Chemistry, 243*(10), 2665-2672. doi:10.1016/s0021-9258(18)93424-1

Mobasheri, H., Ficht, T. A., Marquis, H., Lea, E. J., & Lakey, J. H. (1997). *Brucella* Omp2a and Omp2b porins: single channel measurements and topology prediction. *FEMS Microbiol Lett, 155*(1), 23-30. doi:10.1111/j.1574-6968.1997.tb12681.x

Mohammadi, T., van Dam, V., Sijbrandi, R., Vernet, T., Zapun, A., Bouhss, A., Diepeveen-de Bruin, M., Nguyen-Disteche, M., de Kruijff, B., & Breukink, E. (2011). Identification of FtsW as a transporter of lipid-linked cell wall precursors across the membrane. *EMBO J, 30*(8), 1425-1432. doi:10.1038/emboj.2011.61

More, N., Martorana, A. M., Biboy, J., Otten, C., Winkle, M., Serrano, C. K. G., Monton Silva, A., Atkinson, L., Yau, H., Breukink, E., den Blaauwen, T., Vollmer, W., & Polissi, A. (2019). Peptidoglycan Remodeling Enables *Escherichia coli* To Survive Severe Outer Membrane Assembly Defect. *MBio, 10*(1). doi:10.1128/mBio.02729-18

Moreno, E. (2021). The one hundred year journey of the genus *Brucella* (Meyer and Shaw 1920). *FEMS Microbiol Rev, 45*(1). doi:10.1093/femsre/fuaa045

Moreno, E., Stackebrandt, E., Dorsch, M., Wolters, J., Busch, M., & Mayer, H. (1990). *Brucella abortus* 16S rRNA and lipid A reveal a phylogenetic relationship with members of the alpha-2 subdivision of the class Proteobacteria. *J Bacteriol, 172*(7), 3569-3576. doi:10.1128/jb.172.7.3569-3576.1990

Mullineaux, C. W., Nenninger, A., Ray, N., & Robinson, C. (2006). Diffusion of green fluorescent protein in three cell environments in *Escherichia coli*. *J Bacteriol, 188*(10), 3442-3448. doi:10.1128/JB.188.10.3442-3448.2006

Mutolo, M. J., Jenny, L. L., Buszek, A. R., Fenton, T. W., & Foran, D. R. (2012). Osteological and molecular identification of Brucellosis in ancient Butrint, Albania. *Am J Phys Anthropol, 147*(2), 254-263. doi:10.1002/ajpa.21643

Narita, S. (2011). ABC transporters involved in the biogenesis of the outer membrane in gram-negative bacteria. *Biosci Biotechnol Biochem, 75*(6), 1044-1054. doi:10.1271/bbb.110115

Narita, S., & Tokuda, H. (2007). Amino acids at positions 3 and 4 determine the membrane specificity of *Pseudomonas aeruginosa* lipoproteins. *J Biol Chem, 282*(18), 13372-13378. doi:10.1074/jbc.M611839200

Nikaido, H. (1992). Porins and specific channels of bacterial outer membranes. *Mol Microbiol, 6*(4), 435-442. doi:10.1111/j.1365-2958.1992.tb01487.x

Noinaj, N., Kuszak, A. J., Gumbart, J. C., Lukacik, P., Chang, H., Easley, N. C., Lithgow, T., & Buchanan, S. K. (2013). Structural insight into the biogenesis of beta-barrel membrane proteins. *Nature, 501*(7467), 385-390. doi:10.1038/nature12521

Normark, S., Bartowsky, E., Erickson, J., Jacobs, C., Lindberg, F., Lindquist, S., Weston-Hafer, K., & Wikström, M. (1994). Mechanisms of chromosomal β-lactamase induction in Gram-negative bacteria. In *Bacterial Cell Wall* (pp. 485-503).

Okuda, S., & Tokuda, H. (2009). Model of mouth-to-mouth transfer of bacterial lipoproteins through inner membrane LolC, periplasmic LolA, and outer membrane LolB. *Proc Natl Acad Sci U S A, 106*(14), 5877-5882. doi:10.1073/pnas.0900896106

Okuda, S., & Tokuda, H. (2011). Lipoprotein sorting in bacteria. *Annu Rev Microbiol, 65*, 239-259. doi:10.1146/annurev-micro-090110-102859

Palmer, T., & Berks, B. C. (2012). The twin-arginine translocation (Tat) protein export pathway. *Nat Rev Microbiol, 10*(7), 483-496. doi:10.1038/nrmicro2814

Pappas, G., Kiriaze, I. J., & Falagas, M. E. (2008). Insights into infectious disease in the era of Hippocrates. *Int J Infect Dis, 12*(4), 347-350. doi:10.1016/j.ijid.2007.11.003

Paquet, J. Y., Diaz, M. A., Genevrois, S., Grayon, M., Verger, J. M., de Bolle, X., Lakey, J. H., Letesson, J. J., & Cloeckaert, A. (2001). Molecular, antigenic, and functional analyses of Omp2b porin size variants of *Brucella* spp. *J Bacteriol, 183*(16), 4839-4847. doi:10.1128/JB.183.16.4839-4847.2001

Park, J. S., Lee, W. C., Yeo, K. J., Ryu, K. S., Kumarasiri, M., Hesek, D., Lee, M., Mobashery, S., Song, J. H., Kim, S. I., Lee, J. C., Cheong, C., Jeon, Y. H., & Kim, H. Y. (2012). Mechanism of anchoring of OmpA protein to the cell wall peptidoglycan of the gram-negative bacterial outer membrane. *FASEB J, 26*(1), 219-228. doi:10.1096/fj.11-188425

Park, J. T. (1993). Turnover and recycling of the murein sacculus in oligopeptide permease-negative strains of *Escherichia coli*: indirect evidence for an alternative permease system and for a monolayered sacculus. *J Bacteriol, 175*(1), 7-11. doi:10.1128/jb.175.1.7-11.1993

Park, J. T. (2001). Identification of a dedicated recycling pathway for anhydro-N-acetylmuramic acid and N-acetylglucosamine derived from *Escherichia coli* cell wall murein. *J Bacteriol, 183*(13), 3842-3847. doi:10.1128/JB.183.13.3842-3847.2001

Pasquevich, K. A., Carabajal, M. V., Guaimas, F. F., Bruno, L., Roset, M. S., Coria, L. M., Rey Serrantes, D. A., Comerci, D. J., & Cassataro, J. (2019). Omp19 Enables *Brucella abortus* to Evade the Antimicrobial Activity From Host's Proteolytic Defense System. *Front Immunol, 10*, 1436. doi:10.3389/fimmu.2019.01436

Pautsch, A., & Schulz, G. E. (1998). Structure of the outer membrane protein A transmembrane domain. *Nat Struct Biol, 5*(11), 1013-1017. doi:10.1038/2983

Peters, J. M., Koo, B. M., Patino, R., Heussler, G. E., Hearne, C. C., Qu, J., Inclan, Y. F., Hawkins, J. S., Lu, C. H. S., Silvis, M. R., Harden, M. M., Osadnik, H., Peters, J. E., Engel, J. N., Dutton, R. J., Grossman, A. D., Gross, C. A., & Rosenberg, O. S. (2019). Enabling genetic analysis of diverse bacteria with Mobile-CRISPRi. *Nat Microbiol, 4*(2), 244-250. doi:10.1038/s41564-018-0327-z

Peters, K., Pazos, M., Eddoo, Z., Hugonnet, J.-E., Martorana, A. M., Polissi, A., VanNieuwenhze, M. S., Arthur, M., & Vollmer, W. (2018). Copper

inhibits peptidoglycan LD-transpeptidases suppressing β-lactam resistance due to bypass of penicillin-binding proteins. *PNAS, 115*(42), 10786-10791. doi:10.1073/pnas.1809285115

Pisabarro, A. G., de Pedro, M. A., & Vazquez, D. (1985). Structural modifications in the peptidoglycan of *Escherichia coli* associated with changes in the state of growth of the culture. *J Bacteriol, 161*(1), 238-242. doi:10.1128/JB.161.1.238-242.1985

Pizarro-Cerda, J., Meresse, S., Parton, R. G., van der Goot, G., Sola-Landa, A., Lopez-Goni, I., Moreno, E., & Gorvel, J. P. (1998a). *Brucella abortus* transits through the autophagic pathway and replicates in the endoplasmic reticulum of nonprofessional phagocytes. *Infect Immun, 66*(12), 5711-5724. doi:10.1128/IAI.66.12.5711-5724.1998

Pizarro-Cerda, J., Moreno, E., Sanguedolce, V., Mege, J. L., & Gorvel, J. P. (1998b). Virulent *Brucella abortus* prevents lysosome fusion and is distributed within autophagosome-like compartments. *Infect Immun, 66*(5), 2387-2392. doi:10.1128/IAI.66.5.2387-2392.1998

Plummer, A. M., & Fleming, K. G. (2015). BamA Alone Accelerates Outer Membrane Protein Folding In Vitro through a Catalytic Mechanism. *Biochemistry, 54*(39), 6009-6011. doi:10.1021/acs.biochem.5b00950

Ponting, C. P., Aravind, L., Schultz, J., Bork, P., & Koonin, E. V. (1999). Eukaryotic signalling domain homologues in archaea and bacteria. Ancient ancestry and horizontal gene transfer. *J Mol Biol, 289*(4), 729-745. doi:10.1006/jmbi.1999.2827

Porte, F., Liautard, J. P., & Kohler, S. (1999). Early acidification of phagosomes containing *Brucella suis* is essential for intracellular survival in murine macrophages. *Infect Immun, 67*(8), 4041-4047. doi:10.1128/IAI.67.8.4041-4047.1999

Pratviel-Sosa, F., Mengin-Lecreulx, D., & van Heijenoort, J. (1991). Over-production, purification and properties of the uridine diphosphate N-acetylmuramoyl-L-alanine:D-glutamate ligase from *Escherichia coli*. *Eur J Biochem, 202*(3), 1169-1176. doi:10.1111/j.1432-1033.1991.tb16486.x

Quintela, J. C., de Pedro, M. A., Zollner, P., Allmaier, G., & Garcia-del Portillo, F. (1997). Peptidoglycan structure of *Salmonella typhimurium* growing within cultured mammalian cells. *Mol Microbiol, 23*(4), 693-704. doi:10.1046/j.1365-2958.1997.2561621.x

Raman, S., Vernon, R., Thompson, J., Tyka, M., Sadreyev, R., Pei, J., Kim, D., Kellogg, E., DiMaio, F., Lange, O., Kinch, L., Sheffler, W., Kim, B. H., Das, R., Grishin, N. V., & Baker, D. (2009). Structure prediction for

CASP8 with all-atom refinement using Rosetta. *Proteins, 77 Suppl 9*, 89-99. doi:10.1002/prot.22540

Reboul, A., Carlier, E., Stubbe, F. X., Barbieux, E., Demars, A., Ong, T. A. P., Gerodez, A., Muraille, E., & De Bolle, X. (2021). PdeA is required for the rod shape morphology of *Brucella abortus*. *Mol Microbiol*. doi:10.1111/mmi.14833

Redko, Y., Bechhofer, D. H., & Condon, C. (2008). Mini-III, an unusual member of the RNase III family of enzymes, catalyses 23S ribosomal RNA maturation in *B. subtilis*. *Mol Microbiol, 68*(5), 1096-1106. doi:10.1111/j.1365-2958.2008.06207.x

Robichon, C., Vidal-Ingigliardi, D., & Pugsley, A. P. (2005). Depletion of apolipoprotein N-acyltransferase causes mislocalization of outer membrane lipoproteins in *Escherichia coli*. *J Biol Chem, 280*(2), 974-983. doi:10.1074/jbc.M411059200

Rogers, S. D., Bhave, M. R., Mercer, J. F., Camakaris, J., & Lee, B. T. (1991). Cloning and characterization of *cutE*, a gene involved in copper transport in *Escherichia coli*. *J Bacteriol, 173*(21), 6742-6748. doi:10.1128/jb.173.21.6742-6748.1991

Rojas, E. R., Billings, G., Odermatt, P. D., Auer, G. K., Zhu, L., Miguel, A., Chang, F., Weibel, D. B., Theriot, J. A., & Huang, K. C. (2018). The outer membrane is an essential load-bearing element in Gram-negative bacteria. *Nature, 559*(7715), 617-621. doi:10.1038/s41586-018-0344-3

Ross, H. M., Foster, G., Reid, R. J., Jahans, K. L., & MacMillan, A. P. (1994). *Brucella* species infection in sea-mammals. *Vet Rec, 134*(14), 359. doi:10.1136/vr.134.14.359-b

Salcedo, S. P., Chevrier, N., Lacerda, T. L., Ben Amara, A., Gerart, S., Gorvel, V. A., de Chastellier, C., Blasco, J. M., Mege, J. L., & Gorvel, J. P. (2013). Pathogenic Brucellae Replicate in Human Trophoblasts. *J Infect Dis, 207*(7), 1075-1083. doi:10.1093/infdis/jit007

Salhi, I., Boigegrain, R. A., Machold, J., Weise, C., Cloeckaert, A., & Rouot, B. (2003). Characterization of new members of the group 3 outer membrane protein family of *Brucella* spp. *Infect Immun, 71*(8), 4326-4332. doi:10.1128/IAI.71.8.4326-4332.2003

Salmond, G. P., Lutkenhaus, J. F., & Donachie, W. D. (1980). Identification of new genes in a cell envelope-cell division gene cluster of *Escherichia coli*: cell envelope gene *murG*. *J Bacteriol, 144*(1), 438-440. doi:10.1128/JB.144.1.438-440.1980

Samsudin, F., Boags, A., Piggot, T. J., & Khalid, S. (2017). Braun's Lipoprotein Facilitates OmpA Interaction with the *Escherichia coli* Cell Wall. *Biophys J, 113*(7), 1496-1504. doi:10.1016/j.bpj.2017.08.011

Samsudin, F., Ortiz-Suarez, M. L., Piggot, T. J., Bond, P. J., & Khalid, S. (2016). OmpA: A Flexible Clamp for Bacterial Cell Wall Attachment. *Structure, 24*(12), 2227-2235. doi:10.1016/j.str.2016.10.009

Sandoz, K. M., Moore, R. A., Beare, P. A., Patel, A. V., Smith, R. E., Bern, M., Hwang, H., Cooper, C. J., Priola, S. A., Parks, J. M., Gumbart, J. C., Mesnage, S., & Heinzen, R. A. (2021). beta-Barrel proteins tether the outer membrane in many Gram-negative bacteria. *Nat Microbiol, 6*(1), 19-26. doi:10.1038/s41564-020-00798-4

Sauvage, E., Kerff, F., Terrak, M., Ayala, J. A., & Charlier, P. (2008). The penicillin-binding proteins: structure and role in peptidoglycan biosynthesis. *FEMS Microbiol Rev, 32*(2), 234-258. doi:10.1111/j.1574-6976.2008.00105.x

Schiffer, G., & Holtje, J. V. (1999). Cloning and characterization of PBP1C, a third member of the multimodular class A penicillin-binding proteins of *Escherichia coli*. *J Biol Chem, 274*(45), 32031-32039. doi:10.1074/jbc.274.45.32031

Schindelin, J., Arganda-Carreras, I., Frise, E., Kaynig, V., Longair, M., Pietzsch, T., Preibisch, S., Rueden, C., Saalfeld, S., Schmid, B., Tinevez, J. Y., White, D. J., Hartenstein, V., Eliceiri, K., Tomancak, P., & Cardona, A. (2012). Fiji: an open-source platform for biological-image analysis. *Nat Methods, 9*(7), 676-682. doi:10.1038/nmeth.2019

Schlabritz-Loutsevitch, N. E., Whatmore, A. M., Quance, C. R., Koylass, M. S., Cummins, L. B., Dick, E. J., Jr., Snider, C. L., Cappelli, D., Ebersole, J. L., Nathanielsz, P. W., & Hubbard, G. B. (2009). A novel *Brucella* isolate in association with two cases of stillbirth in non-human primates - first report. *J Med Primatol, 38*(1), 70-73. doi:10.1111/j.1600-0684.2008.00314.x

Schleifer, K. H., & Kandler, O. (1972). Peptidoglycan types of bacterial cell walls and their taxonomic implications. *Bacteriological Reviews, 36*(4), 407-477. doi:10.1128/br.36.4.407-477.1972

Schneider, T., & Sahl, H. G. (2010). An oldie but a goodie - cell wall biosynthesis as antibiotic target pathway. *Int J Med Microbiol, 300*(2-3), 161-169. doi:10.1016/j.ijmm.2009.10.005

Scholz, H. C., Hubalek, Z., Sedlacek, I., Vergnaud, G., Tomaso, H., Al Dahouk, S., Melzer, F., Kampfer, P., Neubauer, H., Cloeckaert, A., Maquart, M., Zygmunt, M. S., Whatmore, A. M., Falsen, E., Bahn, P., Gollner, C., Pfeffer, M., Huber, B., Busse, H. J., & Nockler, K. (2008). *Brucella*

microti sp. nov., isolated from the common vole *Microtus arvalis*. *Int J Syst Evol Microbiol, 58*(Pt 2), 375-382. doi:10.1099/ijs.0.65356-0

Schulz, G. E. (2002). The structure of bacterial outer membrane proteins. *Biochimica et Biophysica Acta (BBA) - Biomembranes, 1565*(2), 308-317. doi:10.1016/s0005-2736(02)00577-1

Schulze, R. J., & Zuckert, W. R. (2006). *Borrelia burgdorferi* lipoproteins are secreted to the outer surface by default. *Mol Microbiol, 59*(5), 1473-1484. doi:10.1111/j.1365-2958.2006.05039.x

Sham, L. T., Butler, E. K., Lebar, M. D., Kahne, D., Bernhardt, T. G., & Ruiz, N. (2014). Bacterial cell wall. MurJ is the flippase of lipid-linked precursors for peptidoglycan biogenesis. *Science, 345*(6193), 220-222. doi:10.1126/science.1254522

Sheik, J., Hicks, S., Dall'Agnol, M., Phillips, A. D., & Nataro, J. P. (2001). Roles for Fis and YafK in biofilm formation by enteroaggregative *Escherichia coli*. *Mol Microbiol, 41*(5), 983-997.

Sidhu-Munoz, R. S., Sancho, P., Cloeckaert, A., Zygmunt, M. S., de Miguel, M. J., Tejedor, C., & Vizcaino, N. (2018). Characterization of Cell Envelope Multiple Mutants of *Brucella ovis* and Assessment in Mice of Their Vaccine Potential. *Front Microbiol, 9*, 2230. doi:10.3389/fmicb.2018.02230

Silva-Herzog, E., Ferracci, F., Jackson, M. W., Joseph, S. S., & Plano, G. V. (2008). Membrane localization and topology of the *Yersinia pestis* YscJ lipoprotein. *Microbiology (Reading), 154*(Pt 2), 593-607. doi:10.1099/mic.0.2007/013045-0

Smith, E. P., Miller, C. N., Child, R., Cundiff, J. A., & Celli, J. (2016). Postreplication Roles of the *Brucella* VirB Type IV Secretion System Uncovered via Conditional Expression of the VirB11 ATPase. *MBio, 7*(6). doi:10.1128/mBio.01730-16

Sola-Landa, A., Pizarro-Cerda, J., Grillo, M. J., Moreno, E., Moriyon, I., Blasco, J. M., Gorvel, J. P., & Lopez-Goni, I. (1998). A two-component regulatory system playing a critical role in plant pathogens and endosymbionts is present in *Brucella abortus* and controls cell invasion and virulence. *Mol Microbiol, 29*(1), 125-138. doi:10.1046/j.1365-2958.1998.00913.x

Song, Y., DiMaio, F., Wang, R. Y., Kim, D., Miles, C., Brunette, T., Thompson, J., & Baker, D. (2013). High-resolution comparative modeling with RosettaCM. *Structure, 21*(10), 1735-1742. doi:10.1016/j.str.2013.08.005

Sonntag, I., Schwarz, H., Hirota, Y., & Henning, U. (1978). Cell envelope and shape of *Escherichia coli*: multiple mutants missing the outer

membrane lipoprotein and other major outer membrane proteins. *J Bacteriol, 136*(1), 280-285.

Sowa, B. A. (1990). Membrane proteins of *Brucella* spp. In *Advances in Brucellosis Research: An International Symposium* (pp. 87-103): Texas A&M University Press.

Sowa, B. A., Kelly, K. A., Ficht, T. A., Frey, M., & Adams, L. G. (1991). SDS-soluble and peptidoglycan-bound proteins in the outer membrane-peptidoglycan complex of *Brucella abortus*. *Veterinary Microbiology, 27*(3-4), 351-369. doi:10.1016/0378-1135(91)90160-h

Stankeviciute, G., Miguel, A. V., Radkov, A., Chou, S., Huang, K. C., & Klein, E. A. (2019). Differential modes of crosslinking establish spatially distinct regions of peptidoglycan in *Caulobacter crescentus*. *Mol Microbiol, 111*(4), 995-1008. doi:10.1111/mmi.14199

Starr, T., Child, R., Wehrly, T. D., Hansen, B., Hwang, S., Lopez-Otin, C., Virgin, H. W., & Celli, J. (2012). Selective subversion of autophagy complexes facilitates completion of the *Brucella* intracellular cycle. *Cell Host Microbe, 11*(1), 33-45. doi:10.1016/j.chom.2011.12.002

Starr, T., Ng, T. W., Wehrly, T. D., Knodler, L. A., & Celli, J. (2008). *Brucella* intracellular replication requires trafficking through the late endosomal/lysosomal compartment. *Traffic, 9*(5), 678-694. doi:10.1111/j.1600-0854.2008.00718.x

Stathopoulos, C. (1996). An alternative topological model for *Escherichia coli* OmpA. *Protein Sci, 5*(1), 170-173. doi:10.1002/pro.5560050122

Stenberg, F., Chovanec, P., Maslen, S. L., Robinson, C. V., Ilag, L. L., von Heijne, G., & Daley, D. O. (2005). Protein complexes of the *Escherichia coli* cell envelope. *J Biol Chem, 280*(41), 34409-34419. doi:10.1074/jbc.M506479200

Sternon, J. F., Godessart, P., Goncalves de Freitas, R., Van der Henst, M., Poncin, K., Francis, N., Willemart, K., Christen, M., Christen, B., Letesson, J. J., & De Bolle, X. (2018). Transposon Sequencing of *Brucella abortus* Uncovers Essential Genes for Growth In Vitro and Inside Macrophages. *Infect Immun, 86*(8). doi:10.1128/IAI.00312-18

Stewart, E. J., Madden, R., Paul, G., & Taddei, F. (2005). Aging and death in an organism that reproduces by morphologically symmetric division. *PLoS Biol, 3*(2), e45. doi:10.1371/journal.pbio.0030045

Stoenner, H. G., & Lackman, D. B. (1957). A new species of *Brucella* isolated from the desert wood rat, *Neotoma lepida* Thomas. *Am J Vet Res, 18*(69), 947-951.

Suarez-Esquivel, M., Chaves-Olarte, E., Moreno, E., & Guzman-Verri, C. (2020). *Brucella* Genomics: Macro and Micro Evolution. *Int J Mol Sci, 21*(20). doi:10.3390/ijms21207749

Sugawara, E., & Nikaido, H. (1992). Pore-forming activity of OmpA protein of *Escherichia coli*. *Journal of Biological Chemistry, 267*(4), 2507-2511. doi:10.1016/s0021-9258(18)45908-x

Sutcliffe, I. C., Harrington, D. J., & Hutchings, M. I. (2012). A phylum level analysis reveals lipoprotein biosynthesis to be a fundamental property of bacteria. *Protein Cell, 3*(3), 163-170. doi:10.1007/s13238-012-2023-8

Suzuki, H., Nishimura, Y., & Hirota, Y. (1978a). On the process of cellular division in *Escherichia coli*: a series of mutants of *E. coli* altered in the penicillin-binding proteins. *Proc Natl Acad Sci U S A, 75*(2), 664-668. doi:10.1073/pnas.75.2.664

Suzuki, H., Nishimura, Y., Yasuda, S., Nishimura, A., Yamada, M., & Hirota, Y. (1978b). Murein-lipoprotein of *Escherichia coli*: a protein involved in the stabilization of bacterial cell envelope. *Mol Gen Genet, 167*(1), 1-9. doi:10.1007/bf00270315

Takeda, K., Miyatake, H., Yokota, N., Matsuyama, S., Tokuda, H., & Miki, K. (2003). Crystal structures of bacterial lipoprotein localization factors, LolA and LolB. *EMBO J, 22*(13), 3199-3209. doi:10.1093/emboj/cdg324

Tanaka, K., Matsuyama, S. I., & Tokuda, H. (2001). Deletion of *lolB*, encoding an outer membrane lipoprotein, is lethal for *Escherichia coli* and causes accumulation of lipoprotein localization intermediates in the periplasm. *J Bacteriol, 183*(22), 6538-6542. doi:10.1128/JB.183.22.6538-6542.2001

Tang, X., Chang, S., Zhang, K., Luo, Q., Zhang, Z., Wang, T., Qiao, W., Wang, C., Shen, C., Zhang, Z., Zhu, X., Wei, X., Dong, C., Zhang, X., & Dong, H. (2021). Structural basis for bacterial lipoprotein relocation by the transporter LolCDE. *Nat Struct Mol Biol, 28*(4), 347-355. doi:10.1038/s41594-021-00573-x

Taniguchi, N., Matsuyama, S., & Tokuda, H. (2005). Mechanisms underlying energy-independent transfer of lipoproteins from LolA to LolB, which have similar unclosed beta-barrel structures. *J Biol Chem, 280*(41), 34481-34488. doi:10.1074/jbc.M507388200

Templin, M. F., Ursinus, A., & Holtje, J. V. (1999). A defect in cell wall recycling triggers autolysis during the stationary growth phase of *Escherichia coli*. *EMBO J, 18*(15), 4108-4117. doi:10.1093/emboj/18.15.4108

Terada, M., Kuroda, T., Matsuyama, S. I., & Tokuda, H. (2001). Lipoprotein sorting signals evaluated as the LolA-dependent release of lipoproteins from the cytoplasmic membrane of *Escherichia coli*. *J Biol Chem, 276*(50), 47690-47694. doi:10.1074/jbc.M109307200

Tibor, A., Decelle, B., & Letesson, J. J. (1999). Outer membrane proteins Omp10, Omp16, and Omp19 of *Brucella* spp. are lipoproteins. *Infect Immun, 67*(9), 4960-4962. doi:10.1128/IAI.67.9.4960-4962.1999

Tibor, A., Saman, E., de Wergifosse, P., Cloeckaert, A., Limet, J. N., & Letesson, J. J. (1996). Molecular characterization, occurrence, and immunogenicity in infected sheep and cattle of two minor outer membrane proteins of *Brucella abortus*. *Infect Immun, 64*(1), 100-107. doi:10.1128/iai.64.1.100-107.1996

Tibor, A., Wansard, V., Bielartz, V., Delrue, R. M., Danese, I., Michel, P., Walravens, K., Godfroid, J., & Letesson, J. J. (2002). Effect of omp10 or omp19 deletion on *Brucella abortus* outer membrane properties and virulence in mice. *Infect Immun, 70*(10), 5540-5546. doi:10.1128/IAI.70.10.5540-5546.2002

Tibor, A., Weynants, V., Denoel, P., Lichtfouse, B., De Bolle, X., Saman, E., Limet, J. N., & Letesson, J. J. (1994). Molecular cloning, nucleotide sequence, and occurrence of a 16.5-kilodalton outer membrane protein of *Brucella abortus* with similarity to PAL lipoproteins. *Infect Immun, 62*(9), 3633-3639. doi:10.1128/iai.62.9.3633-3639.1994

Tipper, D. J., & Berman, M. F. (1969). Structures of the cell wall peptidoglycans of *Staphylococcus epidermidis* Texas 26 and *Staphylococcus aureus* Copenhagen. I. Chain length and average sequence of cross-bridge peptides. *Biochemistry, 8*(5), 2183-2192. doi:10.1021/bi00833a060

Tomasek, D., & Kahne, D. (2021). The assembly of beta-barrel outer membrane proteins. *Curr Opin Microbiol, 60*, 16-23. doi:10.1016/j.mib.2021.01.009

Traum, J. (1914). *Report to the chief of the Bureau of Animal Industry*.

Turner, J. D., Langley, R. S., Johnston, K. L., Gentil, K., Ford, L., Wu, B., Graham, M., Sharpley, F., Slatko, B., Pearlman, E., & Taylor, M. J. (2009). *Wolbachia* lipoprotein stimulates innate and adaptive immunity through Toll-like receptors 2 and 6 to induce disease manifestations of filariasis. *J Biol Chem, 284*(33), 22364-22378. doi:10.1074/jbc.M901528200

Typas, A., Banzhaf, M., Gross, C. A., & Vollmer, W. (2012). From the regulation of peptidoglycan synthesis to bacterial growth and

morphology. *Nat Rev Microbiol, 10*(2), 123-136. doi:10.1038/nrmicro2677

Umbreit, J. N., Stone, K. J., & Strominger, J. L. (1972). Isolation of polyisoprenyl alcohols from *Streptococcus faecalis*. *J Bacteriol, 112*(3), 1302-1305. doi:10.1128/JB.112.3.1302-1305.1972

Vassen, V., Valotteau, C., Feuillie, C., Formosa-Dague, C., Dufrene, Y. F., & De Bolle, X. (2019). Localized incorporation of outer membrane components in the pathogen *Brucella abortus*. *EMBO J, 38*(5). doi:10.15252/embj.2018100323

Vazquez-Laslop, N., Lee, H., Hu, R., & Neyfakh, A. A. (2001). Molecular sieve mechanism of selective release of cytoplasmic proteins by osmotically shocked *Escherichia coli*. *J Bacteriol, 183*(8), 2399-2404. doi:10.1128/JB.183.8.2399-2404.2001

Vergalli, J., Bodrenko, I. V., Masi, M., Moynie, L., Acosta-Gutierrez, S., Naismith, J. H., Davin-Regli, A., Ceccarelli, M., van den Berg, B., Winterhalter, M., & Pages, J. M. (2019). Porins and small-molecule translocation across the outer membrane of Gram-negative bacteria. *Nat Rev Microbiol*. doi:10.1038/s41579-019-0294-2

Verstreate, D. R., Creasy, M. T., Caveney, N. T., Baldwin, C. L., Blab, M. W., & Winter, A. J. (1982). Outer membrane proteins of *Brucella abortus*: isolation and characterization. *Infect Immun, 35*(3), 979-989. doi:10.1128/iai.35.3.979-989.1982

Vizcaíno, N., Cloeckaert, A., Verger, J.-M., Grayon, M., & Fernández-Lago, L. (2000). DNA polymorphism in the genus *Brucella*. *Microbes and Infection, 2*(9), 1089-1100. doi:10.1016/s1286-4579(00)01263-6

Vizcaino, N., Cloeckaert, A., Zygmunt, M. S., & Dubray, G. (1996). Cloning, nucleotide sequence, and expression of the *Brucella melitensis omp31* gene coding for an immunogenic major outer membrane protein. *Infect Immun, 64*(9), 3744-3751. doi:10.1128/iai.64.9.3744-3751.1996

Vogt, J., & Schulz, G. E. (1999). The structure of the outer membrane protein OmpX from *Escherichia coli* reveals possible mechanisms of virulence. *Structure, 7*(10), 1301-1309. doi:10.1016/s0969-2126(00)80063-5

Vollmer, W., & Bertsche, U. (2008a). Murein (peptidoglycan) structure, architecture and biosynthesis in *Escherichia coli*. *Biochim Biophys Acta, 1778*(9), 1714-1734. doi:10.1016/j.bbamem.2007.06.007

Vollmer, W., Blanot, D., & De Pedro, M. A. (2008b). Peptidoglycan structure and architecture. *FEMS Microbiol Rev, 32*, 149-167. doi:DOI:10.1111/j.1574-6976.2007.00094.x

Vollmer, W., Joris, B., Charlier, P., & Foster, S. (2008c). Bacterial peptidoglycan (murein) hydrolases. *FEMS Microbiol Rev, 32*(2), 259-286. doi:10.1111/j.1574-6976.2007.00099.x

Whitfield, C., & Valvano, M. A. (1993). Biosynthesis and Expression of Cell-Surface Polysaccharides in Gram-Negative Bacteria. *35*, 135-246. doi:10.1016/S0065-2911(08)60099-5

Wild, J., Hennig, J., Lobocka, M., Walczak, W., & Klopotowski, T. (1985). Identification of the *dadX* gene coding for the predominant isozyme of alanine racemase in *Escherichia coli* K12. *Mol Gen Genet, 198*(2), 315-322. doi:10.1007/BF00383013

Williams, M. A., Aliashkevich, A., Krol, E., Kuru, E., Bouchier, J. M., Rittichier, J., Brun, Y. V., VanNieuwenhze, M. S., Becker, A., Cava, F., & Brown, P. J. B. (2021). Unipolar Peptidoglycan Synthesis in the Rhizobiales Requires an Essential Class A Penicillin-Binding Protein. *MBio*, e0234621. doi:10.1128/mBio.02346-21

Willmann, R., Lajunen, H. M., Erbs, G., Newman, M. A., Kolb, D., Tsuda, K., Katagiri, F., Fliegmann, J., Bono, J. J., Cullimore, J. V., Jehle, A. K., Gotz, F., Kulik, A., Molinaro, A., Lipka, V., Gust, A. A., & Nurnberger, T. (2011). Arabidopsis lysin-motif proteins LYM1 LYM3 CERK1 mediate bacterial peptidoglycan sensing and immunity to bacterial infection. *Proc Natl Acad Sci U S A, 108*(49), 19824-19829. doi:10.1073/pnas.1112862108

Winkle, M., Hernandez-Rocamora, V. M., Pullela, K., Goodall, E. C. A., Martorana, A. M., Gray, J., Henderson, I. R., Polissi, A., & Vollmer, W. (2021a). DpaA Detaches Braun's Lipoprotein from Peptidoglycan. *MBio, 12*(3). doi:10.1128/mBio.00836-21

Winkle, M., Hernández-Rocamora, V. M., Pullela, K., Goodall, E. C. A., Martorana, A. M., Gray, J., Henderson, I. R., Polissi, A., & Vollmer, W. (2021b). DpaA detaches Braun's lipoprotein from peptidoglycan. *bioRxiv*. doi:10.1101/2021.02.21.432140

Wolf, A. J., & Underhill, D. M. (2018). Peptidoglycan recognition by the innate immune system. *Nat Rev Immunol, 18*(4), 243-254. doi:10.1038/nri.2017.136

Wood, W. A., & Gunsalus, I. C. (1951). D-ALANINE FORMATION: A RACEMASE IN *STREPTOCOCCUS FAECALIS*. *Journal of Biological Chemistry, 190*(1), 403-416. doi:10.1016/s0021-9258(18)56082-8

Yakushi, T., Masuda, K., Narita, S., Matsuyama, S., & Tokuda, H. (2000). A new ABC transporter mediating the detachment of lipid-modified proteins from membranes. *Nat Cell Biol, 2*(4), 212-218. doi:10.1038/35008635

Yakushi, T., Yokota, N., Matsuyama, S., & Tokuda, H. (1998). LolA-dependent release of a lipid-modified protein from the inner membrane of *Escherichia coli* requires nucleoside triphosphate. *J Biol Chem, 273*(49), 32576-32581. doi:10.1074/jbc.273.49.32576

Yamaguchi, K., Yu, F., & Inouye, M. (1988). A single amino acid determinant of the membrane localization of lipoproteins in *E. coli*. *Cell, 53*(3), 423-432. doi:10.1016/0092-8674(88)90162-6

Yamashita, E., Zhalnina, M. V., Zakharov, S. D., Sharma, O., & Cramer, W. A. (2008). Crystal structures of the OmpF porin: function in a colicin translocon. *EMBO J, 27*(15), 2171-2180. doi:10.1038/emboj.2008.137

Yang, J., Anishchenko, I., Park, H., Peng, Z., Ovchinnikov, S., & Baker, D. (2020). Improved protein structure prediction using predicted interresidue orientations. *Proc Natl Acad Sci U S A, 117*(3), 1496-1503. doi:10.1073/pnas.1914677117

Yao, X., Jericho, M., Pink, D., & Beveridge, T. (1999). Thickness and elasticity of Gram-negative murein sacculi measured by atomic force microscopy. *J Bacteriol, 181*(22), 6865-6875. doi:10.1128/JB.181.22.6865-6875.1999

Yeh, Y. C., Comolli, L. R., Downing, K. H., Shapiro, L., & McAdams, H. H. (2010). The caulobacter Tol-Pal complex is essential for outer membrane integrity and the positioning of a polar localization factor. *J Bacteriol, 192*(19), 4847-4858. doi:10.1128/JB.00607-10

Yu, F., Yamada, H., Daishima, K., & Mizushima, S. (1984). Nucleotide sequence of the *lspA* gene, the structural gene for lipoprotein signal peptidase of *Escherichia coli*. *FEBS Letters, 173*(1), 264-268. doi:10.1016/0014-5793(84)81060-1

Zammit, T. (1905). A preliminary note on the susceptibility of goats to Malta fever. *Proceedings of the Royal Society of London. Series B, Containing Papers of a Biological Character, 76*(510), 377-378. doi:10.1098/rspb.1905.0030

Zawadzke, L. E., Bugg, T. D., & Walsh, C. T. (1991). Existence of two D-alanine:D-alanine ligases in *Escherichia coli*: cloning and sequencing of the *ddlA* gene and purification and characterization of the DdlA and DdlB enzymes. *Biochemistry, 30*(6), 1673-1682. doi:10.1021/bi00220a033

Zhang, W. Y., & Wu, H. C. (1992). Alterations of the carboxyl-terminal amino acid residues of *Escherichia coli* lipoprotein affect the formation of murein-bound lipoprotein. *Journal of Biological Chemistry, 267*(27), 19560-19564. doi:10.1016/s0021-9258(18)41811-x

Zheng, S., Sham, L. T., Rubino, F. A., Brock, K. P., Robins, W. P., Mekalanos, J. J., Marks, D. S., Bernhardt, T. G., & Kruse, A. C. (2018). Structure and mutagenic analysis of the lipid II flippase MurJ from Escherichia coli. *Proc Natl Acad Sci U S A, 115*(26), 6709-6714. doi:10.1073/pnas.1802192115